Friction Stir Welding of Commercially available Superplastic Aluminium

A thesis submitted for the degree of Doctor of Philosophy

by

Timothy J Minton

Department of Engineering and Design, Brunel University

September 2008

Summary

A series of Friction Stir Welds (FSW) has been produced in order to optimise tool designs and weld/process variables to minimise flaws in the weld and obtain the best possible microstructure for superplastic Forming (SPF). Therefore the main goal is to produce friction stir welds which do not fail during subsequent SPF processes. The friction stir welds have been created using novel tools which are oversized for the material thickness used; this creates a wider weld region of fine equiaxed grains which are suitable for SPF. These original tools have been compared to tools which are already in mainstream FSW production. The welds created for this investigation also represent an evolution of friction stir welding by starting with a milling machine; a very basic piece of engineering workshop equipment. This was then replaced by a modified milling machine with force monitoring capabilities and finally using a state of the art dedicated FSW machine for the final welds. Room temperature properties are not usually a good indicator of high temperature response; however in this thesis the room temperature properties are closely linked to the FSW microstructure and have been used to assess the suitability of the weld structure for subsequent superplastic forming operations. The welds created for this thesis have been completed using hot and cold welding conditions, evaluated for room temperature properties and microstructural stability. The results have then been used to assess the welds and select the most suitable structure for cone testing, which is used to test the welds' performance during SPF. Friction stir welds were then recreated and cone tested which reveals the different levels of deformation occurring across the entire weld section and the unaffected parent material. Specimens in the as-welded, post-weld annealed and post-SPF have been analysed using standard microscopy techniques and Electron Back-Scattered Diffraction (EBSD). Welds in Aluminium Alloy (AA) 2004 with excellent room temperature properties have been created and shown to be capable of superplastic deformation achieving strain greater than 200%. Welds in AA5083, although producing excellent room temperature properties are unable to deform superplastically due to the difference in strengthening mechanisms employed by the different alloys. AA2004 contains Al_3Zr which effectively pins the microstructure allowing grain boundary sliding to occur, AA5083 lacks this grain refinement element and so suffers from abnormal grain growth leading to early failure.

Acknowledgements

The work described in this thesis has been carried out at Brunel University, TWI's Cambridge facility and Superform Aluminium's UK facility in Worcester. The work has been carried out between the autumn of 2005 and the summer of 2008. The work has been carried out under the guidance of academic supervisors at Brunel University and friction stir welding experts at TWI. The materials and cone testing facilities for this investigation have been donated by Superform Aluminium. Funding for this thesis has been provided by Brunel University and the EPSRC.

The undertaking of this Ph.D research would not have been possible without the support of the members of staff from Brunel University, who have significantly developed my skills through my undergraduate degree and postgraduate research doctorate. The financial support from the EPSRC has been invaluable in completing the course; providing both academic and industrial resources for this project. I would also like to thank Superform Aluminium UK for their support during the project and the donation of the materials investigated for this thesis.

Personal thanks is given to the staff from TWI's Friction and Forging department in Cambridge for their constant support throughout this research project, notably: Dr Michael Russell and Dr Phil Threadgill for the experience I have gained from working with them at the birth place of Friction Stir Welding.

Sincere personal thanks go to my academic supervisor Dr Joe Au for taking me as a student when I was without an academic supervisor and for his tireless efforts in making sure this project was a success. Thanks also go to Dr Bob Bulpett from Brunel's Experimental Techniques Centre for the training and experience gained in the field of metallography and finally to Dr Diane Mynors for introducing me to Friction Stir Welding and giving me the drive and determination to complete this Ph.D project.

This thesis is dedicated to my parents for their constant belief, enthusiasm and never ending support throughout.

Nomenclature

Abbreviation or Symbol	Description	Units
FSW	**F**riction **S**tir **W**elding	
SPF	**S**uper**P**lastic **F**orming	
FSP	**F**riction **S**tir **P**rocessing	
AA	**A**luminium **A**lloy	
TWI	**T**he **W**elding **I**nstitute	
FW	**F**riction **W**elding	
MIG	**M**etal **I**nert **G**as	
TIG	**T**ungsten **I**nert **G**as	
ISO	**I**nternational **O**rganization for **S**tandardization	
TMAZ	**T**hermo **M**echanical **A**ffected **Z**one	
HAZ	**H**eat **A**ffected **Z**one	
AGG	**A**bnormal **G**rain **G**rowth	
DRX	**D**ynamically **R**ecrystallization	
CDRX	**C**ontinuous **D**ynamic **R**ecrystallization	
FSS	**F**ine **S**tructure **S**uperplasticity	
ISS	**I**nternal **S**tress **S**uperplasticity	
T_m	**M**elting **T**emperature	°K
TMP	**T**hermo **M**echanical **P**rocessing	
σ	**F**low **S**tress	MPa
K	**M**aterial **C**onstant	
ἑ	**S**train **R**ate	
m	**S**train **R**ate **S**ensitivity **I**ndex	
ε	**S**train	
n	**S**train **H**ardening **I**ndex	
GBS	**G**rain **B**oundary **S**liding	
ECAP	**E**qual-**C**hannel **A**ngular **P**rocessing	
HPT	**H**igh **P**ressure **T**orsion	
Fx	**F**orce in **X** **D**irection	KN
Fy	**F**orce in **Y** **D**irection	KN
Fz	**F**orce in **Z** **D**irection	KN
Q	**H**eat **I**nput	KJ/mm
E	**E**fficiency **F**actor	
r	**S**pindle **S**peed	Rpm
T	**S**pindle **T**orque	Nm
v	**T**raverse **S**peed	mm/min
UTS	**U**ltimate **T**ensile **S**trength	MPa
EBSD	**E**lectron **B**ack-**S**cattered **D**iffraction	
HSRS	**H**igh **S**train **R**ate **S**uperplasticity	

Contents

1 Introduction

1.1 Abstract

Friction stir welds have been created in two commercially available superplastic aluminium alloys AA5083 and AA2004 in bead on plate trials and butt welding configurations. These welds have been created using a variety of tooling designs ranging from simple smooth tools to more complex tools with re-entrant features. These tools have been used in conjunction with different friction stir welding machines ranging from a basic vertical milling machine to a dedicated, purpose built friction stir welding machine. The welding process has been carried out under hot and cold welding conditions by varying the spindle rotation and weld speed. The room temperature mechanical properties have been tested in order to assess the success of the welding process under the different experimental conditions. The tensile strength has been measured to quantify to the overall strength of the entire weld cross section; with microhardness testing to identify the varying hardness and inferred strength of the different regions within the friction stir welds. Microstructural observations of the welds have been carried out after the welding process and after subsequent annealing and superplastic forming operations. Electron backscatter diffraction has been utilized in order to identify the second phases within the welds and distinguish any preferential textures resulting from the welding and or forming processes.

1.2 Project Introduction

Friction stir welding is a relatively new technology with many benefits over conventional welding techniques. This rapidly evolving process makes use of frictional heat and deformation to join materials. Due to the benefits it has become a readily researched area with many industrial applications emerging, such as aerospace, automotive, ship building and construction [1]. Another large scale research area is superplasticity. This metallurgical phenomenon has been rigorously studied for centuries but it is only now that it can be fully utilized for large scale manufacturing. Superplastic material can achieve strains that are at least two hundred percent without any necking or failure. This means it can be used to form complex shapes. During friction stir welding fusion is never reached, the degradation of mechanical properties due to heat input is minimised and a microstructure containing

recrystallized material is produced. All of these attributes makes the FSW process an ideal candidate to be used in conjunction with superplastic material and superplastic forming. Superplastic microstructures are very sensitive to heat and deformation and are usually destroyed by conventional fusion welding techniques. Both friction stir welding and superplasticity are large subject areas and require a lot of background information. It is the intention of this thesis to provide the reader with the information required to understand the dynamics of both subjects and how they interact in this partnership.

The aims of this investigation are three fold. The first and most important aim is to create quality friction stir welds in both aluminium alloys AA5083 and AA2004. This requires the friction stir welds to be defect free with minimal strength loss across the entire weld cross-section. The two alloy systems are very different and present different challenges in order to achieve the best possible welds. The second aim is to create friction stir microstructures which are suitable for subsequent superplastic forming. Fine structure superplasticity is reliant on prerequisite material characteristics in order for superplastic strains to be achieved. Superplastic strains are only possible when the deformation is uniform. Creating a homogeneous structure throughout the friction stir weld region is very difficult; inducing structural differences into the weld region will cause heterogeneous deformation and lead to early failure. The last aim is to create friction stir welds which can accommodate superplastic strains of greater than two hundred percent. To be deemed superplastic a material must be able to achieve greater than two hundred percent strain before failure [2,3].

To achieve the aims set out above a series of objective must be met. All the sets of tooling are trialled under the different experimental conditions in order to establish the best possible welding conditions for the two different alloy systems; this requires mechanical property testing at room temperature and comparisons drawn against the parent materials and previous studies from the literature review. The next objective is to evaluate the friction stir microstructure, using optical light microscopy; the produced weld region is compared and contrasted with the unaffected parent material. The stability of the weld region is tested in order to establish the extent of the structural change which occurs at elevated temperatures; once again these

findings are compared with materials covered in the literature review in order to continuously improve the weld properties and create the best possible welds for forming. The next objectives are to create welds which can withstand the immense forces involved with biaxial straining under gas pressure. Once weld seams which stand up to the gas pressure have been created, the friction stir welding parameters and subsequent forming parameters can be altered in order to achieve the highest possible equivalent superplastic strains. The post-formed structure can then be analysed with a view to improving the welding process and the associated welding parameters to obtain a better understanding of the material interaction with the friction stir welding process.

Bead-on-plate experiments involve welding on a single piece of material with no joint interface. Intensive bead on plate trials followed by conventional butt welding trials have been carried out and the full weld transverse sections have been tested for mechanical properties and formability. Room temperature results from mechanical property testing and microstructural observations from welds in the as-welded condition have been used to assess the success of the welding process for the subsequent forming process. Room temperature properties vary greatly from high temperature properties and so room temperature properties do not usually act as good precursors to superplastic ability [4]. However friction stir weld microstructures can be assessed by their room temperature properties by considering the friction stir welding heat input as a measure of the amount of disruption to the original microstructure which has occurred within the weld region. By running the welding trial with a fast feed speed the tool is influencing a large amount of material for every tool rotation, reducing the heat input and the disruption to the original superplastic material.

1.3 Chapter Abstracts

Chapter 2 describes the history of the Friction Stir Welding process and the steps involved in creating a solid state join. Firstly the material flow and process requirements are explained, this includes details of the complex flow of plasticised material around the FSW tool, machine variables and considerations for the materials to be joined. Next the advantages of the process are listed followed by some examples of different FSW tool setups.

Chapter 3 details the Friction Stir Welding tool and its fundamental role in producing the join. Some different aspects of the tool and its design are described and their functionality in terms of the resulting welds is also included.

Chapter 4 details the microstructure of Friction Stir Welds. Information is given about the key processes and mechanisms at work within the material during and after the FSW process has taken place. The evolution and final resulting microstructures of FSW welds in aluminium are explained along with their differing properties.

Chapter 5 illustrates the fundamentals of superplasticity and the mechanisms which allow this phenomenon to take place. It will also include details of enhanced superplastic flow by friction stir processing, a variant of FSW carried out on monolithic material with no joint interface.

Chapter 6 lists the various experimental setups used to create the welds and subsequently test their mechanical and material properties.

Chapter 7 lists all the welds carried out during this project and details the analysis carried out in order to establish their room temperature response and their superplastic properties.

Chapter 8 describes the work required to prepare a sample for metallography. Each stage of preparation is explained from initial choice of sample to the etching procedure before examination under a light microscope, scanning electron microscope and electron backscatter detector.

Chapter 9 provides a discussion of all the mechanical properties coupled with the microstructural observations in order to present a clear understanding of mechanisms at work during forming of friction stir welded materials.

Chapter 10 contains all the conclusions drawn from this project including the observations made from the mechanical testing, microstructural investigations and superplastic testing. It also provides details of current work and scope for future studies.

2 Introduction to Friction Stir Welding

2.1 History and Invention

Developed by The Welding Institute (TWI) [1,5] the Friction Stir Welding (FSW) process was invented and patented in 1991 meaning that in terms of a manufacturing process it is a relatively new one. FSW is a modification on an already known method of joining metal via frictional heating known simply as Friction welding.

Friction welding (FW), shown in Figure 2.1, is a joining process which has been in development for more than 100 years. This form of joining is most suited to material which is in rod or pipe form. It involves rotating or oscillating one rod whilst keeping the other stationary (Figure 2.1.a). The two are brought together and friction results (Figure 2.1b). This in turn causes heat. Once sufficient heat has been generated the two rods are pushed together with a force which forges the two rod sections together (Figure 2.1.c). The excess extruded material from the circumference of the join can then be removed leaving a welded section (Figure 2.1.d).

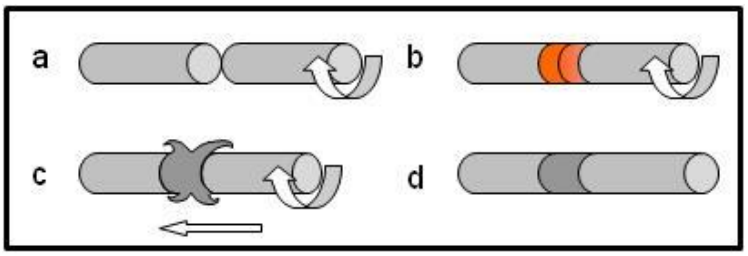

Figure 2.1, Friction Welding Process Steps

In FSW the heat is generated by a non-consumable tool which is rotated at high speed, plunged into and traversed through the material creating a join at the rear of the tool. The forging force in this case is the downwards force exerted by the spindle. Figure 2.2 details the separate parts of the process from start to finish.

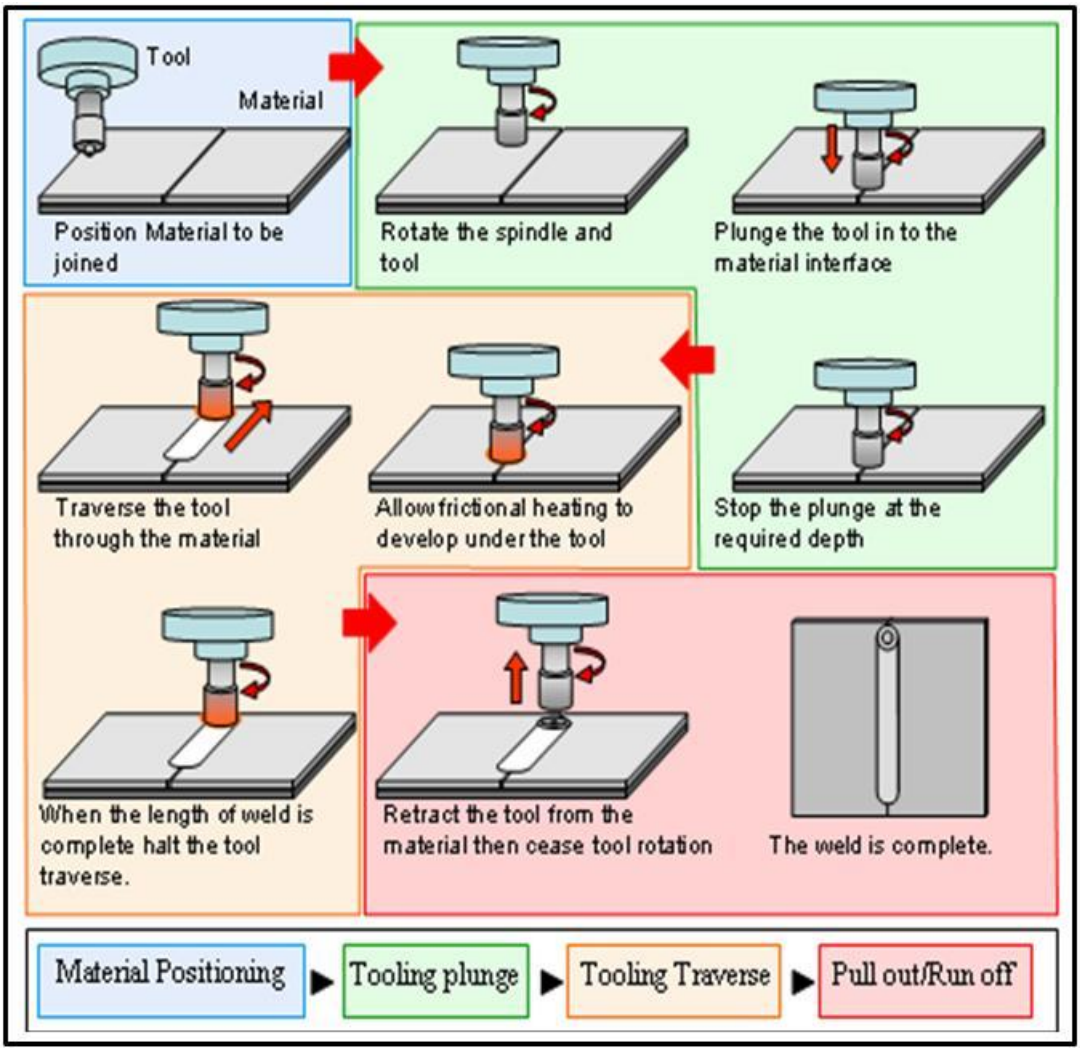

Figure 2.2, Friction Stir Welding process flow chart

2.2 Process Steps

The friction stir welding process is a simple one by its nature. It uses simple technology to produce state-of-the-art joins in previously difficult to weld or un-weldable materials [6]. A simple breakdown of the processing steps result in: Material positioning, tool plunge, tooling traverse and pull out/run off, these stages will be described in detail below.

2.2.1 Material Positioning

The material positioning is strictly linked to both the configuration of the desired weld and the application for the finished material. The material must be held together with a very small tolerance for gaps and constrained so there is no possible movement in the x, y or z axis i.e. zero degrees of freedom. Figure 2.3 defines the

axis system used throughout this thesis and highlights the main points for consideration during the material setup.

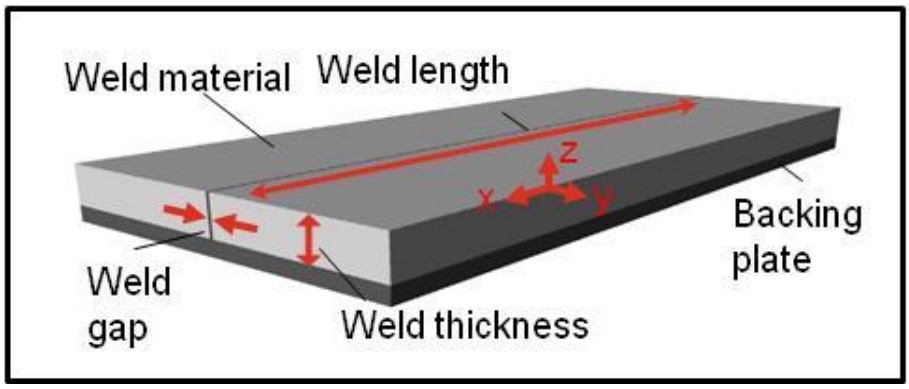

Figure 2.3, Schematic Diagram of Material Constraints.

From previous studies it has been determined that a gap of 10% of the weld thickness is tolerable before the weld quality is affected [1]. This need for accuracy may hinder repeatability unless this factor is controlled. Significant movement during the process can cause unsatisfactory welds due to poor bonding of the material, caused by either intolerable gaps or poor oxide break up on the abutting surfaces.

The forces experienced during FSW can be very high, meaning FSW requires a heavy duty rigid fixture. It is this rigid fixture of an FSW join which plays a significant part in the build up of residual stresses in the welded material. The inability of the weld to contract when cooling causes the build up of these stresses in both the longitudinal and transverse directions [7]. Holding the material sections in place, whilst the FSW process takes place, is difficult when dealing with more complex shapes of parts, these will require complex jigging to secure the work pieces. Some simple clamping methods for butt welding include bolting the sections to the backing plate, using finger clamps or use of vacuum tables. FSW requires a rigid backing plate of stronger material than the weld material. The backing plate or anvil will experience a proportion of the heat experienced by the weld nugget and so must not warp or deform under the heat applied. It must also be free from coatings and oxides as these may be drawn into the weld root by the process causing failures due to inclusions [8]. The downward force exerted by the tooling is resisted by the backing plate and prevents some distortion of the welded material. To make sure

there is no deflection or gap between the weld material and the backing plate, a roller can lead or follow the tool applying a constant force to press the material to the anvil [9], this is further described in Appendix A.

2.2.2 Tool Plunge

The tool plunge is an important part of the process as it is in this stage the tool is most susceptible to damage from unheated, pre-welded material. The depth of this tool movement is critical in maintaining a quality weld. Insufficient depth will result in poor bonding in the weld root; too much depth may break the tool but would also cause flaws, due to inclusions from the backing plate [9]. Position or force control or a combination of both can be used to regulate the plunge depth.

2.2.3 Traverse

This stage of the operation creates the join between the pre-welded sections of material. Once the tool is plunged to the correct depth and has been allowed to produce sufficient heat the feed table or tool traverse is initiated. As the tool is pulled through the heated and ultimately plasticised material, the material flows around the contours of the tool towards the rear of the tool where it cools to form the join.

2.2.4 Pull Out or Run Off

Once the length of the weld is completed the tool can be retracted from the material. This produces a dimple left by the tool profile as shown in Figure 2.4. For this reason a run off area is required at the end of the weld which is usually trimmed off after the process. Advancements in tooling have moved towards a retracting probe which allows for no run off or dimple [10].

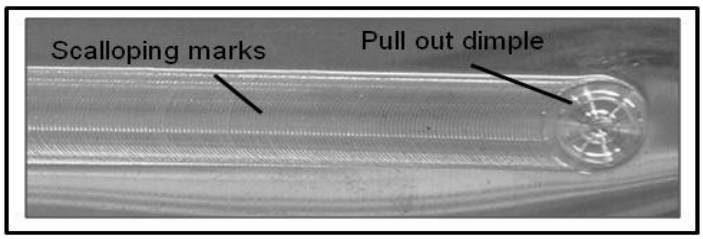

Figure 2.4, Dimple Feature Produced when the Tool is removed from the Material

2.3 FSW Requirements

To be able to carry out the FSW process there are two main requirements: a machine and a tool, these are explained in Sections 2.3.1 and 2.3.2 respectively.

2.3.1 Friction Stir Welding Machinery

The first requirement is a machine capable of rotating and traversing a tool through a resistive medium. This can be a vertical mill, robotic arm or gantry mounted spindle as shown in Figure 2.5.

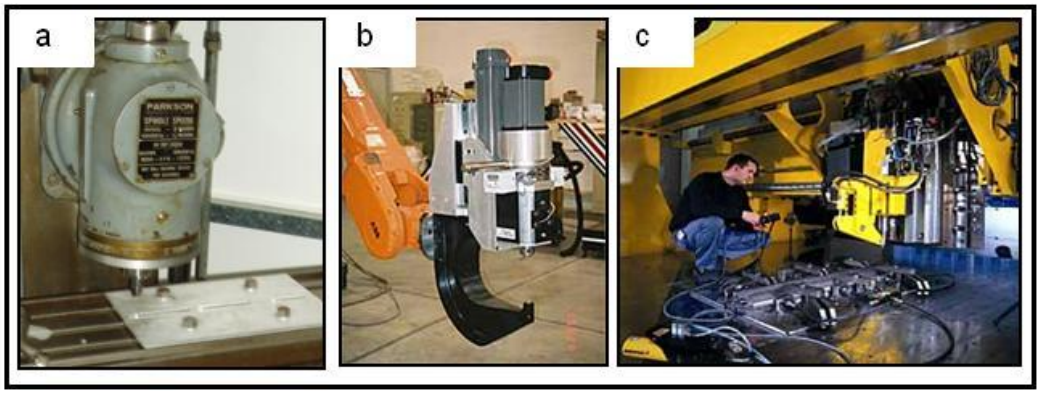

Figure 2.5, FSW Machines: a) Milling Machine Spindle, b) Robotic Arm Mounted Spindle [11], c) Gantry Mounted Spindle [9].

When choosing a machine the two major welding parameters must be dealt with first. These are spindle speed and feed speed [12]. The speed of the spindle determines the amount of frictional heat generated beneath the tool. The feed speed determines the amount of time for which the pre-welded material is subjected to the heat and deformation. An optimum balance between these factors must be struck to produce good quality joins. Other factors associated with the machine are the tilt angle and downward force. FSW requires a large downward force through the tool, currently vertical mills and gantry mounted spindles are the perfect candidates to withstand the forces required but research is ongoing to improve the acceptance of the process for use on robotic arms [13].

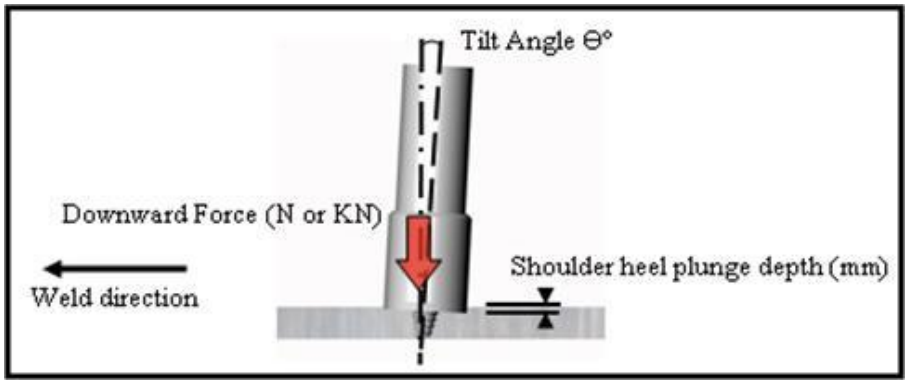

Figure 2.6, Schematic Diagram of: Tilt Angle, Shoulder Heel Plunge and Downward Force.

Tilting the spindle produces a lower shoulder heel as shown in Figure 2.6. This means a greater compressing force at the rear of the tool. During the welding process the material beneath the tool is being deformed. A complex material flow takes place around and beneath the tool which must be contained. The tool shoulder compresses the top of the weld and stops any weld material escaping. The downward force, which maintains the constant contact between the tool and the material, must be regulated to prevent defective welds due to too much or too little downward force through the tool [14].

2.3.2 Friction Stir Welding Tools

The second requirement is a tool specially designed for the process; a simple tool is shown in Figure 2.7. The tool is designed to heat the material and deform it to produce a void free joint [5]. The design of friction stir welding tooling is a large subject area in itself [15-17]. Friction stir welding tooling and tooling design will be detailed in Chapter 3 entitled FSW Tooling.

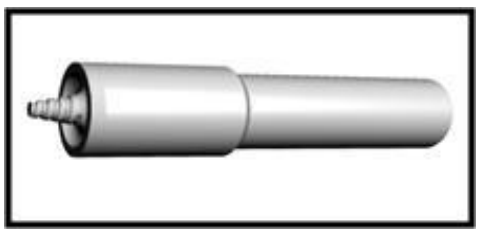

Figure 2.7, A Basic Friction Stir Welding Tool.

2.4 The Fundamental Premise of FSW

The FSW process is a solid state joining process [5]. This means the temperatures experienced beneath the shoulder never reach the melting point of the parent material. When material is heated it becomes more malleable and easier to deform. The rotating tool heats and deforms the material causing it to be displaced and deposited in another region of the cooling weld. Material under the tool is plasticised and extruded to the back of the tooling where it cools, creating a joint [18]. The process can be likened to an extrusion process between the advancing side of the tool and the cool, undeformed material close to the retreating side [19] (see Figure 2.8).

2.4.1 Material Flow

Several different techniques have been employed to try to understand the complicated material flow acting during FSW. These include experimental methods such as marker insert techniques [20, 21], powder insert techniques [22] and stop action techniques [21, 23-25], as well as computer modelling using FEA techniques [26,27]. Heating and deformation of the material take place at the same time. As the tool is moving in a line as well as rotating this creates asymmetry in the cross-section of the weld [18]. This asymmetry gives rise to the terms advancing side and retreating side as described in Figure 2.8.

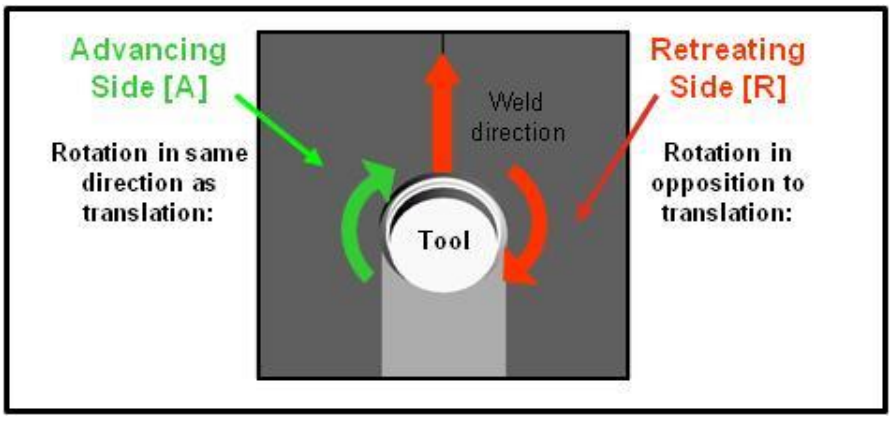

Figure 2.8, Schematic of the Advancing and Retreating Sides of a Friction Stir Weld.

This difference in velocities causes the asymmetric weld nugget although the effects of the advancing and retreating sides are generally very small, especially at higher spindle speeds [19]. The distinct banded structure present in FSW shows the extent of the material's movements throughout the process. The rotation of the tool transports material in relation to its movement. This means material is moved from

advancing side to retreating side at the front of the tool and in the same way, but to a lesser extent, from retreating side to advancing side at the rear of the tool [20]. The FSW process can be visualised as a continuous shearing of material in a semi-circular arc around the tool where it is then deposited behind the tool [24]. This is not the only deformation experienced by the material beneath the tooling. Material moves in different ways in different regions during the welding process, depending on which part of the tool it is influenced by. The top of the weld, closest to the shoulder, moves and is influenced by only the shoulder. This in turn is different for the advancing and retreating sides. On the advancing side the material is transported with the shoulder rotation to form the arc or banded structure associated with FSW. On the retreating side the material fills in the gaps at the rear of the tool left as material is swept forwards. This is rotational flow and only influences the top third of the weld. Further through the thickness of the weld the greatest influence becomes the probe and its features. The deformation caused by the probe features cause vertical or vortex material flow [21]. The material flow can be characterised by the trail left by the tool as it passes over the material. These semi-circular features are caused by the tool being forcibly traversed through the material, the spacing of the bands is equal to the distance travelled by the tool in one revolution. This banded feature also appears within the weld [28], and will be detailed in Chapter 4 FSW microstructure.

2.4.2 Heating and Deformation

The primary inputs to the process are heat and deformation caused by the tool's contact with the material. Temperatures in the weld have been reported to be around eighty percent of the solidus temperature [29]; however it is generally considered that the peak temperature next to the tool is very close to the solidus temperature, but with a very steep temperature gradient. This suggests that this process is actually a solid state extrusion process. The material is heated, but not melted, then subjected to deformation which causes it to take another form in this case a solid joint [19,21,28].

2.4.3 Weld Consolidation and Closure

The joint is formed by the destruction of the interface between the pre-welded materials during the hot, extrusion phase of the process [19]. As the tool passes over the material, the weld begins to cool and the plasticised material becomes more solid.

2.5 Process Parameters

The ***process parameters*** are the direct inputs to the process which will ultimately affect the outcome i.e. spindle and feed speeds and downforce. Other considerations which affect the weld include material type and material thickness; these will be called ***weld variables*** and will be detailed later in Chapter 3 Section 3.4.

2.5.1 Material Feed Speed

This is the most important variable in terms of success of the weld. In some cases for industry, the faster the weld can be made the cheaper it is, studies have been carried out in efforts to minimise the lead time for FSW parts by increasing the traverse speed, currently the fastest welding speed for FSW using an ESAB SuperStir machine and GSP5651 tooling is 6000 mm/min [30]. In other cases the weld quality is the governing factor so the traverse speed is not the driving factor [19]. The traverse speed governs how much time the tool spends in contact with a given area. A fast moving tool will spend less time over an area and so will heat it less than a slow moving tool. This variable determines the length of time the material is subjected to the process and so will have a large influence on the microstructure and properties of the weld [18]. The maximum traverse speed can be increased by advanced tooling designs and concepts. It is difficult to traverse the tool through the material because although in a more malleable state the material is still resistive. Sufficient heat must be generated by the spindle rotation and tool before the translation can begin. Designs of tooling and how the tool traverse is made easier will be described in Chapter 3 - FSW tooling.

2.5.2 Spindle Rotation

Another important variable is the spindle rotation. The speed of this will influence how much friction and so how much heat is generated by the process. The spindle rotation determines the amount of friction applied to an area per unit of time. That is to say that up to a point, the faster the tool is rotated the more heat and deformation is

generated by the resulting friction in a given time span. After a certain critical point the amount of heat generated will decrease with an increase of spindle speed due to a decrease in traction between the tooling and the weld material caused by localised melting [30,31].

2.5.3 Weld Pitch

Combining the process variables gives the feed rate or 'weld pitch'. This figure, with units of mm/revolution gives a first assessment of the heat input associated with the welding conditions as it provides an estimate for the amount of material being processed by each revolution of the tool. A fast spindle speed and a slow travel speed gives rise to a low weld pitch and so therefore is considered to be a hot weld; low spindle speeds and fast travel speeds result in a high value of weld pitch and is considered a cold weld [30].

2.5.4 Heat Input

The FSW heat input relationship behaves in the same way as in conventional rotational friction welding [30]. As the heat input rises, the torque decreases, up until a critical point. After this point no further increase in heat input is possible due to extreme softening and localised melting of the material directly beneath the shoulder, resulting in a loss of traction between the tool and the weld material. As the welding pitch is increased the torque rises; the tool requires more power to rotate the tools as the weld material is harder under cold welding conditions. When the weld pitch is low the material becomes soft and in some extreme cases can cause localized melting of material in direct contact with the tool shoulder. This thin layer of melted material acts as a lubricant and so decreases the amount of torque; this makes FSW a self regulating process unable to attain fusion of the bulk material [30, 31].

The heat input for a friction stir weld can be calculated using the spindle torque. The tool rotation accounts for as much as 99% of the total heat generated, with the remaining heat derived from the traverse of the tool. A dimensionless efficiency factor represents the amount of heat which remains in the work piece and has been estimated to be ~0.85 [14, 31, 32].

(2.1) $$Q = E\frac{2\pi rT}{1000v}$$ (KJ/mm)

Where: Q is Heat Input, E is Efficiency factor (0.85), r is Spindle rotation speed (rpm), T is Spindle torque (Nm) and v is Traverse speed (mm/min) [32].

Applying the spindle torque, spindle rotation speed and the feed speed to equation (2.1) gives the FSW heat input measured in KJ/mm. Table 2.1 shows the estimated power requirements for welding 6mm thick AA6082-T6 aluminium. It is clearly visible that FSW requires far less power than MIG welding and produces considerably less heat input.

Process	Welding Speed (mm/min)	Power at Work (KW)	Gross Power Required (KW)	Heat Input (KJ/mm)
FSW	500	2	2.5	0.24
MIG	300	7.5	8.6	1.5
CO_2 Laser	5000 1600	10 5	112 55	0.12 0.18

Table 2.1, Estimated Power Requirements for 6mm AA6082-T6 material, Recreated from [14]

2.6 Types of Friction Stir Welding Operations

Since the invention of this technology many variants to both the tooling specification and process motions have been tried. The variations used to create the different welds in this thesis are explained below. More information on some of the many other variations can be found in Appendix A.

2.6.1 Rotary FSW

The first and most commonly used technique is known as rotary FSW. This is the basic process outlined at the start of this chapter. A single tool is rotated and plunged into the abutted faces of the materials to be joined. It is then traversed through the material to form a join. Variations using this type of FSW can be single pass operations, multiple passes and multiple welding tool operations.

2.6.2 Single Pass

This is where the FSW process is completed in one single traverse of the tooling. This is nearly always the case [19].

2.6.3 Multiple Pass

This is where more than one traverse is completed by the tooling. Either consecutive passes on the top surface, Figure 2.9.a, or one pass on the top one pass on the bottom, Figure 2.9.b. This can be simultaneous, but there is normally a delay between each pass [19]. The different passes can also be offset from the weld centre line as shown in Figure 2.9.c.

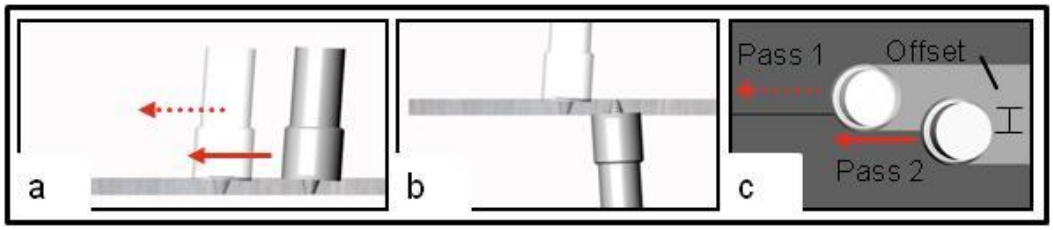

Figure 2.9, Multiple Pass FSW. a) Consecutive Passes on the Top Surface. b) One Pass on the Top Surface one on the Bottom Surface, c) Multiple Passes on the Top Surface with an Offset in the y Axis.

2.6.4 Friction Stir Processing

Friction stir processing is a variation on the FSW operation. The FSW process locally changes the microstructure and properties of the weld region. Friction stir processing applies the FSW process to whole pieces of material. The tool is inserted and traversed back and forth changing the properties of the material.

2.7 Summary

This chapter details the history and invention of the basic process of friction stir welding by The Welding Institute, as well as the complex material flow. The basic FSW process and its requirements are described and broken down into its constituent parts: Material positioning, tool plunge, tool traverse and pull out/run off. The process variables (Feed speed and spindle speed) and their effects on the final weld composition are detailed. The basic process (rotate, plunge and traverse the tooling) is the same for most Friction stir welds. The factor which can exert the biggest change in microstructure is the FSW tool itself. Now that the FSW process,

requirements and process variables are clear, how to design a tool to create a Friction Stir Weld is described in Chapter 3 - FSW Tooling.

3 FSW Tooling

3.1 Introduction

Ever since the invention of FSW the tools used to perform the process have advanced considerably. Early tools used simple cylindrical extrusions with a profiled end, when this is compared to modern tools such as retractable pin tools the advancement of the technology is clearly evident. This chapter looks at just FSW tooling, their design, construction and properties.

3.1.2 Tool Requirements

The friction stir welding process is advancement on traditional rotational friction welding described in Chapter 2. The tool must be designed to generate sufficient heat, through means of rotational surface contact, to create a plasticised region beneath the tool.

3.1.3 Basic Form and Construction

It was realised early on in the development of FSW that the tool's design is critical in producing sound welds [33]. A basic and conventional design for a FSW tool is shown in Figure 3.1. This cylindrical probe design will be compared to other more complex and still emerging tool variants. FSW tools follow the same basic trends in terms of their shapes and geometries. They are generally comprised of three generic features: 1) A shoulder section; 2) A probe (also known as a pin); and 3) Any external features on the probe.

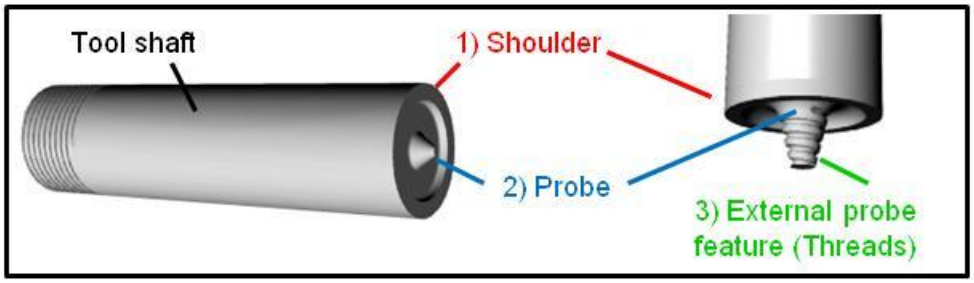

Figure 3.1, A Schematic View of a, Generic, FSW Tool.

3.2 General Features

The three generic features have key roles to play during the process, a failure in the design of one or more sections may lead to a failure in the process. The initial design of the tool is tested and optimised to find the ideal specifications for the geometry.

3.2.1 Tool Shoulder

The shoulder is designed as a relatively large, when compared to the probe, profiled surface. Although the probe makes the initial contact with the pre-welded material the shoulder has a larger contact area and produces more friction.

3.2.1.1 Shoulder Diameter

The diameter of the shoulder will determine the amount of contact area applied to the weld material's surface. A shoulder diameter which is too small could result in insufficient heat being applied to the process through an inadequate contact area between tool and material to be joined and therefore a failed weld or broken tooling. To generate sufficient heat during the process the shoulder diameter should be a minimum of 50% larger than the root diameter of the probe with contact areas up to three times larger deemed to be satisfactory [5]. The diameter of the tooling determines the width of the plasticised region beneath the shoulder and the width of the thermo-mechanically affected zone (TMAZ). The distinct semi-circular trail indentation left in the wake of the tool is evidence of the deformation caused by the shoulder rotation and its width is related to the shoulder diameter [28].

3.2.1.2 Shoulder Profile

The amount of heat generated by the shoulder contact depends on the profile of this surface. The shoulder profile can be designed to suit the material being joined. This profile can increase or decrease the contact surface area and so increase or decrease the amount of heat supplied. This will also change the amount of deformation experienced by the material at the top of the weld. This enables the tool to be specifically designed for the materials or conditions in which it will be used. As the shoulder profile rotates and makes contact with the material it traps material within any contours of the profile and transports them with the rotation of the tool. The material which has become caught in the shoulder causes like-to-like frictional

contact and superior weld closure [33]. Figure 3.2 shows examples of possible shoulder profiles.

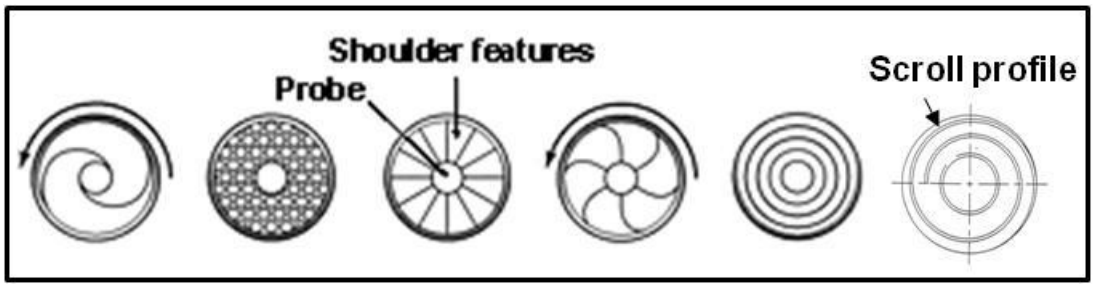

Figure 3.2, FSW Tool Shoulder Profiles Viewed from Beneath [33], Including Scroll Profile [34].

One special shoulder profile called the scroll shoulder enables the process to be carried out with the spindle set to a zero degree tilt angle. This eliminates flashes of material extruded under the shoulder before the weld is compressed but is far more difficult to set the tool's plunge depth as there is no heel plunge. The material is channelled towards the probe in the spiral shaped groove. The ability to weld with no spindle tilt angle allows the completion of non-linear welds, i.e. circumference welds [12]. An example of a scroll profile is shown in Figure 3.2.

3.2.1.3 Frictional Heating and Deformation

The shoulder of the tool generates the majority of the heat required for the process due to its larger contact area. The rotating surface of the tool contacts the top surface of the material causing friction. The softened material beneath the tool is said to be plasticised [30]. The material does not melt, but is heated, to become softer and more malleable. The plasticised region extends down through the weld directly beneath the shoulder as it is translated through the material [33]. The plasticised region of material undergoes heating from the friction and also deformation from the rotation of the tool. As the tool shoulder heats the material it is deformed and stirred by the tool's rotation. As the tool is traversed through the weld material it compresses the joint, stopping any plasticised material from being expelled from the top of the weld [33].

3.2.2 Tool Probe

Protruding from the shoulder profile is a cylindrical probe [5] shown in Figure 3.1. This increases the contact area of the tool and enables heat and deformation to penetrate to the weld root. The probe makes the initial contact with the weld material before being plunged through the material, for a typical butt weld the probe stops when the tool shoulder contacts the material in the region of 0.1mm below the top surface of the material. The probe rotates with the shoulder as it is pulled through the weld material.

3.2.2.1 Probe Length

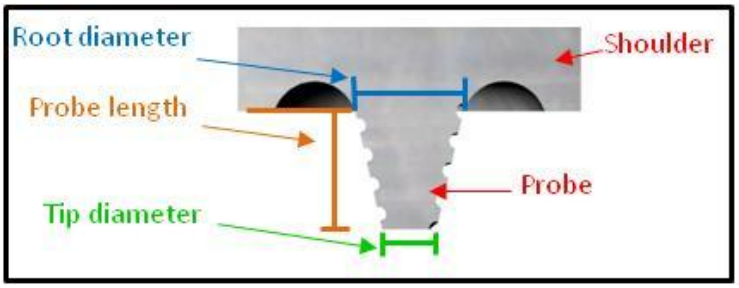

Figure 3.3, Probe Dimensions.

The probe length dimension is shown in Figure 3.3. For a butt weld the probe must be nearly as long as the material thickness [1]. For example the shoulder penetrates the material by a small amount, approximately 0.1mm; the probe must finish a small amount, approximately 0.1mm, before the bottom surface of the weld material to prevent total penetration of the tool. This means that roughly speaking the tool's probe should be designed to be in the region of 0.2mm less than the thickness of the material to be welded [14]. The probe length must be designed for the desired weld depth. The probe must not contact the backing plate as it would cause potential failures in the weld such as root flaws caused by impurities included in the weld from the backing plate, damage to the tool as a result of it being plunged into the backing plate or an unsatisfactory weld root.

3.2.2.2 Root and Tip Diameter

The probe tip and root diameter dimensions are shown in Figure 3.3. A simple cylindrical probe would have an equal root and tip diameter of approximately the same length of the probe [35,36]. A more complex conical shape would have a far

larger root diameter than tip diameter and would stand more chance of the probe breaking whilst under process conditions. However a conical shape yields superior welds than a cylindrical probe [37]. Friction stir welding probes are commonly designed as frustums [1].

3.2.2.3 Probe Profile

The angle the side of a probe makes with the vertical centre line of the tool is the probe angle as shown in Figure 3.4 [37].

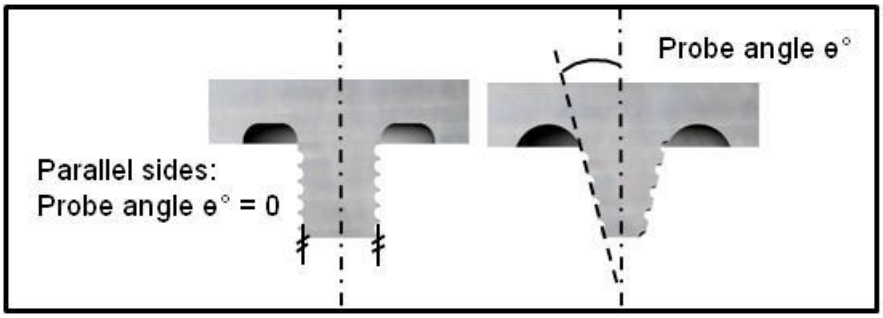

Figure 3.4, Probe Angle Schematic.

The parallel sided cylindrical probe shown on the left hand tool of Figure 3.4 has a probe angle of zero. This is a more prominent protrusion from the shoulder and would be harder to plunge into and traverse through the material to be joined than the tool on the right. The larger probe angle shown on the right allows a suitable radius to be used at its base providing a more gradual transition between the shoulder profile and the probe. This design allows easier plunging and traversing. As this angle increases, the amount of heat generated increases. A tapered cylinder or conical probe produces vertical material flow as well as the rotational flow caused by the tool's rotation [37]. The probe, much like the shoulder, exhibits a profile when viewed from the side or underneath. A probe's profile can be circular, nominally oval, flattened, or re-entrant. Some probe profiles/shapes are shown in Figure 3.5.

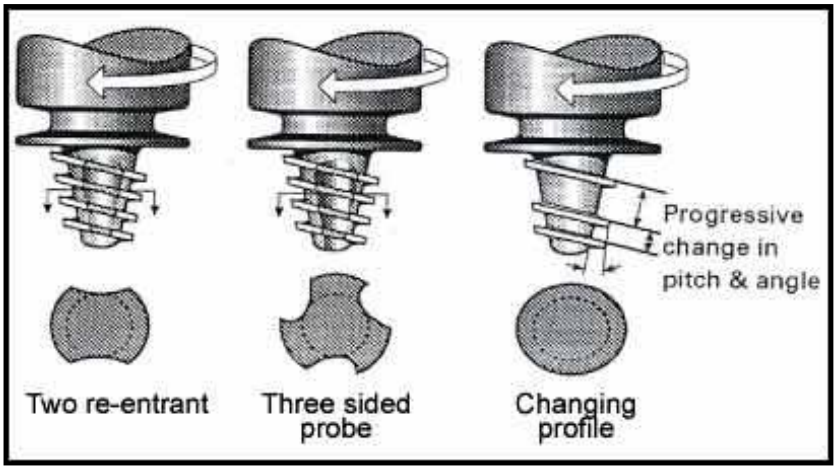

Figure 3.5, Examples of Possible Probe Profiles [1].

3.2.2.4 Frictional Heating and Deformation

The main source of heat for the process comes from the shoulder contact, however for thicker welds (typically of 1.2mm depth and above) the shoulder does not have enough influence on the weld root. It is the probe which generates the heat in the weld root [33]. The probe ensures sufficient deformation and heating of the material throughout the depth of the weld. The probe causes surface contact and therefore frictional heat through the thickness of the material it also causes deformation in the form of a material movement around the probe with the motion of the tool rotation. As explained in Chapter 2, the FSW process is like an extrusion process, the material flows around the probe and consolidates behind the tool. Coinciding with this rotational material movement a vertical movement can occur due to probe shape and or re-entrant features.

3.2.2.5 Threaded Probes

Some probes contain more complex geometry in the form of a helical ridge [1] or external thread. This external thread acts in the same way as any shoulder profile, changing the surface contact and deformation experienced by the weld material. These threads are designed in a specific way. As the tool is rotated the helix would either encourage or resist the plunge into the material depending on the pitch. The pitch of a screw accepts the material when rotated clockwise. This has a right-hand-pitched thread. The thread on an FSW probe is designed to oppose the plunge and push material downwards instead of drawing it upwards. This requires a left-hand-pitched thread (LH thread), when the spindle rotates in a clockwise direction. The

helical ridge pushes the weld material towards the bottom or weld root. This force produces vertical mixing to accompany the rotational mixing. The thread size or pitch will determine how successful the mixing of the weld material is. A small pitch may not produce enough deformation and so bonding of the stirred material is impaired. However too large a pitch will cause the tool to act like a drill and expel weld material before the shoulder makes contact to compresses the material [36]. The probe works as an auger, immersed in the plasticised weld material [33].

3.2.3 Re-entrant Features

More recent tools have moved away from smooth and threaded cylindrical probes and exhibit complex features. These re-entrant features affect the tools' ability to be traversed through the material whilst increasing the tools' influence on the material. Re-entrant features reduce the actual (static) volume of the probe whilst leaving the rotational (dynamic) volume the same. A typical ratio of dynamic volume to static volume for conventional probes would be 1.1:1, this volume is significantly different to that of the MX Triflute™ which is 2.6:1. This difference in ratio aids the material flow. The preferred number of features is an odd number of equally space features, this maintains maximum bending strength [33]. The MX Triflute™, shown in Figure 3.6, has three equally spaced flutes, a frustum probe and a profiled shoulder. This represents a modern FSW tool showing re-entrant features.

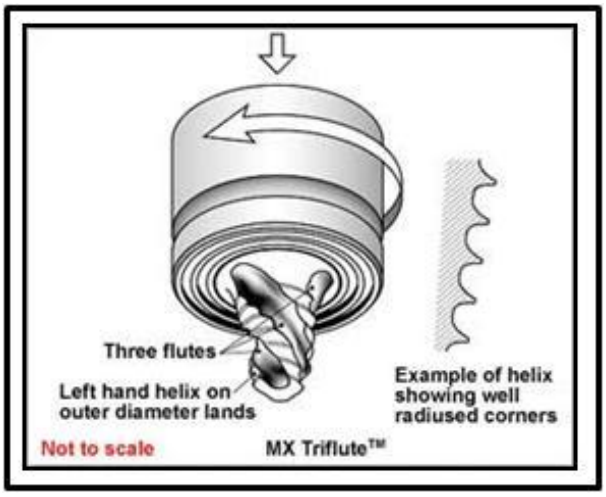

Figure 3.6, MX Triflute™ FSW Tool [33].

3.3 Tooling Variations

Due the amount of interest in the subject of FSW there have been many advancements in the area of FSW tooling. This research has enabled the process to be carried out faster, with longer and more reliable welds produced. As a result of this there are many variations on the basic FSW tool design from single piece basic shapes to composite tools. The tools used for the experimental work in this thesis comprised of single piece and composite tooling. These will be outlined here with information regarding other tooling designs included in Appendix A.

3.3.1 Single Piece Tools

The simplest of tools are those made completely out of one piece of material, usually steel. These tools are hard to make because the probe and shoulder have complex geometries and must be machined out of the same piece of material.

The probe shape is usually a flat ended, smooth, cylinder as shown in the top left corner of Figure 3.7. This extends to threaded cylinders and fluted cylinders. A truncated cone or frustum is a more commonly used design. Like the cylindrical probe this can be smooth, threaded, fluted or a combination.

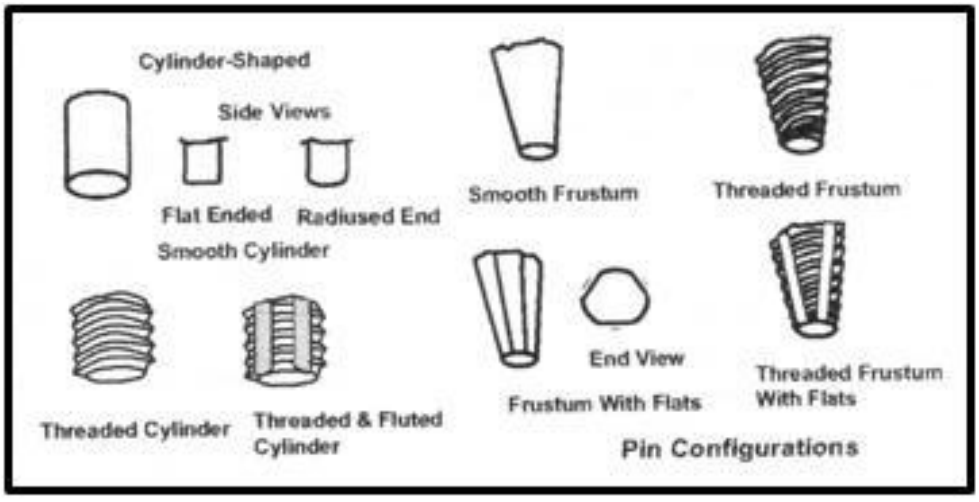

Figure 3.7, Possible Probe Designs [12].

3.3.2 Composite Tooling

A simple but effective improvement to the basic conical probe design allows for more specific process optimisation for the application involved. As the name suggests the tool is not made from a single piece of material. The probe and shoulder

are made from different materials. This allows the probe to be made from a substantially harder, more durable material while the shoulder is made from cheaper less wear resistant material. The difference in materials gives rise to further optimisation. For example the probe for a thick section weld tool can be made from a high temperature, physically resistive material such as Polycrystalline Cubic Boron Nitride (PCBN). This is an abrasive but expensive material so making the entire tool from PCBN is not cost effective. The probe can be made from this physical and chemically resistant material but the shoulder only needs a surface coating, this allows the majority of the tool to be crafted from a less expensive but still temperature resistant material such as high carbon content steel [12].

3.4 Weld Variables

The weld variables are the factors which must be taken into account when designing and building FSW tools. These are different to the process variables such as spindle speed and feed speed.

3.4.1 Weld Material Type

The most commonly FS Welded material is aluminium and its alloys. This material is deemed difficult to join using conventional fusion welding techniques due to its susceptibility to porosity and flaws due to inclusions. A wide selection of materials can be potentially joined using this process; a definitive list would be metals, alloys, composites and some thermoplastics [5].

3.4.1.1 Metals and Alloys

The FSW is a solid state joining process and so accommodates a wide range of possible applications for joining metals. So far research has been made into the continuous welding of aluminium, lead, copper, magnesium, steel and titanium [16, 33]. This represents a cross-section of the metals which could be used. Aluminium is regarded as an easy material to join using this technique when previously some of its alloy compositions had been deemed virtually impossible to join using conventional fusion welding methods [14].

3.4.1.2 Dissimilar Materials

The process can also join dissimilar materials. A join of aluminium 6xxx to aluminium 2xxx would cause problems during fusion welding when the molten weld pool cools. The FSW process is a solid state process and has been proven to be a reliable welding technique to join dissimilar metals, for example, the joining of aluminium to mild steel [1].

3.4.1.3 Thermoplastics

It is typically metals which are friction stir welded, plastics could be joined but the process is heavy handed and many simpler means of plastic bonding are commercially available [5].

3.4.2 Tool Material

The tool must be made from a material which can withstand the process and offer enough frictional heat generation. When selecting a material from which to manufacture the FSW tool the material to be welded must be considered. The tool material must be sufficiently stronger and more wear resistant than the material to be welded and must also have a higher melting temperature. A tool made from a material which is too soft will wear down to an unusable state very quickly due to the constant abrasive contact involved in the process. Tools currently used for industrial applications are capable of completing over 1000m of FSW without the need to change tool [1]. Aluminium can be joined using a tool made from silver steel [38], however if the weld material was to be steel, the tool would have to be more temperature resistant, for example tungsten with a ceramic coating. This means the selection of an FSW tool material must be based on the weld material properties. Another type of tool material under investigation is ceramic tools. A ceramic tool is more resistant to abrasion and so will not wear as much. This tool would also be able to generate the temperatures required to join steels. Ceramic although tough is a more brittle substance than metal and so the traversing of the tool would be its biggest challenge.

3.4.3 Weld Depth

The depth of the weld will dictate the overall geometry of the tool, more critically the probe length. Research in to the friction stir welding process has commonly been in the range of 1.2mm to 6mm thick plates in a butt or lap weld configuration. Thinner than 1.2 mm is considered to be thin section and thicker than 6mm is considered to be thick section [30]. Thin section FSW in the order of 0.4mm has been reported to have been carried out by Airbus [39], whilst thick section materials in the order of 50-75mm thick section have been successfully joined at TWI in Cambridge [40] representing the extremes of the scale. The range of material thicknesses welded is consistently within 1mm (thin gauge) and 50-75mm (thick gauge). The interest for the joining of material less than 1mm thick lies in the aeronautical area, joining air craft frames and body panels. With FSW making ground in the attempts to reduce weight on aeroplanes replacing riveted lap joints with thin gauge FSW butt joints. A TWI project investigating thin gauge of less than 1mm has produced sound butt welds in aluminium with thicknesses of 0.5mm. Sound lap welds have been created in 0.3mm thick aluminium giving rise to the title Micro Friction Stir Welding (μFSW) [41].

3.5 Tool Design in Literature

Due to the reluctance of authors to openly discuss their friction stir welding tooling a direct comparison between the welds produced by different authors is very difficult. Many authors do not give any indication to the shape or dimensions of tools used [28] some choose to give just the shoulder dimension and probe diameter [18]. Many design features are completely ignored. This may be down to several reasons and speculation can be made about these reasons. The weld produced in the FSW process is completely dependent on the tooling used to produce it, if no tooling information is given a comparison between work by different authors is hard, if not impossible, to make due to uncertainty as to how the weld was produced. The shoulder diameter and probe diameter are the most commonly given dimensions when describing a FSW tool. The shoulder dimension gives an idea of how wide the weld region will be and the probe root diameter gives an indication as to the width of the weld nugget. The most common welding arrangement is a butt weld so the probe length is assumed to be consistent with the depth of material to be joined, so is rarely mentioned. With there being no distinct rules for the design of FSW tooling a lot of

trial and error work can be expected. The failing of one tooling design is not documented and so others repeat the same mistake and design a flawed tool. Similarly a particularly successful tool may be designed but because it is not documented this success can be re-created and tested further by the same or different authors. FSW has picked up many followers since its invention; this explosion of interest has prompted International Organization for Standardization (ISO) standards for FSW which are currently under consideration [42].

3.5.1 TWI - The Welding Institute.

Many of the variations on the basic FSW tooling come from TWI. As the inventors of the technology they are constantly working on improving the technology, the main way in which the process is improved is by the design and optimisation of superior tooling. For TWI it is not in their best interest as a research business to divulge exact specification of all of their tools into the public domain. A licence to carry out the procedure from TWI, being the owner of the technology, is required to carry out this process; any improvements to the process will ultimately lead back to and be covered under the original patent relating to the process [5]. Some tooling is created for specific industrial applications and so the information is protected under an embargo.

3.6 FSW Tooling used in this Investigation

This chapter details all the requirements, considerations and features for designing and implementing friction stir welding tools. The friction stir welding tools for use in this investigation have been created using the principles discussed above. The tooling was designed using 3D CAD to produce detailed engineering drawings which were either sent to the mechanical engineering workshop in the case of the simple probed tools or to an independent tool maker for the more complex tool designs. Complete specifications for the tools used in this investigation can be found in Appendix B.

3.7 Summary

The friction stir welding tools used coupled with the process parameters used ultimately govern the final microstructure produced by the welding process. Through the evolution of the FSW process tool designs have become more complex and optimised to produce quality welds in most materials. It has been shown that features on the tool probe are vital in creating friction stir welds which are fully bonded in the

weld root. Threads, flats and flutes have been utilised to increase the deformation and heat generated by the tool, ensuring a suitably bonded weld root. All the tools used for this thesis are for use with conventional rotary friction stir welding, some more recent variants of FSW and their advanced tooling designs will be covered in Appendix A.

4 FSW Microstructure

4.1 Introduction

The microstructure of a friction stir weld is very characteristic and so a transverse section can be easily identified. The FSW process changes the microstructure and properties of the material. The amount of change is dependent on the position within the join as well as many other variables such as alloy type, original microstructure and the process and weld parameters used to create the join. The higher heat and more plastic deformation occurring towards the centre of the weld results in a different microstructural evolution than in the regions of lower heat and no deformation towards the weld extremities. The resulting microstructure is due to a combination of all the process and weld variables described earlier. When tools or processes are said to have been optimised, this means that the variables associated with the process have been tailored to provide the best microstructure possible for the required application of the weld. FSW is still an emerging technology, understanding the evolution of the microstructure is important for a wider acceptance of the technology.

Friction stir welds undergo complex changes to their microstructures. Information regarding the mechanisms for microstructural change can be found in Appendix A to assist in understanding the microstructural evolution of a friction stir weld this includes: recovery, recrystallization and grain growth.

4.2 Microstructural Evolution

The friction stir welding process can be used to intentionally change the structure of a material. FSW provides the structure with heat and deformation; both of which are beneficial for microstructural change. The asymmetry of the process coupled with both the rotation and linear movements of the tool make this a very complex evolution from parent material to refined equiaxed structures in the weld region. An FSW will differ in the transverse and longitudinal direction. To aid with the visualisation of the weld structure the transverse section will be tackled first followed by the longitudinal section.

4.2.1 Weld Section – Perpendicular to Weld Direction

The cross-section of an FSW weld in an aluminium alloy is easy to distinguish. Certain features are present which indicate the tool and process used to carry out the join. The simplest joint configuration is the butt joint and so this will be used for the examples of weld regions. These features are present in all the other joint configurations and are shown below in Figure 4.1.

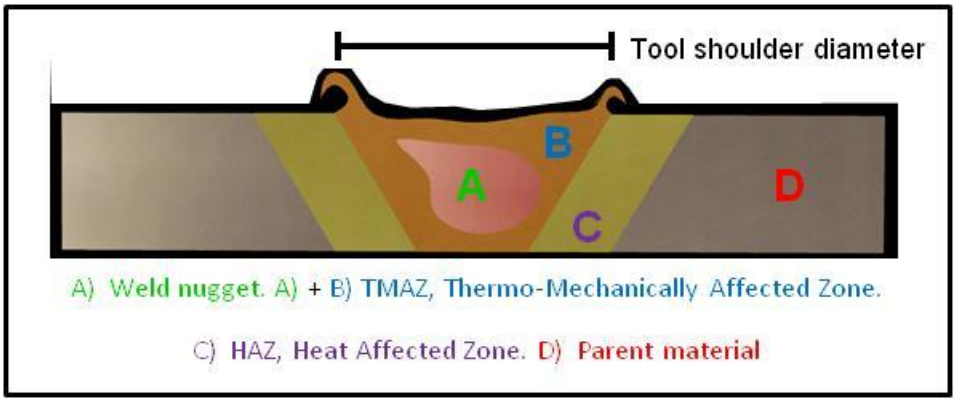

Figure 4.1, Cross Section of an FSW Butt Weld, Detailing the Weld Regions.

To help classify FSW welds, work has been completed at TWI to characterise the different parts of a friction stir weld. These definitions will enable aspects of any kind of friction stir weld made in any kind of material to be easily identified and direct comparisons to be made. This is also to aid the implementation of ISO standards. This thesis will use the terminology set out as guidelines by TWI [43, 44].

A friction stir weld contains different regions. These different regions have different mechanical properties and microstructures depending on what level of heat and deformation was experienced. The weld region comprises of the area directly beneath the tool shoulder. In Figure 4.1 the width of the weld region is approximately that of the tool diameter. The weld region is narrower at the bottom due to less influence from the tool shoulder and the tapering of the probe. However, this is not always the case, other variants of FSW processes and every different design of tool will create a differently shaped weld region but they contain the same features [43, 44].

4.2.1.1 Weld Nugget

This section of the weld region, marked as A in Figure 4.1, experiences high levels of heat and deformation. Aluminium is the only material studied which contains a separate nugget region. In other materials the nugget is part of the thermo-mechanically affected zone and is not a separate area [44]. The nugget region refers to the area which is passed through by the probe of the tool. Material is forced around the front of the tool probe before being extruded round the tool and filling in behind it.

During the process the combined heat and deformation acting on the material tends to cause recrystallization. This recrystallization is dynamic in nature and is confined to the weld nugget for aluminium and its alloys [18, 45]. For this reason the weld nugget is also referred to as the Dynamically Recrystallized Zone (DRX), the 'dynamic' part referring to the mechanism of recrystallization occurring during the presence of deformation as well as heat [46]. There are many different terms being used to describe the various regions. Some of the names used for the weld nugget include, Stir zone, swirl zone and dynamically recrystallized zone [14,44]; to simplify this, TWI terminology will be used throughout this document.

Recrystallization occurs as an evolution from the pre-welded base material structure. The evolution starts by introducing dislocations in the grains by plastic deformation. As the process goes on subgrains are formed by dynamic recovery. This is where the temperature causes the grains to move and become rearranged. This reduces residual stress in the grains [47, 48]. The recrystallization and recovery steps continue until the driving force (residual stresses within the grain boundaries) diminishes, at this point grain growth takes over. The recrystallization process usually takes place as a discontinuous process with cycles of high heat and deformation, however it has been reported that the recrystallization occurring within FSW takes place continuously and is referred to as continuous dynamic recrystallization (CDRX) [49,50,51]. However, this theory is not accepted by everybody, with some considering the mechanism to be geometrical dynamic recrystallization (GDRX) [19].

CDRX is a continuous increase in subgrain boundary misorientation within the microstructure of the material. This is achieved by continuous heat and deformation

as exhibited in the FSW process. This continuous misorientation is in turn attributed to dislocations being absorbed by the subgrain boundaries in order to accommodate plastic strains acting on the subgrains. This ultimately yields a fine grain structure containing fewer dislocations. Figure 4.2 shows dislocations being absorbed in the subgrain boundary. Figure 4.3 shows the difference between the base material structure and a recrystallized structure, a and b respectively.

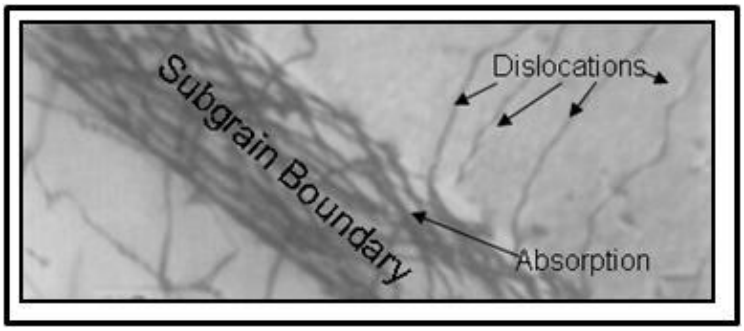

Figure 4.2, Dislocation Absorption by Subgrain Boundary during Dynamic Recrystallization [52].

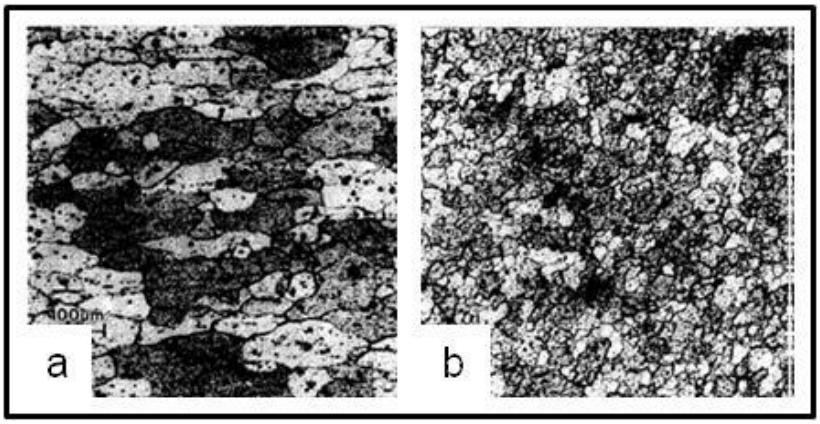

Figure 4.3, Grain Refinement after FSW via Dynamic Recrystallization.
a) Pre-welded Microstructure, b) Fine Grain Structure after Recrystallization [51].

The creation of the fine grain structure is based on a system of dynamic recovery and continuous dynamic recrystallization. Grains are heated and deformed which dislocates the grains, making them smaller and more uniform in size [48]. This uniform structure is very beneficial to FSP as mentioned in Section 2.7.4. The weld nugget's structure is dramatically changed by applying localised heat and deformation to the material.

4.2.1.2 Thermo Mechanically Affected Zone- TMAZ

This area marked as B in Figure 4.1 is not subjected to the same amounts of heat or deformation experienced by the weld nugget material. As the name suggests however this area is both heated and deformed by the tool. Recrystallization in the weld nugget is homogeneous, recrystallization in the TMAZ in inhomogeneous. The same fundamental process exists within this area. The amount of heat and deformation is at its peak inside the weld nugget and then generally dissipates as the distance from this weld nugget increases. It is common for aluminium to exhibit both a weld nugget and a TMAZ which both contain recrystallization. However, it is possible for the TMAZ to not experience the dynamic recrystallization when deformation or temperature is insufficient [53]. Generally in aluminium there is only partial recrystallization in the TMAZ, mostly recovery. This applies to aluminium but not necessarily other materials where a separate weld nugget is seldom observed. This is due to the very high resistance of aluminium alloys to recrystallize [19]. The high stacking fault energy in aluminium means that the critical level of driving force for recrystallization is not reached in the TMAZ or is only reached sporadically meaning this part of the weld does not fully recrystallize.

4.2.1.3 Heat Affected Zone - HAZ

This is the last region of the weld cross section which experiences any change in structure or properties due to the FSW process. This area is located just outside the foot print of the tool and marked as ‘C’ in Figure 4.1. As the name suggests this area is heated by the presence of the tool as it traverses the join. There is no macroscopic deformation occurring in this area and so it is affected by possible aging and or over aging [12,44]. Without induced deformation the structure of the HAZ is either strengthened or weakened by the heat from the process, this depends on the temper of the aluminium being welded. Recovery acts upon this region, the grains remain larger in size compared to the previous zones described above because there is no deformation to recrystallize the structure.

The HAZ can be compromised due to an over-aging effect of the tool. If a fully aged alloy was subsequently friction stir welded the tool would overage and weaken the HAZ region, however if an O temper material is used the tool may age and therefore strengthen the HAZ [19]. Aging, especially artificial aging is applied to evolve the

physical properties of a material [12]. The material is heated to a precise temperature for a precise amount of time to maximise mechanical properties like strength and hardness. The time and temperature of this is critical. Too higher temperature or too long a time or both will result in over aging and weakening of the material. This means that the amount by which the HAZ is weakened depends on the inputs to the process, tool rotation and travel speed. A slow tool rotation and fast travel speed (high welding pitch) would yield a far smaller and shorter period at elevated temperature. Consider a fast tool rotation and slow travel speed (low welding pitch), this would result in a far larger temperature and longer time at this high temperature and so would be more influential to the properties of the HAZ [12]. The general weakness of this region, in fully heat treated materials, is associated with larger grains and is easily characterised by a hardness profile plot containing hardness minima at the point corresponding to the HAZ region. Figure 4.4 shows such a hardness plot for a precipitation hardening alloy. The distinct 'W' shape shows the weakness associated with the HAZ region. Towards the centre of the weld the material is deformed allowing recrystallization to occur. The further from the weld centre the less deformation influences the material until the edge of the tool shoulder is met and deformation stops. When the material is heated without the presence of deformation it causes weakening of the material due to coarsening or even dissolution of the strengthening precipitates [44] giving rise to the minima seen in Figure 4.4.

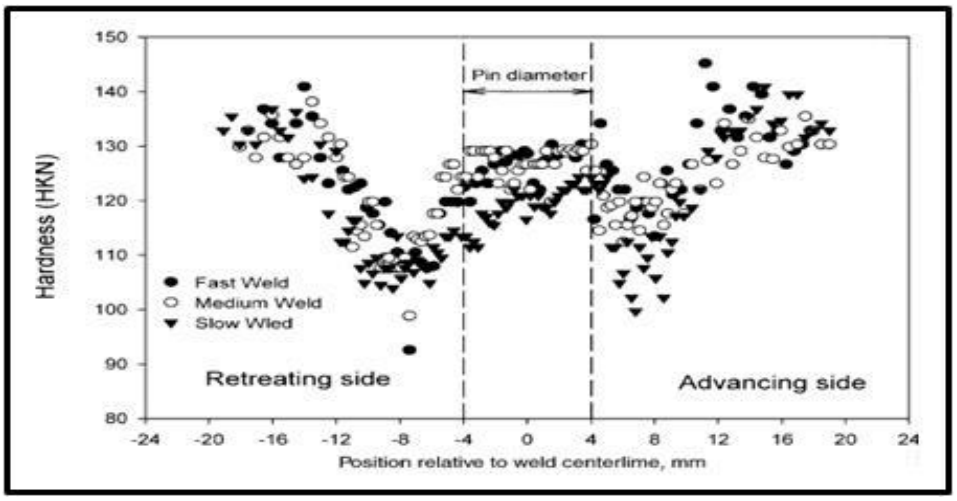

Figure 4.4, Common Hardness Profile of a Cross Section of a Weld made in AA2024-T351 [54].

4.2.1.4 Parent Material

This area, marked as ‘D’ in Figure 4.1, is unchanged throughout the entire process. The heat emanating from the tool does not affect this region. The HAZ is not under the tool footprint and so it is a transitional region between the unchanged parent material, the highly deformed TMAZ and weld nugget. Generally the physical properties of the parent material are superior to those of the welded zone; however it has been known for welds to fail in this unaffected zone rather than the weld itself.

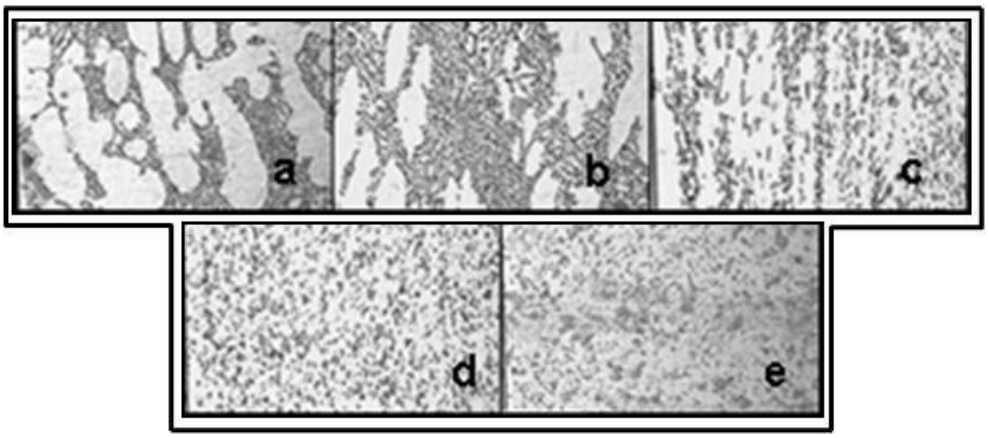

Figure 4.5, Macrographs of Weld Regions a) Parent Material, b) HAZ, c) TMAZ, d) Weld Nugget Extremity, e) Weld Nugget Centre [29].

Figure 4.5 shows the transition of a cast aluminium parent material structure through the different weld regions from the cast structure in a) to the fine equiaxed structure within the weld nugget in e). This represents the extremes of the structural change at work during FSW. The first considerations are the fine structures in pictures d) and e). This is the weld region and so exhibits fine equiaxed grains. These grains are larger in c) which shows the difference in recrystallization between the two regions. Larger grains still are found in the HAZ, picture b), along with some of the dendrite parent material structure. The completely unaffected material shown in a) contains only the casting solidification structure.

4.2.2 Weld Section – Parallel to Weld Direction

FSW creates a very distinguishable transverse cross section as detailed above, however it also creates a highly characteristic longitudinal cross section. When an FSW is observed the track left by the tool is instantly noticeable. This track also known as scalloping and consists of individual bands of swept material. In Chapter 2

section 2.4.1, the material flow is described; material is swept by the tool from advancing side to retreating side, this action results in the banded structure shown in Figure 4.6.

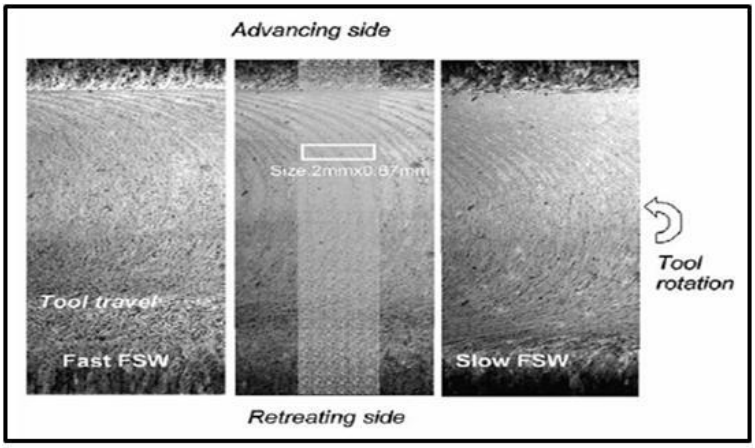

Figure 4.6, Banded Structure of FSW Exhibited in a Longitudinal Cross Section [54].

This banded structure exhibits two distinct alternating structures. These bands are shown in greater detail in Figure 4.7. The microstructure and hence grain sizes are different for the two bands.

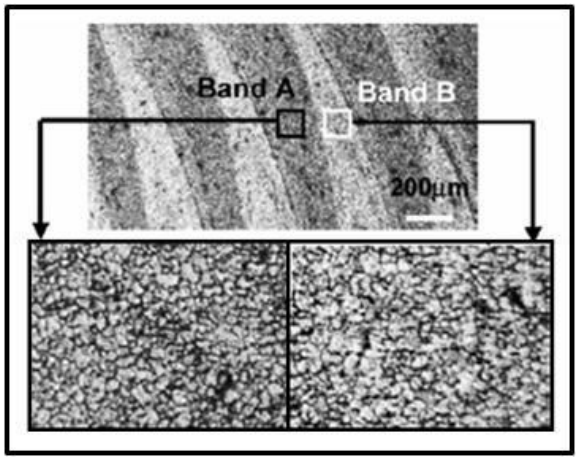

Figure 4.7, Banded Structure Grain Variance [54].

Sometimes the grain size separates the two bands; band A can show finer grains when compared to band B. The causes of the banded structure are not fully understood, but are not considered important as there are no detrimental effects caused by them [19]. It is however hypothesised that this structure is due to the distribution of second phase particles within the weld. Studies show that band A contains a higher density of second phase particles [54]. These particles affect the

hardness of the material, the more particles the harder the material, and this is clarified by Figure 4.8. It is also hypothesised by Yang et al that the difference in precipitation density in the banded structure could affect the microstructure at high temperatures; resulting in the bands experiencing recrystallization, recovery and abnormal grain growth at different intervals.

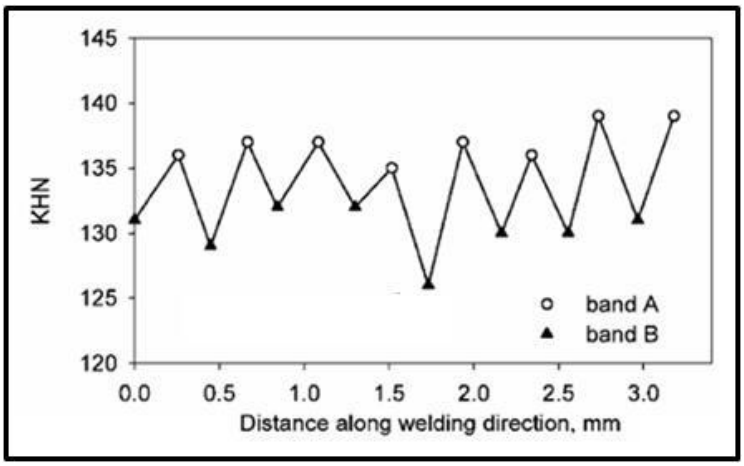

Figure 4.8, Knoop Micro-Hardness (KHN) Vs Distance in Weld Direction (mm) for Bands A and B [54].

In studies of these bands it has been noted that the spacing of the bands is equal to the distance travelled along the weld direction by the tool in the time taken to complete one tool revolution [28, 54].

4.2.3 Precipitation Distribution and Coarse Grain Dispersal.

Coarse precipitates within the structure are broken down and refined by FSW but are still far larger than the fine grains created in the weld region by the CDRX process. These second phase particles or precipitates affect the properties. It is reported that more, smaller particles are found on the advancing side of friction stir welds with the retreating side containing larger particles [54]. These particles and their arrangements are believed to affect the properties. The most common failure site for a FSW butt weld is on the retreating side of the weld. This suggests that larger particles are detrimental to the weld properties [54].

4.2.4 Variation of FSW Microstructure with Process and Weld Variables

The final microstructure of an FSW is reliant on the process variables and tooling geometry used to create the weld. For a given tool, variations to the primary process variables; spindle speed and welding speed (feed speed), have the most influence over the microstructural evolution of a friction stir weld [43]. However the tool itself has the greatest say on the final weld structure created by determining the size and shape of the weld region, the amount of heat and deformation experienced and the size and position of any weld defects.

4.2.4.1 Variation of Structure with Process Variables

It has been established that fast welding speeds coupled with slow spindle rotations give rise to low heat inputs during welding [31]. Low levels of heat input for FSWs allows for significant reduction in grain size via the dynamic recrystallization mechanisms in the weld nugget [25, 26, 27, 55] and more favourable microstructures for subsequent forming operations. Generally the lower the FSW heat input, the finer the grain size and so more strength is retained post welding; this occurs due to a reduction of static annealing processes induced by the tooling as it processes the weld material; minimising the amount of recovery and therefore grain coarsening within the weld region [56].

Taking the spindle rotation first; the faster the spindle is rotated the more frictional heat is generated beneath the tool, increasing the extent of the influence of the heat field generated by the FSW tooling. This means that increasing the spindle speed will increase the final grain size of the weld material [56]. This can occur due to the FSW process offering the weld material sufficient energy for microstructural change for recovery or secondary recrystallization allowing the grains to grow within the weld region. The increased spindle speed and therefore increased heat input can also destabilise the microstructure due to coarsening or dissolution of important second phase strengthening particles which pin the grain boundaries. If the size and distribution of these second phases are significantly affected the weld region may be prone to abnormal grain growth. Figure 4.9.a) shows grain size versus FSW spindle rotation speed for AA2524-T351 [56]. For a constant feed speed, as the rotation speed increases the grain size also increases. At first there is a sharp increase in grain size before it levels off to a plateau in a similar way the FSW heat input; where

above a certain point no more increase in heat is possible for an increase in spindle rotation; due to the self-regulating frictional heating mechanism which stops fusion temperatures from being reached. Figure 4.9.b) shows the variation of grain size versus with welding speed. The trend here shows that the faster the welding speed the greater the grain refinement and therefore the smaller the final grain size [56].

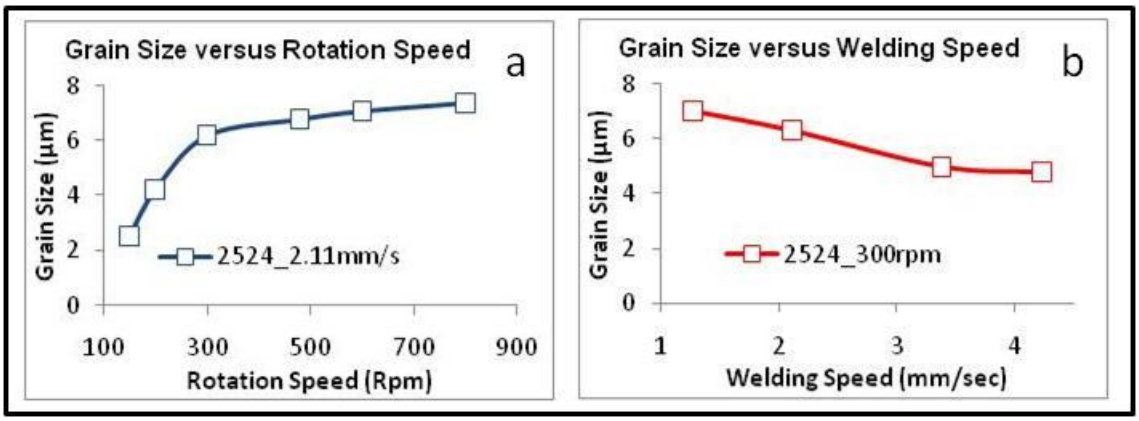

Figure 4.9, Effects of Rotation Speed and Welding Speed on Nugget Grain Size, a) Grain Size versus Rotation Speed. b) Grain Size versus Welding Speed. Recreated from [56].

Manipulating the grain size data from Yan el al [56] to give the grain size versus welding pitch gives the graph shown in Figure 4.10. The welding pitch is a useful value for estimating the heat input for a friction stir weld; a high welding pitch represents a cold welding parameter set with a large amount of material processed for each revolution of the tooling, compared to a low welding pitch where a small amount of material is process for each tool revolution. It is clearly visible that as the welding pitch increases (heat input decreases) the grain size of the material in the weld nugget decreases for both a constant rotation speed and a constant welding speed.

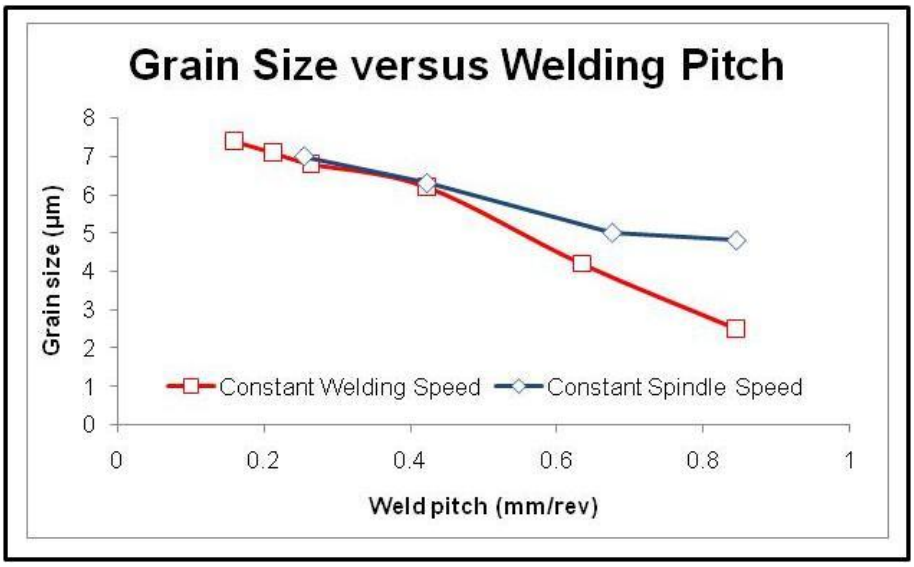

Figure 4.10, Grain Size versus Welding Pitch (Results Obtained by Yan et al [56]).

This grain refinement, for a reduction in FSW heat input, is mirrored in AA7010 [57], AA2024 [58] and AA5083 [59]. Reducing the heat input applied during welding reduces the grain size of the weld material; a fine grain size is more favourable for subsequent high temperature forming. Looking briefly at material from outside of the weld region, the FSW heat input plays a part in the size and strength of the Heat Affected Zone. As the FSW heat input decreases (either by decreasing the rotation speed or increasing the welding speed) the hardness of the HAZ increases due to the reduced annealing effects of the tooling. The heat field generated by the tool as it passes over the material is reduced in magnitude and has a reduced affect on the weld material [56]. The final grain size of the FSW microstructure can be further refined using quenching techniques and or low temperature welding techniques. Benavides et al [60] have produced grain sizes in the nano range using a liquid nitrogen cooled FSW system. Removing the vast majority of the heat from the process; ultra fine grains are produced, the liquid nitrogen also acts as an instant quench, locking in the refined microstructure and maintaining its size even after the tooling has left the vicinity of the material.

4.2.4.1 Variation of Structure with Tool geometry

Many studies have been carried out in order to establish the best tooling for friction stir welding [1, 7, 11, 12, 14, 33, 61, 62]. It is now recognised that tooling with external probe features produce the best welds and most favourable microstructures. This is due to the influence of the tool probe during FSW. It is the job of the tool probe to deliver heat and deformation to the weld root; allowing total annihilation of the joint interface. Smooth, featureless tooling does not exert enough influence towards the weld root and so the joint interface remains and acts as a failure initiation site and ultimately a flawed weld. The inclusion of re-entrant features such as threads, flats and flutes increases the size of the weld nugget and so also the deformation throughout the through thickness of the weld material; ensuring bonding right to the very bottom of the weld. They also play a part in refining the grain structure and reducing FSW heat input by reducing the static volume while maintaining the dynamic rotating volume [33].

For a given process variable set; the choice of tooling makes a difference in the weld structures produced. Smooth tooling will produce larger grains than re-entrant tooling due to a decrease in interaction between the tooling and the weld material [63]. Smooth tooling will slide over the weld material and reduce the amount of deformation; whereas re-entrant tooling will entrap weld material and distribute it within the weld region and so will cause more deformation and more grain refinement [33]. The tooling geometry may also influence the size and position of any weld defects such as worm holes, kissing bonds and voids. This is mostly associated with smooth tooling as they exert less deformation on the weld material and may leave unprocessed material within the weld region. A tool with threads and either flutes or flats is considered to be the best for friction stir welding of aluminium [30]

4.2.5 Friction Stir Welding in 5xxx Series Aluminium Alloys

This series of alloys derives the majority of its strength from dislocations within the structure. Dislocations impede each other's movement and form dislocation tangles which greatly improve the material's strength; this is known as strain hardening. Strain hardened materials are non-heat-treatable as the application of heat without the presence of deformation causes the dislocations to become more mobile; allowing

them to be annihilated by interacting with other dislocations of opposite sign and thus removing their affects on the material. Strain hardened materials contain internal stresses and thus energy for microstructural change; this allows these materials to recrystallize in a static manner; without the presence of deformation. When friction stir welding 5xxx series alloys the resulting weld microstructure and associated properties are based on the condition of the material prior to welding. If welding in the 'O' condition (Fully annealed condition) the intense plastic deformation occurring under the tool causes dynamic recrystallization of the weld nugget via material shear [24, 50, 64]. This makes the weld nugget stronger than the rest of the weld material and the parent material; which is fully soft and so cannot be reduced in strength by the heat field generated by the tooling [43, 44]. It has also been suggested that the forging action of the tool heel can induce dislocations in the weld nugget material as the tool is traversed; strain hardening this part of the weld nugget [65]. If the AA5083 is welded in a strain hardened condition, the weld nugget will still be recrystallized but the surrounding material within the TMAZ extremities and HAZ will be annealed by the tooling as it moves along the weld line resulting in the weld region exhibiting reduced strength when compared to the parent material [18]. The weld region in all cases contains a fine recrystallized grain structure; this means that the strength of the weld nugget is independent of the starting condition of the material, with the FSW process governing the strength of the weld region [43, 44].

4.2.6 Friction Stir Welding in 2xxx Series Aluminium Alloys

This aluminium alloy series is classed as precipitation strengthened. Hard second phase particles are distributed throughout the matrix enhancing the strength of the material. The fine second phase particles precipitate during natural and artificial aging techniques; this means that this series of alloys is heat treatable. The friction stir welding process affects how these second phase particles precipitate. Fine precipitates are required for strengthening; the heat field generated by FSW can cause coarsening of the strengthening precipitates. Coarse particles reduce the strength of the material giving rise to the 'W' shaped hardness profile showing minima situated at the HAZ/TMAZ interface [12]. After FSW the material within the weld region is fine and equiaxed; this structure has evolved via dynamic or geometric recrystallization [25]. Recrystallized material in the weld nugget is lower in strength than the parent material due to the relaxation of strain hardening in the deformation

free recrystallized grains and the dissolution of precipitates within the weld nugget. This means that generally the weld region will have a lower strength than the parent material; with joint efficiencies ranging from 70% to 96% [30]. The properties of the weld region are said to be independent of the original condition of the material due to the complex heat and deformation cycles occurring during FSW [44]. This structure is capable of grain boundary sliding as it fulfils the two major requirements for fine structure superplasticity, fine equiaxed grains and a distribution of fine second phase particles. The distribution of second phase is very important as the deformation under the tooling can cause the second phases to be heterogeneously distributed; leading to particle rich and particle deficient regions. This in turn can lead to abnormal grain growth within the weld region where the second phase distribution is disrupted the most [66]. Retention of superplasticity is capable in 2xxx series alloys [4, 58, 67]; stability of the microstructure is paramount. This can be further highlighted by looking at a similar alloy series, 7xxx series aluminium. This is also precipitation strengthened and can achieve superplasticity after processing has produced a fine equiaxed structure [68-75]. This also further highlights the need for microstructural stability at high temperatures; coherent second phase precipitates which arrest grain growth and maintain the fine structure during high temperature deformation.

4.3 Superplastic Microstructures

The original microstructure can vary dramatically from cast to wrought structures. The friction stir welding process takes this starting structure and changes it to form a fine equiaxed structure in the weld nugget. This structure is very different from one of a conventional fusion welding process, in which the structure contains large grains and is prone to solidification defects due to shrinkage and porosity. The FSW process' ability to refine a grain structure is most noticeable when starting with a cast material; the dendrite structure is so different from the FSW structure. The ability to further refine the structure is possible but far less noticeable when the starting structure is already highly processed to yield a fine grain structure. Many superplastic aluminium alloys have to go through thermo-mechanical processes to produce their very specific structures. It is this structure which is the key to the material's ability to deform at high temperatures. These thermo-mechanical processes usually consist of hot and cold rolling [2, 3] but other techniques such as Equal Channel Angular Processing (ECAP) [76-78] High Pressure Torsion (HPT)

[76] and Friction Stir Processing (FSP) [65, 79] can achieve a fine equiaxed structure capable of superplastic deformation. Usually a fusion weld will destabilize the microstructure, due to high heat and absence of any deformation, causing a coarsening of the structure [80]. However the FSW process can produce a join with a similar structure to that which is required for superplastic deformation. The ability of FSW to produce a superplastic microstructure has been recognised and now many authors are reporting using FSW not for welding but for processing [4, 58, 65, 68, 69, 81, 82]. FSP is being used to change a usually non-superplastic structure into a superplastic structure capable of hundreds of percent of elongations [65]. The grain size requirement for superplasticity is < ~10μm. The FSW process is capable of grain refinement; however the stability of the weld microstructure during forming now becomes the problem. During the SPF process high temperature cause the grain structure to coarsen via recovery mechanisms. Grain refinement elements are included within aluminium alloys in order to pin the structure and prevent grain coarsening, such elements include: Mn, Cr, Zr and Sc [67, 76, 81-83].

4.4 Chapter Summary

A brief explanation of some key microstructural terminology is offered before explaining the resulting weld regions. The friction stir welding process' characteristic weld regions are depicted and explained. These regions undergo very different thermal and deformation cycles and so produce very different microstructures. These different structures are described along with how the starting structure has evolved into its final form.

5 Superplasticity

5.1 Introduction to Superplasticity

To provide a better understanding of superplasticity a description the material prerequisites and primary deformation mechanisms will be given. A brief overview of the constituent equations as well as a description of the different forming processes and applications of SPF parts will be offered for reference in Appendix A.

First described in 1912, superplasticity is a property associated with certain materials which allows them to deform uniformly at elevated temperatures [3, 84]. In a non-superplastic material under tension the material will elongate forming a neck or reduced cross-sectional area before finally failing at a certain load usually before the 100% elongation mark. A superplastic material will have the same reduction in cross-sectional area but this reduction is uniform and so the material will continue to stretch to elongations typically in the range of 400 – 2000% and in some cases as much as 8000% before any failure [85] as shown in Figure 5.1. Superplasticity is best described as: “The ability of a polycrystalline material to exhibit, in a generally isotropic manner, very high elongations prior to failure.” Superplastic materials can be described as: “Metallic, ceramic, intermetallic, or composite multiphase materials with uniform or non-uniform, relatively coarse (20μm) to ultra fine (30nm) grain sizes that have isotropic or anisotropic grain (phase) shape, size, or orientation.”

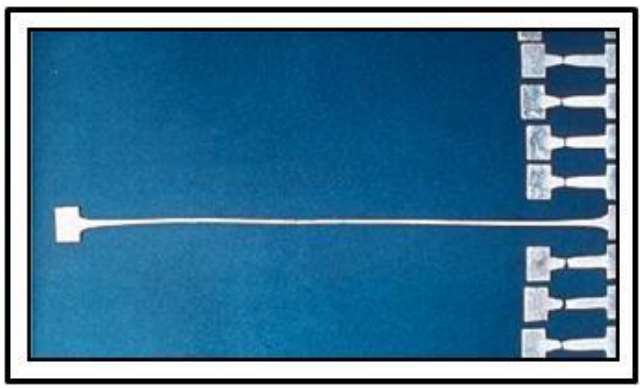

Figure 5.1, The Difference in Elongation Potential between Normal Aluminium Alloys and Superplastic Aluminium Alloys [84].

5.2 Types of Superplasticity

There are two different types of superplasticity; the first is called fine structure superplasticity (FSS). The second type is called internal stress superplasticity (ISS) [3]. Aluminium and its alloys fall under the fine structure superplasticity category, so only this will be discussed.

5.2.1 Fine-Structure Superplasticity

As the name suggest this form of superplasticity is reliant on a fine microstructure i.e. a very small grain size.

5.2.1.1 Grain Size

The main requirement for superplasticity in an FSS material is a very fine equiaxed grain structure with distributed, stable, particles which exert a pinning force inhibiting grain growth during the elevated temperatures imposed by superplastic forming [3,86]. A fine grain structure allows the material to be slowly stretched without failure at a certain temperature normally greater than half the melting temperature ($>0.5T_m$ where T_m is the melting temperature). For metals these well rounded, small grains are in the order of around 10μm [4, 86-89]. As the grain size decreases, the strain rate increases when grain boundary sliding is the driving force for the deformation. At the same time the flow stress of the material decreases as the grain size decreases requiring less force to deform the material. A decrease in grain size results in better superplastic properties, higher optimum strain rates, increased superplastic ductility, reduced flow stresses and reduced optimum temperatures [69]. The fine grain structure is not the only requirement for superplastic behaviour [3]. There are some other prerequisite characteristics which are as follows.

5.2.1.2 Second Phase Particles

High temperatures are required for grain boundary sliding to occur, in a single phase material these high temperatures will cause the grains to grow in a recovery cycle. Strengthening precipitates can inhibit the grain growth allowing the material to retain its fine equiaxed structure even when substantially heated. The grains are prevented from growing due to Zenner-pinning forces [86]. The hard phase should be fine and uniformly distributed throughout the matrix. Fine particles can inhibit cavitation; however, coarse, hard particles can cause cavitation. The strength of this second

phase should be similar to the matrix material as during superplastic flow the presence of the hard particles can cause cavitation. These particles act as stress concentration points allowing heterogeneous deformation to occur.

5.2.1.3 Grain Boundary Structure

Grain boundary sliding is the preferred mechanism for superplastic deformation. This only occurs with high angle or high energy boundaries. A material consisting of low angle boundaries should be first converted to a high energy structure by an appropriate thermo-mechanical process (TMP). A grain's ability to slide is primarily based on the boundary structure; however the chemical composition is also important. A boundary between grains of a similar chemical composition (homophase boundary) does not slide as willingly as a boundary between grains of a dissimilar composition (heterophase boundary) [3].

5.2.1.4 Grain Shape

For superplastic behaviour to be achieved the grains must be able to slide, a fine equiaxed structure allows this to happen, however a non-equiaxed structure will experience only a limited amount of grain boundary sliding. It is the texture of these elongated grains which causes this, strain accommodation at triple points is more difficult and can lead to cavitation [3].

5.2.1.5 Grain Boundary Mobility

During grain boundary sliding stress is concentrated at triple points, as shown in Figure 5.2. The capability of grain boundaries to move allows these stress concentrations to be reduced. The build up of stress concentrations at triple points leads to crack nucleation and failure [3].

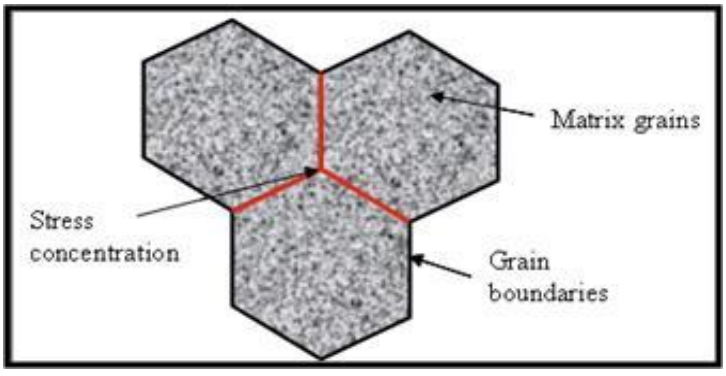

Figure 5.2, Schematic Diagram of a Triple Point.

5.2.1.6 Grain Boundary Tensile Fracture Stress

For a material to be able to be superplastically deformed to vast elongations the grain boundaries must not readily separate from one another. The stress required for plastic flow must be less than the stress required for grain boundary tensile separation [3].

5.3 Superplasticity Mechanisms

Ever since the 1960's [3] research has been carried out in order to model the process mechanisms and understand what happens when superplastic behaviour is observed.

It has been established that superplasticity is a special type of creep behaviour [3]; creep is the time-dependant and permanent deformation of material when it is subjected to a constant load or stress. When considering metals this generally this occurs at temperatures greater than $0.4T_m$ (T_m is the melting temperature) [3]. A description of the different creep mechanisms and the constituent equations, derived from these mechanisms in order to describe the material's behaviour, are given in Appendix A. It is believed that the major contributing creep mechanism which is responsible for superplasticity is Grain Boundary Sliding (GBS). As the name suggests the fine equiaxed grains of the superplastic microstructure move past each other in order to accommodate the deformation; the grain boundaries remain in contact. As the grains move over and past each other the material will become susceptible to cavities forming at triple points where grain boundary separation can take place [3, 86]; for this reason an accommodation process is necessary [3]. The accommodation process is theorised to be either: grain-boundary migration, recrystallization, diffusional flow or a dislocation slip process [3, 85].

5.4 Superplasticity in Aluminium Alloys

Superplastic aluminium can fall into three different categories [85]. They are:

1. Alloys which have been specifically designed to be superplastic.
2. Alloys designed for both ambient properties and superplasticity (e.g. SUPRAL 100: AA2004).
3. Commercial alloys which have been altered by a thermo-mechanical process to become superplastic (e.g. AA7475 and AA5083).

5.4.1 Alloys Covered

The aluminium alloys featured in this thesis fit into categories 2 and 3 above; AA2004 has been specifically designed to be superplastic but maintaining good ambient and post formed properties. AA5083 is a commercial alloy; modified to be superplastic. Normally AA5083 is not superplastic but, using the right TMP route this alloy can be processed to give moderate SP behaviour.

5.4.1.1 AA5083-H19

Aluminium alloy 5083 is a non-heat-treatable Al-Mg-Mn alloy. Following its thermo-mechanical processing the alloy contains two types of particle, larger constituent particles roughly 1-5µm in size (containing AL, Mn, Fe and Si) and Al_6Mn roughly 0.2-0.8µm in size. This mix of particle type is very important for the stability of the material at high temperatures. The alloy now goes through a process of cold working. This reduced the sheet thickness by approximately 70-80%. This strain hardened material is designated as having a temper of H19, meaning that is has been cold worked, with no annealing and is classed as extra hard [90]. The material will statically recrystallize quite rapidly during the SPF pre heat stage (350-570°C). At these temperatures the material is in a state of recovery causing grains to grow. The fine Al_6Mn particles mentioned earlier act to pin the constituent particles hence preserving the fine structure of the material [85].

This alloy has been developed for applications which require the material to be corrosion resistant and able to be welded, but also to exhibit superplastic behaviour and have good room temperature properties. The typical composition of this alloy is shown in Table 5.1 in weight percent.

Mg	Mn	Cr	Fe	Si	Zn	Ti	Cu	others each/Total	Al
4.0-4.9	0.4-1.0	0.05-0.25	0.4	0.4	0.25	0.15	0.10	0.05/0.15	Bal

Table 5.1, Typical Composition of AA5083 in wt% [91].

This alloy is suitable for rail, automotive, architectural and marine applications due to its good compromise between its formability and corrosion resistance as well as its

moderate strength. This alloy is superplastically formed using either bubble or cavity forming at 450 - 500 °C and controlled strain rate.

5.4.1.2 AA2004 - SUPRAL 100

This alloy is a heat treatable Al-Cu-Zr which has post forming properties that are comparable to those of conventional sheet fabricating alloys like AA2014. The processing route for AA2004 is complex but ensures that the microstructure is stable at SPF temperatures. The pinning particles which ensure this stability, in this case, are Al_3Zr. The alloy is very rapidly solidified from a super high heat to keep the zirconium (Zr) in solid solution and prevent any coarse particles from forming. It is then aged at 360°C during which a fine, homogenous distribution of Al_3Zr particles precipitate. The material is then solution treated at 500°C and hot rolled. Finally the alloy is warm/cold worked (approximately 80% reduction). During this stage recovery and recrystallization are prevented by the Al_3Zr precipitates. Recrystallization instead happens during the hot forming (SP) process. The fine grain structure evolves due to subgrain boundary coalescence. These small equiaxed grains give favourable conditions for GBS [85].

During the early stages of the SPF process; AA2004 evolves from a highly elongated structure to the fine equiaxed structure via dynamic recrystallization accommodated by intra-granular slip. This gives rise to fine grains which are highly misorientated and present a random texture; which is beneficial for grain boundary sliding [92]

This alloy allows neck free elongations of 500% meaning deep complex forming is possible. The alloy has a corrosion resistance which is similar to other aluminium alloys which contain copper meaning that it will require extra protection when used in an aggressive environment. The typical composition of this alloy is given in weight percentage in Table 5.2.

Cu	Zr	Mg	Si	Fe	Mn	Zn	Ti	others each/Total	Al
5.5-6.5	0.3-0.5	0.5	0.20	0.2	0.1	0.1	0.05	0.05/0.15	Bal

Table 5.2, Typical Composition of AA2004 in wt% [93].

Due to this alloy's ability to accommodate component strains in excess of 200% this alloy is well suited for complex designs. The alloy is most suited for electronic enclosures, aerospace components and small complex components. The forming of this alloy is carried out between 450 and 470°C and is either bubble or cavity formed.

5.5 The Superplastic Forming Process

The superplastic forming process is a rapidly advancing technology with many industrial applications including automotive, aeronautical and structural [84, 85, 91, 93]. This process is a hot forming process, for aluminium it requires the sheet to be heated to between 450 to 500°C, the temperature regime in which GBS takes places. The hot sheet is then forced into or onto a die via gas pressure. There are several methods in which this can be achieved, each with its own benefits. These superplastic forming processes include: Cavity, bubble, back pressure and diaphragm SPF [85].

5.5.1 Cone Test

In order to test a material's ability to deform under a superplastic regime it can be subjected to a biaxial cone test as illustrated in Figure 5.3. The cone test was developed by Superform Aluminium in order to produce a standard test for superplasticity [85]. The sheet is inserted between two ceramic heaters and brought quickly up to superplastic temperatures in the range of ~400 – 500°C. Clamps are engaged and gas pressure is applied to the underside of the sheet; the process is similar to the cavity forming process where the superplastic sheet is forced into a cone shaped die with an angle of ~57°. The cone test is used to assess the materials acceptance to the superplastic forming process by measuring the dome height; for a material to be accepted it must reach a predetermined height. The superplastic strain achieved during this biaxial forming operation can be obtained by measuring the pole thickness.

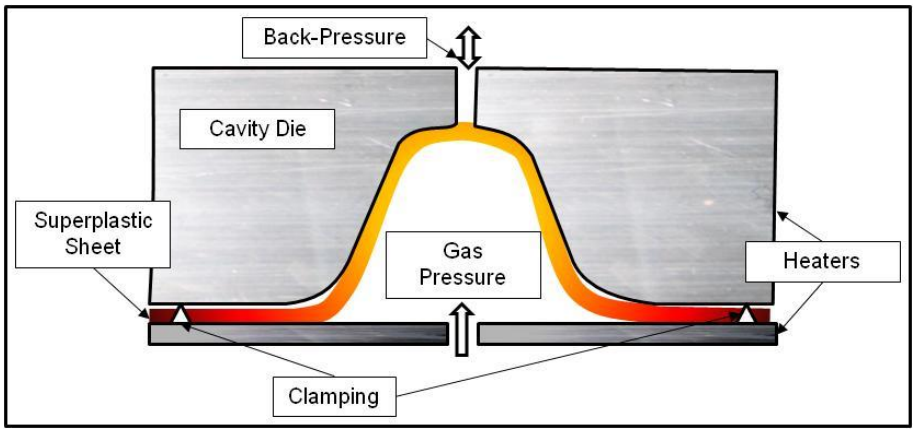

Figure 5.3, Schematic diagram of the cone test.

5.6 Superplasticity and FSW

Over the past decade FSW has taken off as an industrial process which is capable of joining previously impossible to weld materials without melting them. After this initial discovery it was realised that FSW could be used as a material processing tool. The FSW process results in a recrystallized weld nugget which has a fine equiaxed structure with minimal disruption to second phases. This makes FSW the perfect candidate for joining and processing superplastic materials. Many authors have recently investigated the possibilities of processing a standard material to instil superplastic properties upon them [58, 65, 68, 69, 71, 73, 74]. Another route is to take an already superplastic material and retain the superplastic properties post FSW/FSP; allowing large elongations to failure [4]. SPF is a slow operation due to the low strain rates which are required. The jump from low strain rates of 10^{-4} - 10^{-3} to more productive high strain rates of 10^{-1} - 10^{1} has only been possible due to advances in superplastic materials such as grain refinement techniques [3]. Such techniques include: Equal-Channel Angular Processing [76], High Pressure Torsion [76], Reciprocating Extrusion [83] and of course Friction Stir Processing [58, 73]. The post-weld retention of already present superplastic properties represents a great opportunity expand the current capabilities of superplastic forming. The prerequisite structure required for superplasticity is sensitive to any input of heat and deformation so a homogeneous structure is required over the area to be strained. Previous attempts to join superplastic materials give rise to massive mismatches in properties between the parent sheet and the joint interface. Conventional fusion welding cannot be used as the high heat and melting involved will completely destroy the superplastic microstructure [80]. FSW on the other hand provides a very small heat

input but more crucially provides deformation which will provoke recrystallization and grain refinement within the structure [47, 49]. Friction stir, whether it be used to weld superplastic materials or locally process them is a viable process, able to cater for this thermally sensitive phenomenon.

5.7 Summary

Superplasticity is a material phenomenon which allows extremely large elongations when the material exhibits certain microstructural characteristics and is deformed at high temperature. The exact mechanisms by which this process can occur are still a topic of much debate, but the main hypotheses are described. Superplasticity is a sensitive attribute which can be completely removed by conventional welding techniques. The relationships between the microstructural characteristics and creep mechanisms involved with superplastic deformation are described in order to provide good background knowledge of this high temperature deformation process. The stability of each of the superplastic microstructures of the two alloys covered in this investigation are discussed and compared; highlighting the subtle but key differences in terms of the success of the material to remain superplastic after welding.

6 Experimental methods

6.1 Introduction

A number of welds have been created using machines located at Brunel University and TWI's Cambridge facility. These welds were in turn created using different tools and process variables. Upon completion the welds were examined before sampling and sectioning for further analysis. Room temperature mechanical property tests were carried out along with formability trials.

6.2 Experimental Strategy

Friction stir welds have been created in the two superplastic aluminium alloys. In order to assess the weld microstructure without the inclusion of any root defects associated with butt welding; the bulk of the welds were created in a bead-on-plate format. These bead-on-plate FSWs were then tested using standard mechanical property tests such as tensile testing and microhardness and evaluated by incorporating the welding forces and spindle torque data acquired from the LoStir unit and built in force monitoring systems. Annealing experiments were carried out on the FSWs in order to assess their microstructural stability under static annealing conditions and microstructural observations were made in both the as-welded and annealed conditions. The results from these trials and tests carried out on the welded specimens were used in order to determine which of the tools and the process variables created a suitable weld which is capable of superplastic deformation. In order to test for superplasticity cone test specimens were created by friction stir welding in a butt welding configuration using the tools and process variable selected in the bead-on-plate trials. High temperature deformation of the butt welded FSWs was carried out and microstructural observations were made in the as-formed condition.

In order to improve on the results obtained from the welding carried out in the first set of welding trials; subsequent welding trials were carried out using an ESAB SuperStir FSW machine and MXTriflute^{TM} tooling. These are considered to be pieces of state-of-art FSW equipment. Another round of friction stir welding trials was carried out using amended process variables. The process variables were altered within the original range of welding pitches based on previous studies in friction stir

welding of 5xxx and 2xxx series aluminium alloys in literature [30]. Further FSWs were then subjected to another round of mechanical tests and microstructural observations before the final cone testing and post-formed microstructural observations.

After each battery of friction stir welding trials the welds produced were tested for mechanical and microstructural properties in order to improve the welds for the next set of welding trials; to achieve a constant improvement in terms of weld success and forming success.

6.3 Welding Trials

The welding trials were carried out in three distinct stages using three very different machines. The first tests were carried out on a vertical milling machine located at Brunel University. Once it was recognised that this machine was substandard for the task an alternative machine was sought. The next stage was carried out on FW22 located at TWI's site in Cambridge; this involved a much larger scale investigation completing hundreds of welds with many differing tools and process parameters. The final set of welding trials was carried out on a custom built ESAB SuperStir machine. This is a dedicated FSW machine and represents the state-of-the-art in FSW machinery; this is also located at TWI's site in Cambridge.

6.3.1 Testing Schedule

Tool Name	Tool Shoulder Diameter	Weld Material	Material Thickness	BOP/Butt Welding	Spindle Speed	Feed Speed
Concave with Threaded Probe	19mm	AA6082-T6	6.3mm	Butt Welding	1550 - 464 Rpm	190.5 - 15.9 mm/min
Concave with Threaded Probe	19mm	AA6082-T6	4.6mm	Butt Welding	1550 - 464 Rpm	190.5 - 15.9 mm/min
Concave001	16mm	AA5083-H19	1.6mm	Butt Welding	1550 - 250 Rpm	190.5 mm/min
Concave002	16mm	AA5083-H19	1.6mm	Butt Welding	1550 - 250 Rpm	190.5 mm/min
Concave003	16mm	AA5083-H19	1.6mm	Butt Welding	1550 - 250 Rpm	190.5 mm/min
Concave001	16mm	AA2004-F	1.6mm	Butt Welding	372 Rpm, 250 Rpm	190.5 mm/min
Concave002	16mm	AA2004-F	1.6mm	Butt Welding	620 Rpm, 464 Rpm	190.5 mm/min
Concave003	16mm	AA2004-F	1.6mm	Butt Welding	620 Rpm, 464 Rpm	190.5 mm/min

Table 6.1, Welding Trials Carried Out on the Parkson Milling Machine.

Tool Name	Tool Shoulder Diameter	Weld Material	Material Thickness	BOP/Butt Welding	Spindle Speed	Feed Speed
Concave004	16mm	AA5083-H19 AA2004-F	1.6mm	Bead-On-Plate	700 Rpm, 500 Rpm	175 - 746 mm/min
Concave005	16mm	AA5083-H19 AA2004-F	1.6mm	Bead-On-Plate	700 Rpm, 500 Rpm	175 - 746 mm/min
Concave006	16mm	AA5083-H19 AA2004-F	1.6mm	Bead-On-Plate	700 Rpm, 500 Rpm	175 - 746 mm/min
TriFlute001	16mm	AA5083-H19 AA2004-F	1.6mm	Bead-On-Plate	700 Rpm, 500 Rpm	175 - 746 mm/min
TriFlute002	16mm	AA5083-H19 AA2004-F	1.6mm	Bead-On-Plate	700 Rpm, 500 Rpm	175 - 746 mm/min
TriFlute003	16mm	AA5083-H19 AA2004-F	1.6mm	Bead-On-Plate	700 Rpm, 500 Rpm	175 - 746 mm/min
TriFlat001	16mm	AA5083-H19 AA2004-F	1.6mm	Bead-On-Plate	700 Rpm, 500 Rpm	175 - 746 mm/min
TriFlat002	16mm	AA5083-H19 AA2004-F	1.6mm	Bead-On-Plate	700 Rpm, 500 Rpm	175 - 746 mm/min
TriFlat003	16mm	AA5083-H19 AA2004-F	1.6mm	Bead-On-Plate	700 Rpm, 500 Rpm	175 - 746 mm/min
GSP5651 [Flutes]	7.5mm	AA5083-H19	1.6mm	Bead-On-Plate	700 Rpm, 500 Rpm	175 - 746 mm/min
GSP5651 [Flats]	7.5mm	AA5083-H19 AA2004-F	1.6mm	Bead-On-Plate	700 Rpm, 500 Rpm	175 - 746 mm/min
Large Shoulder	19mm	AA5083-H19 AA2004-F	1.6mm	Bead-On-Plate	700 Rpm, 500 Rpm	175 - 746 mm/min
GSP5651 [Flats]	7.5mm	AA5083-H19 AA2004-F	1.6mm	Single Pass Butt Weld	500 Rpm	746 mm/min
GSP5651 [Flats]	7.5mm	AA5083-H19 AA2004-F	1.6mm	Double Pass Butt Weld	500 Rpm	746 mm/min
Concave005	16mm	AA5083-H19 AA2004-F	1.6mm	Single Pass Butt Weld	500 Rpm	746 mm/min
Concave005	16mm	AA5083-H19 AA2004-F	1.6mm	Double Pass Butt Weld	500 Rpm	746 mm/min
Large Shoulder	19mm	AA5083-H19 AA2004-F	1.6mm	Single Pass Butt Weld	500 Rpm	746 mm/min
Large Shoulder	19mm	AA5083-H19 AA2004-F	1.6mm	Double Pass Butt Weld	500 Rpm	746 mm/min

Table 6.2, Welding Trials Carried Out on the FW22 Machine.

Tool Name	Tool Shoulder Diameter	Weld Material	Material Thickness	BOP/Butt Welding	Spindle Speed	Feed Speed
Concave005	16mm	AA5083-H19	1.6mm	Single Pass Butt Weld	750 Rpm	750 mm/min
Concave005	16mm	AA5083-H19	1.6mm	Single Pass Butt Weld	750 Rpm	750 mm/min
Concave005	16mm	AA5083-H19	1.6mm	Single Pass Butt Weld	750 Rpm	750 mm/min
MXTriflute	15mm	AA5083-H19	1.6mm	Single Pass Butt Weld	750 Rpm	750 mm/min
MXTriflute	15mm	AA5083-H19	1.6mm	Single Pass Butt Weld	1250 Rpm	1250 mm/min
MXTriflute	15mm	AA5083-H19	1.6mm	Single Pass Butt Weld	1250 Rpm	1000 mm/min
MXTriflute	15mm	AA5083-H19	1.6mm	Single Pass Butt Weld	1250 Rpm	750 mm/min
MXTriflute	15mm	AA5083-H19	1.6mm	Triple Pass Butt Weld	750 Rpm	750 mm/min
MXTriflute	15mm	AA2004-F	1.6mm	Single Pass Butt Weld	750 Rpm	750 mm/min
MXTriflute	15mm	AA2004-F	1.6mm	Single Pass Butt Weld	1250 Rpm	1250 mm/min
MXTriflute	15mm	AA2004-F	1.6mm	Single Pass Butt Weld	1250 Rpm	1000 mm/min
MXTriflute	15mm	AA2004-F	1.6mm	Single Pass Butt Weld	1250 Rpm	750 mm/min
MXTriflute	15mm	AA2004-F	1.6mm	Triple Pass Butt Weld	750 Rpm	750 mm/min
MXTriflute	15mm	AA2004-F	1.2mm	Single Pass Bead-On-Plate	1250 Rpm	1000 mm/min
MXTriflute	15mm	AA2004-F	1.2mm	Triple Pass Bead-On-Plate	1250 Rpm	1000 mm/min

Table 6.3, Welding Trials Carried Out on the ESAB SuperStir Machine

6.3.1 Parkson Milling Machine

The first machine used to perform FSW at Brunel University was a Parkson vertical milling machine c1950 [38]. As shown in Figure 6.1. The tools were designed to fit into a Clarkson chuck for a secure fixing and a safety screen erected for added operator protection. The weld material and backing plate were bolted directly to the feed table. The material feed speed range is from 6-190mm/minute, it should be noted that the feed speed is converted from imperial measurements, the spindle speed ranges from 23-1550rpm. The plunge depth is completely manual; the operator winds the feed table up to engage the tool.

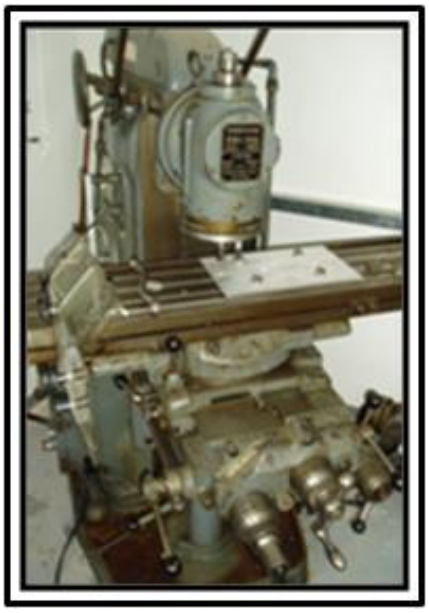

Figure 6.1, Parkson Milling Machine used for FSW.

6.3.1.1 Feasibility Studies

A short study had been previously completed as part of an undergraduate dissertation project in order to establish the suitability of the machine for carrying out FSW experiments. This study successfully created a small number of 100mm long butt welds in 6.3mm thick AA6082. Having proved that the Parkson milling machine is capable of FSW; it was not known whether the machine was capable of carrying out a large volume of welds or the full extent of the machine's operating window.

A feasibility study was carried out during the initial planning stages of the doctoral research experimental work and completed as part of this thesis [38]. This study primarily established the operating process window for the Parkson milling machine and secondly established the machine's capability of creating a larger number of welds for a more comprehensive trial schedule using superplastic materials.

6.3.1.1.1 AA6082-T6

The first experiments were carried out on 6.3 and 4.6mm thick aluminium alloy 6082. This is a relatively easy alloy to friction stir weld as it falls into a category of extrusion alloys. As the FSW process is likened to an extrusion process this alloy copes well with the heat and deformation applied by FSW. The tool used in this study is shown in Figure 2.7. The machine was shown to be capable of joining the

materials at a variety of spindle speeds, between 620 and 1550rpm, and material feed speeds of 15 to 190mm.min [38].

6.3.1.1.2 AA5083

Thicker weld material increases the force required to join the material. In this respect the machine is easily capable of joining 1.6mm thick aluminium. It is however the tolerances for plunge depth and weld interface gaps which cause the larger problems for this machine when welding thinner sheets. As was mentioned earlier a gap of around 10% is tolerated [14], this tolerance is small when the total thickness of the material to be joined is only 1.6mm. The manual plunge depth is difficult as the tool must be plunged extremely close to the backing plate. A number of welds were produced using basic tools, Concave001 – 003, which can be easily manufactured using standard university workshop equipment. The material feed speed remained constant at 190mm/min, the fastest available speed but still considered slow, and the spindle speed was reduced from 1550 rpm to 250 rpm using the machine's different spindle gears. Table 6.4 shows the process variables used in this investigation and the successful process window for this machine. At spindle speeds of over 620rpm the welds exhibited large surface cracks due to the build up of stresses within the materials. The material was bolted directly to the backing plate and not allowed to relax. During welding the excessive heat caused overheating of the top surface and the residual stresses caused this weakened material to crack. Some of the macrographs of the welds produced in this experiment are compared to later welds to show the improvements in weld quality from basic milling machine and tools to state-of-the-art machinery and tooling.

Spindle speed (Rpm)	Feed speed (mm/min)	Weld pitch (mm/rev)
250	190.5	0.762
372	190.5	0.512
464	190.5	0.411
620	190.5	0.307
920	190.5	0.207
1164	190.5	0.164
1550	190.5	0.123

Table 6.4, Process variables used for trials on the Parkson milling machine.

6.3.1.2 Tooling Design

Many of the tools used to carry out this investigation were designed to fit the Parkson milling machine. This involved cutting a thread into the tool shaft which would engage in a Clarkson chuck. This chuck allows lateral force to be applied to the tool without the tool becoming loose as it spins. The tools are divided into 5 groups: Concave (x6), Triflute (x3), Triflat (x3), large shoulder (x1) and GSP5651 (x3). The dimensions and specifications of the tooling can be found in Appendix B. The friction stir welding tools used for this investigation are larger diameters than usually considered for the material thickness in order to produce wider weld regions. These are compared to the TWI designed GSP 5651 tool which is considerably smaller. The tool probes include smooth conical, threaded cylinder and threaded Triflute and Triflat designs. The final welds created on the ESAB SuperStir machine were created using an MX Triflute^{TM} tool supplied and modified by TWI.

6.3.1.3 Limitations

The Parkson milling machine is a robust machine capable of performing the FSW process. It is however the controlling of the process which lets it down. The spindle and feed speed settings are predetermined sets of values and so the ideal values may never be achievable. The maximum feed speed of 190mm/min is slow in comparison to most FSW machinery. A low value for this setting severely reduces the available range of spindle speeds which can be used.

The plunge depth can be set quite accurately by winding the feed table up towards the tooling, however there is no way of knowing whether the large forces required to maintain constant contact are overcome and some vertical movement from the tool

has been permitted during the process. This completely manual control hampers the repeatability of the process. It was recognised that this machine was not suitable for a full scale FSW trial and alternative arrangements were made.

6.3.2 FW22

This was possibly the first customised machine used to carry out FSW experiments and is shown in Figure 6.2. It is a screw-driven, gantry mounted spindle with a heavy duty machine table bolted directly to the workshop floor. The spindle and feed speeds can be set to the nearest 1rpm and 1mm/min; allowing for finer adjustments of the process parameters. The material was held to the machine table using finger clamps with the option to use a vacuum table if necessary. This machine was used to carry out the vast proportion of the welds used in this investigation. The tooling was originally designed to fit the Parkson milling machine so they were fitted with an adapter so as to fit FW22's tool holder and the LoStir device.

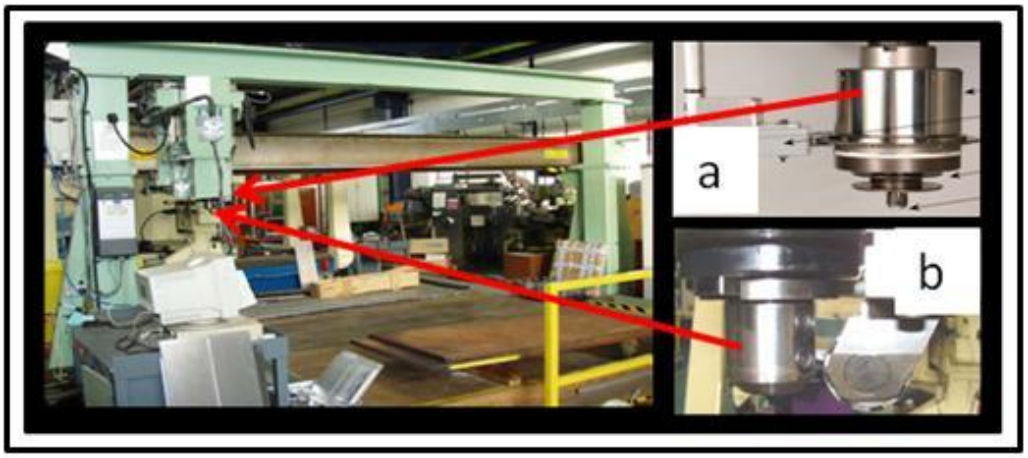

Figure 6.2, FW22 FSW Machine Inset: a) LoStir Force Monitoring System, b) Conventional Tool Holder and Tool Heel Roller.

6.3.2.1 Improvements on the Parkson Milling Machine

FW22 has the ability to join the material with greater control over the process variables. Although it is more difficult to set the plunge depth there is more certainty over the machine being able to maintain constant tool/material contact and plunge depth, in order to weld to the very bottom of the material. The machine also has a much larger process window than the Parkson mill. The feed speed and spindle speed can be varied from 0 - 750mm/min and 0 - 2000rpm respectively.

6.3.2.2 Weld Force Monitoring

The machine came fitted with a force monitoring system. This took measurements for weld force, down force and spindle torque at regular time intervals. However at the time of the trial TWI were testing a low cost FSW monitoring tool named the LoStir device [32]. This tool takes measurements for weld force, down force and spindle torque, as well as having the ability to measure the tool temperature. This system was deemed to be more reliable than the dated system installed on the machine and so was used in preference.

6.3.2.3 FW-22 Bead on Plate Trials

Initial trials were carried out using a bead on plate technique. This essentially removes any set up related flaws whilst still maintaining the ability to study the microstructure and properties of the welds produced, in effect an FSP action was carried out in order to produce different FSW microstructures. Each of the 13 tools was used in 5 welds for each of the alloys investigated. Taking the Spindle speed first, a value of 500 Rpm was set, this is based on the welds produced on the Parkson milling machine. Next feed speed values were set and the weld pitch calculated. For the feed speed a range of 175 – 746 mm/min, was set out which encompasses the maximum feed speed and at the lower end a value which falls into the process window from the Parkson milling machine. The process parameters used for each of the trials is displayed in Table 6.5.

Spindle speed (Rpm)	Feed speed (mm/min)	Weld pitch (mm/rev)
500	746	1.49
500	500	1
500	375	0.75
500	250	0.5
700	175	0.25

Table 6.5, Process Variables used for Bead on Plate Welding Trials on FW22.

The material was supplied by Superform Aluminium UK [84] in the form of 1.6mm thick, 100mm wide 1m long sheets. These were then cut into ~330mm lengths and clamped to the anvil using just finger clamps. The tool was selected and installed.

After the plunge sequence but before the traverse was initiated a short 15 second dwell time was introduced to minimise the chance of tool failure. The first and last 50mm of weld was trimmed from the plate and discarded. The remaining weld was then ready for property and formability testing. The first test carried out was a quality test to ensure the FSP region extends to the bottom of the material. A small 10mm wide transverse strip of weld was removed and subjected to a 180° bend test with the root in tension. This test is usually used for butt welds to test the joint interface, however the bead on plate samples have no interface. In this case the test still has its uses in order to assess the plunge depth of the FSP region and make sure there are no apparent root flaws due to inclusions from the backing plate. It should be noted that all the welds passed this test due to there not being an interface between two plates. A complete overview of all the welds produced can be found in the data overview tables in Chapter 7 - Results and Analysis.

6.3.2.4 FW-22 Butt Weld Trials

On completion of the bead-on-plate welding trials the data collected from the material property and microstructural analysis was used to assess the best candidates in terms of the tools and process variables; these were then used for subsequent butt welding trials. The bead-on-plate trials carried out on the FW22 machine indicated that a high welding pitch (low heat input) yielded superior mechanical properties and a fine equiaxed structure within the weld region. The most successful tools were the tools which included re-entrant features such as threads, flutes and flats. Butt welding experiments were conducted using the selected tooling and process variable, as shown in Table 6.6; creating butt welded specimens of sufficient size to fit within the cone testing equipment. As the there is extra difficulty in setting up the machine and the weld material prior to welding the 180° bend test was again applied with the root in tension to assess the weld's ability to withstand weld root separation.

Tooling	Alloy	Spindle speed (Rpm)	Feed speed (mm/min)	Weld pitch (mm/rev)
GSP5651	AA5083-H19 AA2004-F	500	746	1.49
Concave005	AA5083-H19 AA2004-F	500	746	1.49
Large Shoulder	AA5083-H19 AA2004-F	500	746	1.49

Table 6.6, Tooling and Process Variables used for Butt Welding Trials on FW22.

When considering a butt weld, compared to bead on plate, there are many more problems in setting the machine up. The first and most significant set up is making sure the joint interface is correctly aligned with the tool's centre. Once this has been achieved steps must be made to prevent plate separation. Steel blocks were secured to the anvil and adjusted with screws to engage the weld material and ensure the material sheets remain in contact at the joint interface. When the tool first engages the material the two sheets will have a tendency to move with the rotation of the tool, that is to say that the advancing side sheet moves in the weld direction and retreating side sheet moves in the opposite direction. This movement was also restricted by steel blocks mounted to the anvil.

Even a very small lack of penetration gives rise to a failure in the root of the weld when the root is in tension. Many of the single pass welds created continuously failed the bend test and were subsequently discarded. Only welds which passed the 180° bend tests were selected for cone testing; this meant that there were a limited number of single-pass welds which passed the test and could be subsequently used in the cone testing experiments.

Time on the cone testing apparatus was limited so to ensure that welds were produced ,which could be subjected to a cone test without a root flaw failure, an additional set of friction stir welds were produced using a multiple-pass welding operation (as explained in Chapter 3). The welds were made using two consecutive FSW passes. The process variables and tooling used to create the double pass welds are the same as those used to create the single pass butt welds as shown in Table 6.6. The material sheets were welded from one side, flipped over and welded again from

the other side. This ensures a total penetration weld with no plunge depth related defects in the weld root.

6.3.2.5 Limitations

Once again the critical part of the set up involves the plunge depth. This machine uses position control, but once again there is a manual setting. The spindle is lowered using hydraulics onto adjustable steel blocks mounted to the machine's frame. These blocks determine the maximum extension permitted by the spindle hydraulics. The plunge depth has to be checked prior to welding as it is possible that the blocks may move during process due to the very high downward forces acting through the spindle and vibration from the process. For this reason many welds failed the bend test due to lack of penetration, essentially an inherent flaw runs the entire length of the welds due to poor bonding in the weld root.

6.3.3 ESAB SuperStir

The ESAB SuperStir machine used for the last set of welding trials is located at TWI's Cambridge facility along with FW22. This machine represents the state-of-the-art in terms of FSW equipment and is shown in Figure 6.3.

Figure 6.3, ESAB SuperStir Machine.

6.3.3.1 Improvements on FW22

The ESAB machine is a fully programmable 5 axis machine. This means that once a program for the weld has been written it can be easily reproduced. The machine can use both position and force control. In this case it was used in the position control mode. A number of welds were created using concave tool BRUTJMCON005, it was noted that although the plunge depth related problem were completely eradicated this tool did not create satisfactory welds. Welding was poor due to the tool geometry. A lack of features on the probe leads to poor joint interface break up towards the weld root and an inherently flawed weld. This tool was swapped for an MXTriflute^{TM} tool. This tool, as described in Chapter 3, exhibits re-entrant features on the probe and so allows for superior weld closure. Enhanced mixing of the material towards the weld root allows for excellent interface break up and so superior bonding of the extremities of the weld root. The welds created using this tool passed the subsequent bend tests, showing that the MXTriflute^{TM} is a superior tool. The clamping method for this machine involves both mechanical fasteners, i.e. finger clamps and blocks mounted to the anvil, and also a vacuum table. It also makes use of a roller mounted in front of the tool to prevent deflection of the material.

The ESAB machine also makes use of real time force monitoring equipment. The same values as the LoStir device are obtainable with the addition of measurements for the y-Force.

6.3.3.2 ESAB SuperStir Bead on Plate Trials

The bead on plate trials carried out on this machine used 1.2mm thick AA2004. In August 2007 aluminium supplier, Dolgarrog Aluminium Limited, went into administration and so were unable to supply additional AA2004 material. To enable the continuation of welding trials in AA2004 a substitution had to be made for any available stock from Superform Aluminium UK. Additional 1.6mm thick material was unavailable; spare material was found but was a reduced sheet thickness of 1.2mm. Each plate was ~200mm wide and 500mm long. Each plate was welded straight down the middle to create 2 cone test samples each ~200mm^2. The process parameters used for welds created on the ESAB machine are given in Table 6.7.

Tooling	Alloy	Spindle speed (Rpm)	Feed speed (mm/min)	Weld pitch (mm/rev)
MXTriflute	AA2004-F	1250	1000	0.8
MXTriflute	AA2004-F	1250	1000	0.8

Table 6.7, Process Parameters used for the Bead-On-Plate Welding trials on the ESAB SuperStir Machine.

6.3.3.3 ESAB SuperStir Butt Weld Trials

Butt welds were also carried out using the ESAB SuperStir machine; using the parameters and tooling; as listed in Table 6.8. Welds were created in both AA5083 and AA2004 using the MXTriflute™ tool supplied by TWI. This machine uses CNC to control the tool plunge and so the lack of penetration root flaws associated with the welds created on FW22 are reduced. Using the MXTriflute™ tool also removes the root defect from single pass welds as the influence of the tool in terms of deformation and heat extends downwards past the very bottom of the tool. These two factors meant that quality single pass welds were created which passed the 180° bend tests. Multiple pass welds carried out on this machine were carried out in order to assess the ability of friction stir processed regions to withstand the subsequent superplastic forming operations.

Tooling	Alloy	Spindle speed [Rpm]	Feed Speed [mm/minute]	Weld Pitch [mm/rev]
Concave005	AA5083-H19	750	750	1
MXTriflute	AA5083-H19 AA2004-F	750	750	1
MXTriflute	AA5083-H19 AA2004-F	1250	750	0.6
MXTriflute	AA5083-H19 AA2004-F	1250	1000	0.8
MXTriflute	AA5083-H19 AA2004-F	1250	1250	1

Table 6.8, Tooling and Process Variables used for Butt Welding Trials on the EASB SuperStir Machine.

6.3.4 Weld Quality Testing

The first examination of the weld is purely instinctive. All the welds produced on the three different machines were vetted for weld quality as soon as the process finished. The weld is visually examined to make sure there are no obvious flaws on top and bottom surfaces. Large flaws such as excessive flash generation can be easily identified in this way so as to prevent analysis of fatally flawed welds.

To further test the validity of the join every single weld and bead on plate specimen was subjected to a 180° bend test. The material is clamped into a customized jig and bent with the root in tension.

6.4 Weld Mechanical Property Analysis

The welds were tested for room temperature properties first. This involved removing tensile and hardness specimens from the completed welds. The analysis was carried out on the transverse direction of the FSWs as this has the most variation of properties associated with the different weld regions. The tensile test will show to some extent the amount of recrystallization and softening within the weld nugget. The microhardness plots will also highlight the differing weld regions and the effect of the tool on the HAZ regions.

6.4.1 Tensile Testing

Four tensile testing specimens were blanked out of the welds using a punch and die mounted to a ball-screw press. Care was taken during this stage to align the centre of the weld with the centre of the tensile specimen. Tensile testing was carried out on an Instron 8501 machine fitted with an extensometer for accurate readings for the displacement.

6.4.2 Microhardness

Hardness measurements were carried out on polished transverse sections using a Future Tech Vickers microhardness tester FM – 1E with a 1Kg load and a standard ‘B’ grade Vickers hardness indenter with an angle of 136° between opposite faces. The test produced indents with mean averaged diagonals measuring ~120-140μm for AA5083 and ~130-150μm for AA2004. A maximum of 33 measurements were taken

on each sample spaced every 1mm in the weld region and every 5mm outside of the tools footprint.

6.5 Formability

The key tests for the friction stir welds completed for this thesis involve biaxial strain. The critical part of the weld is the interface between the sheets. During the forming process if there is a flaw along this interface or if the properties of the parent sheet differ greatly from the weld region then the sheet will not form homogeneously and will fail in the weld region.

6.5.1 Dome Testing

A small number of the welds were initially tested at room temperature using an Erichsen dome testing machine. This was used to test the weld's ability to strain in both the longitudinal and transverse directions, and also to test the quality of the joint interface. This test was discontinued as the room temperature formability of the aluminium is low. Superplastic deformation requires elevated temperature test which are not possible with this particular machine.

6.5.2 Cone Tests

The formability of the welds produced is measured by the cone test. The cone test is a simple simulation of the complex superplastic forming process. The specimen is heated to ~450°C and clamped in place. Gas pressure is used to force the heated sheet into a cone shaped female die at a low strain rate. The final thickness of the material at the pole of the cone is used to measure the biaxial strain and thus determine whether the material has been deformed under a superplastic regime.

6.6 Microstructural Stability at High Temperatures

A number of annealing experiments were carried out on the welds produced and the parent material sheets in order to establish the effect of significant heat increases on the material. At elevated temperature the driving force for structural change is increased and allows the cycle of recovery, recrystallization and grain growth to occur. The material must be stable, allowing no significant grain growth in order to withstand the SPF process. The matrix material is pinned by a fine distribution of second phase; this zenner-pinning limits the growth of grains at high temperatures.

Weld and parent samples were taken and subjected to annealing at 350°C in an air furnace for ~25 minutes. These annealed samples were then tested for tensile strength variation.

6.7 Accuracy

The utmost care has been taken to ensure the accuracy of the measurements taken during testing of the friction stir welded specimens. All machinery used for property testing has a current and valid calibration certificate. All in-process measurements such as spindle speed and weld speed have been assessed using the friction stir welding equipment's built-in systems and verified using independent equipment.

6.7.2 Process variables

The spindle speed and welding speed are set using the control system for the FSW machine. These variables can be selected to the nearest 1 Rpm and 5 mm/min. After selecting the ranges of values to be used each variable was verified using independent equipment. Spindle speeds have been checked using a hand held tachometer, feed speed has been checked by measuring the spindle travel time over a known distance.

6.7.2 Weld forces

The welding forces are measured using built-in systems, the forces measured using FW22 are also measured using an additional force measuring system developed by TWI [32]. The measurements are taken at intervals of 1ms and are compiled to produce force/torque versus time charts. Friction stir welding settles into a steady state regime where the weld force, down force and spindle torque remains relatively constant until the weld is complete. The steady state average of the forces/torque is then used to describe the relationships between the tooling and the process variables along with the calculated FSW heat input.

6.7.2 Tensile testing

Tensile testing has been carried out on a calibrated Instron 8501 tensile testing machine with an additional extensometer for additional accuracy when dealing with small strains. After removing and discarding the beginning and end sections of the weld, tensile specimens have been taken from each end of the steady state region and averaged to produce the figures used in the tensile strength versus heat input charts.

Error bars have been excluded from these charts to ensure that the charts are clear and easy to read.

6.7.3 Cone test pole thickness

To evaluate the equivalent superplastic strain of the formed FSWs the pole thickness has been measured using a dial gage which is accurate to ± 0.1 mm. These measurements have been re-evaluated using the onscreen measurement functions on the SEM which is accurate to ~ ± 1µm using a magnification of 20x to ensure the thickness of the material fills the entire SEM view screen.

6.7.4 Grain size measurements

All grain size measurements are taken using the linear intercept method from a minimum of three different images taken from the particular region of the weld which is under investigation.

7 Material property and weld force analysis

7.1 Introduction

The post weld material properties are strictly linked to the process variables used during the FSW operation. The amount of heat and deformation experienced by the weld material can be evaluated by looking at the welding forces and torque produced throughout the weld. The analysis of the force/torque measurements can then be used as a quality measure to further optimise the process variables in order to produce the best weld possible for the desired application. To some extent the welding force/torque analysis can be used as a loose precursor to material properties of the weld. For example welds created using hot weld parameters are expected to yield lower weld forces and generally lower strength and hardness values. This is linked to the amount of energy for microstructural change within the weld material. A fully recrystallized material can be weaker and softer than the pre-welded material. This is the case for the AA5083 and AA2004 used here due to strain and precipitation strengthening mechanism. However, if the material if fully annealed prior to welding the FSW will make the weld nugget stronger than the parent material [12, 43, 44]. It should be made clear at this point that the room temperature properties usually have little bearing on how well the weld will perform in a high temperature regime. This is down to microstructural stability throughout the entire structure. The heterogeneous nature of the FSW process makes it difficult to obtain a homogeneous structure; there will be differing levels of recrystallization, recovery, grain growth and precipitation coarsening throughout the weld region. Essentially the FSW tooling creates a certain amount of disruption to the original microstructure, for example a cold weld will exhibit more of the original material properties and less softening effects due to less heat, deformation and relaxation of stored energy.

7.2 Data Overviews

The data overviews are a series of tables which contain all the results from the welding trials and the testing carried out post welding. Table 7.1 shows the welding trials carried out on the Parkson milling machine. Table 7.2.a) and b shows the results from welding trials carried out on FW22. The last overview table 7.3.a) and b) contains the trials performed on the ESAB SuperStir machine, this is by far the

largest of the overview tables as it contains the results from the entire bead on plate trial.

Tool ID	Concave003	Concave003	Concave002	Concave002	Concave001	Concave001
Tool Diameter [mm]	16	16	16	16	16	16
Weld Id	P1	P2	P3	P4	P5	P6
Spindle Speed [Rpm]	464	620	464	620	250	372
Feed Speed [mm/min]	190.5	190.5	190.5	190.5	190.5	190.5
Weld Pitch [mm/rev]	0.41	0.31	0.4	0.3	0.76	0.5
AA5083						
Displacerment at max load [mm]	0.34	0.14	0.1	0.05	0.13	1.25
Max load [KN]	2.44	2.06	2.01	1.36	2.27	2.95
Stress at max load [Mpa]	234.7	198.1	192.8	131.1	218	283.8
Strain at max load	0.014	0.006	0.004	0.002	0.005	0.05
Young's Modulus	69950	71250	75190	71520	80310	71590
Drawing force [T]	1	0.9	0.7	0.4	0.7	1.05
Measured Erichsen value [mm]	9.4	7.1	6.5	5	6.15	9.4
AA2004						
Displacerment at max load [mm]	0.05	0.005	0.08	0.08	0.22	0.04
Max load [KN]	1.35	1.07	1.83	1.77	1.89	1.01
Stress at max load [Mpa]	129.5	103.2	175.9	170.3	181.3	97.3
Strain at max load	0.002	0.002	0.003	0.003	0.009	0.002
Young's Modulus	68990	69030	73090	70560	71310	66830
Drawing force [T]	0.2	0.15	0.35	0.15	0.9	0.2
Measured Erichsen value [mm]	4.5	4	5.5	3.8	6.9	4

	Weld Id
	Weld variables
	Process parameters
	As-welded tensile data
	Erichsen dome test data

Table 7.1, Data Overview Table: Friction Stir Welds Created using the Parkson Milling Machine.

Weld ID #	Tool	Spindle Speed Vs [Rpm]	Feed Speed Vf [mm/min]	Weld Pitch Vf/Vs [mm/rev]	AVG Weld Force [KN]	AVG Down Force [KN]	AVG Spindle Torque [Nm]	Heat Input [KJ/mm]	Displacement at Max Load [mm]	Load at Max Load [KN]	Stress at Max Load [Mpa]	Strain at Max Load	Young's Modulus	Fracture Location	Displacement at Max Load [mm]	Load at Max Load [KN]	Stress at Max Load [Mpa]	Strain at Max Load	Young's Modulus	Fracture Location
F78	BRUTJMCR003	700	175	0.25	0.63	17.20	26.35	0.56	1.92	3.04	292.4	0.08	69630	N	2.35	2.65	255.2	0.09	53970	N
F77		500	250	0.50	1.04	14.35	34.42	0.37	1.84	3.16	303.9	0.07	70440	N	5.12	3.15	303	0.20	85320	N
F79		500	376	0.75	1.02	17.08	40.39	0.29	1.75	3.20	307.6	0.07	103400	N	4.37	3.10	298.4	0.17	69130	N
F76		500	500	1.00	1.63	10.84	35.52	0.19	1.72	3.29	316.5	0.07	81910	N	5.63	3.22	309.4	0.23	81220	P//H [A]
F80		500	746	1.49	1.65	14.22	45.77	0.16	1.60	3.27	314.7	0.06	71540	N	4.92	3.14	302.2	0.20	81170	N
F3	Concave004	700	175	0.25	0.58	14.48	23.35	0.50	1.80	3.21	308.2	0.07	75810	T [R]	5.48	3.26	313.6	0.22	82130	T [R]
F2		500	250	0.50	0.83	14.96	30.06	0.32	1.56	3.23	310.4	0.06	74600	N	4.52	3.17	304.5	0.18	81350	N F
F4		500	376	0.75	0.84	14.77	32.85	0.23	1.38	3.21	308.1	0.06	69630	N	5.40	3.24	311.2	0.22	76240	T [R]
F1		500	500	1.00	1.01	13.77	33.99	0.18	1.48	3.34	320.8	0.06	65730	N	4.47	3.13	300.9	0.18	74570	N F
F5		500	746	1.49	1.11	12.69	36.62	0.13	1.33	3.25	312.9	0.05	73910	N	5.95	3.25	312.1	0.24	81440	N
F18	Concave005	700	175	0.25	0.62	11.05	21.54	0.46	1.60	3.14	302.1	0.06	69160	N	4.44	3.11	298.8	0.18	75410	T [R]
F17		500	250	0.50	0.86	9.78	26.17	0.28	1.36	3.36	323.5	0.05	82310	N	5.45	3.25	312.4	0.22	80000	P
F19		500	376	0.75	0.96	11.24	29.34	0.21	1.60	3.37	323.9	0.06	73030	N	5.71	3.27	314	0.23	76360	P//H [R]
F16		500	500	1.00	0.98	8.17	27.33	0.15	1.41	3.38	324.8	0.06	73920	T [R]	6.11	3.24	311.2	0.24	76880	P//H [R]
F20		500	746	1.49	0.97	9.42	29.76	0.11	0.82	3.24	311.7	0.03	91230	N	5.45	3.23	310.6	0.22	79170	T [R]
F33	Concave006	700	175	0.25	0.49	13.56	24.28	0.52	1.67	3.14	302.3	0.07	74020	N	4.33	3.09	296.7	0.17	72730	N
F32		500	250	0.50	0.47	20.57	37.32	0.40	1.54	3.06	294.3	0.06	62860	N	4.08	3.05	292.8	0.16	64070	N
F34		500	376	0.75	0.76	14.20	34.42	0.24	1.43	3.23	310.2	0.06	72870	T [R]	5.08	3.19	306.6	0.20	72600	P//H [R]
F31		500	500	1.00	0.49	20.73	41.76	0.22	1.43	3.21	308.4	0.06	77330	N	5.55	3.19	306.6	0.22	77210	P//H [R]
F35		500	746	1.49	0.69	14.79	39.18	0.14	1.41	3.23	311	0.06	66750	N	5.12	3.12	300.4	0.21	72910	T [R]
F138	TriFlat001	700	175	0.25	0.34	13.84	22.19	0.47	1.63	3.01	289.6	0.07	84350	N	3.92	2.97	285.3	0.16	66940	N
F137		500	250	0.50	0.28	13.73	32.76	0.35	1.91	3.18	305.4	0.08	92650	N	4.42	3.13	301.4	0.18	70230	N
F139		500	376	0.75	0.30	13.56	34.86	0.25	1.49	3.20	307.3	0.06	74830	N	5.13	3.17	304.3	0.21	76850	N
F136		500	500	1.00	0.18	15.39	41.45	0.22	1.52	3.13	301.2	0.06	75200	N	4.63	3.15	302.8	0.19	71530	N
F140		500	746	1.49	0.66	12.74	38.03	0.14	1.55	3.33	319.9	0.06	71930	N	5.20	3.21	308.6	0.21	73910	P//H [A]
F153	TriFlat002	700	175	0.25	0.44	9.33	19.63	0.42	1.63	3.10	297.6	0.07	67960	T [R]	4.34	3.12	300	0.17	68640	T [R]
F152		500	250	0.50	0.72	8.53	25.25	0.27	1.66	3.30	317.2	0.07	72380	N	5.27	3.21	309	0.21	71080	H [A]
F154		500	376	0.75	0.70	8.66	27.82	0.20	1.38	3.26	313.7	0.06	76790	N	5.83	3.25	312.8	0.23	72940	P//H [A]
F151		500	500	1.00	1.01	10.82	29.24	0.16	1.35	3.41	328.2	0.05	75170	N	5.97	3.24	311.7	0.24	77310	P//H [A]
F155		500	746	1.49	1.11	7.75	31.26	0.11	0.61	2.97	285.8	0.02	71570	N	5.89	3.24	311.1	0.24	69260	T [R]
F168	TriFlat003	700	175	0.25	0.50	10.37	21.42	0.46	1.70	3.13	300.8	0.07	68480	N	4.61	3.13	301	0.18	74790	N
F167		500	250	0.50	0.85	9.72	30.73	0.33	1.70	3.25	312.3	0.07	78460	N	5.51	3.24	311.3	0.22	68310	P//H [R]
F169		500	376	0.75	0.81	9.35	27.43	0.19	1.54	3.28	315.7	0.06	80950	N	5.55	3.23	310.1	0.22	79610	P//H [R]
F166		500	500	1.00	1.21	7.72	29.85	0.16	1.54	3.31	318.3	0.06	78120	N	5.22	3.20	307.9	0.21	83780	P//H [A]
F170		500	746	1.49	1.46	7.39	31.07	0.11	1.45	3.40	326.5	0.06	71390	N	4.75	3.16	303.4	0.19	76950	T [R]
F93	TriFlute001	700	175	0.25	0.43	10.71	20.51	0.44	1.40	3.11	299.1	0.06	77140	N	4.74	3.13	301.1	0.19	70580	N
F93		500	250	0.50	0.83	10.02	26.09	0.28	1.44	3.28	315.4	0.06	73820	N	5.92	3.24	311.5	0.24	80140	P
F94		500	376	0.75	0.94	10.85	28.67	0.20	1.40	3.39	326.1	0.06	79220	N	5.01	3.20	307.4	0.20	74610	T//H [R]
F91		500	500	1.00	1.16	9.49	29.24	0.16	1.39	3.41	328	0.06	76660	N	5.48	3.18	305.7	0.22	76310	P//H [R]
F95		500	746	1.49	1.34	9.24	30.90	0.11	1.30	3.41	327.4	0.05	77650	N	5.64	3.20	307.8	0.23	80620	P
F108	TriFlute002	700	175	0.25	0.42	11.91	22.23	0.47	1.76	3.15	302.8	0.07	66110	N	4.47	3.10	297.6	0.18	74420	N
F107		500	250	0.50	0.70	11.71	29.10	0.31	1.53	3.29	316.3	0.06	76520	N	5.51	3.22	310	0.22	72560	P//H [R]
F109		500	376	0.75	0.59	12.26	32.25	0.23	1.42	3.28	315.5	0.06	77390	N	5.53	3.21	308.2	0.22	68610	P//H [R]
F106		500	500	1.00	1.09	9.00	30.38	0.16	1.32	3.40	326.8	0.05	70430	N	5.33	3.22	309.7	0.21	74860	P//H [A]
F110		500	746	1.49	1.25	10.17	33.34	0.12	1.32	3.38	324.8	0.05	78920	N	5.46	3.23	310.8	0.22	82150	P//H [A]
F123	TriFlute003	700	175	0.25	0.38	15.64	23.24	0.50	1.61	2.90	278.6	0.06	47350	N	3.72	2.87	276.3	0.15	69540	N
F122		500	250	0.50	0.63	16.34	31.74	0.34	1.65	3.16	303.9	0.07	82080	N	4.81	3.09	297.5	0.19	73410	N
F124		500	376	0.75	0.31	16.05	36.68	0.26	1.61	3.22	309.1	0.06	77980	N	5.05	3.15	303.2	0.20	76810	N
F121		500	500	1.00	0.95	10.78	32.02	0.17	1.61	3.28	315.7	0.06	87660	N	5.49	3.20	308	0.22	95060	P//H [A]
F125		500	746	1.49	0.81	16.35	39.94	0.14	1.47	3.30	317.1	0.06	72580	N	6.00	3.24	311.5	0.24	73570	P//H [R]
F213	Triton FLATS	700	175	0.25	0.22	5.35	10.23	0.22	0.88	3.22	309.9	0.04	84420	N	3.33	2.83	271.7	0.13	76140	N
F212		500	250	0.50	0.22	5.95	12.13	0.13	0.76	3.60	346.1	0.03	75680	N	4.31	3.06	294.1	0.17	88560	N
F214		500	376	0.75	0.28	5.80	12.11	0.09	0.71	3.77	362.2	0.03	75980	N	4.99	3.20	307.2	0.20	73030	N
F211		500	500	1.00	0.26	5.70	13.17	0.07	0.75	3.74	359.4	0.03	75870	N	4.53	3.12	300.4	0.18	68780	N
F215		500	746	1.49	0.36	5.43	12.12	0.04	0.74	3.98	382.7	0.03	79890	N	4.75	3.14	301.5	0.19	79560	N
F198	Triton RH	700	175	0.25	0.27	4.16	9.13	0.19	0.71	2.95	283.5	0.03	82670	T [A]	2.73	2.57	246.9	0.11	79930	T [R]
F197		500	250	0.50	0.29	5.17	10.94	0.12	0.92	3.56	342.3	0.04	80300	N	3.98	3.01	289	0.16	83870	T [R]
F199		500	376	0.75	0.32	5.14	11.36	0.08	0.71	3.70	355.7	0.03	80670	T [R]	4.28	3.03	290.9	0.17	89780	T [R]
F196		500	500	1.00	0.41	5.40	12.44	0.07	0.80	3.80	365.2	0.03	82180	T [A]	4.54	3.09	297.3	0.18	82870	T [R]
F200		500	746	1.49	0.38	5.14	11.42	0.04	1.01	4.07	391	0.04	78780	N	5.62	3.18	305.5	0.23	79300	N

	Weld ID
	Weld variables
	Process parameters
	LoStir Force/Torque data
	Calculated data
	As-Welded tensile data
	Annealed tensile data

N	Nugget
T	TMAZ
H	HAZ
P	Parent material
_//_	Interface between 2 regions
[A]	Advancing side
[R]	Retreating side

Table 7.2.a) Data Overview Table: Bead on Plate Welds in AA5083 completed onFW22.

Weld ID #	Tool	Spindle Speed Vs [Rpm]	Feed Speed Vf [mm/min]	Weld Pitch Vf/Vs [mm/rev]	AVG Weld Force [KN]	AVG Down Force [KN]	AVG Spindle Torque [Nm]	Heat Input [KJ/mm]	Displacement at Max Load [mm]	Load at Max Load [KN]	Stress at Max Load [Mpa]	Strain at Max Load	Young's Modulus	Fracture Location	Displacement at Max Load [mm]	Load at Max Load [KN]	Stress at Max Load [Mpa]	Strain at Max Load	Young's Modulus	Fracture Location
F83	BRUTJMCR003	700	175	0.25	0.38	11.68	26.81	0.57	1.19	2.76	265.2	0.05	71780	T [R]	0.46	2.01	193.5	0.02	77970	N
F82		500	250	0.5	0.46	12.24	36.17	0.39	0.92	2.74	263.1	0.04	91980	T [R]	1.14	2.24	215.4	0.05	112700	N
F84		500	376	0.752	0.72	11.97	37.71	0.27	0.76	2.65	255.2	0.03	70870	T [R]	0.95	2.20	211.7	0.04	82790	N
F81		500	500	1	0.80	11.04	39.94	0.21	0.91	2.83	272.2	0.04	85190	T [R]	0.81	2.33	223.5	0.03	63090	N
F85		500	746	1.492	1.23	10.03	40.50	0.14	0.41	2.63	253.3	0.02	80460	T [R]	0.75	2.39	229.3	0.03	68460	N
F8	Concave004	700	175	0.25	0.44	12.49	24.29	0.52	1.05	2.57	247.5	0.04	42360	T [R]	1.05	1.83	175.6	0.04	83370	N
F7		500	250	0.5	0.15	14.11	33.62	0.36	1.49	2.73	262.7	0.06	51800	T [R]	1.09	2.05	197	0.04	41610	N
F9		500	376	0.752	0.18	14.07	35.88	0.25	1.02	2.68	258.1	0.04	72800	T [R]	0.93	2.19	210.6	0.04	80780	N
F6		500	500	1	0.31	13.93	39.09	0.21	1.34	2.72	261.3	0.05	63850	N	0.96	2.15	206.2	0.04	65220	N
F10		500	746	1.492	0.47	14.17	41.70	0.15	0.90	2.66	255.3	0.04	84880	T [R]	0.80	2.26	217.1	0.03	86790	N
F23	Concave005	700	175	0.25	0.29	10.76	22.38	0.48	1.61	2.83	272	0.06	69630	T [R]	0.94	2.20	211.9	0.04	86260	N
F22		500	250	0.5	0.64	11.14	29.94	0.32	1.01	2.70	259.5	0.04	76590	T [R]	1.01	2.06	198.1	0.04	72738	N
F24		500	376	0.752	0.25	11.14	32.16	0.23	0.81	2.61	250.6	0.03	99820	T [R]	0.92	2.22	213.2	0.04	106200	N
F21		500	500	1	0.37	10.77	34.46	0.18	0.90	2.69	259.1	0.04	97490	T [R]	0.86	2.29	220.3	0.03	89140	N
F25		500	746	1.492	0.43	11.31	38.45	0.14	0.79	2.66	255.8	0.03	81540	T [R]	0.89	2.37	228.1	0.04	100200	N
F38	Concave006	700	175	0.25	0.17	12.93	25.49	0.54	1.35	2.64	253.4	0.05	46470	N	1.17	1.76	169.1	0.05	46550	N
F37		500	250	0.5	0.12	16.14	37.00	0.40	1.56	2.68	257.4	0.06	58160	N	1.17	1.92	184.2	0.05	51130	N
F39		500	376	0.752	0.13	11.59	34.85	0.25	0.92	2.75	264.3	0.04	75550	T [R]	0.94	2.27	217.8	0.04	105300	N
F36		500	500	1	0.18	15.93	43.24	0.23	0.45	2.56	245.6	0.02	76280	H [R]	1.06	2.27	218	0.04	93790	N
F40		500	746	1.492	0.29	11.56	40.87	0.15	0.85	2.64	254.1	0.03	85730	T [R]	0.96	2.30	220.8	0.04	87120	N
F143	TriFlat001	700	175	0.25	0.25	11.08	23.00	0.49	0.95	2.50	240.3	0.04	56300	H [R]	0.77	1.60	154.3	0.03	33230	T//H [R]
F142		500	250	0.5	0.24	14.69	35.82	0.38	0.16	0.89	85.19	0.01	27480	H [R]	1.15	1.83	175.9	0.05	39560	N
F144		500	376	0.752	0.34	8.96	29.79	0.21	0.89	2.61	251.2	0.04	75790	T [R]	0.90	2.24	215.1	0.04	61210	N
F141		500	500	1	0.16	14.77	41.42	0.22	1.50	2.68	257.8	0.06	49920	N	1.03	2.07	198.6	0.04	85430	N
F145		500	746	1.492	0.83	7.13	34.64	0.12	0.90	2.57	246.8	0.04	82660	N	0.82	2.23	214.5	0.03	80220	N
F158	TriFlat002	700	175	0.25	0.16	9.33	21.45	0.46	0.74	2.57	246.7	0.03	65730	H [R]	1.02	1.96	188.4	0.04	78400	N
F157		500	250	0.5	0.28	8.98	31.27	0.33	1.38	2.85	273.7	0.06	94550	N	1.02	2.06	198.2	0.04	93640	N
F159		500	376	0.752	0.24	9.80	30.53	0.22	0.96	2.77	266.3	0.04	95560	T [R]	0.84	2.31	221.8	0.03	79540	N
F156		500	500	1	0.60	8.40	33.11	0.18	1.01	2.78	266.9	0.04	95940	T [R]	0.86	2.25	216.3	0.03	81220	N
F160		500	746	1.492	0.55	8.73	36.41	0.13	0.87	2.67	257	0.03	82020	T [R]	0.84	2.34	224.9	0.03	81840	N
F173	TriFlat003	700	175	0.25	0.17	10.02	23.55	0.50	0.62	2.55	245	0.02	55090	H [R]	1.03	2.11	202.7	0.04	57080	N
F172		500	250	0.5	0.25	10.80	30.66	0.33	1.24	2.86	275.3	0.05	79400	T [R]	1.05	2.29	220.3	0.04	64240	N
F174		500	376	0.752	0.31	11.15	32.79	0.23	0.98	2.72	261.2	0.04	76780	T [R]	0.92	2.30	221.2	0.04	78180	N
F171		500	500	1	0.35	10.23	36.22	0.19	1.00	2.76	265.5	0.04	102200	T [R]	0.96	2.36	226.9	0.04	106100	N
F175		500	746	1.492	0.59	9.45	37.14	0.13	0.85	2.64	253.7	0.03	94380	T [R]	0.54	2.31	221.6	0.02	80320	T//H [R]
F98	Triflute001	700	175	0.25	0.25	10.28	21.22	0.45	0.80	2.69	258.3	0.03	58630	H [R]	1.05	2.12	203.7	0.04	84020	N
F97		500	250	0.5	0.34	10.68	29.52	0.32	0.95	2.79	268	0.04	86780	T [R]	1.02	2.28	219.1	0.04	95390	N
F99		500	376	0.752	0.35	10.58	31.29	0.22	0.78	2.80	269.6	0.03	70190	T [R]	0.89	2.38	229	0.04	75150	N
F96		500	500	1	0.35	8.92	35.00	0.19	1.18	2.68	258.1	0.05	86690	N	0.94	2.18	209.7	0.04	92330	N
F100		500	746	1.492	0.41	10.16	36.77	0.13	0.79	2.74	263.7	0.03	79150	T [R]	0.84	2.41	231.7	0.03	88710	N
F113	Triflute002	700	175	0.25	0.12	10.39	23.93	0.51	1.36	2.85	273.7	0.05	67410	N	0.91	2.01	192.9	0.04	87940	N
F112		500	250	0.5	0.23	10.45	32.25	0.34	1.15	2.73	262.9	0.05	83070	T [R]	0.89	2.17	208.5	0.04	79020	N
F114		500	376	0.752	0.27	9.95	33.21	0.24	0.80	2.67	256.9	0.03	101900	N	0.93	2.27	217.9	0.04	97960	N
F111		500	500	1	0.36	8.98	38.02	0.20	1.14	2.71	260.5	0.05	86870	N	0.97	2.24	215.7	0.04	91570	N
F115		500	746	1.492	0.54	8.93	37.38	0.13	0.89	2.63	253.2	0.04	92180	N	0.82	2.29	220.5	0.03	89680	N
F128	Triflute003	700	175	0.25	0.32	8.37	21.41	0.46	1.23	2.92	280.5	0.05	90680	T [R]	0.94	2.29	219.7	0.04	80900	N
F127		500	250	0.5	0.18	12.26	33.85	0.36	1.32	2.72	261.6	0.05	80590	N	1.05	2.06	197.9	0.04	88980	N
F129		500	376	0.752	0.59	7.58	31.59	0.22	0.90	2.72	261.9	0.04	78070	T [R]	0.85	2.32	222.8	0.03	79540	N
F126		500	500	1	0.28	12.13	38.95	0.21	1.12	2.73	262.8	0.04	78830	T [R]	0.95	2.21	212.9	0.04	90350	N
F130		500	746	1.492	1.10	6.52	31.23	0.11	0.36	2.57	247.3	0.01	100800	N	0.47	2.30	221.5	0.02	119800	T [R]
F218	Triton FLATS	700	175	0.25	0.19	3.68	11.30	0.24	0.47	2.39	229.4	0.02	98910	H [R]	0.50	2.04	195.9	0.02	88160	T//H [R]
F217		500	250	0.5	0.15	4.40	12.22	0.13	0.49	2.46	236	0.02	89760	N	0.63	2.25	216.3	0.03	91340	N
F219		500	376	0.752	0.33	4.87	12.14	0.09	0.32	2.50	240.2	0.01	71390	N	0.49	2.27	217.8	0.02	59680	N
F216		500	500	1	0.26	5.90	13.49	0.07	0.28	2.80	268.7	0.01	115100	N	0.48	2.50	240.1	0.02	88380	N
F220		500	746	1.492	0.31	5.63	12.78	0.05	0.26	2.92	280.4	0.01	86430	N	0.50	2.42	232.8	0.02	85940	N

	Weld ID
	Weld variables
	Process parameters
	LoStir Force/Torque data
	Calculated data
	As-Welded tensile data
	Annealed tensile data

N	Nugget
T	TMAZ
H	HAZ
P	Parent material
_//_	Interface between 2 regions
[A]	Advancing side
[R]	Retreating side

Table 7.2. b) Data Overview Table: Bead on Plate Welds in AA2004 Carried out on FW22.

AA5083

Tool	Concave005	Concave005	Concave005	MX Trifilute™	MX Trifilute™	MX Trifilute™	MX Trifilute™	MX Trifilute™	MX Trifilute™	MX Trifilute™
Tool diameter [mm]	16	16	16	15	15	15	15	15	15	15
Configuration	C	C	C	C	C	C	C	C-5	C	C+5
	SP	SP	SP	SP	SP	SP	SP	3P		
Weld Id	E1	E2	E3	E4	E11	E12	E13	E5-A	E5-B	E5-C
Spindle Speed [Rpm]	750	750	750	750	1250	1250	1250	750		
Feed Speed [mm/min]	750	750	750	750	1250	1000	750	750		
Weld pitch [mm/rev]	1	1	1	1	1	0.8	0.6	1		
Weld force (Fx) [Kn]	3.72	1.39	3.44	3.33	2.16	1.03	2.71	2.63	2.89	1.99
Side force (Fy) [KN]	2.93	3.57	3.13	2.33	2.61	2.42	2.46	2.31	2.61	2.53
Down force (Fz) [KN]	14.83	17.52	17.61	13.42	15.95	16.07	15.48	13.78	15.56	16.6
Spindle torque [Nm]	32.4	32.41	33.48	29.82	22.15	20.83	19.27	29.87	29.13	29.33
FSW Heat input [KJ/mm]	0.173	0.173	0.179	0.159	0.118	0.139	0.172	0.16	0.156	0.157
180° Bend test [P/F]	F	F	F	P	P	P	P	P	P	P
Displacement at max load [mm]	-	-	-	1.658	1.763	1.673	1.629	0.1146		
Max load [KN]	-	-	-	3.1	3	3	2.8	3		
Stress at max load [Mpa]	-	-	-	295	291	289	273	292		
Strain at max load	-	-	-	0.066	0.071	0.067	0.065	0.005		
Young's Modulus	-	-	-	71400	67090	69090	65190	63900		
Oringinal thickness [mm]	-	-	-	1.6	1.61	1.61	1.61	1.6		
Formed thickness [mm]	-	-	-	1.28	0.844	0.772	0.97	1.18		
SPF strain [%]	-	-	-	46.88	72.27	79.02	62.89	50.85		
Formed thickness [mm]	-	-	-	-	-	-	-	-		
SPF strain [%]	-	-	-	-	-	-	-	-		

	Weld Id
	Weld variables
	Process parameters
	Force/Torque
	Calculated data
	As-welded tensile data
	Cone test data

	Surface finished Cone test data
SP	Single pass
3P	Triple pass
C-5	Tool position weld centre line -5mm
C	Tool position weld centre line
C+5	Tool position weld centre line +5mm
BOP	Bead on plate

Table 7.3.a) Data Overview Table: Welds in AA5083 Created using the ESAB Machine.

AA2004

Tool	MX Trifflute™	MX Trifflute™	MX Trifflute™	MX Trifflute™	MX Trifflute™	MX Trifflute™	MX Trifflute™	MX Trifflute™	MX Trifflute™	MX Trifflute™	MX Trifflute™	MX Trifflute™
Tool diameter [mm]	15	15	15	15	15	15	15	15	15	15	15	15
Configuration	C	C	C	C	C	C-5	C	C+5	C-5	C	C+5	
	SP	SP	SP	SP	SP/BOP	3P			3P/BOP			
Weld Id	E6	E10	E9	E8	E14	E7-A	E7-B	E7-C	E15-A	E15-B	E15-C	
Spindle Speed [Rpm]	750	1250	1250	1250	1250	750			1250			
Feed Speed [mm/min]	750	1250	1000	750	1000	750			1000			
Weld pitch [mm/rev]	1	1	0.8	0.6	0.8	1			0.8			
Weld force (Fx) [Kn]	0.62	4.89	2.1	1.03	2.09	2.33	0.73	0.56	3.07	1.52	2.82	
Side force (Fy) [KN]	2.23	2.4	2.32	2.31	2.21	2.11	2.43	2.41	2.22	2.68	2.79	
Down force (Fz) [KN]	11.52	14.83	14.65	13.99	12.26	14.02	15.44	15.44	12.6	14.81	15.95	
Spindle torque [Nm]	29.59	23.15	22.27	19.72	19.59	29.46	29.61	29.61	19.46	19.65	19.46	
FSW Heat input [KJ/mm]	0.158	0.1236	0.1487	0.1755	0.1308	0.16	0.158	0.157	0.13	0.131	0.13	
180° Bend test [P/F]	P	P	P	P	P	P	P	P	P	P	P	
Displacement at max load [mm]	1.076	1.007	1.117	1.443	1.246	0.8774		0.2689	0.9887		1.784	
Max load [KN]	2.443	2.598	2.619	2.727	2.112	2.24		2.005	2.283		2.221	
Stress at max load [Mpa]	234.9	249.8	251.8	262.2	270.7	215.4		192.8	292.7		284.7	
Strain at max load	0.043	0.0403	0.0447	0.0577	0.0498	0.0395		0.0108	0.0395		0.0714	
Young's Modulus	86200	57900	64070	59210	90440	50730		59340	71000		54680	
Oringinal thickness [mm]	1.6	1.61	1.61	1.6	1.21	1.61			1.23			
Formed thickness [mm]	0.42	0.306	0.29	0.46	0.3	0.7			0.306			
SPF strain [%]	142.86	199.35	210.34	130.43	70	87.14			75.16			
Formed thickness [mm]	-	-	-	-	0.294	-			0.278			
SPF strain [%]	-	-	-	-	71.429	-			82.73			

	Weld Id
	Weld variables
	Process parameters
	Force/Torque
	Calculated data
	As-welded tensile data
	As-welded Cone test data

	Surface finished Cone test data
SP	Single pass
3P	Triple pass
C-5	Tool position weld centre line -5mm
C	Tool position weld centre line
C+5	Tool position weld centre line +5mm
BOP	Bead on plate

Table 7.3.b Data Overview Table: Welds in AA2004 Created using the ESAB Machine.

7.3 Real Time Force Monitoring

The real time force monitoring only applies to the welds carried out on FW22 and the ESAB SuperStir machines. All welds carried out of FW22 were collected using the LoStir device [32]. The ESAB machine utilises built in systems. Values are taken at 10ms intervals creating a force/torque versus time plot. Figure 7.1 shows an example of the plots derived from the different force monitoring systems.

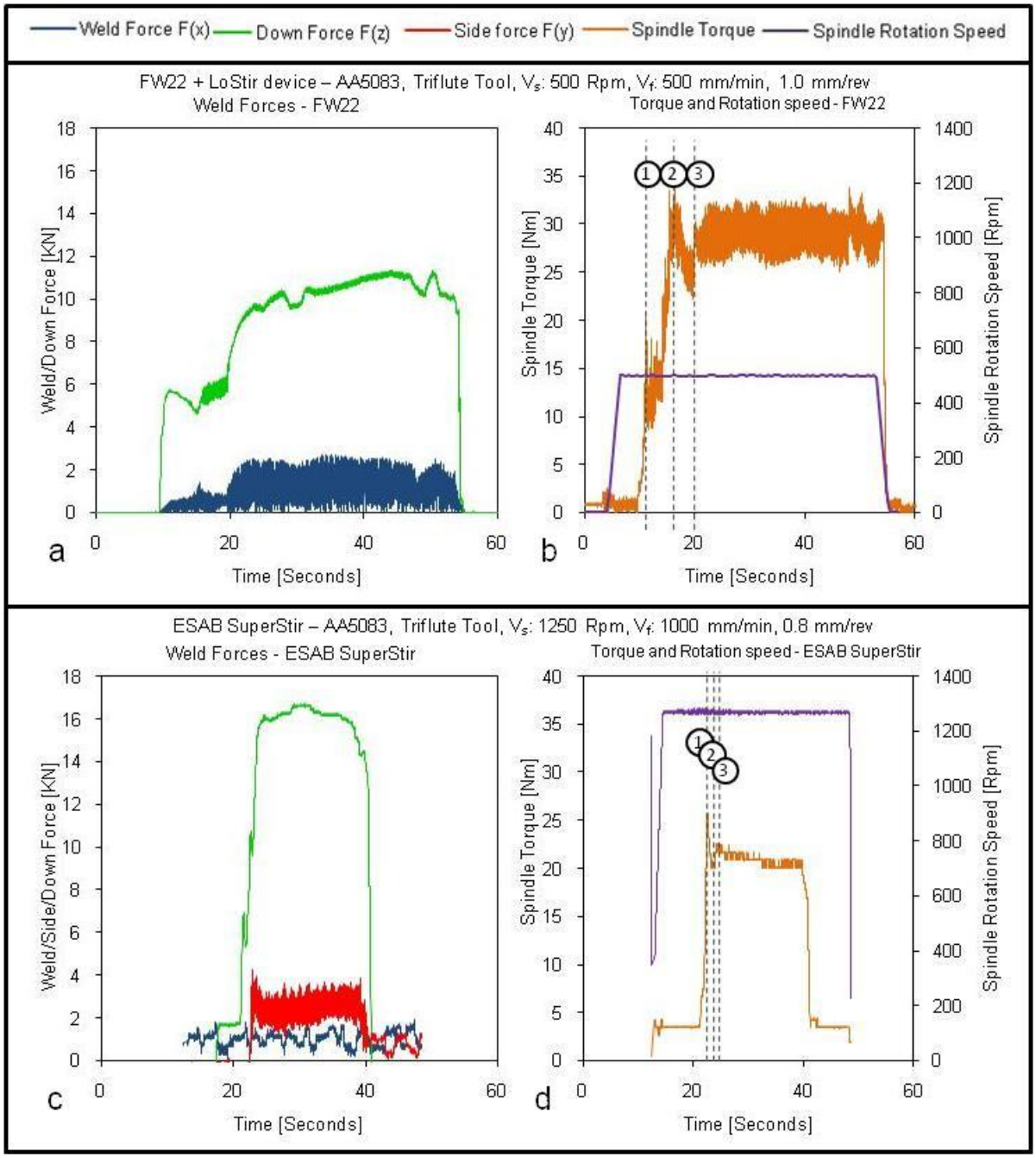

Figure 7.1, Real Time Force Data. a) FW22: Weld Forces versus Time. b) FW22: Spindle Torque versus Time. c) ESAB SuperStir: Weld Forces versus Time. d) ESAB SuperStir: Spindle Torque and Rotation Speed versus Time.

From the plots produced the most significant is the torque versus time plot shown in Figure 7.1 c) and d). This plot shows the initial tool touchdowns for both the probe and shoulder these are annotated on the plots as 1 and 2. It also shows start of the tool traverse, annotated as 3 and the onset of the steady state regime. During FSW it will take some time for the process to become steady state hence the removal of material at the start of the weld when testing is carried out. This steady state region is present for the weld force versus time plots but is a little noisy and less distinct. Using the torque plots the steady state regions were defined and averages for the forces and torque have been taken from this time span to be included in the data overviews.

7.3.1 Weld-Force

The weld-force is strongly linked to the amount of heat supplied by the FSW tooling and process variables. It equates to the amount of force the machine requires to traverse the tooling through the plasticised material. More heat implies softer material beneath the tool making it easier to traverse. This is what is expected, as the weld pitch increases the force required to traverse the tooling increases; this trend is shown in Figure 7.2, for the welds created using FW22. The difference between the hot welding conditions (low weld pitch) and the cold welding conditions (high weld pitch) ranges between ~50% for the small diameter tooling and ~232% for the largest tooling.

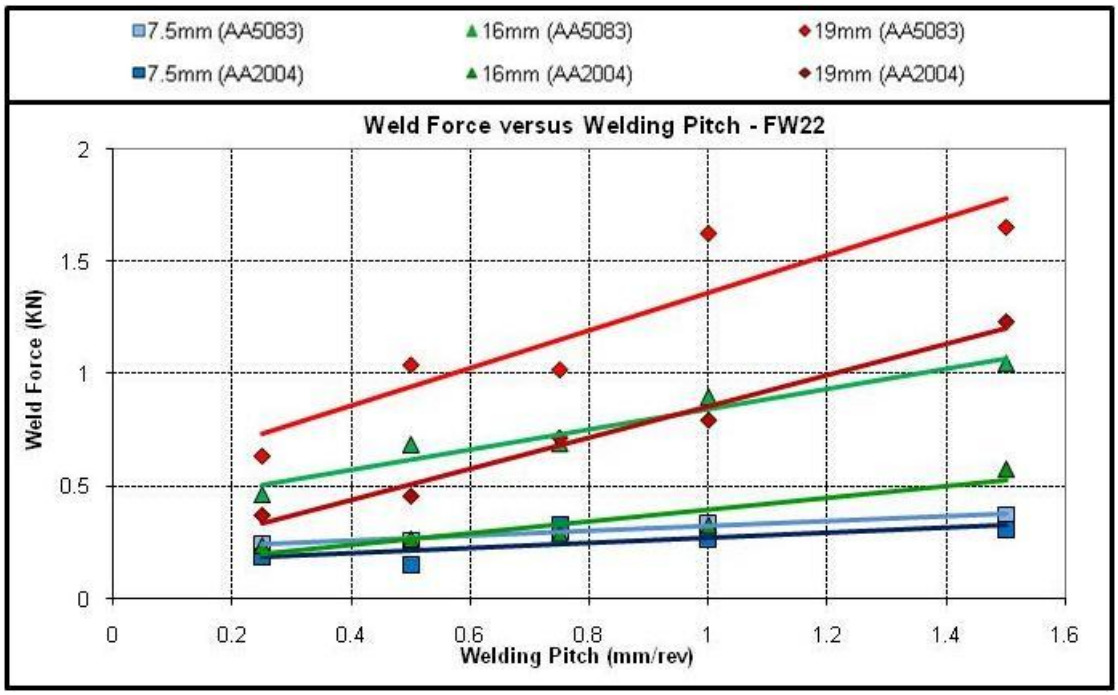

Figure 7.2, Weld-Force Versus Weld Pitch for Bead-On-Plate Welds Created on FW22.

7.3.2 Down-Force

The downwards force acting through the tooling is much larger in magnitude than the welding force. This is the force required to maintain constant contact between the FSW tools and weld material. The down-force through the tool is relatively constant; with only very small changes in force for changes in weld pitch, this suggests that the major process variables (spindle speed and feed speed) have less affect on the down-force than the tooling used to create the welds and the material being welded. The same trend as the weld force was expected for the down-force, hot welding conditions implying softer material beneath the tool requiring less force through the tooling. This however is not the case. For all the tooling, with the exception of the 7.5mm tool welding the AA2004, the down-force decreased slightly. This difference is much less in magnitude than the weld force, only ~10-20%. It can be seen in Figure 7.3, that the forces experienced when welding AA5083 is higher than that for the AA2004, this can be attributed to the differences in the alloy systems, implying that it is harder to plasticise the AA5083 due to its strain hardening effects of this alloy.

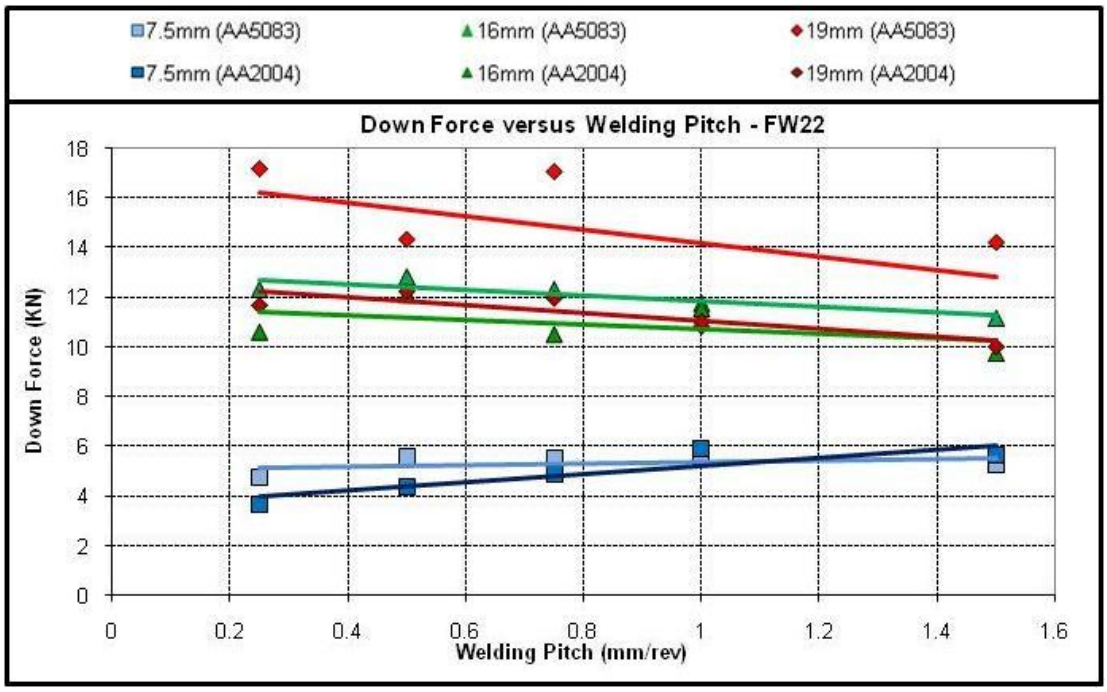

Figure 7.3, Down-Force Versus Weld Pitch for Bead-On-Plate Welds Created on FW22.

7.3.3 Side-Force

The side force measurements only apply to the welds carried out on the ESAB machine. Only a small number of welds have been created and so a complete analysis of the side force cannot be made, therefore the side force F_y will not be discussed further.

7.3.4 Spindle Torque

The spindle torque produced during the process gives a good initial estimate of the amount of heat generated during the FSW process. A high torque value yields a low heat input and vice versa. Spindle torque (Nm) is the tendency of a force vector to rotate an object about an axis. For a high value of spindle torque more force is required to rotate the spindle, this in turns means more power is required to rotate the tooling; indicating that the material is not fully plasticized; further indicating a low heat input to the weld. As the weld pitch falls, moving from cold to hot welding conditions, the material is more plasticised resulting in a reduction in the spindle torque and therefore the power required to rotate the tool. This torque/heat input relationship behaves in the same way as in conventional rotational friction welding. As the heat input rises, the torque decreases, up until a critical point. After this point

no further increase in heat input is possible due to extreme softening and localised melting of the material directly beneath the shoulder, resulting in a loss of traction between the tool and the weld material [30, 31]. Figure 7.4 shows the torque versus increasing weld pitch. As the welding pitch is increased the torque rises; indicating that the tool requires more power to rotate the tools as the weld material is harder under cold welding conditions. When the weld pitch is low the material becomes soft and in some extreme cases can cause localized melting of material in direct contact with the tool shoulder. This thin layer of melted material acts as a lubricant and so decreases the amount of torque; this makes FSW a self regulating process unable to attain fusion of the bulk material.

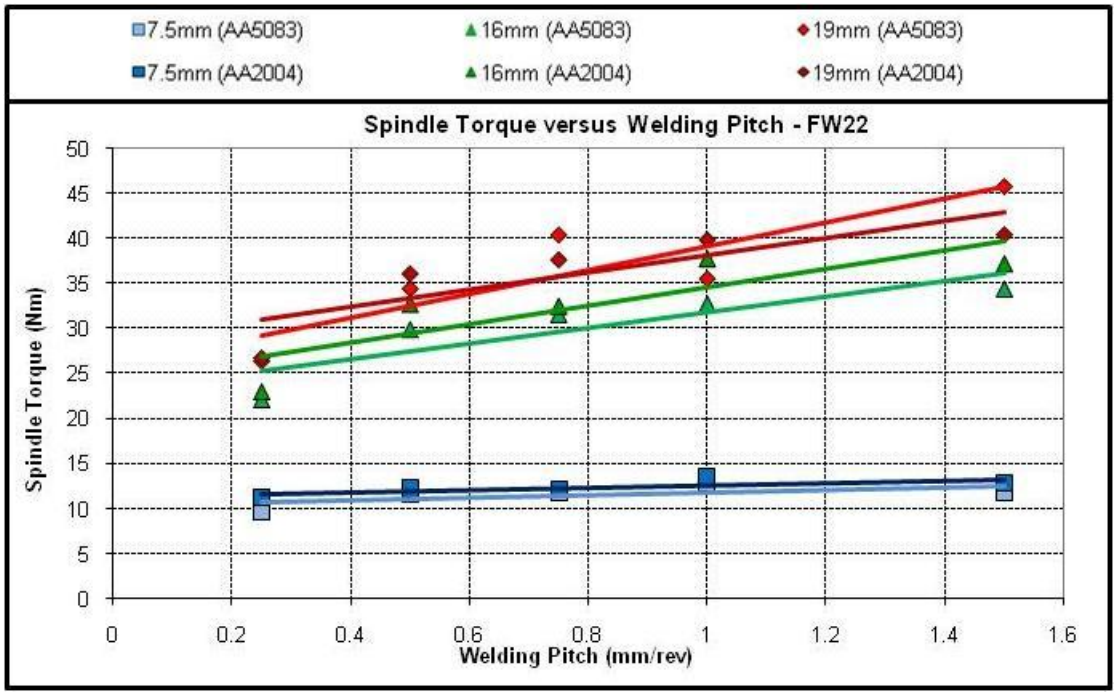

Figure 7.4, Spindle Torque Versus Weld Pitch for Bead-On-Plate Welds Created on FW22.

7.3.5 Heat Input

The heat input for a friction stir weld is best estimated using the spindle torque. It has been suggested that the rotation of the tool in contact with the weld material accounts for as much as 99% of the total heat generated, with the remaining heat derived from the traverse of the tool. The efficiency factor represents the amount of heat which remains in the work piece and has been estimated to be ~0.85 [14, 30, 31].

(2.1) $$Q = E\frac{2\pi rT}{1000v}$$ (KJ/mm)

Where: Q is Heat Input, E is Efficiency factor (0.85), r is Spindle rotation speed (rpm), T is Spindle torque (Nm) and v is Traverse speed (mm/min) [31, 32].

Figure 7.5 shows the calculated heat input from equation (2.1) versus the welding pitch. It is clearly visible that as the welding pitch increases the amount of heat supplied falls. This is expected as the higher the welding pitch, the more material is processed for each rotation of the tooling. This supports the notion of using the welding pitch as a preliminary evaluation of the heat supplied to the weld.

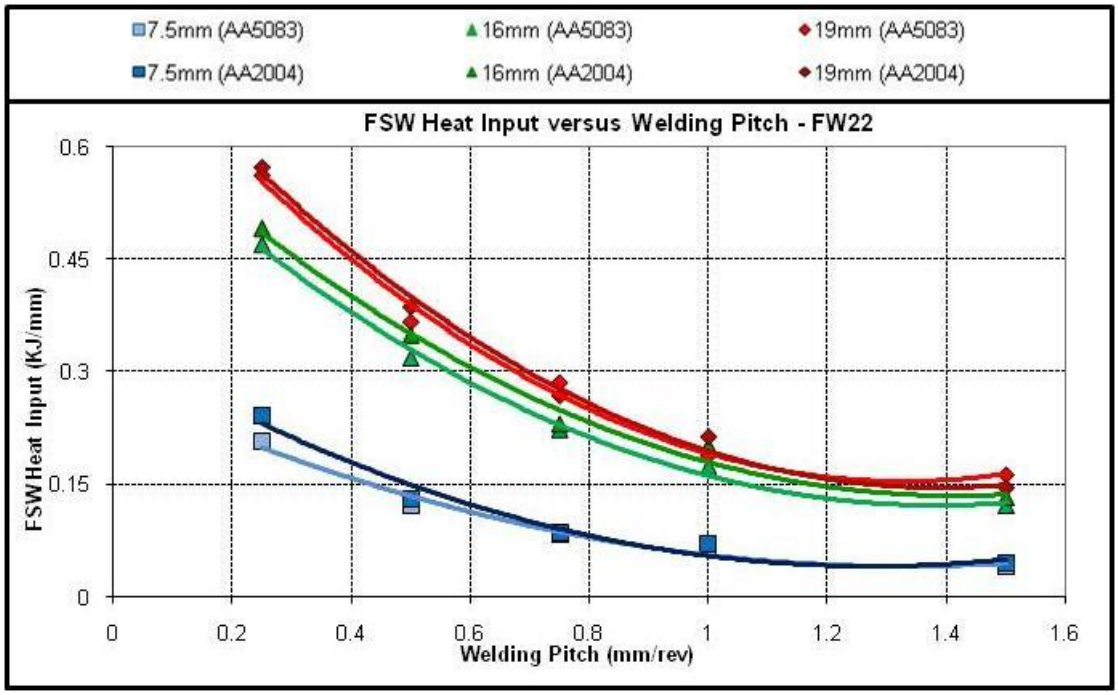

Figure 7.5, Calculated Heat Input Versus Welding Pitch for Bead-On-Plate Welds Created on FW22.

7.4 Mechanical Property Testing

Tensile testing is the most convenient way of determining the overall strength of the weld. If the weld is tested in its entirety, i.e. the weld region, heat affected zones and some parent material is included in the gage length, then the test will show the strength of the weakest part of the gage length. This is usually the weld region itself unless the weld material starts in a fully annealed condition; in this case the weld region can be much stronger than the parent material [12, 43]. Tensile testing of the bead on plate specimens allows the microstructures produced to be tested for strength

without any joint interface flaws affecting this result. Tensile tests have been carried out on welds created on all three machines.

Hardness profiles have been collected in the transverse direction and readings taken at 1mm intervals within the tool footprint, extending to readings every 5mm outside the tool footprint. The hardness profile is a useful tool used in conjunction with the tensile test results in order to establish the strength of the weld and possible variations in strength for the different weld regions.

Formability tests have been carried out as elevated temperature cone testing, mimicking the cavity forming variant of superplastic forming.

The analysis will be described in chronological order starting with the initial welds carried out on the Parkson milling machine and ending with the welds created using the ESAB machine.

7.4.1 Parkson Milling Machine

The Parkson milling machine is the least technologically advanced machine used to create the FSWs in this thesis. This is essentially the first part of the learning curve and further highlights the growing gulf between basic machines which are capable of FSW, but with limited success and the state-of-the-art FSW machines. Most of the limitations of the machine are due to its completely manual control and are highlighted by poor mechanical property tests. The welds created on the Parkson milling machine are butt welds.

7.4.1.1 Tensile Test Results

It is clearly visible from Figure 7.6 that the welds are well below quality standards required for subsequent forming operations. The ultimate tensile strength falls well short of the strength of the annealed material. Subsequent microstructural observations concluded that the poor tensile strength is due to poor breakup of the joint interface.

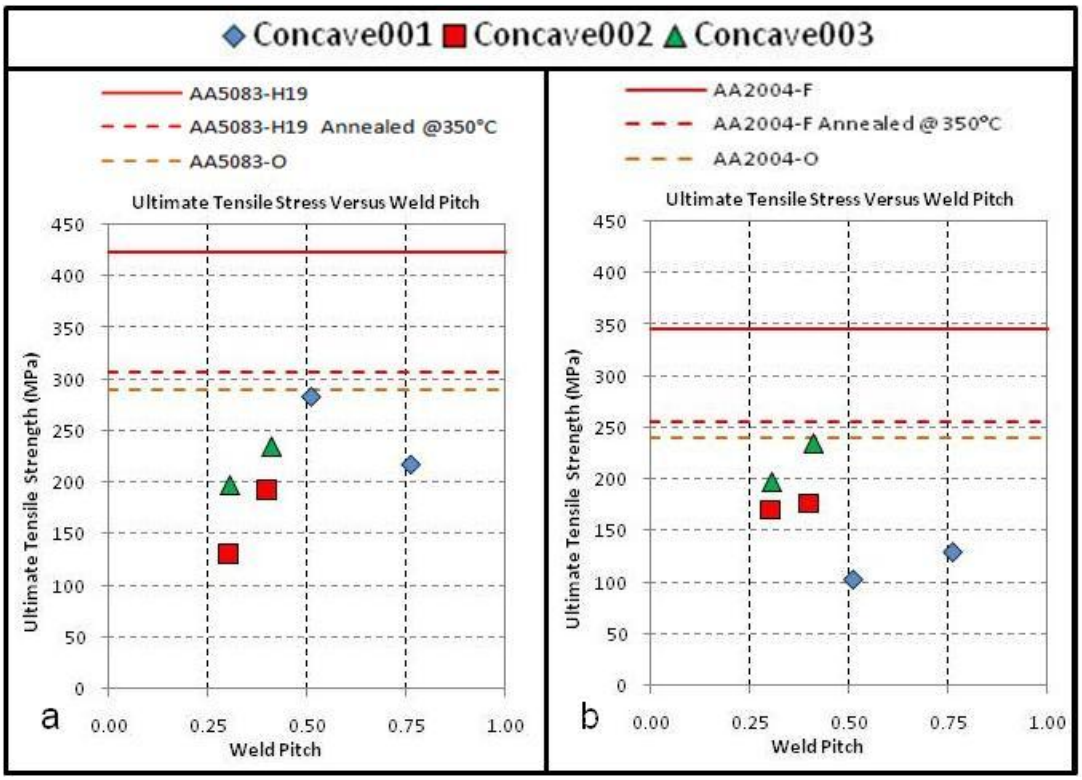

Figure 7.6, Ultimate Tensile Strength Versus Welding Pitch for FSWs Created on the Parkson Milling Machine: a) AA5083, b) AA2004.

As shown in Figure 7.6 the tensile strength of the welds fall below the original parent material strength (shown as the red, solid line) and the strength of a fully annealed parent material (shown as the orange, dashed line), this suggests that there are faults within the weld which contribute to the reduced ultimate tensile strength. Both the AA2004 and AA5083 FSWs created on the Parkson milling machine contain root flaws. Deformation and heat is transferred to the weld root via the tool probe and its features. The simple smooth probes of the concave tooling group do not allow enough probe induced deformation in the weld root; this means that the weld produced has an inherent flaw running the length of the weld. During tensile testing this flaw is pulled apart causing early failure of the weld.

7.4.1.2 Dome Test Results

This type of test is not readily applicable for testing superplastic formability as room temperature properties alter dramatically from properties at superplastic temperatures. This does however test the weld's ability to be stretched by a force normal to the top surface of the welded specimens and can give an indication to the

success of the join via its failure mode. The test can establish whether the weld root has received enough heat and deformation to sufficiently bond the material. If this bonding is poor the test will yield a split or rupture at the joint interface. If the bonding is suitable the test will yield cracking of the top surface (surface in tension) due to poor room temperature ductility of the aluminium. The Parkson Overview shown in Table 7.1 contains the dome test results. It can be seen from these results that the higher spindle speed produces a lower drawing force implying a reduction in strength. This reduction in strength however is not present in conjunction with an improvement in ductility as the Erichsen value (Dome height) does not increase. It would be expected that a recrystallized FSW microstructure would yield a reduced strength compared to the parent material accompanied with an increase in ductility; allowing a reduced drawing force and an increased dome height. This further suggests that there is a root flaw associated with the smooth, non-re-entrant tooling, which acts as an initiation site for the failure.

Re-entrant tooling is more susceptible to breaking during the process than the simple design used on this machine. The Parkson milling machine has a manual plunge which is difficult to rely on for accuracy and may change throughout the process. This difficult setting is critical to the success of the weld and so measures were taken to secure alternative machinery for a more intensive trial.

7.4.2 FW22

FW22 is a superior machine with greater control of the process variables but once again with a manually set plunge distance. For these runs the plunge depth was set using thickness gauges to set the height of two large bolts which support the milling head. There is more confidence that this machine; once set it can maintain a constant depth and so be considered as position control. The Parkson milling machine engages the tool and weld material by raising the feed table rather than bringing a heavy milling head down on the weld as with FW22. This machine represents the middle of the technology tree for FSW carried out in this thesis. It is still a milling machine but it has been enhanced with force monitoring systems and heavy duty rigid fixture; secured directly to the workshop floor.

The largest bulk of trials have been carried out on this machine [94], most of these being bead on plate trials, designed to create differing microstructures for analysis without the problems relating to the plunge depth flaws. The second stage of the trials for this machine involves butt welding using process parameters selected based on the bead on plate results. These butt welds are wider in physical size allowing cone testing to be carried out.

7.4.2.1 Tensile Test Results - As-Welded Specimens

FW22 samples have been tested in an ‘As-welded’ condition. These tests have been carried out approximately one month after the welding operation to allow any precipitation and aging phenomena to stabilise.

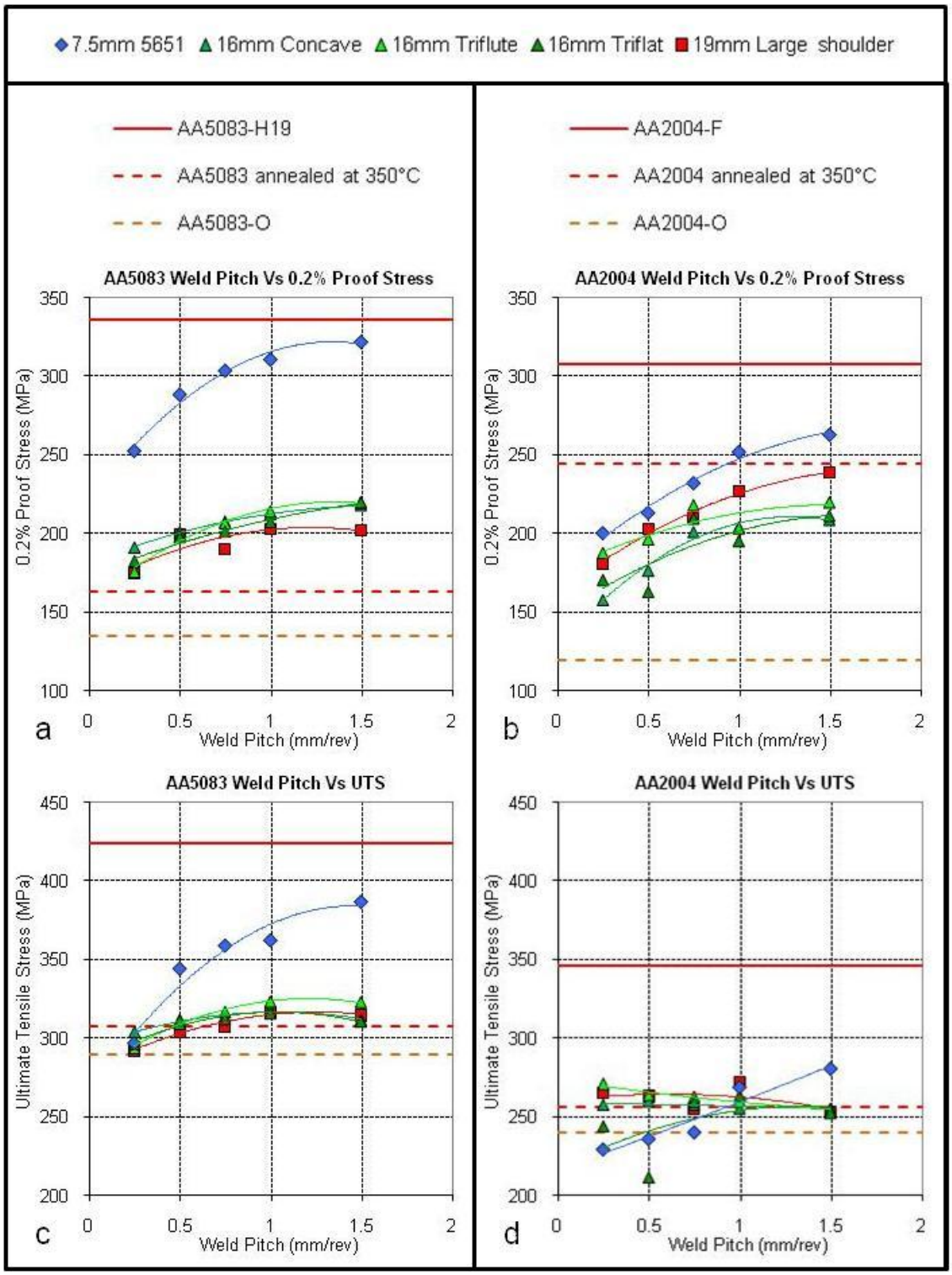

Figure 7.7, Tensile Strength versus Weld Pitch.

a) A2004 – 0.2% Yield Stress. b) AA2004 – Ultimate Tensile Stress.

c) AA5083 – 0.2% Yield Stress. d) AA5083 – Ultimate Tensile Stress.

It is clear from Figure 7.7 that the smaller 5651 tools, in blue, yield superior strength compared to the larger tools. The largest tool at 19mm diameter and the three groups

of 16mm diameter tools provide very similar results. It can also be seen that the results are different for the two alloy systems. Figure 7.7.a) and c) shows the AA5083, this is a strain hardening material, which means that some of the strength derived from the cold rolling processes carried out on the sheet is retained when a high welding pitch is used in conjunction with a small tool. There is insufficient heat over a small time to cause full softening of the weld region. This is in contrast with the AA2004, shown in Figure 7.7.b) and d), where all the tools used at any of the welding pitches investigated caused softening of the weld region. AA2004 is a precipitation hardening alloy that relies on second phase particles for its strength. This alloy is also susceptible to continuous dynamic recrystallization, the kind of recrystallization commonly associated with the evolution of the weld nugget. The welds created in this alloy all soften to a point which is comparable to a partially annealed material. Figure 7.8 shows the ultimate tensile strengths versus the heat input generated during the welding operation. It can be seen from Figure 7.8.a) that above a critical value of heat input, ~0.1 KJ/mm, the strength of the AA5083-H19 is lost and resembles an annealed AA5083-O material. For the AA2004, Figure 7.8 b), all the welds resembled an annealed material indicating that the critical value for retention of strength was exceeded by all the tools and all the welding pitches investigated.

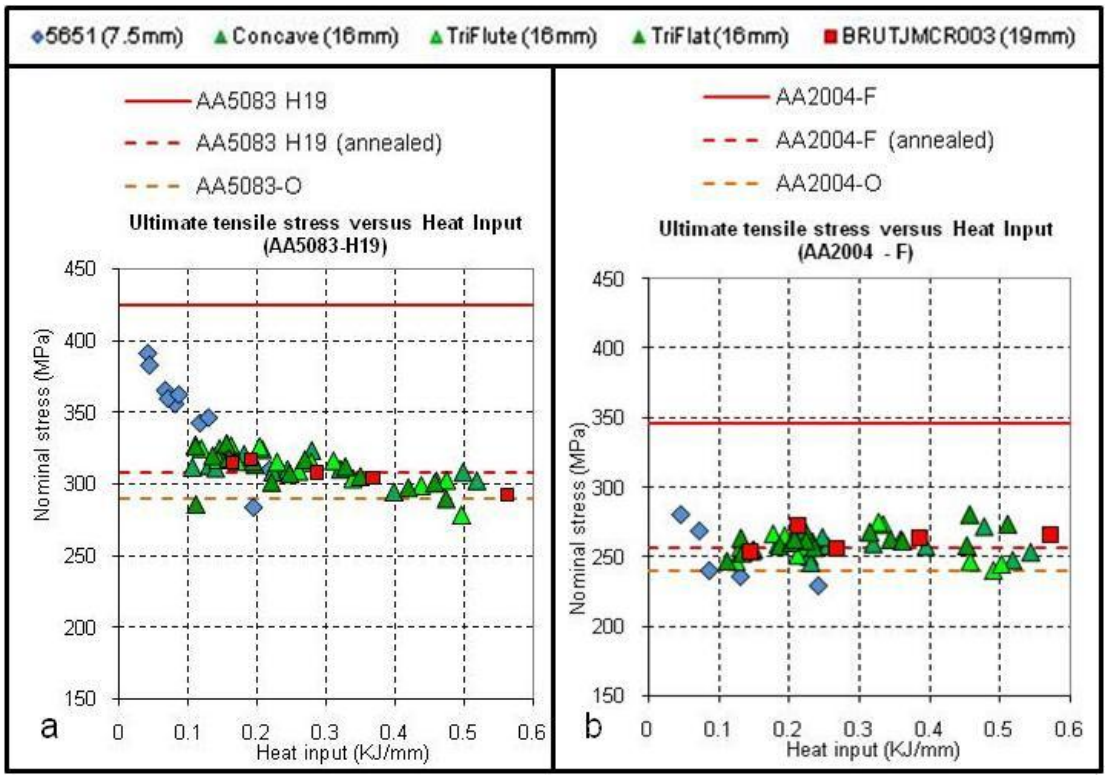

Figure 7.8, Ultimate Tensile Strength versus Heat Input. a) AA5083 (as-welded). b) AA2004 (as-welded).

The tensile test results are summarised as joint efficiencies in Table 7.4. It can be seen that the FSW process causes softening of the material within the tool footprint. The amount of softening is linked to the size of the tooling, the heat input into the weld and effectiveness of the probe in supplying heat and deformation to the bottom of the weld. The very different strengthening mechanisms of the alloys are a major factor in determining the success of the welds. From these results it can be said that the AA5083 accepts the FSW process better than the AA2004, but this is only in terms of room temperature response. The 5651 tooling group utilises a fluted and threaded probe and flatted and threaded probe, it is these features which increase the effectiveness of the tooling. The amount of heat supplied is enough to plasticise the material and makes welding possible, without completely softening the weld region. The concave tooling on the other hand has a very simple probe with no re-entrant features this means that weld closure is difficult; welds created using this group of tools yielded poor transfer of heat and deformation to the weld root. This is somewhat masked by the bead-on-plate configuration of the welding experiments. The smooth tooling profiles are unable to complexly annihilate the joint interface,

weakening the joint (butt welding); however as there is no joint interface in a bead-on-plate trial, the joint efficiencies are improved.

		AA5083			AA2004		
		Joint efficiency (%)					
Tool diameter (mm)	Tool group	Minimum	Maximum	Average	Minimum	Maximum	Average
19	Large shoulder	68.92	74.61	72.37	73.19	78.66	75.65
16	Concave	69.37	76.56	73.43	70.99	78.6	74.3
16	Triflute	65.67	77.32	73.96	71.46	81.05	75.88
16	Triflat	67.37	77.36	72.91	24.62	79.55	71.13
7.5	5651 Triflute	68.83	92.17	81.92	-	-	-
7.5	5651 Triflat	73.05	90.21	82.99	66.29	81.02	72.51

Efficiency = $Uts_{(Weld)}/Uts_{(Parent)} \times 100$

Table 7.4, Summary of As-welded Tensile Test Results: Joint Efficiency.

7.4.2.2 Tensile Test Results - Annealed Specimens

Tensile specimens from FW22 have also been tested in an annealed condition. A short annealing process has been carried out at 350°C for ~25 minutes. These specimens exhibit a pseudo formed condition. For annealed material it is expected that the weld region has a similar strength to the parent material. This is shown in Figure 7.9.a) where the AA5083 tensile results closely mimic those of the parent material results. Figure 7.9.b) shows the AA2004 results, it shows the tensile strength of the welds falling as the FSW heat input rises.

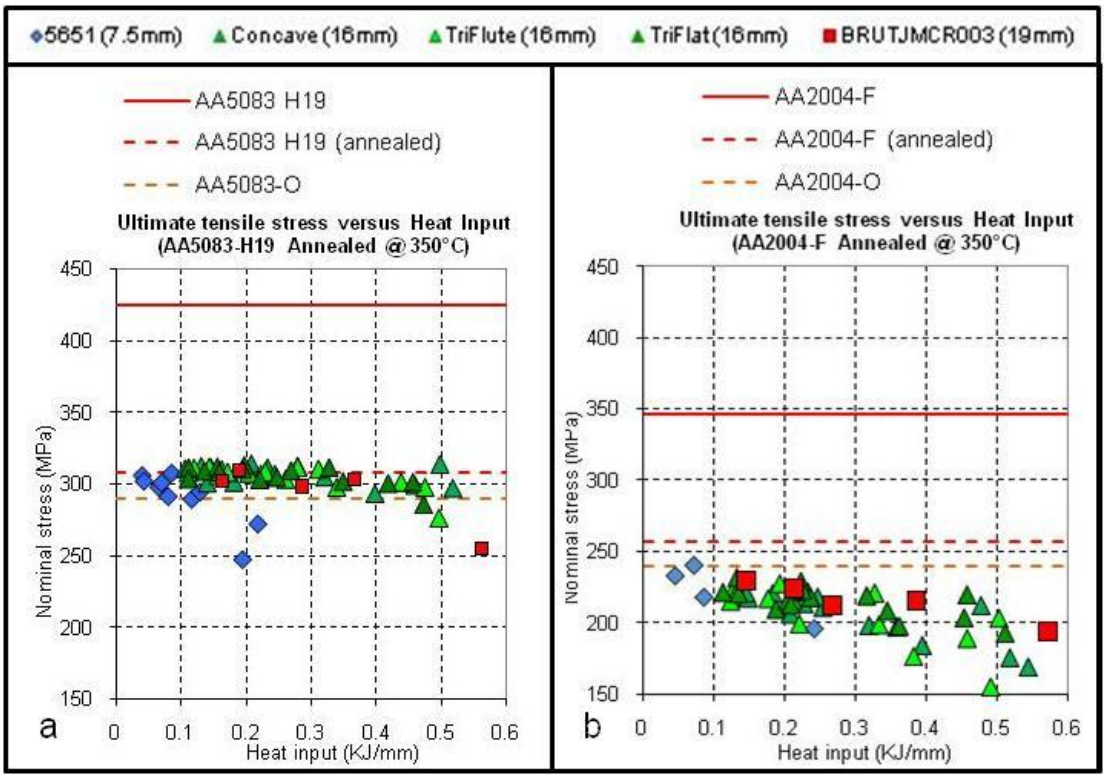

Figure 7.9, Ultimate Tensile Strength Versus Heat Input. a) AA5083 (annealed). b) AA2004 (annealed).

Material properties are affected by the microstructural stability of the material at elevated temperatures. From Figure 7.9 it can be seen that the FSWs react differently to the parent material when heated. Figure 7.9 a) shows the tensile results for the annealed AA5083 welds. This is non-heat treatable alloy and so resembles a fully annealed material. AA5083 statically recrystallizes at ~350°C. This ability to recrystallize without any introduction of deformation suggests that this alloy will start to recrystallize during the pre-heating stage of any superplastic deformation. Any microstructural instability is temporarily masked by the recrystallization at moderate temperatures. Once full forming temperatures, > 430°C, are reached the instability of the weld region will manifest itself in the form of recovery and abnormal grain growth. This is in contrast with Figure 7.9 b) which shows the response of the annealed AA2004. This material does not statically recrystallize; the presence of both heat and low levels of deformation, occurring during the early stages of SPF, are essential to dynamic recrystallization of this material. The heat response of the FSWs created in the AA2004 shows that there is induced instability in the microstructures of these welds. All of the welds produced a tensile strength which is less than the strength of AA2004-O. This suggests that the friction stir

welding process has produced a heterogeneous structure which is susceptible to grain growth during the pre-heat stage of the SPF process. This is highlighted by the drop in tensile strength as the FSW heat input increases; the hotter welds become more unstable.

		AA5083			AA2004		
		Joint efficiency (%)					
Tool diameter (mm)	Tool group	Minimum	Maximum	Average	Minimum	Maximum	Average
19	Large shoulder	95.11	99.59	97.65	75.53	89.50	83.79
16	Concave	95.11	101.99	99.45	66.00	89.03	80.35
16	Triflute	89.75	101.18	98.88	75.29	90.44	83.88
16	Triflat	92.67	101.60	99.19	60.23	88.56	80.68
7.5	5651 Triflute	80.20	99.23	92.87	-	-	-
7.5	5651 Triflat	88.25	99.78	95.81	76.46	93.72	86.10

Efficiency = $Uts_{(Weld)}/Uts_{(Parent)}x100$

Table 7.5, Summary of Annealed Tensile Test Results: Joint Efficiency.

This is further highlighted by the joint efficiency of the welds shown in Table 7.5. For the AA5083 the temperature response for the weld is very similar to that of the parent material producing joint efficiencies of around 100%. This is different to the response of the AA2004 where the efficiencies show that the strength of the welds is significantly lower than that of the parent sheet.

7.4.2.3 Vickers Microhardness

The hardness of a material is another indicator of the strength of the weld. A transverse hardness profile will also indicate the sizes of the different weld regions discussed in Chapter 4. Figure 7.10 a) shows the hardness profile of the AA5083 welds tested for hardness. The most striking trend is the minimal hardness loss within the weld region. Figure 7.10.b) shows a characteristic hardness plot for a friction stir welded, strain hardened material [12]. It is usually expected to exhibit a small reduction in hardness due to localized annealing and possible recrystallization within the weld nugget. This is the minima in the picture, the hardness will then return to the level of the parent material as it moves through the TMAZ which only contains partial recrystallization. AA5083 gains the vast majority of strength from solid solution hardening and cold work; it is not strengthened by second phase precipitation and so is not susceptible to dissolution or coarsening of these precipitates. The minimal drop in hardness is characteristic for the material but is not as defined in the hardness profiles as was expected. AA5083 statically recrystallizes

at ~350°C. In effect, as the tooling passes by the heat from the process should soften the material within the weld zone giving rise to the reduction in hardness. This is not the case, suggesting that the tool has a far greater influence than expected.

The same can be said of Figure 7.11 a) which shows the hardness profile for the AA2004. In the characteristic FSW hardness profile shown in Figure 7.11.b), a distinct 'W' shape is present. The weld nugget has undergone recrystallization and so is slightly less than the unaffected parent material. As the plot moves further away from the centre, through the partially recrystallized TMAZ, the hardness falls. The minima in this case represent the HAZ of the weld. AA2004's precipitation hardening mechanism means that the presence of heat without deformation will have detrimental effects on the microstructure. The heat from the tool will cause coarsening of the second phase strengthening particles which will in turn reduce the Zenner pinning of the structure and allow recovery and grain growth mechanisms. Once again the actual plots recorded do not match the literature for hardness profiles in similar precipitation hardened materials. The plot shows a trend that is very similar to the AA5083. The amount of softening is very similar for all the tooling and process parameters used. Regardless of the tool size and whether the weld is hot or cold the hardness drops to roughly the same level. The striking difference between the two materials is the amount by which it has dropped. From the profiles the AA5083 has dropped by only ~15% from the parent material value, this is small when compared to the ~25% drop for the AA2004. The FSW process has affected the hardness of the AA2004 more than that of the AA5083 which mirrors the effects seen in the tensile testing where joint efficiencies are lower for the AA2004 than the AA5083.

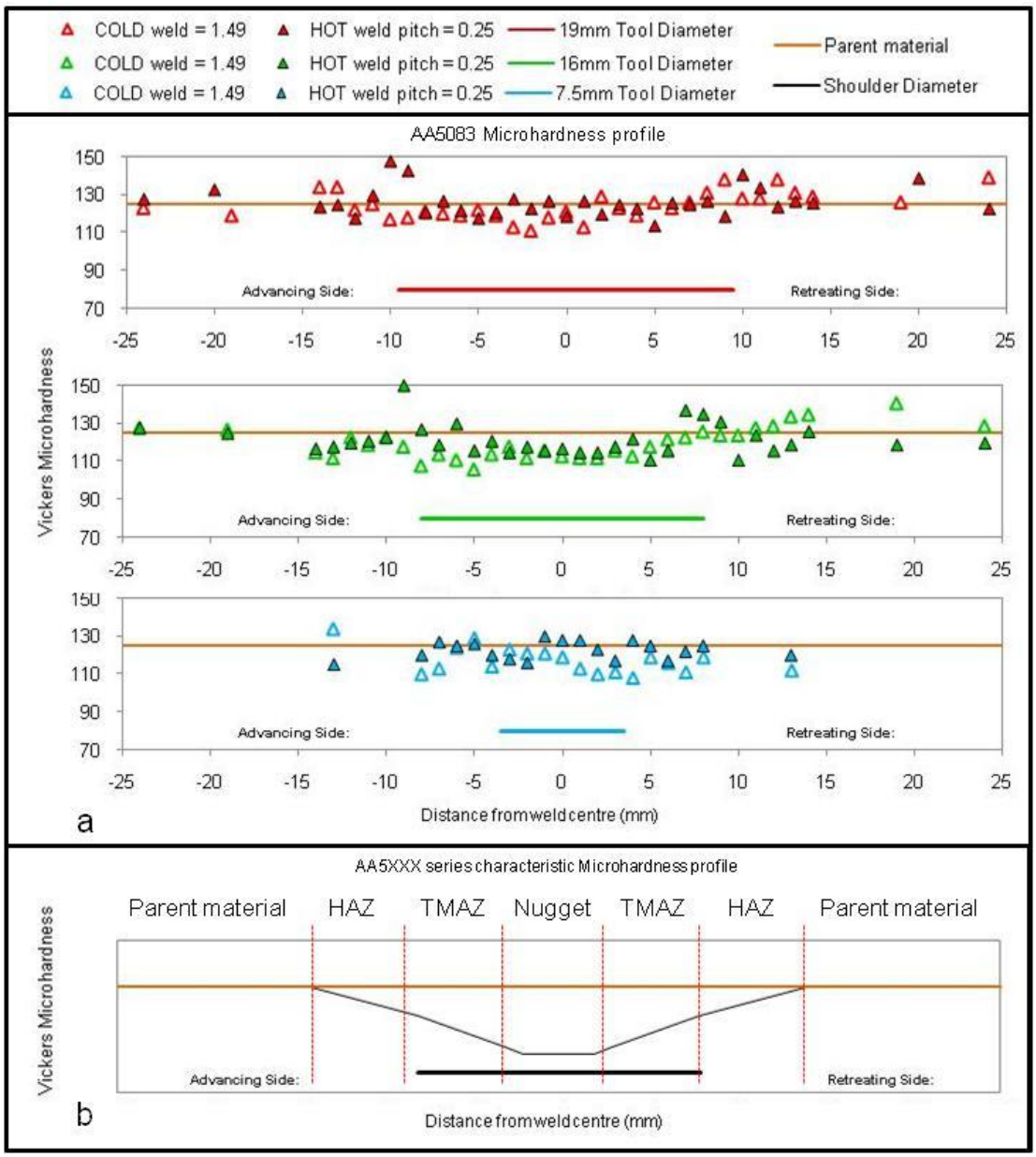

Figure 7.10, AA5083 Microhardness Profile, Vickers Hardness versus Distance from Weld Centre. a) 19mm, 16mm and 7.5mm tools, b) Characteristic Profile for 5XXX Series Aluminium Alloy, recreated from [12].

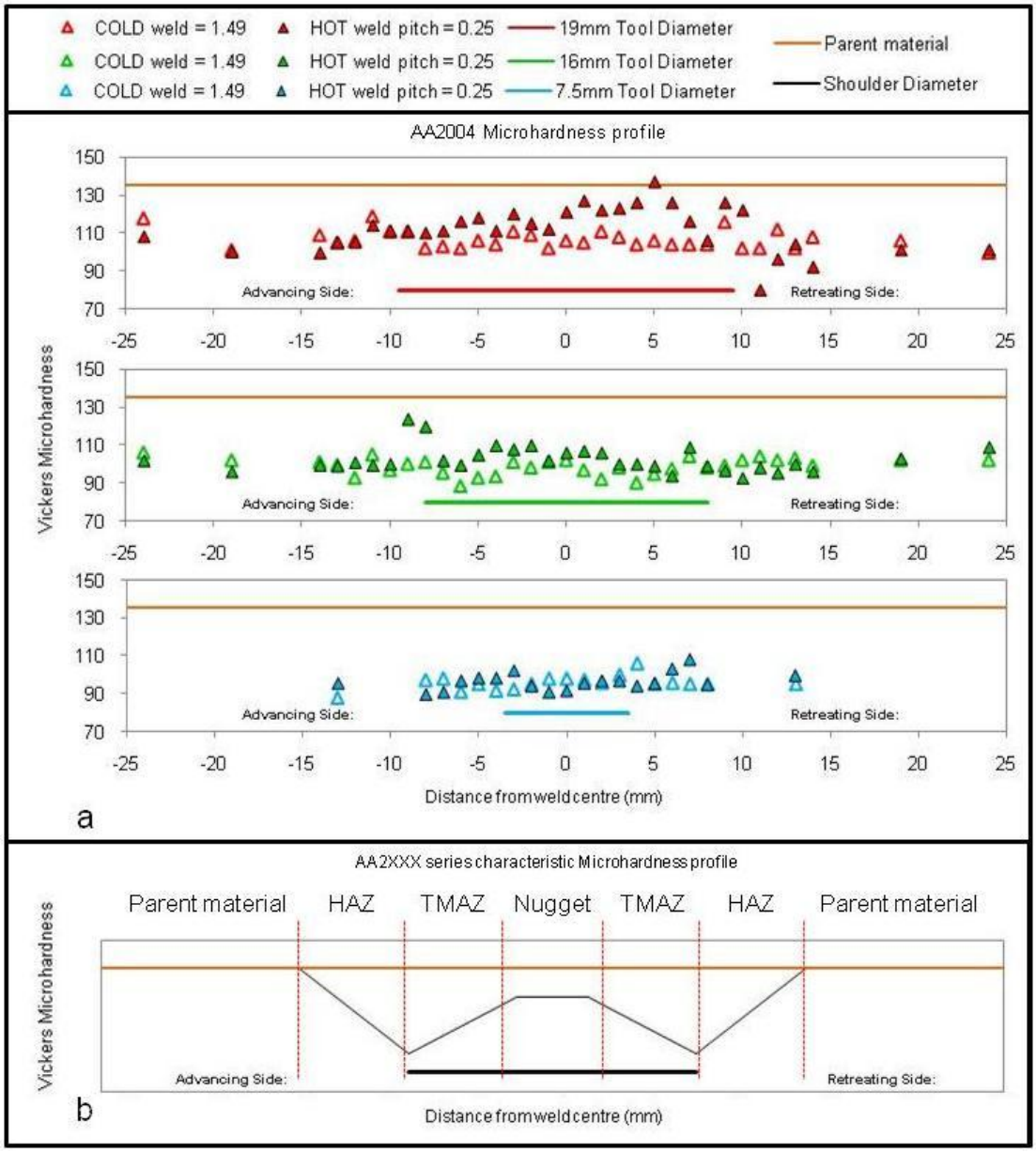

Figure 7.11, AA2004 Microhardness Profile, Vickers Hardness Versus Distance from Weld Centre. a) 19mm, 16mm and 7.5mm tools, b) Characteristic Profile for 2XXX Series Aluminium Alloy, recreated from [12].

7.4.2.4 Cone Testing

Cone tests require a square specimen ~200x200mm. The bead on plate welds created here are far too small for this test. Bead on plate welds have been recreated in a butt weld configuration with specimens measuring 200x330mm. These can be successfully cone tested but throw up many more issues with the setting up of the welds and general success of the welds. The butt configuration re-introduces the plunge depth issues highlighted in the Parkson milling machine welds. The recreated

welds used the cold welding parameters (500Rpm, 746mm/min and 1.49 mm/rev) and have been carried out using the 5651 tool (7.5 mm diameter), a simple concave tool (16mm diameter) and the large shoulder tool (19mm diameter). The setting up of the welding process is hampered by the manual plunge depth of this machine. Welds have been created and immediately tested for quality using the 180° bend testing with the root in tension. Although the welds passed the bending test it was feared that these welds would not survive the elevated temperature cone tests and would rupture when exposed to the gas pressures used during forming. One weld created by each tool was selected for a multiple pass welding trial where the FSW was carried out in two consecutive passes on the top surface and then again on the bottom surface. Both of the welding passes were carried out using the cold welding parameters (500rpm, 746mm/min) in order to minimise the heat input to the weld. This makes sure that there is sufficient bonding in the through thickness of the material and the removal of root defects so the welded specimen is able to withstand the forming process.

Table 7.6 shows the results of the elevated temperature cone test results for the welds created using FW22. Figure 7.12 shows pictures of the resulting cone test specimens. It is immediately clear that the single pass welds do not fare well in this test. Although more single pass welds were tested the two shown in Table 7.6 are actually the most successful of the single pass welds. The other omitted welds could not achieve gas pressure and so the test could not be completed. This further highlights the significant effects of root flaws in friction stir welds. The single pass welds have proven successful in bend testing but this is a uniaxial test pulling the weld root apart. Cone testing uses gas pressure to apply biaxial stress in the material. Any flaw in the weld root will be immediately exploited by the gas causing the weld seam to rupture. The double pass welds have been much more successful in maintaining pressure but there is still a major difference in success between the two materials used.

Figure 7.12.	Tool (Configuration)	Pitch (mm/rev)	Gas pressure (MPa)	Time to failure (Sec)	Failure description
a)	BRUTJMCR003 (DP)	1.49	0.276	137.92	Grain coarsening
b)	BRUTJMCR003 (DP)	1.49	0.207	59.27	Weld rupture
c)	GSP 5651 (DP)	1.49	0.552	2.0	Weld rupture
d)	GSP 5651 (S)	1.49	0.552	2.0	Weld rupture
e)	Concave005 (S)	1.49	0.552	1.0	Weld rupture

(S) – Single pas weld (DP) – Double pass weld

Table 7.6, Cone Test Results for Welds Created using FW22.

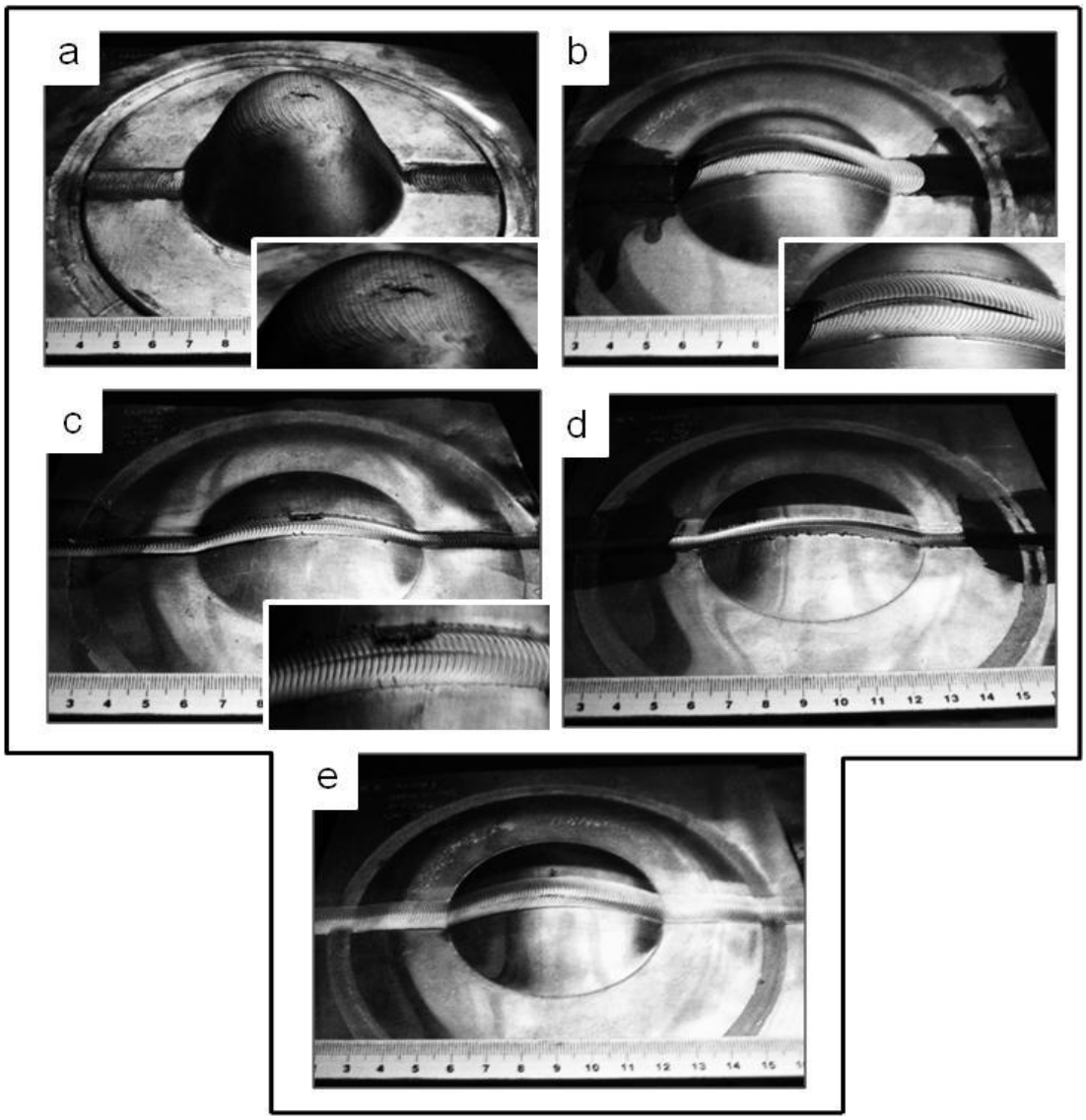

Figure 7.12, Cone Tested Specimens of Welds Created using FW22.

a) AA2004 – Double Pass (19mm tool), b) AA5083 – Double Pass (19mm tool), c) AA5083 – Double Pass (7.5mm tool), d) AA5083 – Single Pass (7.5mm tool), e) AA5083 – Single Pass (16mm tool).

The most significant aspect of this test is that only the AA2004 weld survived the gas pressure applied during the test. This weld shown Figure 7.12.a) formed to an equivalent superplastic elongation of ~260%. This specimen has a completely different failure mode to the other AA5083 specimens. This failure mode is grain coarsening. During SPF the material experiences heat and deformation, this gives the material energy for microstructural change and so the material goes through recrystallization, recovery and grain growth mechanisms. The friction stir weld in these specimens is an introduced heterogeneity in the parent material. The differing structure of the weld causes the recrystallization, recovery and grain growth mechanisms to act differently on this material compared to the surrounding parent material. It can be seen from the photo in Figure 7.12 a) that the weld material has begun coarsening well before the parent material to the extent that the grain structure of the FSW has grown to such proportions that individual grain can be seen with the naked eye; this effect is sometimes referred to as the "orange peel" effect.

The AA5083 welds created for this test were unable to survive the SPF process in both a single and double pass operation. The smallest tool (7.5mm) was tested in both single and double pass operations, but both failed in the same way; weld rupturing when subjected to gas pressure. AA5083 is commercially available structural aluminium alloy which is specially processed to provide a microstructure capable of superplastic elongations. This level of superplasticity is far less than AA2004 which is a specifically designed SPF alloy. In the case of the AA2004 it seems that the weld material begins to deform before the parent material causing the weld material to stretch with the parent material constraining this deformation at the extremities of the weld; this can be seen in Figure 7.12.a) where the deformation is localized within the weld region. For the AA5083 however it is evident that the weld material has become undeformable under these conditions in a similar way to conventional fusion welds [80]. The parent material begins to deform first but the weld material resists the deformation and is pulled apart by the stretching parent material.

FW22 has successfully created FSWs in aluminium which can be subjected to subsequent SPF processes. However, every pass completed by the FSW tool changes the microstructure so a double pass weld will have experienced more disruption and

more deformation and heating phenomena than a single pass weld. This machine was unable to create successfully formed welds in a single pass operation. This is again due to poor bonding in the weld root and an inherent flaw in the weld root. The method by which the plunge depth is set is difficult to improve without serious modification to the machine. A superior, state of the art FSW machine has been selected in order to create the most successful welds possible. This machine is an ESAB SuperStir machine. This programmable 5 axis machine is far more accurate and reliable for constraining all the process parameters and weld variables such as the plunge depth.

7.4.3 ESAB SuperStir

A much smaller selection of weld parameters have been tested on the ESAB SuperStir machine. The selection has been based on the tensile test, cone test and microstructural observations from the bead on plate and butt welds created using FW22. The use of this machine has also enabled faster spindle and traverse speeds to be used. The welding pitch has remained close to the values used for FW22 but both the spindle speed and feed speed have been increased. This increase in spindle speed is based on experimental data from TWI which shows that 2XXX series aluminium alloys respond better to higher spindle speeds [30]. To prevent the higher spindle speeds from completely overheating and destroying the SPF microstructure the welding speed was also increased.

7.4.3.1 Tensile Test Results

The first most noticeable fact from the ESAB tensile results is that the ultimate tensile strength of the butts welds made on the ESAB machine are very similar to the strength of the bead on plate welds created on FW22 given the same size tools, this is shown in Figure 7.13. The 5651 (7.5mm) tool was not used on the ESAB machine but it is hypothesised that the results would be similar to those produced as bead on plate joints on FW22. It can also been seen that the welds produced resemble the strength of annealed material indicating further that the FSW process acts as a localized annealing process in the wake of the tool as it traverses the joint line.

The ESAB SuperStir machine can effectively reduce the chances of plunge depth related flaws by using position control. The programmable nature of the machine

means that once satisfactory set up; welds produced to the same quality can be assured for subsequent welds. Two tools were used on this machine, the simple concave tool Concave005, and an MXTriflute™ tool provided and modified by TWI. The MXTriflute™ tool is 15mm in diameter, has a concave shoulder profile and 5mm diameter, threaded and fluted probe. The comparison between the tools sheds light on the plunge depth issues experienced before. Even with the dramatically improved accuracy of the plunge depth, the few welds created on the ESAB machine using the simple concave tool still exhibit flaws in the weld root and fail the bending tests. This can now be attributed to the simple and smooth profiles of the shoulder and probe for this tool. The lack of threads and re-entrant features on the probe limits the amount of deformation occurring in the weld root, poor interface breakup results and poor joint properties are inevitable. Swapping this smooth tool for the MX TriFlute tool instantly improves results. The welds pass the bending test and provide tensile strengths which are similar to bead on plate results. Tensile test results for the welds created used the MXTriflute™ tool are shown in Figure 7.13.

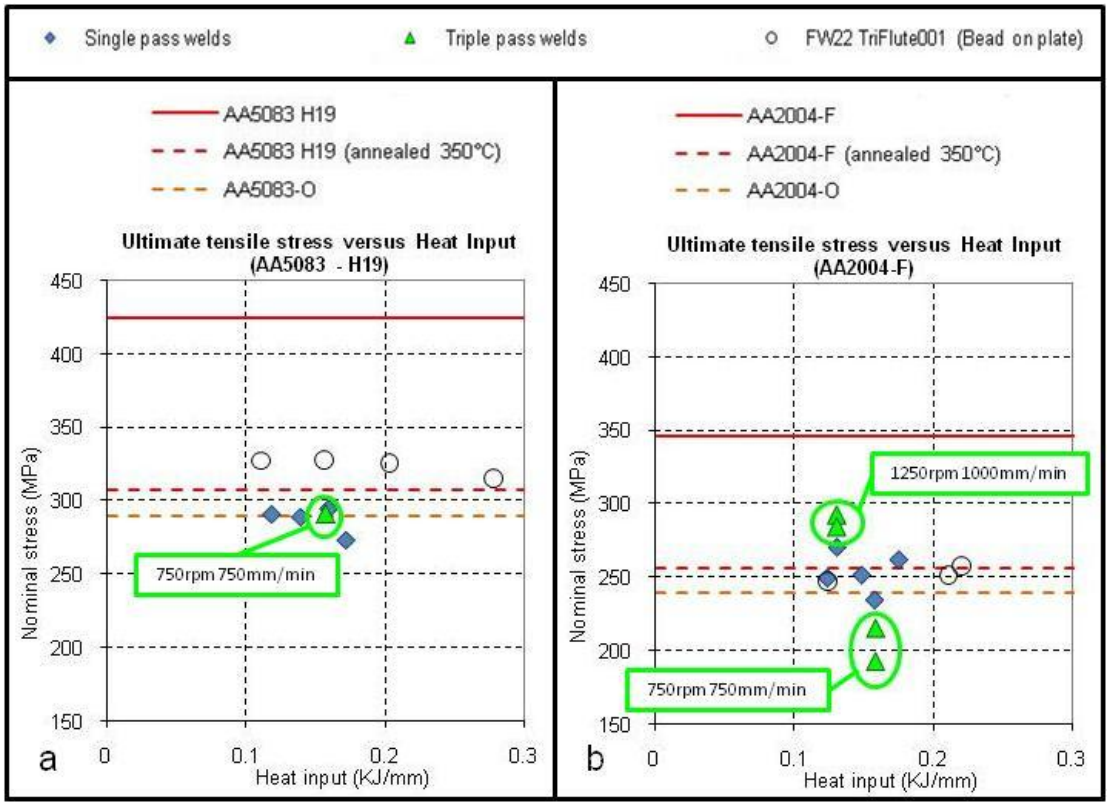

Figure 7.13, Ultimate Tensile Strength Versus Heat Input for Welds Created on the ESAB SuperStir FSW Machine: a) AA5083, b) AA2004.

Triple pass welds have also been created using the ESAB machine. For these welds all three passes are carried out on the top surface, the passes are spaced 5mm apart which coincides with the diameter of the tool's probe. This has created welds with a tool footprint of 25mm, this larger footprint means more FSW material and will act as a friction stir processed material. Figure 7.14 shows a schematic diagram of the overlapped pass configuration.

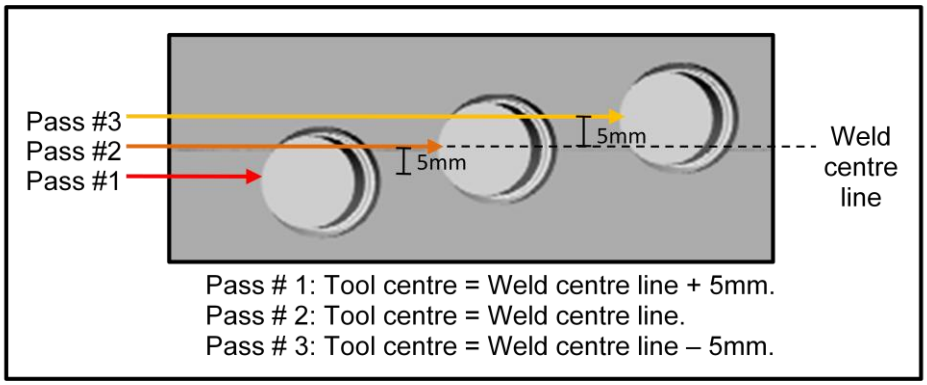

Figure 7.14, Schematic Diagram of the Overlapped Passes of the Multiple Pass FSWs Created on the ESAB SuperStir machine.

7.4.3.2 Cone Testing

Cone testing has been carried out on all the welds completed using the ESAB SuperStir machine. All the specimens have been tested with a gas pressure of 0.138 MPa (20 psi) and a temperature of 460°C. Figure 7.15a-e) shows the results for the cone tests of butt welds created in AA5083 on the ESAB machine.

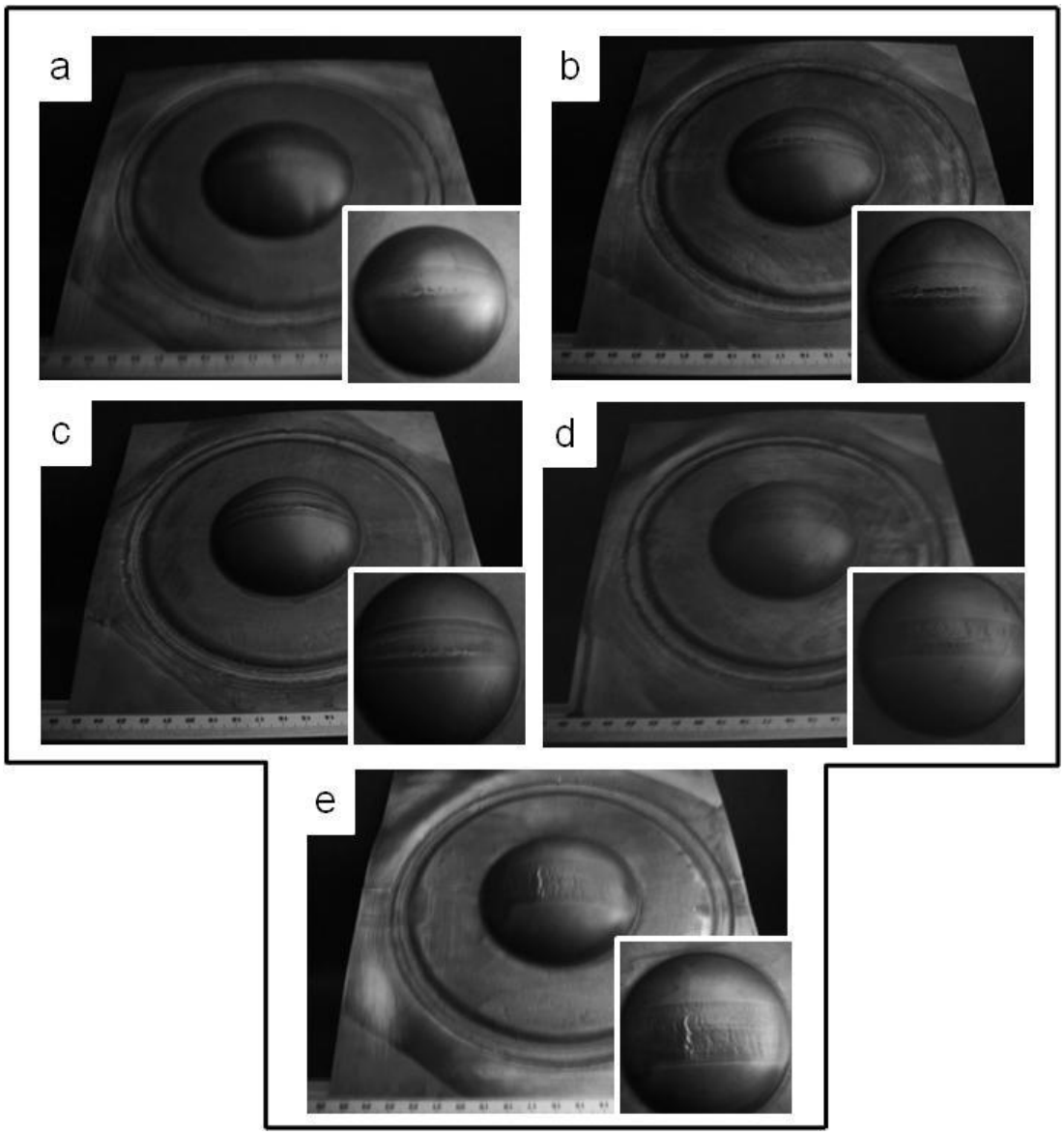

Figure 7.15, AA5083 Cone Test Results (ESAB SuperStir).

a) Single Pass: 1250 Rpm/1250 mm/min, b) Single Pass: 1250 Rpm/1000 mm/min,

c) Single Pass: 1250 Rpm/750 mm/min, d) Single Pass: 750 Rpm/750 mm/min,

e) Triple Pass: 750 Rpm/750 mm/min.

Figure 7.15	Weld pitch	Configuration	Time (sec)	Pole Thickness (mm)	SPF Strain	Failure description
a)	1	1 pass	810	0.844	72%	Grain coarsening, Parallel to joint interface.
b)	0.8	1 pass	1020	0.772	79%	Grain coarsening, Parallel to joint interface.
c)	0.6	1 pass	1103	0.97	63%	Grain coarsening, Parallel to joint interface, separation of weld regions.
d)	1	1 pass	920	1.28	47%	Grain coarsening, Parallel to joint interface.
e)	1	3 pass	790	1.18	51%	Grain coarsening, Perpendicular to joint interface.

Table 7.7, AA5083 Cone Test Results.

The modes of failure and forming time for the AA5083 welds are shown in Table 7.7. It is clearly visible that all of the single pass welds share the same failure mode. The weld material is heterogeneous this means that there will be differing levels of structure coarsening within this region. This is highlighted by Figure 7.16.a) where the weld region has separated, parallel to the welding direction, clearly defining the nugget and TMAZ regions. The nugget consists of recrystallized material; the TMAZ consists of partially recrystallized material, this means that the weld region will coarsen at different rates. This has led to the failure of the specimen at the nugget/TMAZ interface. This is the same for all the single pass welds. The triple pass weld however, has a different failure mode. This weld has failed perpendicular to the weld direction which may be related to the semi-circular bands of material characteristic to the FSW process. Figure 7.16.b) shows a detailed photo of the AA5083 triple pass weld.

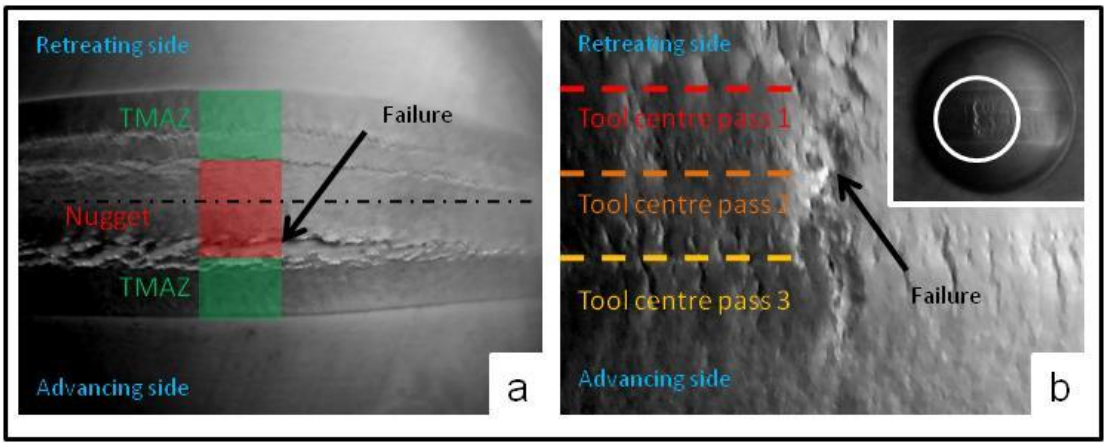

Figure 7.16, Detail of the Failure Mode for Cone Tested AA5083 Specimens: a) Single Pass 1250rpm/750mm/min, b) Triple Pass 750rpm/750mm/min.

The triple pass FSW has undergone three overlapping friction stir welding processes. This means that pass 1 has experienced more heat and deformation from the successive FSW passes, pass 2 has also experienced the extra heat and deformation from pass 3. This has produced a weld region which is 25mm wide with a weld nugget ~15mm wide. Each of the passes has affected the weld region and accounts for the accumulated deformation, heat and ultimately softening of the weld material. The tensile results for the triple pass butt weld (750rpm/750mm/min) show that this weld material has undergone significant softening. The welding process has successfully annihilated the joint interface preventing the FSW microstructure from failing parallel to the welding direction. It is visible from Figure 7.16 that the failure is due to the coarsening of the weld region, this in turn may be related to the FSW's banded microstructure, perpendicular to the weld direction and situated in the weld centre between passes 2 and 3.

The friction stir welds in AA2004 react to the cone test in a very different way. The weld material deforms more readily than the parent material and has undergone superplastic deformation. In each cone test specimen the failure site is located on the advancing side of the weld nugget further highlighting the heterogeneous nature of friction stir welded microstructure. The triple pass weld did not complete the cone test to failure; so it is unsure what the final failure position and extent of the superplastic deformation would be. Figure 7.17 a-e) shows the AA2004 cone tested specimens of the butt welds created on the ESAB machine, with inset pictures of the

failure location. The first most noticeable point is the similarities between all of the AA2004 samples. It can be seen that the weld regions have all undergone extensive deformation, with the weld region stretching more than the parent material. The next most significant point is the location of the failure. Each specimen, with the exception of the triple pass weld, failed on the advancing side of the weld region parallel to the welding direction. This suggests coarsening of the weld microstructure and eventual separation of the interface between the weld nugget and TMAZ regions. The nugget and TMAZ have coarsened at slightly different rates during the process due to heterogeneous microstructures created during FSW. It should also be noted that none of the cone tested welds failed alone the original joint interface.

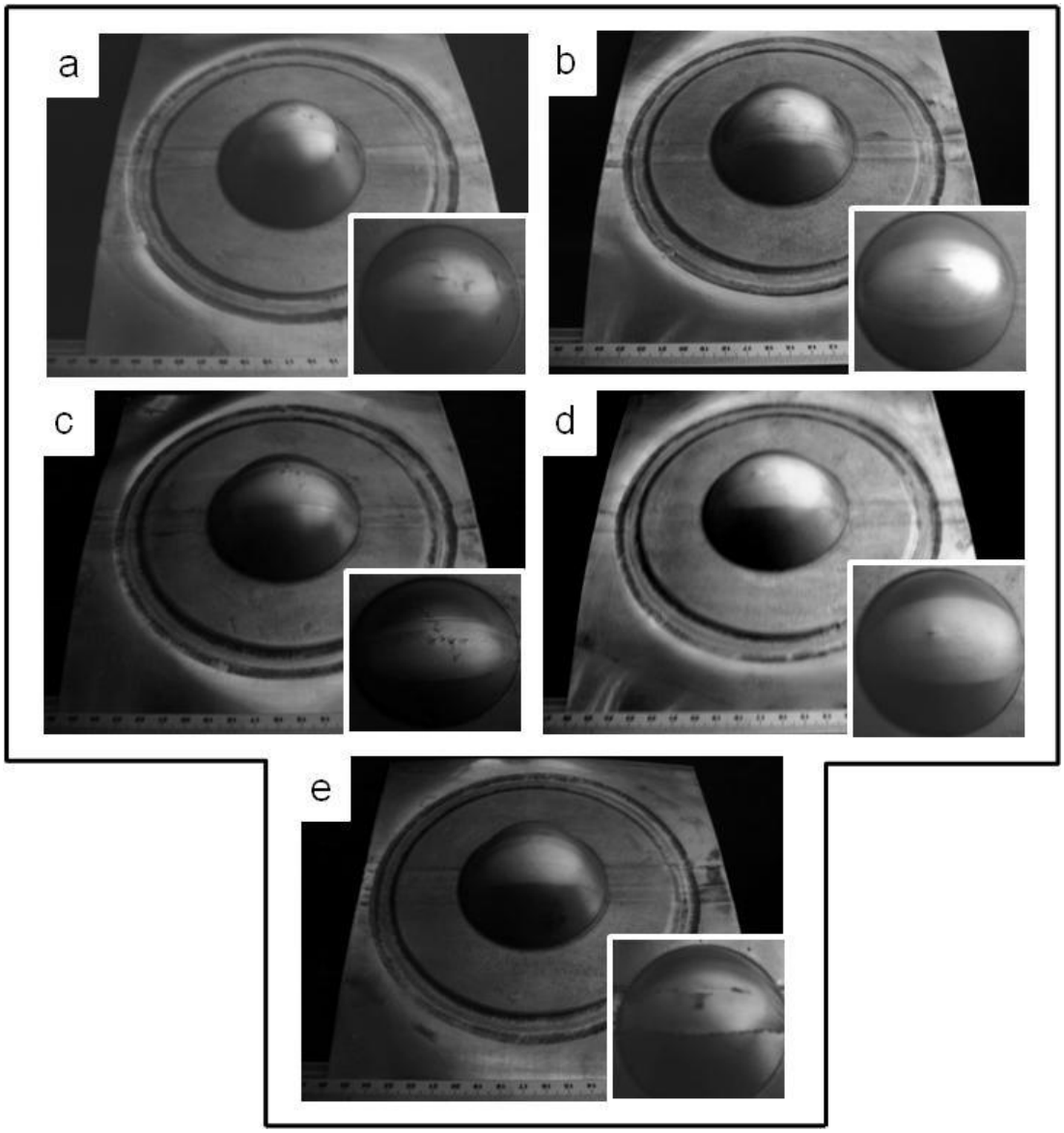

Figure 7.17, AA2004 Butt Welded Cone Test Results (ESAB SuperStir)
a) Single Pass: 1250 Rpm/1250 mm/min, b) Single Pass: 1250 Rpm/1000 mm/min,
c) Single Pass: 1250 Rpm/750 mm/min, d) Single Pass: 750 Rpm/750 mm/min,
e) Triple Pass: 750 Rpm/750 mm/min.

Table 7.8 summarizes the AA2004 butt welded cone test results. The most successful weld has been carried out in a single pass operation using a welding pitch of 0.8mm/rev. This weld has produced an equivalent superplastic strain of 210%. There is no real trend between the weld pitch and the resulting SPF strain. However it can been seen that increasing the spindle speed from 750rpm to 1250rpm, whilst maintaining the weld pitch, improves the results and enable SPF strain of approaching 200%.

Figure 7.17	Weld pitch	Configuration	Time (sec)	Pole Thickness (mm)	SPF Strain	Failure description
a)	1	1 pass	613	0.306	199%	Grain coarsening, Advancing side.
b)	0.8	1 pass	540	0.29	210%	Grain coarsening, Advancing side.
c)	0.6	1 pass	400	0.46	130%	Grain coarsening, Advancing side.
d)	1	1 pass	350	0.42	143%	Grain coarsening, Advancing side.
e)	1	3 pass	360	0.7	87%	No failure

Table 7.8, AA2004 Butt Weld Cone Test Results.

The bead on plate experiments carried out on the ESAB SuperStir machine reveal the same failure locations as the butt welded specimens; parallel to the weld direction on the advancing side of the weld. Further supporting the notion that the failure is a result of differing rates of microstructural coarsening between the weld nugget and neighbouring TMAZ; causing the failure at the interface between the two regions. Figure 7.18 a-d) shows the difference between the bead on plate single and triple pass welds in an as-welded and surface finished condition. The scalloping marks have been removed from for the surface finished specimen and the top surface smoothed and polished to a 9µm finish. Both the single and triple pass welds experienced a very small drop in performance for the surface finished specimens. This drop in performance is not considered to be significant. Surface finishing can therefore be carried out between the FSW operation and the subsequent SPF operation to remove the characteristic scalloping marks left by the process and enabling a high class surface finish for the formed material.

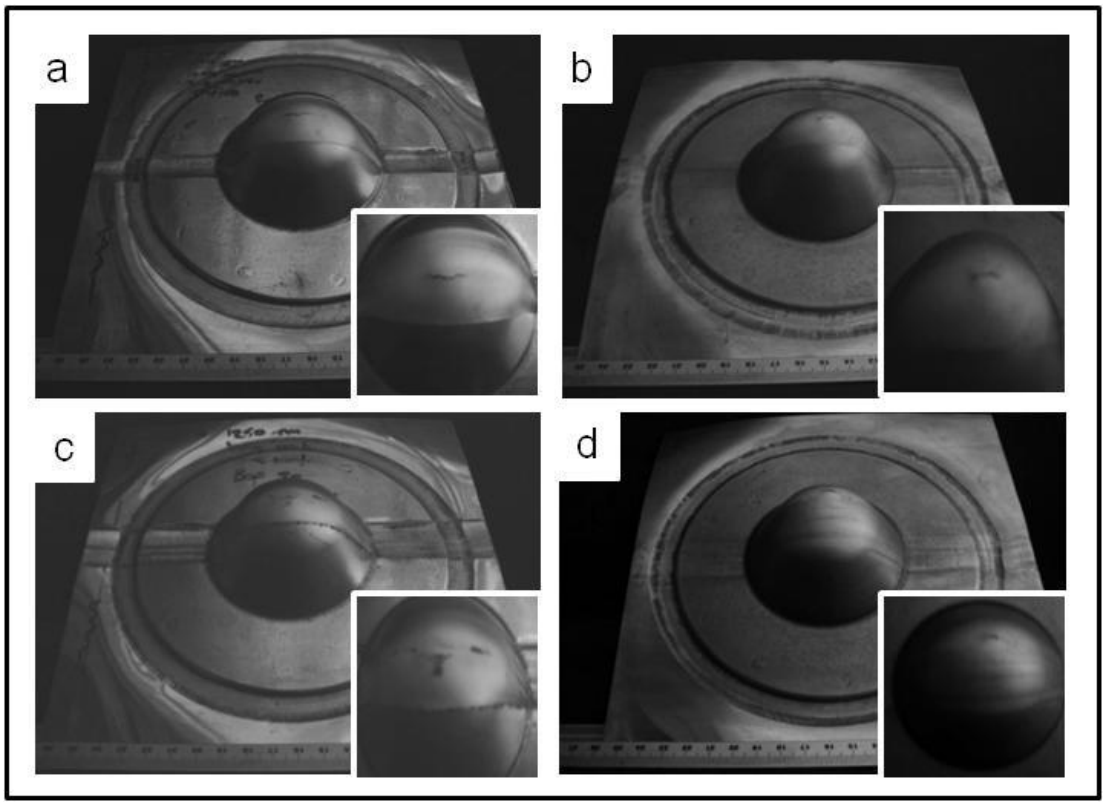

Figure 7.18, AA2004 Bead on Plate Cone Test Results.
a) Single Pass: 1250 Rpm/1000 mm/min-As welded, b) Single Pass: 1250 Rpm/1000 mm/min-Surface Finished, c) Triple Pass: 1250 Rpm/1000 mm/min-As welded, d) Triple Pass: 1250 Rpm/1000 mm/min-Surface Finished.

Table 7.9 shows a summary of the bead on plate cone test results. The equivalent SPF strains for these specimens are significantly lower than the butt welded counterparts. The most significant difference between the two sets of the results is the thickness of the material. The bead on plate material is only 1.2mm thick. The tool used to create the 1.6mm thick welds has been modified for use on this material. The probe length has been altered but the rest of the geometry remains the same effectively increasing the ratio of probe length to probe diameter. The use of this tool on this material has not been very effective, producing welds that fall well short of the 200% equivalent strain required to be deemed superplastic.

Figure 7.18	Weld pitch	Configuration	Time (sec)	Pole Thickness (mm)	SPF Strain	Failure description
a)	0.8	1 pass, As welded	225	0.294	71%	Grain coarsening, Advancing side.
b)	0.8	1 pass, Surface finished	275	0.3	70%	Grain coarsening, Advancing side.
c)	0.8	3 pass, As welded	240	0.29	83%	Grain coarsening, Advancing side.
d)	0.8	3 pass, Surface finished	250	0.3	75%	Grain coarsening, Advancing side.

Table 7.9, AA2004 Bead on Plate Weld Cone Test Results.

It should be noted that the pole thickness is the same as those produced in the 1.6mm material suggesting that this is the limit for the FSW material created using this tool. During the SPF process the microstructure is undergoing intense deformation and at the same time microstructural change including grain growth. When grains grow the strength of the material is reduced until failure occurs. Regardless of the original thickness of the material the pole thicknesses for the AA2004 FSWs fall in the range of ~0.3 to 0.5mm.

7.5 Summary

This chapter has described the results from mechanical property tests and formability tests carried out on AA5083 and AA2004 friction stir welds in butt weld and bead on plate configurations. Details of welding forces, spindle torque and heat input is included with visual observations to assist the assessment of the welds themselves and the quality of the resulting microstructures for subsequent SPF operations.

The results have proved that superplastic deformation is observed in friction stir welded material across a complete transverse section of the weld. That is to say, the tests include material from the weld nugget, TMAZ, HAZ and parent material. The observed results show a heterogeneous structure throughout the weld giving rise to differing levels of microstructural change within different regions of the weld. Although superplastic deformation has been observed this is significantly limited due to the different magnitudes of structural change occurring in the weld. It is impossible to introduce a weld into the parent material without suffering from some

kind of heterogeneous structure which may result in premature failure of the specimen within the weld region. The weld region is an induced heterogeneity. The weld region undergoes the same microstructural changes as the parent material but at different rates and from a different starting point. The parent material undergoes a change from heavily strained, elongated grains to an equiaxed structure during the initial stages of the SPF process. For AA5083 this occurs as static recrystallization in the preheat stage; for AA2004 this occurs as dynamic recrystallization during the initial stages of forming. The FSW process produces a dynamically recrystallized weld nugget and a partially recrystallized TMAZ. This region is already in a recrystallized state and so chronologically is further into the superplastic microstructural change sequence than the parent material. For the AA5083 the recrystallized grains begin to coarsen rapidly and become undeformable. The weld material acts as an undeformable block, much like a fusion weld, which is eventually pulled apart by the deforming parent material causing a rupture type failure. The AA2004 however acts in completely the opposite way. As the weld material is already recrystallized it forgoes the transformation stage of the parent material and immediately begins to deform. The weld region forms before the parent material and is stretched to failure.

8 Metallographic techniques and microstructural analysis

8.1 Introduction

Welds from the AA5083 and AA2004 have been selected for metallographic analysis based on their performance in the tensile and cone tests. Improper care in sample preparation can lead to misleading analysis as the true microstructure may not be revealed. Henry Sorby developed the first successful preparation technique by understanding the importance of removing all the surface deformation. All the welds selected for metallographical investigation have been prepared using standard material sample preparation techniques, which have evolved from Sorby's methods [95], and experimental techniques designed to improve the crystallographic information received from Electron Back-Scatter Diffraction (EBSD) techniques. Chapter 8 outlines these techniques from mounting the specimen to the final picture.

To reveal the true microstructure of a material the following points must be observed during the specimen preparation. Deformation must be completely removed or shallow enough to be removed by an appropriate etchant. Deformation can be implanted into the surface of the specimen by sectioning, grinding and polishing. The severity of the deformation affects how far into the surface the effects of the deformation can be found. Induced deformation falls into two categories, gross deformation and plastic deformation. Figure 8.1 shows the different types of deformations. The gross deformation may be visible before surface preparation and can be attributed to the method used to remove the sample from its original surroundings and the planar grinding steps. The plastic deformation is hidden by the gross deformation and is complementary to it. For successful specimen preparation all the stages of deformation must be removed or reduced to a negligible level.

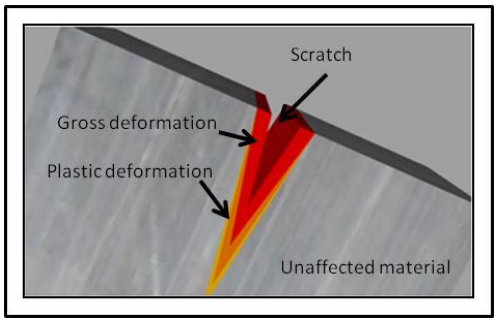

Figure 8.1, Schematic View of Gross and Plastic Deformation.

Non-standard techniques such as EBSD have been used in this study as a routine method for determining the grain structure of the welded material. The material preparation steps must be closely adhered to and meticulously followed to ensure successful maps are acquired. The effects of any underlying deformation in the sample are exacerbated by EBSD. Poor Kikuchi patterns [96] arise from deformation and residual stresses within the structure giving rise to inaccurate or incomplete mapping of the specimen. Techniques such as ion beam thinning [96] have been trialled along with modifications to existing metallography to ensure high quality EBSD patterns.

8.2 Sampling, Sectioning and Specimen Preparation

Metallographic analysis is an experience based practice, many guides to specimen preparation give a basic and universal approach to this science; however each material is different and may require alterations to certain preparation steps in order to produce the correct images. The list below briefly describes the different stages of sample preparation, the main steps will be expanded to discuss the modifications made to ensure a quality surface finish and correct imaging of the aluminium alloys AA2004 and AA5083 investigated in this thesis [95].

1. **Sampling** - Choosing the specimen.
2. **Sectioning** - Removing the area of interest.
3. **Encapsulation** – Mounting the specimen.
4. **Grinding and polishing** - Removing all the deformation to provide a deformation free surface.
5. **Initial visual examination** - Preparation quality assessment.
6. **Etching** - Highlighting of specific material characteristics.

7. **Visual examination** - Microstructural interpretation.
8. **Quantitative metallography** - Obtaining data from the prepared specimen.
9. **Data interpretation** - Drawing conclusions from data.

8.2.1 Metallography

The sampling of Friction Stir Welds for this project is driven by quality control and failure analysis. The welds are completed and tested for their mechanical properties such as tensile strength and formability. From these results successful and failed welds can be highlighted and selected for metallography. For example the most successful welds and the least successful welds can be compared to ascertain the origins of the deviations (quality control). Another example is analysis of welds which failed during the process. Welds have been produced which have failed during the FSW process due to improper welding parameters or conditions, the exact nature and origin of the failure can be identified and steps taken to rectify the failure for subsequent processes (failure analysis).

8.2.2 Sectioning

Once the desired area has been identified it must be removed from the bulk of the material with as little damage to the sample as possible. Any deformation which occurs during this step will be significant and will require a more prolonged planar grinding stage to rectify. Aluminium is a soft material and so must be sectioned carefully. The use of a guillotine is ruled out due to the crushing effect of the clamping and shearing action which accompanies it. In this study the material has been carefully removed from the friction stir welds using a standard hacksaw, which generates less deformation. The section to be removed can only be analysed in relation to its original position within the bulk material so care must be taken to document this. Figure 8.2 shows a schematic of the different orientations of sections taken from different locations within a material.

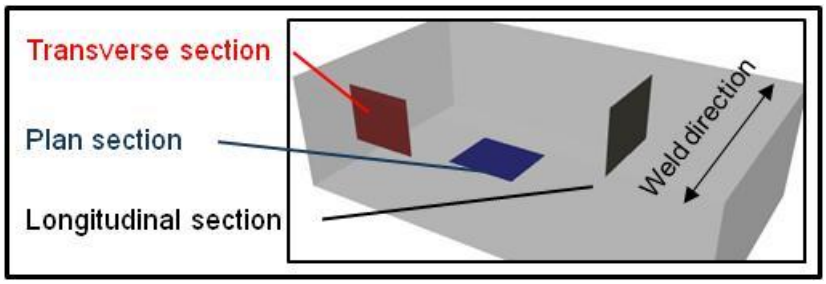

Figure 8.2, Schematic View of Different Sectioning Planes.

8.2.3 Mounting

Hot compression mounting is the most common method and is preferred for rigid specimens that can withstand the heat and pressure required for this mounting technique (150°C, 4200 psi). The resin used for this project is a thermosetting phenolic resin due its low cost and satisfactory properties. The mould is pressurised to a pre-load pressure while a heater is placed over the mould to soften the resin, this requires a temperature of 150°C. Once the resin has completely softened the pressure within the mould is increased to 4200psi. The mould is then left to cure under pressure and high temperature, in this case for around 10-15 minutes. Once the resin has been cured the heater is removed and the mould is cooled under pressure for around 20 minutes. Cooling under pressure reduces the amount of shrinkage experienced by the resin.

8.2.4 Grinding

The initial purpose of the grinding stage is to produce a flat, planar surface on which the subsequent grinding and polishing stages can be based. The first grinding stage also removes the damage inflicted by the sectioning of the sample. Grinding is usually carried out in four or five stages depending on the material being prepared. Each step of the grinding procedure will create damage on the surface of the specimen, but as the abrasive size decreases with each step the subsequent damage is slowly removed. A four stage grinding procedure has been carried out on the specimens to firstly make sure the sample is flat and secondly to remove the damage inflicted by sectioning in carefully controlled manner Table 8.1 shows the grinding steps used. The procedure initially used silicon carbide papers ranging from 240 to 1200 grit numbers. This has been modified, removing the coarser 240 grit paper in exchange for the planar grinding stage being carried out using P400 and the final

grinding stage being carried out with P2500. This has increased the quality of the surface finish for the soft aluminium increasing the success of subsequent polishing, etching and eventually EBSD procedures.

Grinding Stage	FEPA Grit Number	Abrasive size (μm)	Time (minutes)	
1	P240	52	Until flat	
2 (1)	P400	34	1:00	(Until flat)
3 (2)	P600	23	1:00	(2:00)
4 (3)	P1200	15	2:00	(3:00)
(4)	P2500	7	2.00	(3:00)

Table 8.1, Four Stage Grinding Procedure for AA2004 and AA5083 Samples.

8.2.5 Polishing

With the grinding stage complete there is still damage to the surface which is visible to the naked eye. This deformation must be completely removed before successful analysis of the specimen can take place. Just as the grinding stage before it, polishing is carried out in stages using consecutively finer grades of abrasives. The abrasive is polycrystalline diamond suspended in a paste. This paste is applied to a napless or low nap cloth where free abrasion takes place. Coarse, intermediate and final polishing stages are usually required to create a defect free, mirror like finish. Table 8.2 shows the four polishing stages used for the preparation of the aluminium used in this study.

Polishing Stage	Abrasive type	Abrasive size (μm)	Time (minutes)
1	Diamond paste	6	5.00
2	Diamond paste	1	5.00
3	Diamond paste	0.25	3.00
4	Colloidal silica suspension	0.04	5.00-10.00

Table 8.2, Four Stage Polishing Procedure for Aluminium.

Colloidal silica is used for the final polishing because of its ability to produce a chemical and mechanical polishing action. The abrasive particles are nearly spherical in shape meaning the rate of material removal is very slow, hence the longer polishing time. Colloidal silica produces damage free surfaces far more easily than abrasives like alumina, and etchants respond better to surfaces polished in this manner.

8.2.6 Etching

There are two different types of etching; chemical etching and electrolytic etching. Etching is essentially a selective corrosion used to highlight certain microstructural aspects of the sample. Some features such as voids, porosity, cracks, discontinuities, non-metallic inclusions and corrosion products can be viewed in the as polished stage. However greater detail about the structure can be revealed using a suitable chemical etch. Etching the sample selectively attacks or colours areas of the structure, revealing features by producing visual contrast. These details include grain boundaries, material flow, phases, constituents, coring, layer interfaces, heat affected zones, reaction zones, depletion zones, dendrite patterns, segregation and precipitates. A complete list of all the etchants used for the preparation of the aluminium can be found in Table 8.3.

8.2.6.1 Chemical Etching

The sample is swabbed or immersed in a suitable etchant solution. The selective dissolving of the material does not require any electrical current and is based on the different dissolution rates of the different grain orientations or chemistry within the structure. Swabbing is the preferred method of application, however if the etchant works by creating a coloured film, then immersion must be used as swabbing will stop the film from forming. Etching begins by selecting a suitable etchant from a very long list possible chemicals and solutions. Strict laboratory safety conditions must be adhered to as most of the constituents of etchants are damaging or harmful.

8.2.6.2 Electrolytic Etching

The sample is placed in a bath containing an electrolyte. This sample then becomes the anode in a process very similar to electroplating. A cathode made from a suitable material is then placed into the bath. When a low voltage is passed through the bath the anode becomes coated with an oxide layer which may be viewed under crossed polarized light to reveal the grain structure.

Etchant name	Etchant type	Composition	Material	Procedure	Time
Keller's reagent	Chemical Etch	95ml H_2O 2.5ml HNO_3 1.5ml HCL 1.0ml HF	AA2004	Immerse the sample in the acid solution, minor agitation.	10 seconds (Higher magnifications) – 20 seconds (Lower magnifications)
Modified Keller's etch	Chemical Etch	96.5ml H_2O 2.5ml HNO_3 1.0ml HF	AA2004	Used to enhance the contrast of images. Dip the sample and immediately wash	1 second
Graff and Sargent's etchant	Chemical Etch	84ml H_2O 15.5ml HNO_3 0.5ml HF 3g CrO_3	AA2004	Immerse the sample in the acid solution, minor agitation.	30 – 90 seconds. More time is required the longer the time between polishing and etching.
Barker's reagent	Electrochemical/Electrolytic Etch	2% BF_4H in water	AA5083	Set up the electrolytic cell with the sample as the anode. Using 20-30V.	20 – 60 seconds. Dependent on specimen size.
General Etch	Chemical Etch	1% HF in water	AA5083	Immerse the sample in the acid solution, minor agitation.	10 seconds

Table 8.3, List of Etchants used for the Preparation of Aluminium Metallography Samples.

8.2.7 EBSD Preparation

Due to the sensitive nature of the EBSD technique the utmost importance must be given to the surface preparation. EBSD interacts with the top ~50nm of the surface [96], any deformation or large levels of residual stresses within this band will degrade the pattern quality received. To improve the pattern quality a number of techniques have been trialled. Firstly a standard TEM preparation technique has been modified to remove surface material with minimal additional damage. This method utilised ion beam thinning and has been applied to the specimen's surface for the duration of 3 hours, essentially micro machining the surface. This technique had the effect of improving the pattern quality but not sufficiently for the required analysis. This is also a very time consuming technique for a limited gain in pattern quality. The second and preferred method of EBSD preparation is to aggressively etch the sample and follow this by removing the relief from the surface by repeating the colloidal silica final polish. This etch polish sequence is then repeated until the pattern quality is improved to an acceptable standard. In the case of the two alloy systems investigated herein the total number of iterations used is 10 for the AA2004 and 15 for the AA5083.

8.3 Optical Light Microscopy

Optical light microscopy has been carried out in order to investigate the microstructures of the friction stir welded material.

8.3.1 Unetched Samples

Figure 8.3.a) shows an AA2004 sample friction stir welded on the Parkson milling machine. Figure 8.3.b) shows an AA2004 parent material sample. In this case there are small Al-Cu precipitates evenly distributed throughout. Precipitate sizes and aspect ratios are given in Table 8.4. In the parent material sample the precipitates appear in tight bands and stringers, running from left to right in the micrograph, which coincide with the rolling direction of this material. The FSW sample shows the same small precipitates but the distribution of the precipitate material has been disrupted by the FSW process creating fragmented stringers. This is more noticeable towards the top surface of the sample. This section of the material experiences deformation and heat from the shoulder of the tooling only. The relatively large size of the tool shoulder induces a large magnitude of deformation and therefore disruption to the original structure. This has proved to be detrimental to the weld's stability at SPF temperatures invoking unwanted grain growth in the regions within the structure which have been exposed to the most heat and deformation from the tooling. It is surmised that this may be due to precipitate coarsening induced by the FSW process as the precipitates in the FSW samples are larger than the precipitates in the parent material samples, as shown by comparing Table 8.4.a) to b) for AA2004, and Table 8.5.a) to b) for AA5083.

Figure 8.3.c) shows a friction stir welded sample in AA5083, Figure 8.3.d) shows an AA5083 parent material sample. The first and most striking difference between the AA5083 and the AA2004 is the amount and size of the precipitates. The AA5083 samples contain larger Al-Mg-Mn precipitates, as shown in Table 8.5. The Al-Cu precipitates from the AA2004 are smaller than the Al-Mg-Mn precipitates from the AA5083. The sizes of the AA5083's precipitates are larger and they are less evenly distributed, which is then exacerbated by the subsequent FSW processes carried out on the material; coarsening the precipitates and creating an inhomogeneous structure which will be prone to AGG.

It can be seen in Figure 8.3.a) that the distribution of these particles is severely affected by the FSW process, creating particle rich and particle deficient areas giving rise to areas of microstructural instability. AA5083 is not well known for its inclusion of grain refining alloy elements such as Zr, Sc and Mn. These second phase inclusions are designed to pin the structure at high temperature and prevent grain growth. AA5083 only contains a small amount of Mn, this second phase material is not as effective at grain refinement as the relatively large amounts of Zr included in the AA2004

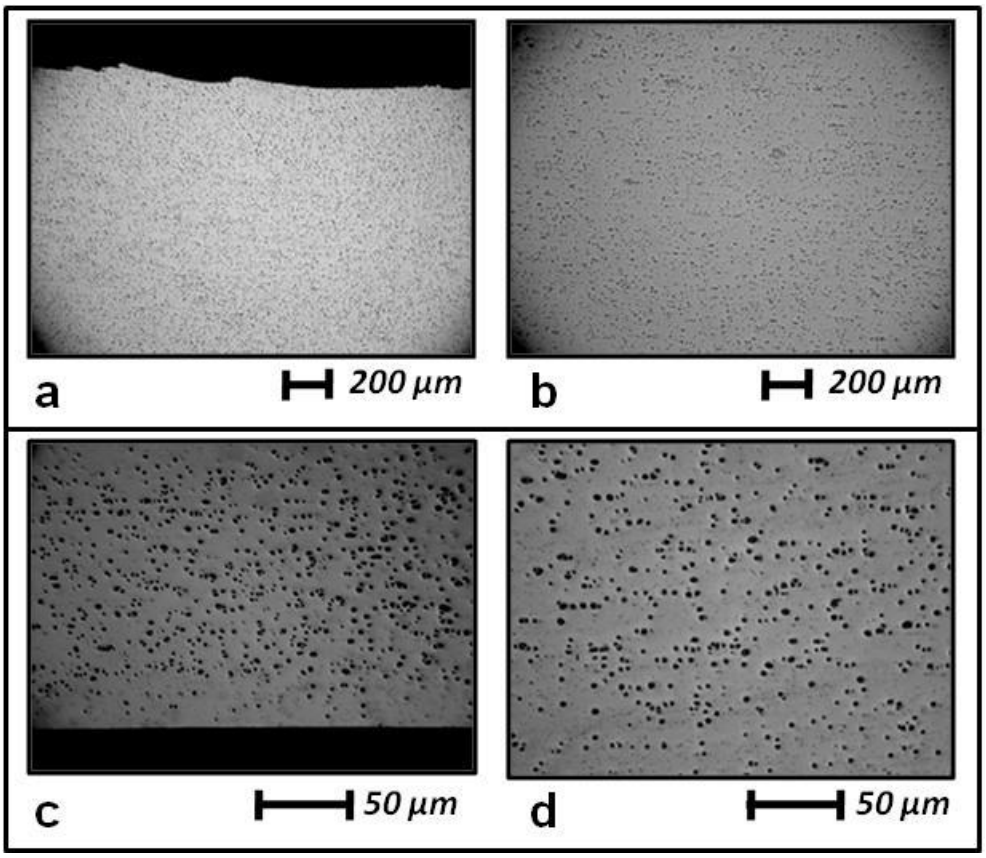

Figure 8.3, Micrographs of Unetched Specimens.
a) AA2004 welded: 620rpm, b) AA2004 parent material.
c) AA5083 welded: 620rpm, d) AA5083 parent material.

A) Particle Size: AA2004 – Parent material				B) Particle Size: AA2004 – Weld material			
Particle #	Dimension 1 (µm)	Dimension 2 (µm)	Aspect Ratio	Particle #	Dimension 1 (µm)	Dimension 2 (µm)	Aspect Ratio
1	6.836	3.174	1:2.2	**1**	10.86	3.418	1:3.2
2	8.179	3.54	1:2.3	**2**	4.517	3.174	1:1.4
3	7.08	2.197	1:3.2	**3**	4.15	3.906	1:1.1
4	4.272	2.808	1:1.5	**4**	4.15	2.93	1:1.4
5	4.883	2.563	1:1.9	**5**	11.47	2.93	1:3.9
6	4.15	2.319	1:1.8	**6**	4.272	4.272	1:1
7	5.615	2.563	1:2.2	**7**	5.615	3.418	1:1.6
8	5.249	2.441	1:2.2	**8**	4.272	3.174	1:1.3
9	4.761	3.052	1:1.6	**9**	5.371	1.831	1:2.9
10	3.662	1.709	1:2.1	**10**	2.93	2.197	1:1.3
AVG	5.4687	2.6366	1:2.1	**AVG**	5.7607	3.125	1:1.8

Table 8.4, Particle Size and Aspect Ratio of Second Phase Particles in AA2004: a) AA2004 Parent Material, b) AA2004 Welded at 620Rpm.

A) Particle Size: AA5083 – Parent material				B) Particle Size: AA5083 – Weld material			
Particle #	Dimension 1 (µm)	Dimension 2 (µm)	Aspect Ratio	Particle #	Dimension 1 (µm)	Dimension 2 (µm)	Aspect Ratio
1	5.039	4.853	1:1.0	**1**	9.644	6.226	1:1.5
2	4.573	4.199	1:1.1	**2**	7.446	7.324	1:1.0
3	8.229	4.304	1:1.9	**3**	9.277	8.667	1:1.1
4	4.051	2.532	1:1.6	**4**	7.324	6.348	1:1.1
5	8.061	4.509	1:1.8	**5**	11.96	7.202	1:1.7
6	6.968	6.148	1:1.1	**6**	10.74	9.888	1:1.1
7	6.436	5.951	1:1.1	**7**	6.226	3.906	1:1.6
8	5.493	4.15	1:1.3	**8**	3.906	3.296	1:1.2
9	4.15	4.028	1:1.0	**9**	10.5	3.54	1:3.0
10	4.517	2.075	1:2.2	**10**	10.13	3.906	1:2.6
AVG	5.7517	4.2749	1:1.3	**AVG**	8.7153	6.0303	1:1.4

Table 8.5, Particle Size and Aspect Ratio of Second Phase Particles in AA5083: a) AA5083 Parent Material, b) AA5083 Welded at 620Rpm.

8.3.2 Parent Material Samples

To fully understand the evolution of FSWs in this material; samples of parent material have been investigated in the condition in which they were welded. The AA5083 is a structural alloy designed for room temperature strength, weldability and corrosion resistance. This strain hardening alloy has been specially processed to yield superplastic properties by TMP. Designated AA5083-H19, the H19 part means that the material is about one third hardened, but has a fine structure normal to the rolling direction. Figure 8.4.a) shows a sample of AA5083 electro-chemically etched with Barker's etch. The rolling direction of this sample extends into the picture; the

macrograph shows a transverse section of the material perpendicular to the rolling direction. Small pancake or plate shaped grains dominate the structure, this structure as it is, is not in the correct form to accommodate superplastic deformation. During the preheating stage of SPF this material undergoes a transformation into fine, more equiaxed structure via static recrystallization.

Figure 8.4.b) shows the AA2004 parent material etched with Keller's reagent. This material has been welded in the 'F' condition. This stands for as-fabricated, i.e. straight from the cold rolling mill. For this sample the rolling direction runs from left to right. The structure is similar to the AA5083 but the grains are far thinner and longer in the rolling direction. The dark portions in the macrograph show the second phases, it can be seen that the matrix material flows around these second phase particles. The structure of the AA2004 is again not accommodating to superplastic deformation in this form. Dynamic recrystallization occurs during the early stages of SPF and transforms into the fine equiaxed structure required for grain boundary sliding to occur.

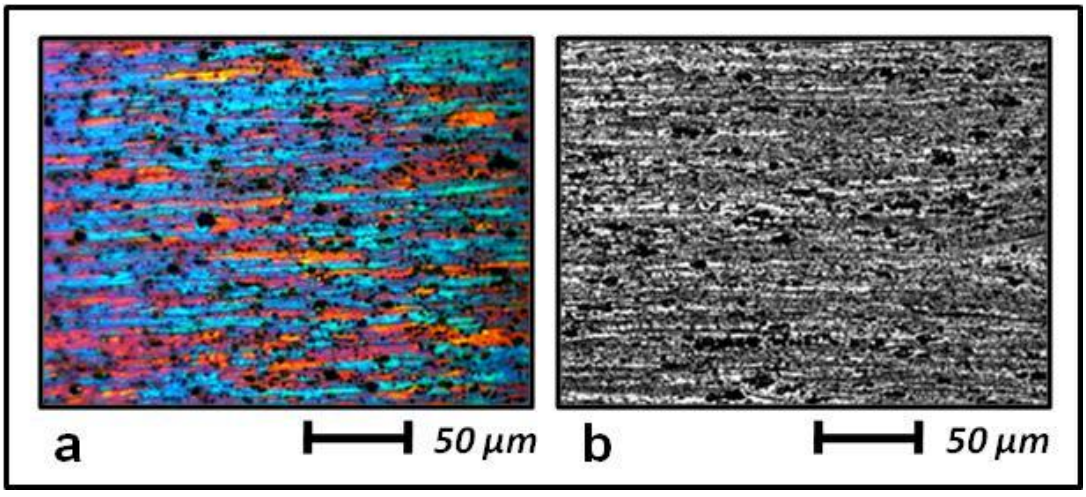

Figure 8.4) Micrographs of the Parent Material, Transverse to the Weld Direction: a) AA5083. b) AA2004.

8.3.3 Samples from the Parkson Milling Machine

The welds created using this machine are not suitable for SPF due to the inclusion of multiple welding faults. Some of these faults are visible to the naked eye during or after the process without the need for destructive testing, in this case transverse sectioning. The most noticeable weld defect present is a hot cracking defect

associated with excess heat and residual stresses during the FSW process. The rigid fixture required for FSW prevents the material from contracting and relaxing during the FSW process. The induced residual stresses coupled with the reduction of strength of the weld material causes the weakest part of the weld to tear itself apart, manifesting itself as visible crack on the top surface of the weld. Figure 8.5.a) shows the top surface of an FSW created using the maximum spindle speed setting for this machine of 1550rpm. Figures 8.5.b-d) show a transverse section of this friction stir weld. It is clearly visible that the defect extends to the very bottom of the weld. The region at the top of the weld, directly influenced by the tool shoulder has been bonded, further away from the tool shoulder, where the probe takes over as the influence; the joint interface has not been entirely destroyed. After welding the plate has attempted to contract, pulling the joint interface apart at the weld root.

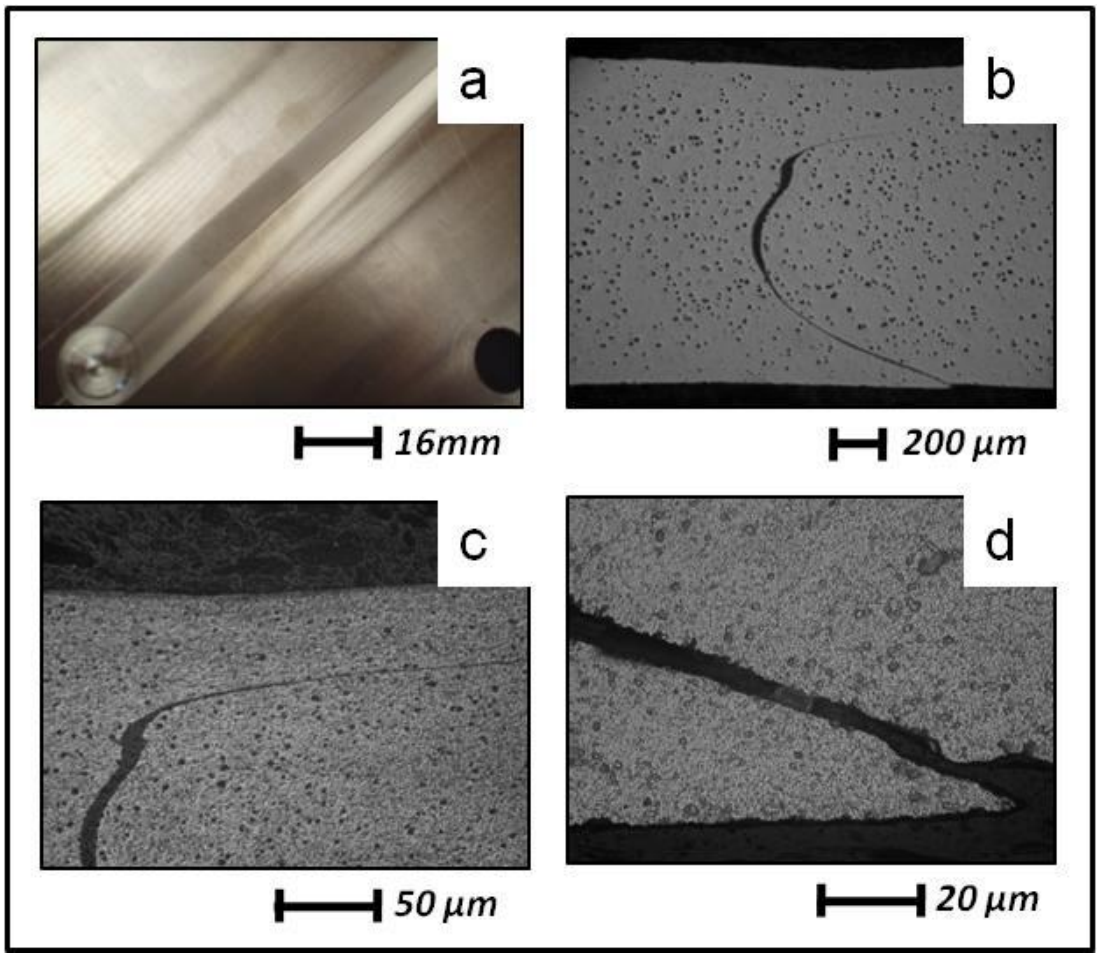

Figure 8.5, Example of Cracked FSW (1550rpm/195mm/min, concave003): a) Photograph of the Top Surface of the FSW, b-d) Micrographs of the FSW Transverse Section.

This defect is directly linked to the process parameters used and tooling geometry. The large tool size provides a large amount of heat and deformation to the material at the top of the weld; however the simple probe with no re-entrant feature does not exert enough influence on the weld root. Reducing the spindle speed will prevent the residual stresses from opening the poorly bonded joint interface and prevent the surface cracking. This will ultimately result in welds which will initially pass a visual examination, however the underlying problem will still be present.

This problem is caused solely by the tooling, making it unsuccessful at destroying the joint interface, consolidating and closing the weld at the root. The joint interface remains intact and results in an inherent flaw running the entire length of the weld. Figure 8.6.a), b), e) and f) show the top section for friction stir welds, created on the Parkson milling machine with reduced spindle speeds, it should be noted that none of these welds suffered from the surface hot cracking defect associated with higher spindle speeds. These welds are suitably bonded at the top of the weld, but as shown in Figure 8.6.c), d), g) and h) although smaller the root of the weld still exhibits a defect.

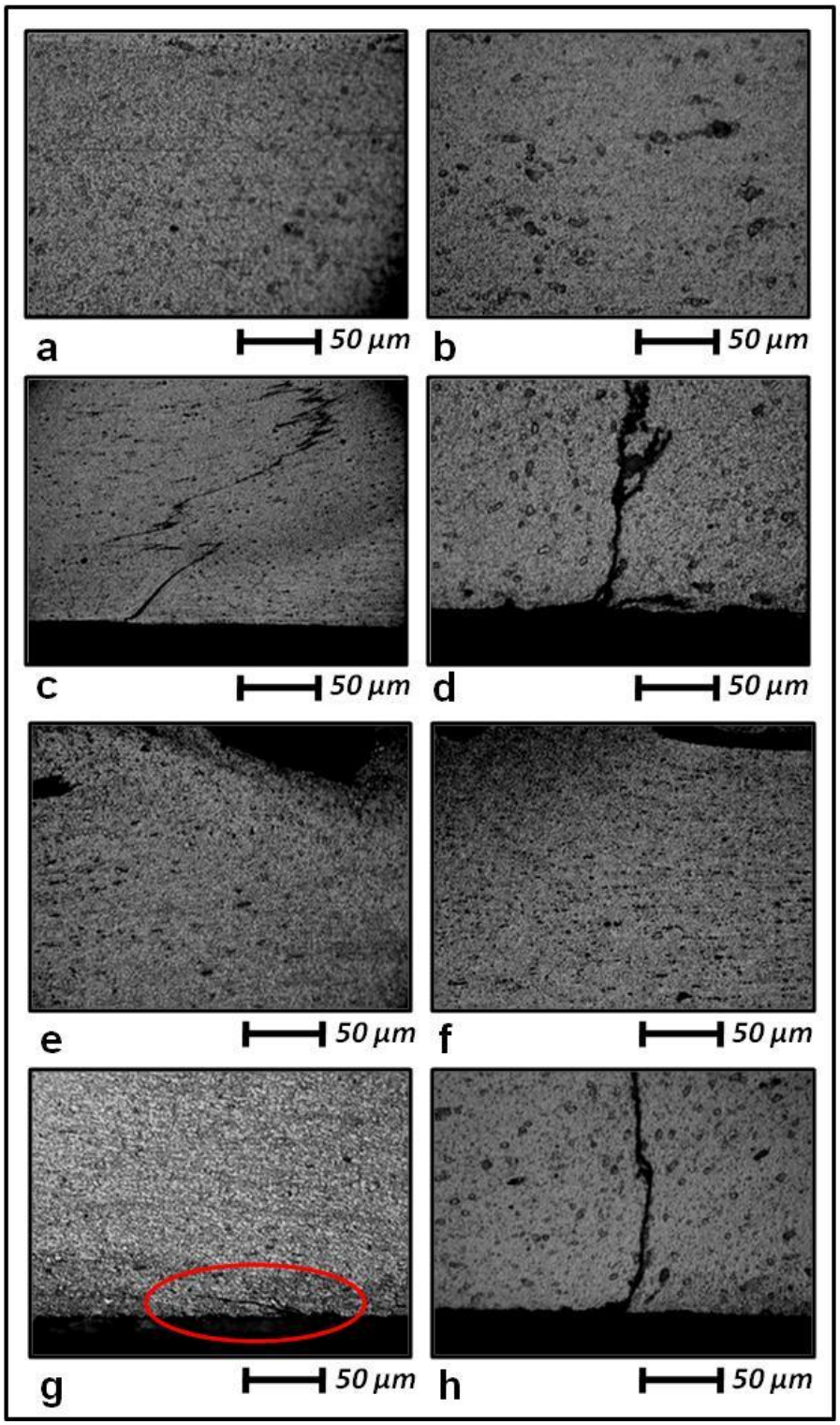

Figure 8.6, Micrograph of the Weld Crown and Weld Root for FSWs Created on the Parkson Milling Machine, a-d) AA5083, e-h) AA2004: a) AA5083: 250rpm, b) AA5083: 620rpm, c) AA5083: 250rpm, d) AA5083: 620rpm, e) AA2004: 250rpm, f) AA2004: 620rpm, g) AA2004: 250rpm, h) AA2004: 620rpm.

8.3.4 FW22

The bead on plate welds created on FW22 allows the FSW microstructure to be analysed without the inclusion of joint interface and root flaws affecting the results. Bead on plate welds are essentially friction stir processed regions, locally modified regions within a monolithic piece of material. The welds selected for microstructural investigation are chosen based on their room temperature responses. This is contrary to normal when dealing with superplastic materials as the room temperature response is not usually a good indicator for elevated temperature properties. In the case of FSW the weld region is an induced area of microstructural upheaval. Strong welds which give superior tensile strength and hardness values have been evaluated to establish the magnitude of microstructural change and the stability of the friction stir processed region. The most successful welds are purely based on their room temperature properties. In the case of the welds produced on FW22 the best welds have been produced using the TWI designed GSP 5651 tool. This is the smallest of the tools investigated and so it is assumed that use of this tool will result in a minimal amount of microstructural disruption. Hot welding conditions, 0.25mm/rev, and cold welding conditions, 1.49mm/rev, have been compared for both the AA2004 and AA5083 materials.

8.3.4.1 AA2004

Figure 8.7.a-c) shows the microstructure of an FSW created using the GSP 5651 tool and cold welding conditions. The most striking structural change is highlighted by Figure 8.7.a) this shows the boundary between the undeformed HAZ and the well deformed weld region. Looking at this in more detail in Figure 8.7.b) it can be seen that the original microstructure, consisting of elongated grains, has been transformed into a much more equiaxed structure containing very fine but very deformed grains. The weld region contains a large proportion of partially recrystallized material with no distinct weld nugget, which is usually present in FSWs in aluminium alloys. This highly disordered structure is a region of heterogeneity and may cause microstructural stability issues when subjected to elevated temperatures, causing the material in the weld region to deform at different rates to the original structure. Figure 8.7.c) shows the detail of the weld region. This is where the weld nugget is expected to be; the nugget would be an area of fully recrystallized material with deformation free grains, but this is not present in these samples.

Figure 8.7.d-f) shows the microstructure of a hot friction stir weld. The weld region has undergone a more intense heating and deformation cycle resulting in the well defined stir patterns displayed in Figure 8.7.d and e). Figure 8.7.f) shows the detail of the centre of the weld region. The biggest difference between this and cold weld is the size of the matrix grains and second phases present. The hot weld contains much larger second phase particles and less deformed matrix grains suggesting that more recrystallization has occurred in the hot samples than the cold samples. The coarser precipitates are detrimental to the microstructural stability of the weld region. Coarser second phase particles exert a smaller magnitude pinning force on the matrix grains and may causes abnormal grain growth during the subsequent SPF operations.

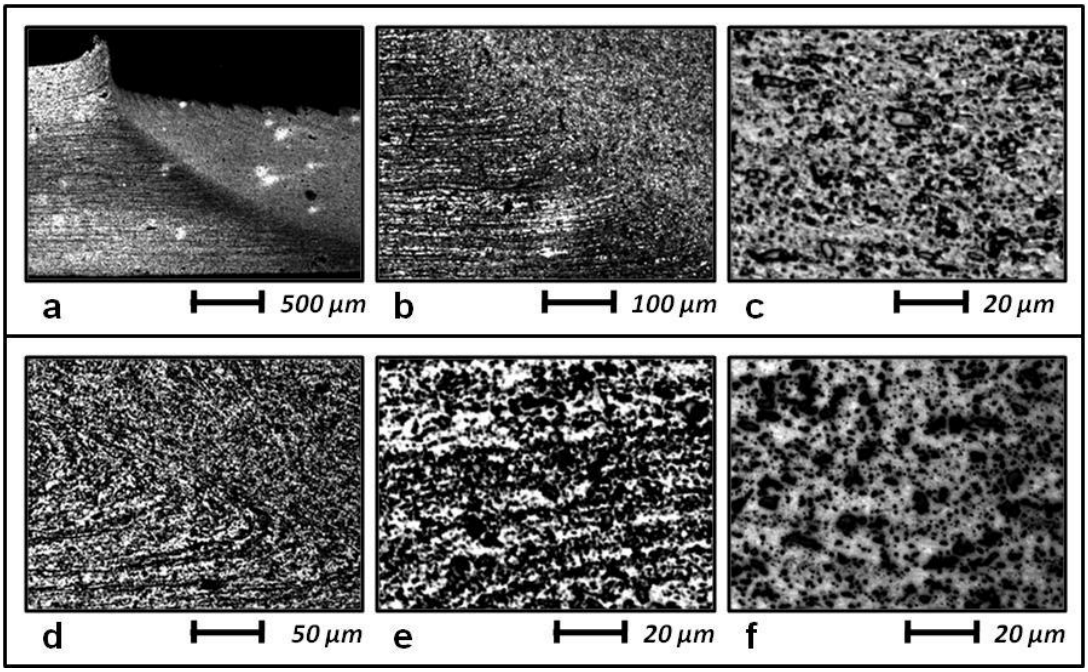

Figure 8.7, Micrographs of the FSW Microstructures for Hot and Cold Welded AA2004:

a-c) Weld Pitch = 1.49mm/rev, d-f) Welding Pitch = 0.25mm/rev. a) HAZ/TMAZ Interface, b) HAZ/TMAZ Interface Detail, c) TMAZ Detail, d) HAZ/TMAZ Interface, e) Stir Patterns in the TMAZ, f) TMAZ Detail.

8.3.4.2 AA5083

The corresponding welds created in AA5083 exhibit the same features as the AA2004 welds; a well defined interface between the HAZ and TMAZ but a lack of distinction between the TMAZ and the weld nugget. The AA5083 samples have been etched in a 1% hydrofluoric acid solution for 90 seconds. Figure 8.8.a-d) shows the weld created using cold welding conditions. The elongated original structure is transformed into a more equiaxed structure within the weld region as shown in Figure 8.8.a) Detail of the weld region is shown in Figure 8.8.b-d) the three macrographs show the advancing side, weld centre and retreating side respectively. It is clear that the grain structure differs from one side to the other with a distinctly coarser structure on the retreating side. This is due to the asymmetric nature of FSW and will cause heterogeneous deformation during SPF processes. The second phases are very disrupted in this sample, the coarse particles visible in the unetched samples in Figure 8.3 are broken down into much smaller pieces which are not visible in this picture suggesting that the colder deformation cycle has produced a finer distribution of second phase; without the static annealing produced by the tooling, causing any coarsening after the tool has left the vicinity.

The hot welding condition for this alloy has produced a very peculiar effect. The TMAZ/HAZ interface in this case is much less defined with some evidence of separation between the top, shoulder influenced material, and the rest of the material, which is directly affected by the tool probe. Figure 8.8.e) and g shows this separation, this is possibly produced by using conditions which are too hot for the thickness of material; causing localized melting of the material directly beneath the tool shoulder. This in turn limits the influence of the tooling on material further into the thickness of the material. Figure 8.8.h) shows the poorly defined interface between the TMAZ and HAZ regions. There is much less flashing compared to the colder welding parameters, producing much less plate thinning but giving rise to the separation of material in the weld crown. Figure 8.8.f) shows the weld centre material. This material has undergone severe plastic deformation but also some degree of static annealing caused by the tool as it passes along the weld. The limited amount of second phase, compared to the AA2004, appears to be coarser than the cold weld centre shown in Figure 8.8.c).

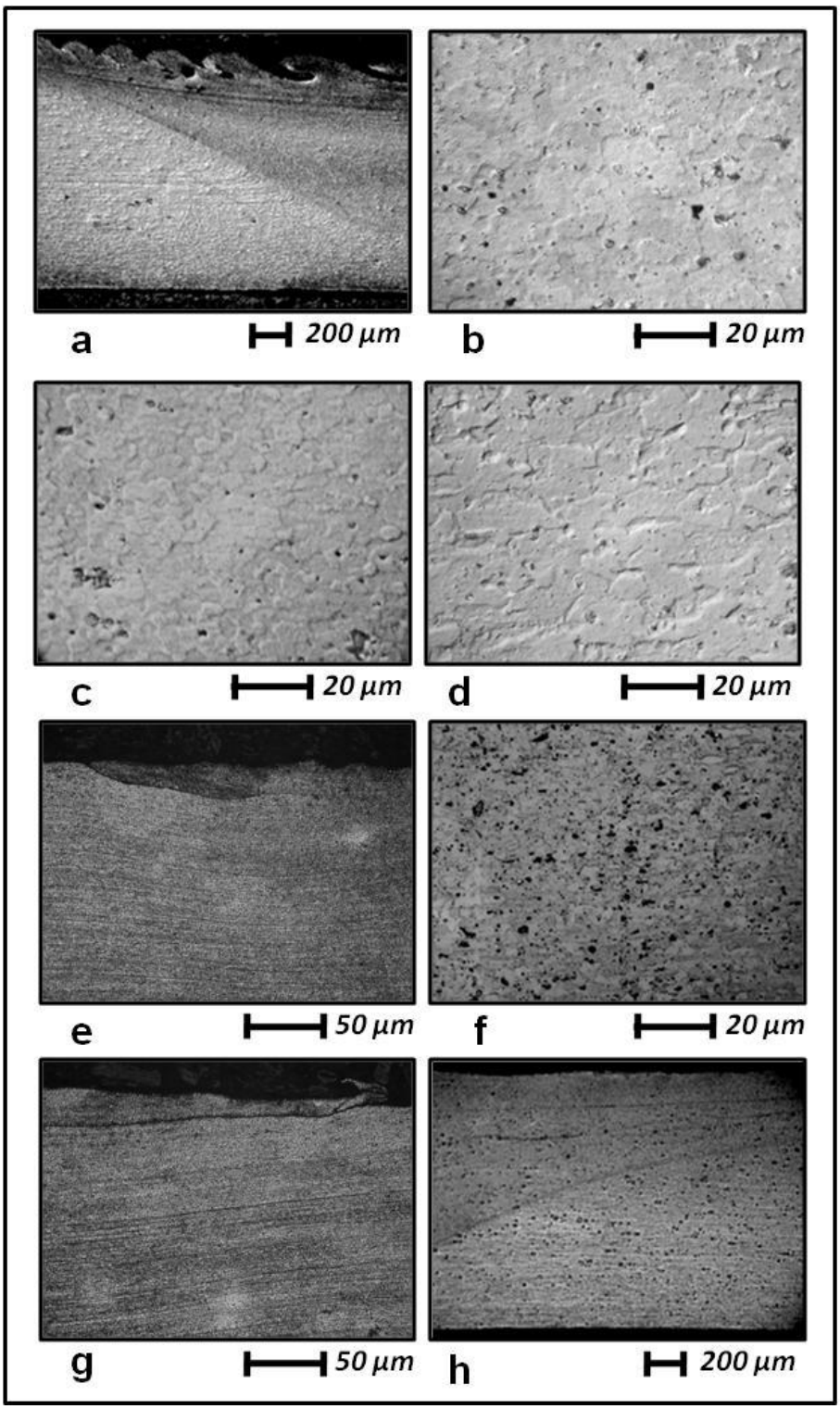

Figure 8.8, Micrographs of the FSW Microstructures in AA5083 Created using Cold (1.49mm/rev) and Hot (0.25mm/rev) Welding Conditions.

a-d) Weld Pitch = 1.49mm/rev, e-h) Welding Pitch = 0.25mm/rev. a) HAZ/TMAZ Boundary, b) Advancing Side TMAZ , c) Weld Centre TMAZ , d) Retreating Side TMAZ, e. Advancing Side TMAZ , f. Weld Centre TMAZ , g) Retreating Side TMAZ, h) TMAZ/HAZ Boundary.

8.3.4.3 Microstructural Stability at Elevated Temperature

The main issue concerning the successful use of FSW for subsequent SFP operations is the stability of the weld region at high temperatures. The introduction of heat into a structure can cause recovery, recrystallization and eventually grain growth. Abnormal grain growth occurs when certain grains grow at a higher rate than others; this is due to microstructural instability. In superplastic materials this is usually prevented by a uniform distribution of hard second phase particles within the aluminium matrix. The FSW process induces a heterogeneous region into the material where the second phase distribution, size and morphology can be significantly changed. To test the stability of an FSW weld, samples have been annealed at 350°C in an air furnace and then sectioned and prepared for microscopy. Figure 8.9 shows the microstructure of an AA2004 weld created using the GSP 5651 tool and cold welding parameters (1.49mm/rev). It is clearly visible from Figure 8.9.a) that some areas within the structure have undergone differing levels of grain growth and abnormal grain growth. It is also clear that the magnitude of the growth is affected by the asymmetric nature of the FSW process; with more growth on the advancing side of the weld region. The banded microstructure is highlighted in the form of horizontal bands originating on the advancing side of the specimen. This is limited to the top third of the weld region; below this the probe influenced stir zone is visible. Figures 8.9.b and c) show this in detail. The darker material in the micrographs remains relatively fine where as the lighter mater has grown allowing individual grains to be visible. Figure 8.9.d) shows the very centre of the weld and depicts the abnormal grain growth present in this sample.

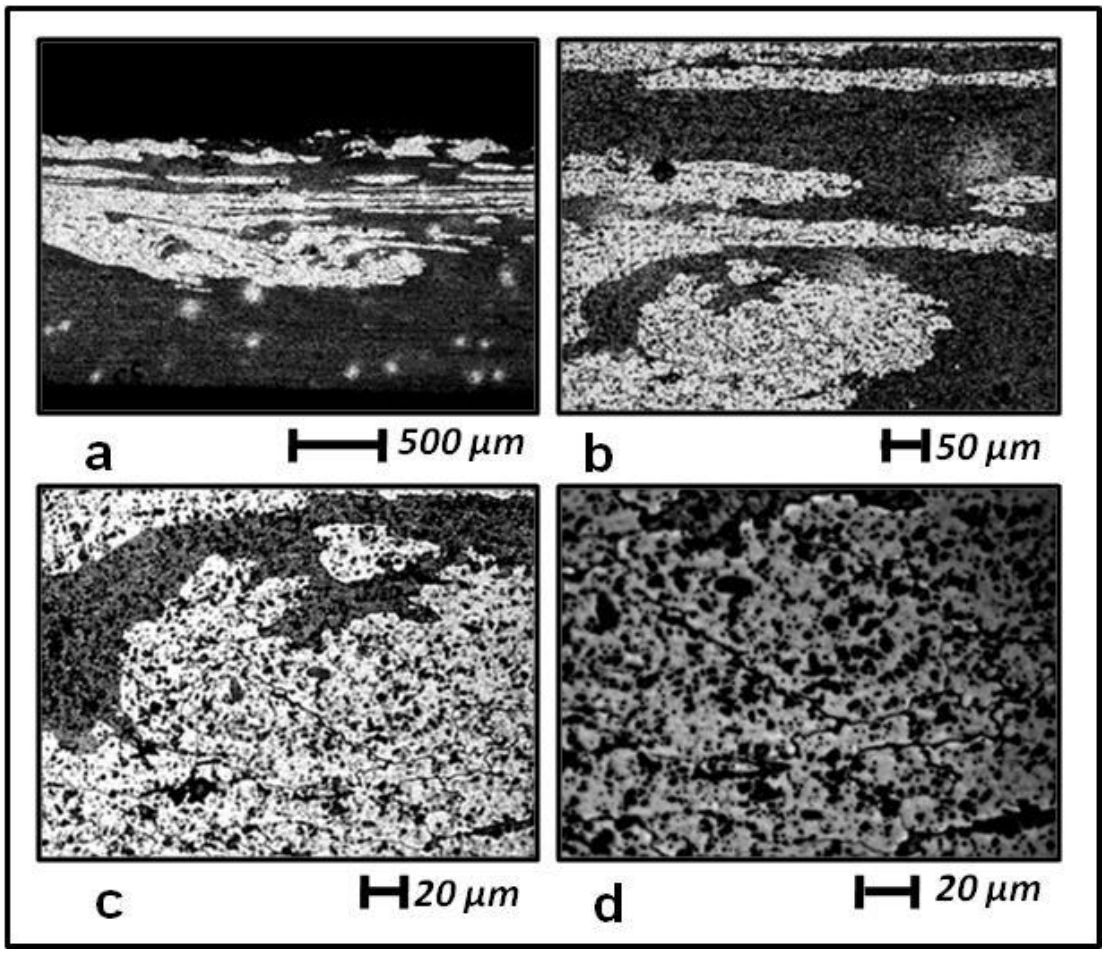

Figure 8.9, Micrograph of an FSW in AA2004 After Annealing at 350°C:
a) Whole Weld Region, b) Separate Shoulder and Pin Influence,
c) Detail of Stir Zone, d) Detail of Area with Grain Growth.

8.3.4.4 Double Pass Friction Stir Welds

A number of double pass welds have been created and cone tested, however only the successful AA2004 weld, created using the large shoulder (19mm) tool, and corresponding weld in AA5083 have been prepared for microstructural evaluation. Figure 8.10 shows the microstructure of the weld region and unaffected parent material after FSW. The shape of the weld region is very different from the single pass welds discussed and there is once again no distinct boundary visible between the HAZ and TMAZ regions, this is shown in Figure 8.10.b) There is significant difference between the completely unaffected parent material and the centre of the weld region, shown in Figure 8.10.a. and c). The original elongated structure derived from the rolling processes has been changed into a heavily deformed, highly disordered structure via multiple friction stir welding passes. The second pass has

been included in order to remove any root defects from the weld. Root defects have been present in the single pass welds created using the simple tooling types. The tool used to create this weld is such a tool. The weld root defects have been removed; however there is still evidence of entrapped oxide in the weld region. The joint interface has been disrupted by the two passes of the tool and has created the feature shown in Figure 8.10.d) this is only a small feature which does not extend to the weld crown or weld root where the FSW passes exert the most influence.

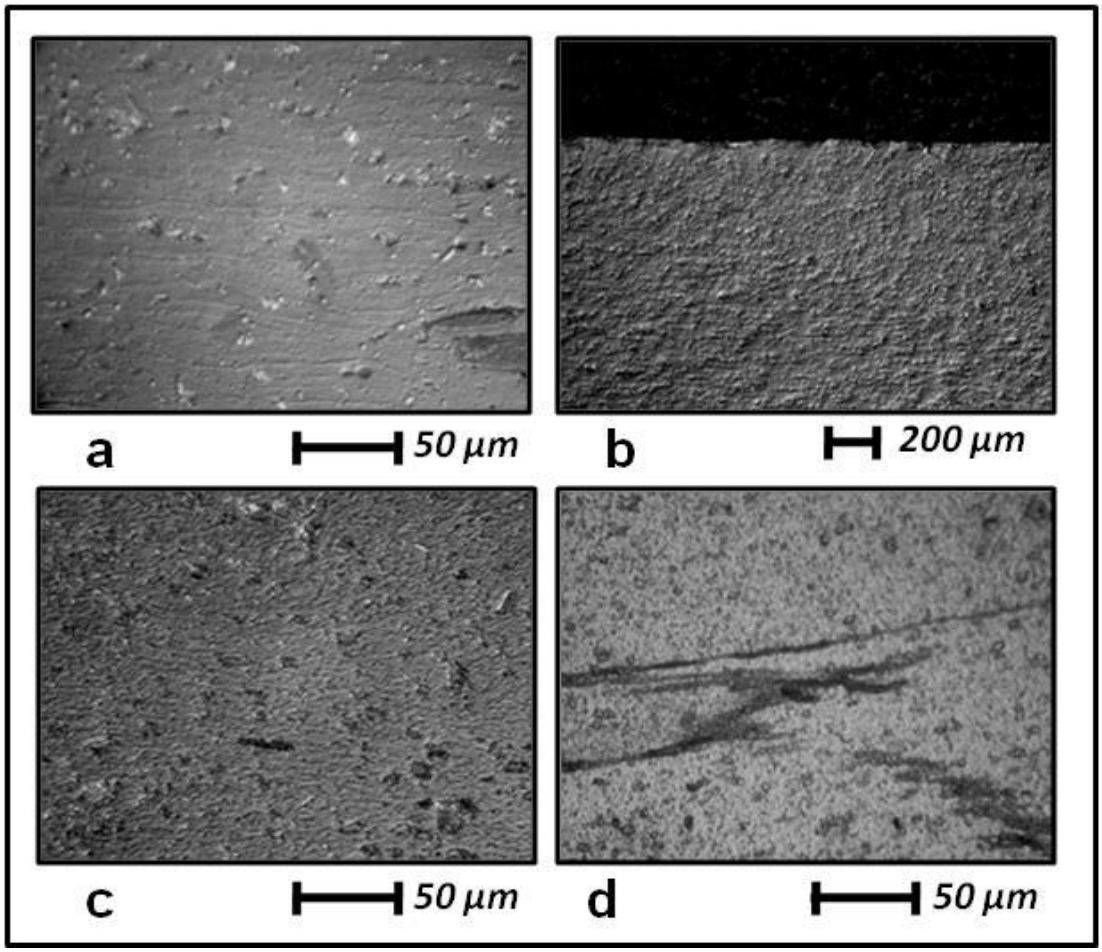

Figure 8.10, Micrographs of Double Pass FSW in AA2004:
a) Parent Material, b) Parent Material-TMAZ Interface,
c) Weld Centre, d) Weld Centre Detail (entrapped oxide).

Figure 8.11 shows the sample after it has been cone tested. The weld has been formed at 460°C to an equivalent SPF strain of ~258%. This microscopy sample has been taken from the pole region of the cone test specimen and is orientated as a plan sample, see Figure 8.2. The scalloping marks left by the FSW process are clearly visible on the cone test specimen; the distinct bands are distinguishable by the naked

eye and have been evaluated in order to establish any microstructural differences between the bands. Figures 8.11.a. and b) show one band, Figures 8.11.c. and d) show the neighbouring band. It can be seen from these micrographs that there is not any visual differences between the two bands. There is however a marked difference between Figure 8.11.c. and d) and Figure 8.11.a. and c). The disordered, highly deformed material has fully recrystallized and has become an equiaxed structure with a mean grain size of ~4.3μm. The main failure mode for this cone tested specimen has been grain growth, the "orange peel" effect; the grains grow whilst under heating and deformation conditions. These dynamically recrystallized grains finally separated away from the joint interface but within the weld region. This suggests that heterogeneity of the weld region has accelerated the failure of this sample.

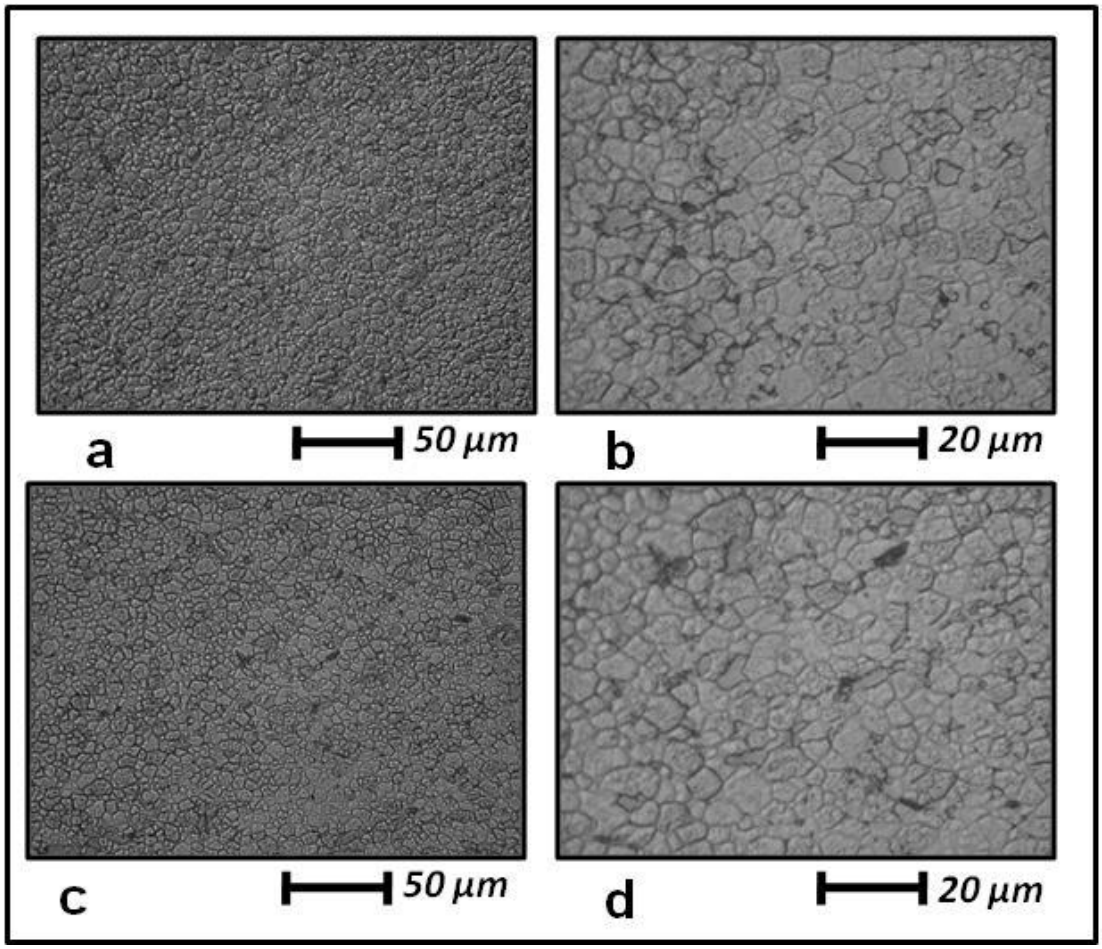

Figure 8.11 Micrograph of Cone Tested FSW in AA2004.
a) Weld Centre Band A. b) Band A Detail.
c) Weld Centre Band B. d) Band B Detail.

The double pass weld made in AA5083 failed to form during the cone test. As gas pressure was applied the weld seam has ruptured causing a catastrophic failure. Figure 8.12 shows the structure of the material before the cone test. It is clearly visible that the grain size is much larger than the AA2004 counterpart. This much larger starting grain size is detrimental to the SPF process and it is suggested that this is the primary reason for the failure. AA5083 statically recrystallizes during the SPF preheat. In this case the weld region is already partially recrystallized, the two consecutive passes has caused two cycles of heat to be delivered by the tooling and has led to the structure shown in Figure 8.12. The static heat from the SPF process relaxes the strain hardening within the microstructure of the material; weakening the material. The addition of deformation whilst the structure is in this weakened state has caused the failure of the specimen at the weakest point, the joint interface.

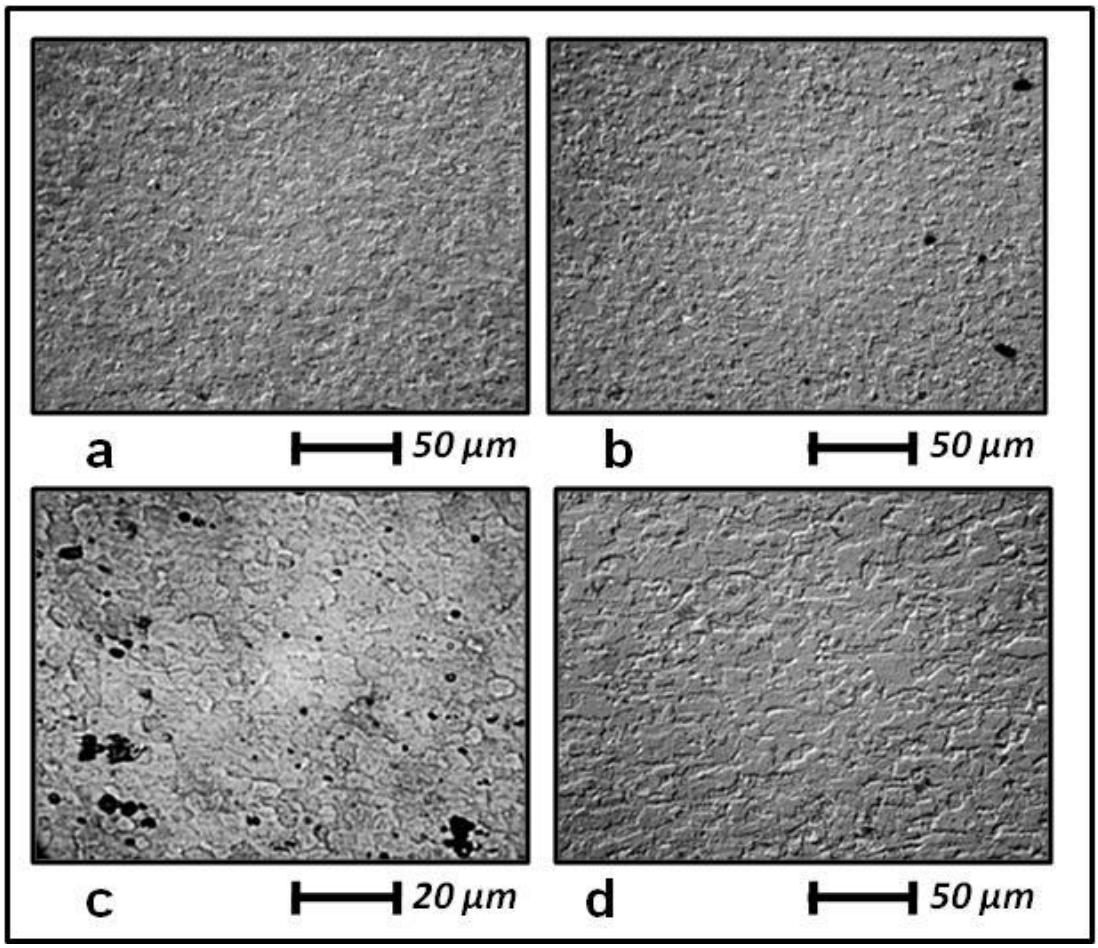

Figure 8.12, Micrograph of Double Pass FSW in AA5083.
a) Advancing Side TMAZ. b) Weld Centre,
c) Weld Centre Detail. d) Retreating Side TMAZ.

8.3.5 ESAB Machine

The friction stir welds made using the ESAB machine are single and triple pass welds; all created by welding on the top surface. This machine is fully programmable and can use both position and force control. These welds have been created using position control as the plunge depth is the most critical parameter due to the thickness of the material.

8.3.5.1 AA2004

The samples have been cone tested at 460°C and a gas pressure of 20psi. The most successful single pass weld in AA2004 obtained an equivalent SPF strain of 210%; the triple pass weld in AA2004 has achieved an SPF strain of 87%. It is suggested that the intense heating and deformation experienced by the material has reduced the weld region's strength by successive passes, causing large levels of dynamic recrystallization. The parent material usually transforms into an equiaxed structure during the SPF process. As the weld regions for both the single and triple pass welds are already in this state it can be said that they are one step further into the superplastic evolution than the parent material. This means that they will experience recovery and grain growth before the parent material. This has also meant that the weld region has deformed before the parent material; suggesting a reduction in flow stress for the FSW material. Most of the superplastic deformation has been confined to the weld region.

Figure 8.13 shows the microstructure of the weld centre and the weld extremities, for the single pass weld in AA2004, after the cone testing. Figure 8.13.a-c) shows the advancing side of the weld region. It is clear that the superplastic deformation has been confined to the weld region due to the neck which has formed on the TMAZ/HAZ interface. The undeformed material on the left of Figure 8.13.a) remains approximately the same thickness as it was before the test. This is true but less noticeable on the retreating side of the weld region shown in Figure 8.13.g). Figure 8.13.d-f) shows the pole region of the cone test specimen. This area has undergone the most deformation and so yields the largest grain size at the point of failure. The grain size changes depending on the position within the weld region. The weld centre contains the largest measured grain at ~6µm. Moving towards the advancing side of the weld the grain size falls slightly to ~5.2µm. The smallest grain

size measured within the weld region is located on the retreating side with a grain size of ~3.1µm. It is expected that weld centre contains the largest grains, the difference between the advancing and retreating sides of the weld is due to the asymmetry of the welding process. Larger levels of residual stresses are found in the advancing side material [18]. This increased residual stress means the advancing side has more energy for microstructural change and this may be the reason for the significantly larger grain size, compared to the retreating side. Figure 8.13.c), f) and i) show evidence of larger grains interspersed with smaller grains. The larger grains are growing at the expense of the smaller grains, although not visible to the naked eye on the cone test specimen this is clear evidence of some abnormal grain growth and further highlights the heterogeneous structure of the FSW region and induced microstructural instability.

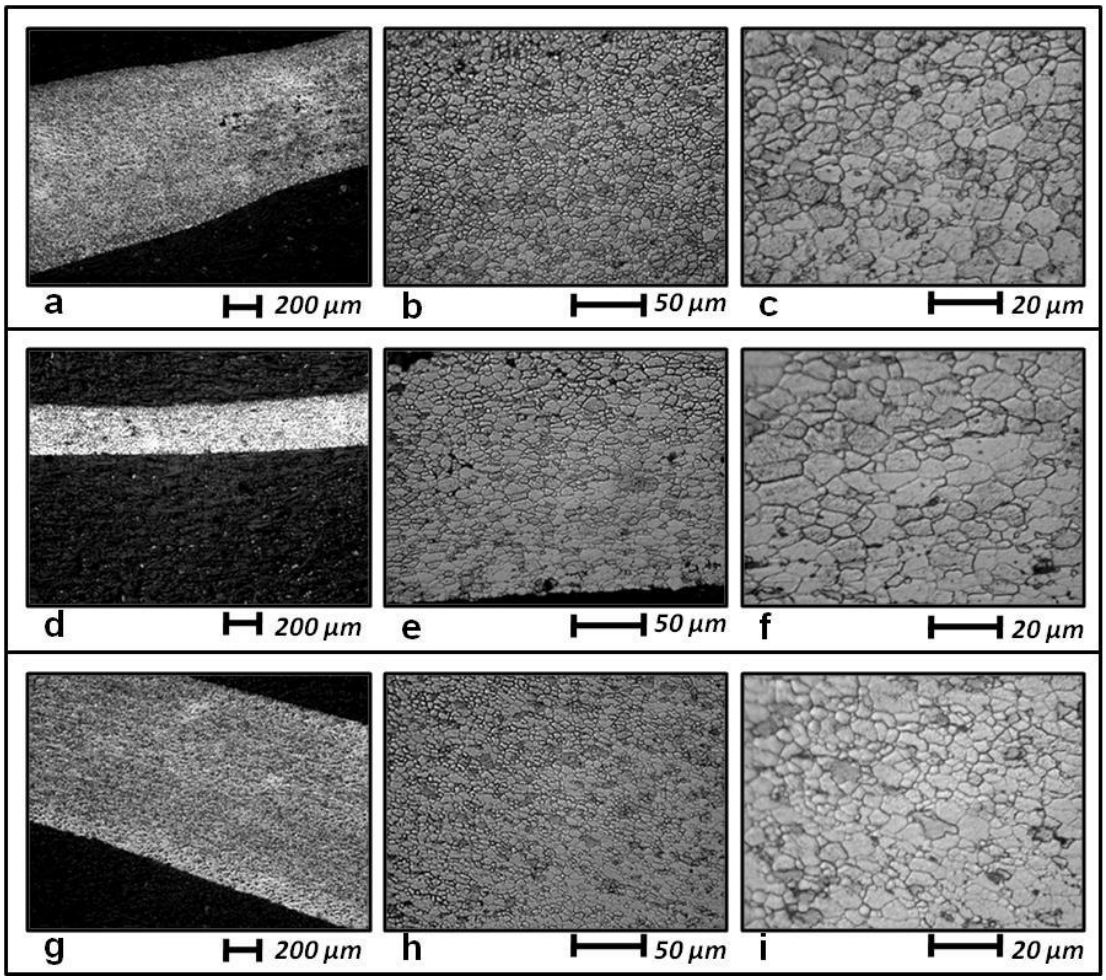

Figure 8.13, Micrograph of Weld Region after Cone Testing, Single Pass, 1250rpm, 750mm/min:

a-c) Advancing Side, d-f) Weld Centre, g-i) Retreating Side.

Figure 8.14 shows the microstructure of the triple pass weld centre and advancing and retreating sides of the weld region. Once again it is noticeable from Figure 8.14.a) and g) that there is some necking and again the most necking is present on the advancing side. In the case of the triple pass weld the advancing side of the weld region is pass number 3. This region has undergone three consecutive heating cycles by the three consecutive overlapping FSW passes but has only experienced 1 deformation cycle. This is highlighted by the average grain sizes present in the three different regions shown in Figure 8.14.c), f) and i). The grain size on the retreating side (pass 1) is the largest recorded in this sample at ~6μm. Moving towards the centre of the weld region (pass 2) the grain size drops to 4.4μm. On the advancing side (pass 3) the grain size drops further to 3.3μm. This suggests that as pass 1 (retreating side) has undergone more heating than the other parts of the weld it has endured more relaxation of strain and so has undergone more grain growth. The overlapping nature of the passes has created a gradient of heat and deformation, decreasing in magnitude from retreating to advancing side of the weld.

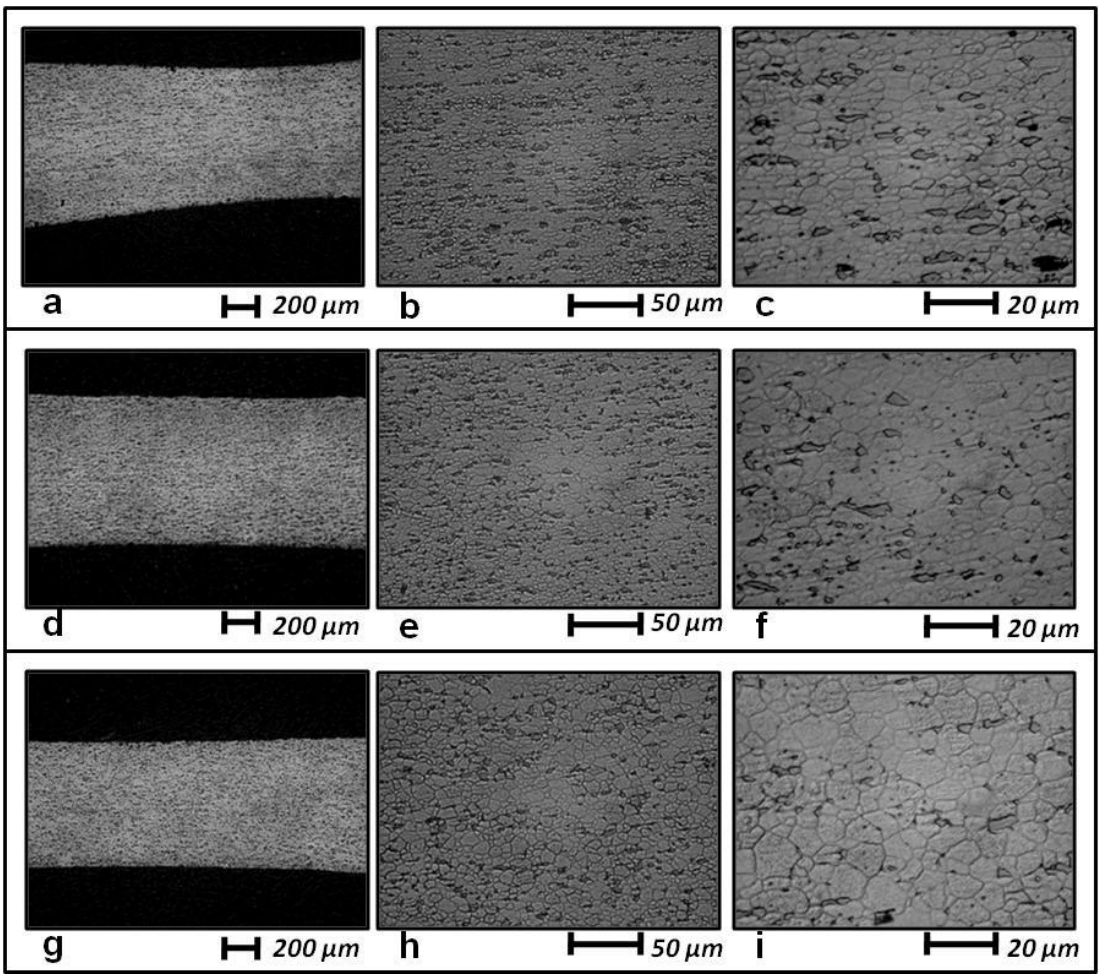

Figure 8.14, Micrograph of Weld Region after Cone Testing, Triple Pass, 750rpm, 750mm/min:

a-c) Advancing Side, d-f) Weld Centre, g-i) Retreating Side.

8.3.5.2 AA5083

The AA5083 alloy transforms into its superplastic microstructure during the preheat stage of the SPF process. This occurs by static recrystallization. This means that the original parent material structure can recrystallize when the thermal field generated by the FSW tool provides a certain amount of heat, in this case ~350°C. The friction stir welded region contains partially recrystallized material. When this material is heated it starts a cycle of recovery, recrystallization and grain growth in an attempt to gain an equilibrium structure. It can be said that the FSW region is one stage further into this cycle and so when the SPF preheat occurs the weld region may already be beginning its grain growth stage. AA5083 lacks the addition of grain refinement elements like the Zr found in AA2004; this means that AA5083 is much more

susceptible to grain growth and abnormal grain growth. The AA5083 samples have also been formed at 460°C and a low gas pressure of 0.138 MPa (20psi).

Figure 8.15 shows the cone tested AA5083 single pass specimen. It is clear that superplastic deformation has not occurred in this sample. An equivalent SPF strain of 62.9% was achieved before the sample failed. The failure is situated on the interface between the weld nugget and TMAZ; and appears to be caused by abnormal grain growth on the top surface of the specimen. Figure 8.15.a) shows the advancing side of the weld region and the apparent starting place for the tear. The top surface in a biaxial strain environment will experience a higher proportion of tensile stress during the forming operation. The grains close to this surface have begun an abnormal grain growth stage and so have become severely weakened compared to the much smaller grains just below the surface. There is also some evidence of cavitation in the structure around the failure site. The microstructure of the FSW region has been made unstable at high temperatures by heating and deforming the material; producing a region which will coarsen rapidly during the SPF preheat stage of the forming operation.

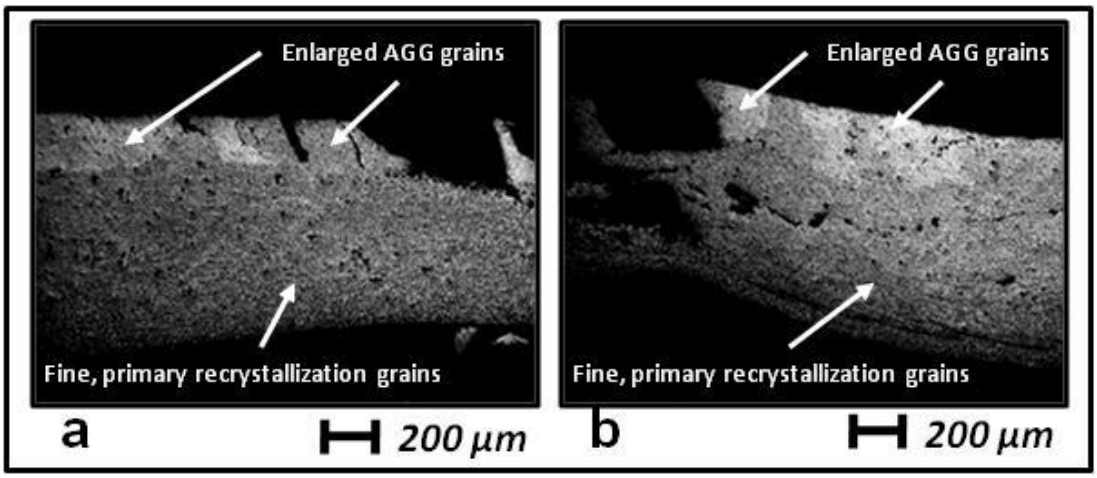

Figure 8.15, Macrograph of FSW Weld Region after Cone Testing, Single Pass, 1250rpm/750mm/min. a) Advancing Side. b) Retreating Side

The triple pass weld in AA5083 exhibits the same abnormal grain growth which contributed to the failure of the previous sample but in a more spectacular fashion. The failure of the triple pass specimen is located in the very centre of the weld region where pass 2 is located; it is also perpendicular to the weld direction and is associated with the banded structure produced by the FSW process rather than the

original joint interface. This sample exhibits abnormal grain growth throughout the entire depth; not just the top surface. Figure 8.16 shows the entire cross section of weld region. It should be noted that red line denotes where the two montage images are joined. The most severe coarsening occurs in the very centre of the weld region where the tool probe passed through the material. The extremities of the region exhibit the same top surface grain coarsening as shown in the Figure 8.15. As the grains grow the strength of the material is lowered and stress required for grain boundary separation is reduced. This has led to several instances of cavities between the enlarged grains.

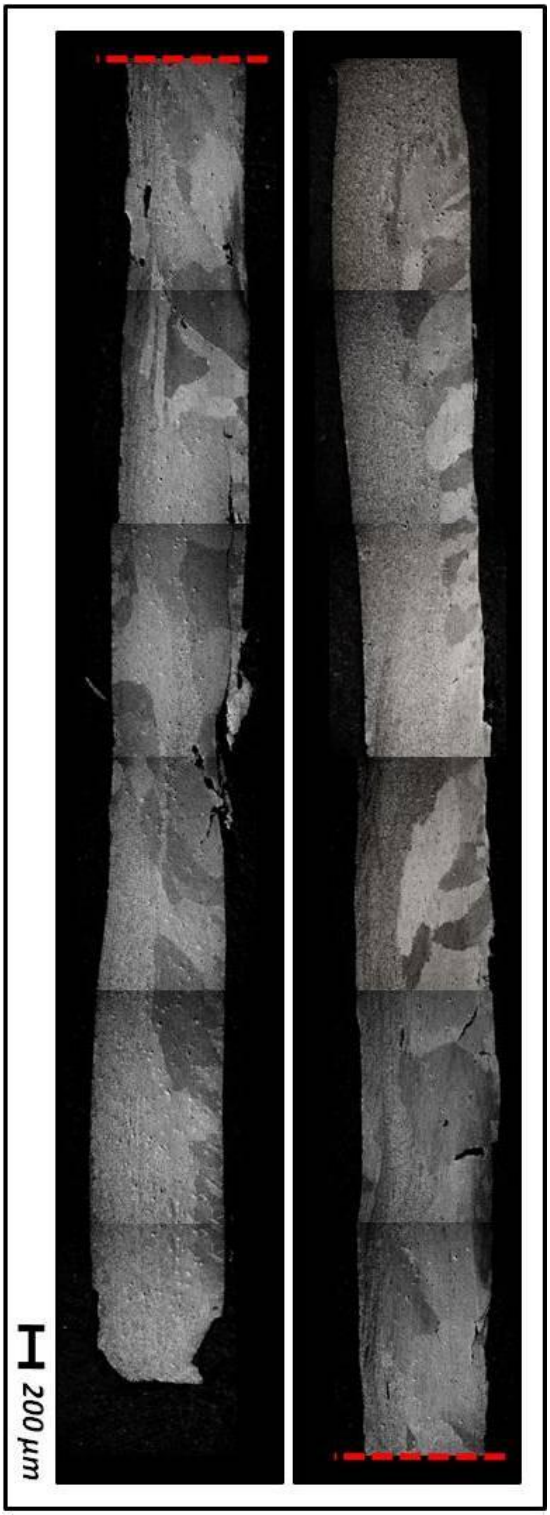

Figure 8.16, Micrograph of FSW Weld Region After Cone Testing, Triple Pass, 750rpm/750mm/min.

8.4 Electron Backscattered Diffraction

This technique uses back scattered electrons to reveal the grain structure, crystallographic orientation and phase distribution of the materials investigated in this thesis. The preparation techniques are stricter due to the sensitive nature of the analysis technique. The orientation of the crystal structure gives a bearing on the level of recrystallization, recovery and grain growth present in the sample and also gives a very clear picture of the distribution of second phases present. The second phases are very important for microstructural stability which is a key aspect in producing superplastic deformation. Materials will attempt to transform to a low energy state when there is sufficient energy for microstructural change; in order to attain an equilibrium state [97]. For aluminium this usually involves recovery and grain growth due to the high stacking fault energy of aluminium, resulting in a reluctance to recrystallize [90]. Fine, second phase particles distributed along grain boundaries are essential to prevent grain growth and maintain the fine matrix grain size required for superplastic deformation mechanisms such as grain boundary sliding to occur.

8.4.1 Double Pass Welds in AA2004

Figure 8.17 shows the EBSD and phase distribution maps for the double pass weld in AA2004. The TMAZ extremities show a fine structure of partially recrystallized material and a significant amount of strengthening precipitates located on the grain boundaries. Comparing Figure 8.17.d) and f) shows that there is a larger quantity on the retreating side. The asymmetry of the FSW process has yielded a heterogeneous distribution of second phase which will cause grain growth problems during forming. Figure 8.17.a) and c) shows the difference in grain size between the advancing and retreating sides. There is more energy for structural change on the advancing side due to the vast differences in residual stresses between the two sides which is in turn caused by the differing periphery speeds of the tooling on the advancing and retreating sides of the weld. More energy causes more recrystallization, recovery and growth of grains. The very centre of the weld shown in Figure 8.17.b) contains more recrystallized material, larger grains and much less of the Al_3Zr precipitates which pin the structure and prevents growth. The fine Al_3Zr particles shown in Figure 8.17 have been highlighted by the EBSD detector and have been established to ~0.3μm.

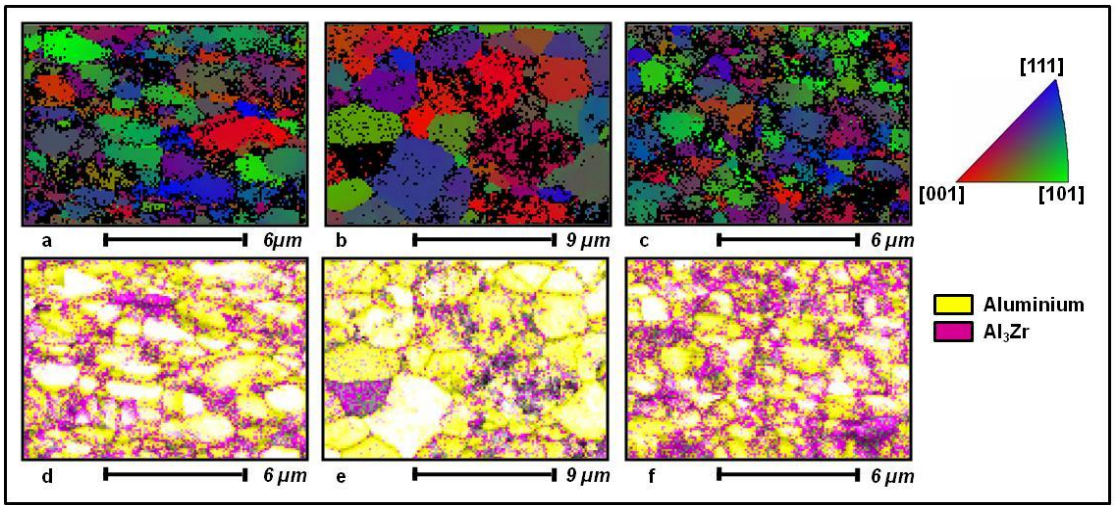

Figure 8.17, Transverse Section EBSD Maps and Phase Maps for the AA2004 Cone Tested Sample Created on FW22. a) EBSD Map from Advancing Side TMAZ, b) EBSD Map from Weld Centre, c) EBSD Map from Retreating Side TMAZ, d-f) Corresponding Phase Maps.

During SPF the original banded and highly deformed structure transforms in the superplastic microstructure. The weld region is already in a recrystallized state and so will be continuously at this more advanced state within the deformation process, than the surrounding parent material. This leads to coarsening of the weld region, mainly in the weld centre where the nugget is located.

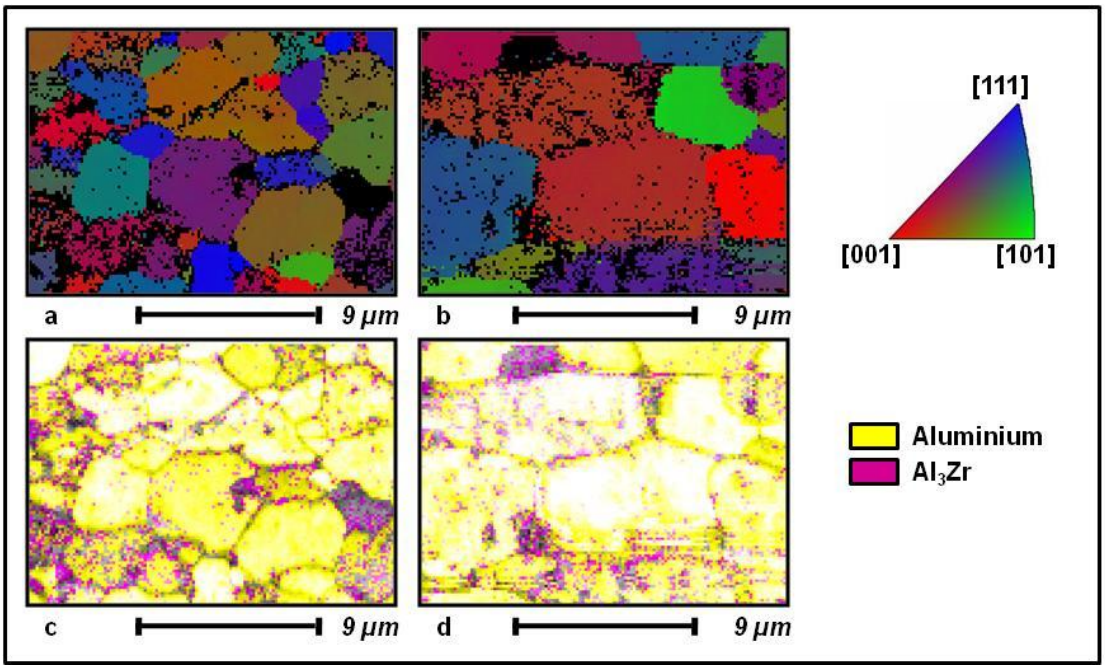

Figure 8.18, EBSD Maps and Phase Maps for the AA2004 Cone Tested Sample Created on FW22. a) EBSD Map from Band A. b) EBSD Map from Band B. c) and d) Corresponding Phase Maps.

The double pass weld in AA2004, created on FW22, has achieved the largest superplastic deformation of all the samples tested in this thesis. It is difficult to see the extent of the grain growth from the optical light microscopy carried out and depicted in Figure 8.11. Figure 8.18 shows EBSD maps from a plan view; maps were taken from two neighbouring bands of the characteristic semicircular bands present in an FSW structure. It is clear that the different bands have undergone different amounts of deformation and therefore their structures have evolved at different rates. Band A contains smaller grains and far larger amount of second phase, which has effectively pinned the grain boundaries and minimised the grain growth during the high temperature deformation. Band B is dominated by far larger grains; this is linked to the significantly reduced amount of Al_3Zr. In band A the distribution of second phase is more uniform and located on the grain boundaries, there is some coarsening of precipitates but overall the distribution is sufficient to prevent abnormal grain growth. Band b is affected by abnormal grain growth. There are a couple of coarse second phase particles but the main issue is the reduced levels of precipitation on the grain boundaries; this reduced pinning force has allowed the grains in the centre of the image to grow significantly. This essentially shows that the

banded structure produced by FSW has the potential to deform at much different rates; this is due to the heterogeneous nature of the FSW structure.

8.4.2 Double Pass Welds in AA5083

The structure of the material must be stable at high temperature in order for successful SPF operations to be able to be carried out. It is clear from Figure 8.19.b-d) that this is a major issue for the AA5083. The pinning of the grains is reliant on the Al_6Mn precipitates distributed along the grain boundaries. Figure 8.19.a) and e) shows a banded structure interlaced with pinning particles. The material within the weld has coarsened and phase maps show they lack the precipitation required to prevent abnormal grain growth during SPF. There is significant grain growth present in the FSW sample; when this sample is then exposed to high temperatures and deformation the structure will coarsen further, leading to abnormal grain growth within the weld region only. The parent material will begin to form, the undeformable weld region will act as a rigid block separating the deforming parent material on each side; the weld region will be torn apart due to a decrease in the stress required for grain boundary separation for larger grains.

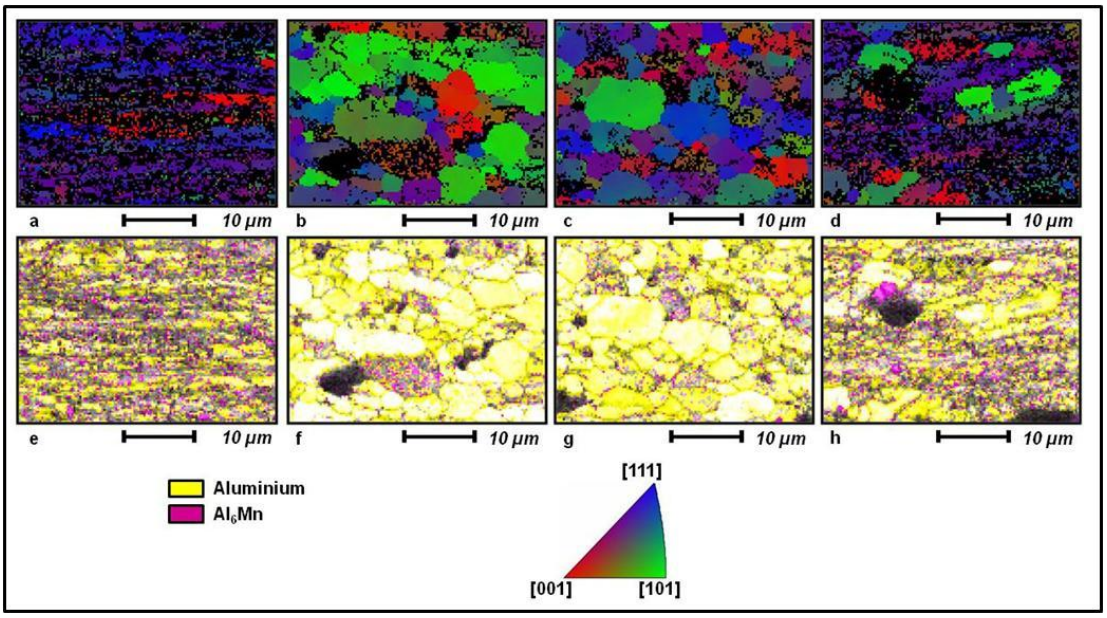

Figure 8.19, EBSD Maps and Phase Maps for the Double Pass Weld in AA5083: a) Parent Material, b) Advancing Side TMAZ, c) Weld Centre d. Retreating Side TMAZ, e-h) Corresponding Phase Distribution Maps.

8.4.3 Friction Stir Welds in AA2004 Created on the ESAB Machine

The EBSD maps for the single pass weld in AA2004 shows a change in grain size for the centre of the weld compared to extremities of the TMAZ. The grain size is slightly larger for the weld centre. This region experiences the most deformation and most disruption to the distribution of second phase precipitates. It also contains more recrystallized material. Figure 8.20.b) and c) shows some small equiaxed grains interspersed with larger grains which have been allowed to grow due to lack of pinning forces acting on the grain boundaries. On both the advancing and retreating sides of the TMAZ, shown in Figure 8.20.a) and d) the grains remain small and the structure is mostly equiaxed. The amount of the energy and amount of recrystallized material within this region has meant that these areas evolve at different rates. The weld centre enters a cycle of recovery and growth before the extremities of the weld, causing grain coarsening and the development of a non-equiaxed structure, which is detrimental to GBS and therefore superplastic deformation. The spindle speed used for this weld is 1250rpm and has a welding pitch of 0.8mm/rev. The double pass weld used a spindle speed of 700rpm and has a welding pitch of 1.49mm/rev. The increased heat input and higher spindle speed has caused significantly more

coarsening of the second phase. The distributions of the second phase is also significantly different, there are more coarse particles and less fine particles distributed along the grain boundaries leading to less superplastic deformation before failure due to grain coarsening.

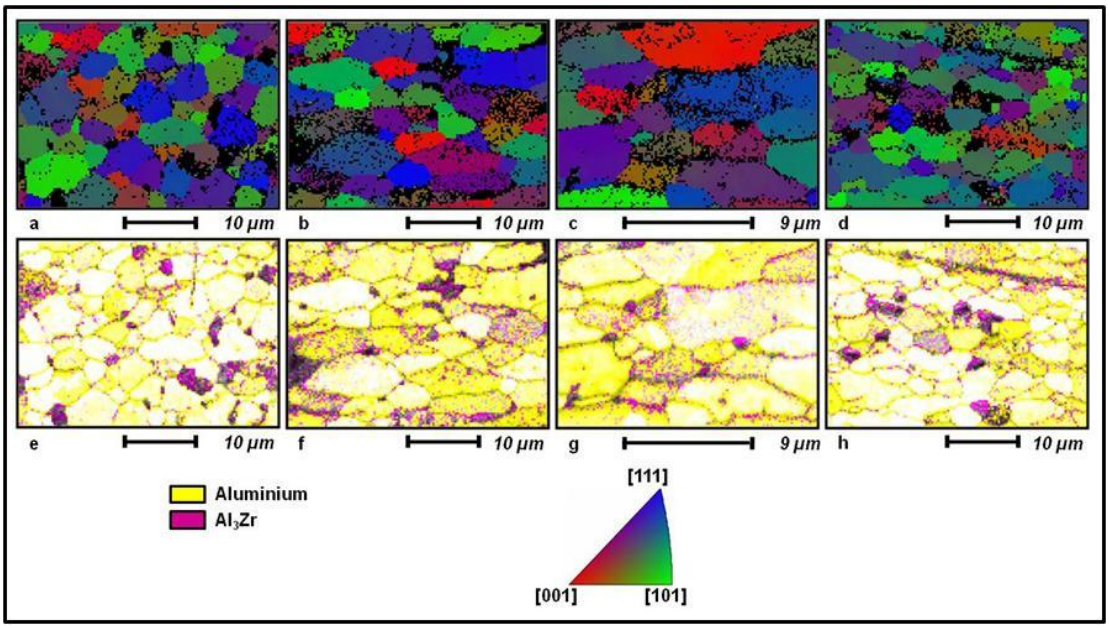

Figure 8.20, EBSD Maps from a Single Pass FSW in AA2004 Created on the ESAB Machine: a) Advancing Side TMAZ Extremity, b) and c) Weld Centre, d. Retreating Side TMAZ Extremity, e-h) Corresponding Phase Maps.

The levels of residual stress in a friction stir weld are higher on the advancing side of the weld, giving this region more energy for structural change, leading to larger grains after during subsequent forming operations. This is true for the single pass weld shown in Figure 8.20. The triple pass weld differs from this pattern. The retreating side undergoes three consecutive heating cycles from the three overlapping passes; the advancing side only experiences one. This has led to the grains on the retreating side becoming larger than the advancing side; this is clear from comparing Figure 8.21.a) and c).

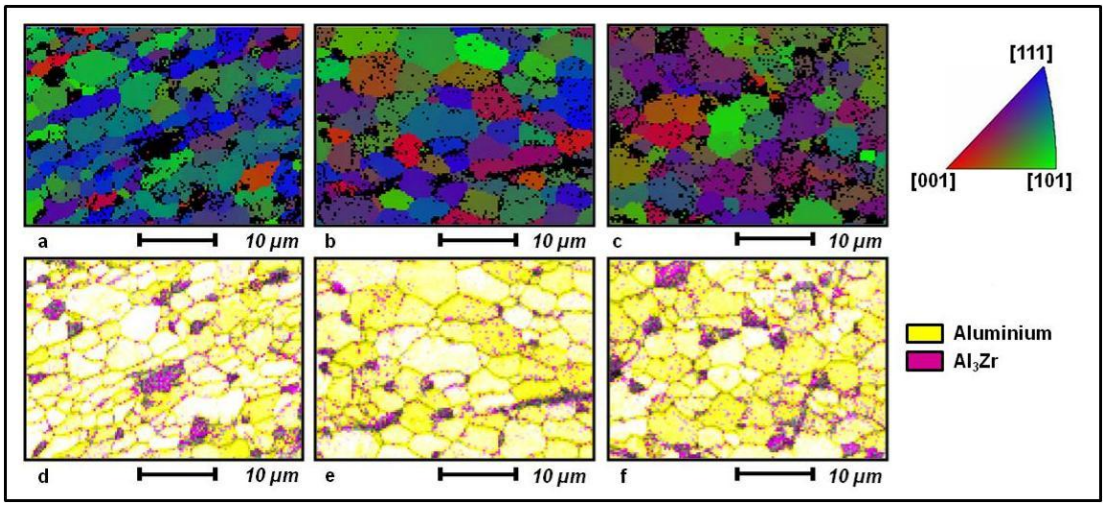

Figure 8.21, EBSD Maps for the Triple Pass Weld in AA2004.
a) Advancing Side (pass 3), b) Weld Centre (pass 2), c) Retreating Side (Pass 1), d-f) Corresponding Phase Maps.

Once again the weld centre exhibits the largest grain size with mostly equiaxed grains; this is also the case on the retreating side. The advancing side has a very different structure; some larger grains in amongst much smaller grains. The differing levels of recrystallization within the structure mean that when the SPF process is applied the weld region experiences heterogeneous structural evolution. This gradient of change affects the overall SPF strain; the grains in the weld centre and retreating side in this case grow faster and get to size where they can deform in a superplastic regime, the advancing side's structure is still fine allowing it to deform and has caused more deformation in this region. For the triple pass weld the pole of the cone test is not the thinnest part of the specimen; this is located on the advancing side of the weld.

8.4.4 Friction Stir Welds in AA5083 Created on the ESAB Machine

It is clear from the optical microscopy that the AA5083 welds react very differently to the SPF process than the welds in AA2004. The amount of grain growth and abnormal grain growth is much higher; causing the structure obtained to resemble a formed fusion weld [80]. Figure 8.22 shows the EBSD and phase distribution for the single pass weld in AA5083. It is clear from Figure 8.22.b) that the failure of the sample originated from the top surface of the weld where the grains are coarse. As the grains coarsen the tensile strength required for grain boundary separation is reduced. The coarse grains separate and the tear then moves quickly through the finer

grained material beneath. There is not much difference between the advancing and retreating sides shown in Figure 8.22.a) and c). Coarse material dominates the top surface which experiences the most strain during forming. The lower part of the sample still exhibits the fine structure present in the unformed FSW material. The phase maps show the distinct lack of second phase particles which are vital for the stability of the material at SPF temperatures. The stabilizing particles in AA5083 are Al_6Mn, but there are insufficient numbers of these to prevent the extreme grain coarsening experienced by the formed FSWs. Most of the second phase is distributed within the grains rather than on the grain boundaries which is the case for the strengthening precipitate Al_3Zr in the AA2004.

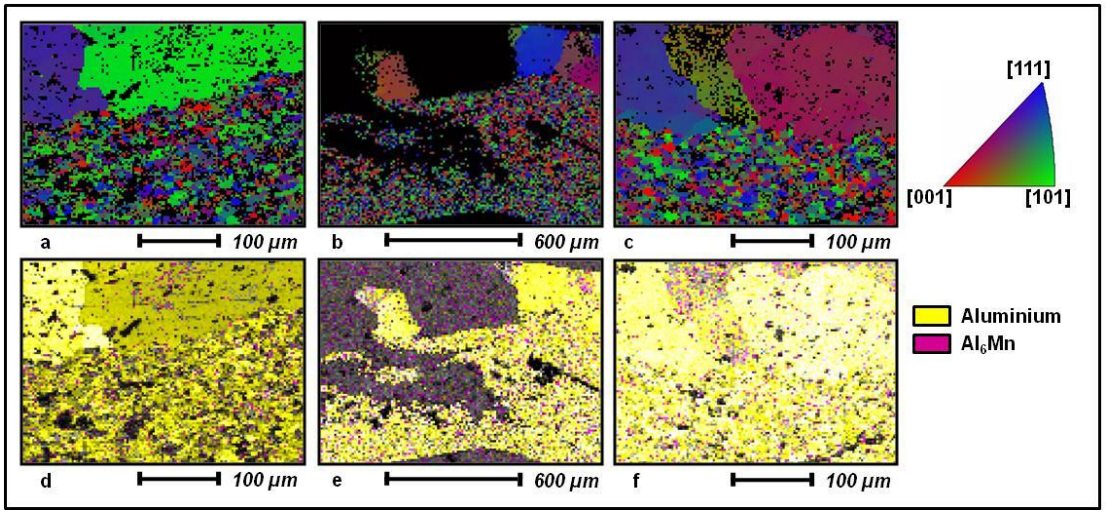

Figure 8.22, EBSD Maps for the Single Pass Weld in AA5083:
a) Advancing Side TMAZ, b) Weld Centre, c) Retreating Side TMAZ,
d-f) Corresponding Phase Maps.

The triple pass weld exhibits the same lack of stabilizing particles situated on grain boundaries as shown by the phase maps in Figure 8.23.d-f). The significantly larger magnitude of heating and deformation experienced by this weld has led to a spectacular amount of abnormal grain growth situated in the weld region. A fine equiaxed structure remains at the very extremities of the weld footprint; transforming to a coarse structure which resembles a fusion weld within the area passed through by the tool probe; this is shown in Figure 8.23.a-c). The joint interface has been completely annihilated and has been proved to be strong enough to withstand the

forces involved in SPF. The failure has occurred in the transverse direction between the bands of the FSW microstructure.

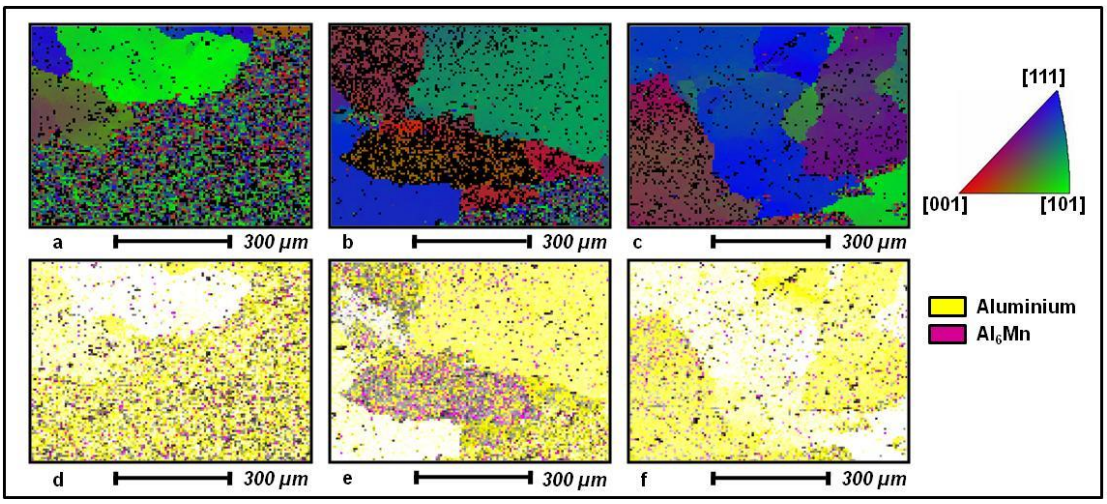

Figure 8.23, EBSD Maps for the Single Pass Weld in AA5083:
a) Advancing Side TMAZ, b) Weld Centre, c) Retreating Side TMAZ,
d-f) Corresponding Phase Maps.

8.5 Crystallographic Texture

EBSD has been used in this investigation primarily to provide clear information on the microstructure of the parent materials and friction stir welds. The EBSD analysis has provided detailed pictures of the grain structure and more importantly the presence, size and distribution of the second phase particles. Additional information from the EBSD analysis enables an understanding of any preferential textures developed during welding or during the SPF process. Crystallographic texture is the distribution of orientation within a material sample; if the crystalline orientation is completely random it is said to have no texture [98]. From the EBSD maps shown in this section is can be clearly seen that after friction stir welding the aluminium's microstructure exhibits a completely random texture. The superplastic parent materials benefit from this random texture. The random texture aids and facilitates the grain boundary sliding mechanism which allows uniform deformation and eventual superplastic straining.

8.6 Summary

Microstructural stability appears to be the biggest limitation of the friction stir weld's microstructure. This is alleviated in the AA2004 by the relatively large amount of

Al_3Zr distributed along the grain boundaries. The grain coarsening is minimised but is still a factor as the rate of coarsening is much higher than the parent or unaffected material outside of the weld footprint. During superplastic forming the evolution of the microstructure starts with dynamic recrystallization of the parent material which then progresses into dynamic recovery and grain coarsening and eventually abnormal grain growth and failure of the material. The FSW weld region contains recrystallized material and so is a step into the superplastic microstructural evolution. While the parent material is recrystallizing the weld region is coarsening, in some cases this is abnormal grain growth due to the disruption of the distribution of stabilizing precipitates. This is highlighted by the AA5083 samples. Manganese is used in this material for structural stability; this element is not as effective as zirconium and is present in much smaller amounts. The Al_6Mn is distributed within the matrix grains; not along the grain boundaries which is far more effective for pinning the grains during high temperature deformation. The AA5083 welds produce an undeformable weld region which is pulled apart by the deforming parent material; this usually results in a failure along the joint interface. The AA2004 behaves in a very different manner. The recrystallized material in weld region requires a much lower flow stress to start the deformation and as a result starts to deform before the parent material. In this case most of the deformation is localized within the weld region.

9 Discussion

9.1 Introduction

Friction stir welding and processing has been a heavily researched area since its invention in 1991 with academic research, industrial research and patent applications increasing on a yearly basis. FSP has been successfully linked to the production and retention of superplastic properties in a number of aluminium alloys and has led to the production of aluminium alloy which can be formed via high strain rate superplasticity (HSRS). This decreases the forming time per part, thus increasing the production rate of SPF parts, making superplastic forming an effective and more competitive method of producing complex parts.

FSW/FSP is capable of producing superplastic microstructures which outperform those created using standard thermo-mechanical processing. Creating enhanced superplastic responses from already superplastic materials and providing non-superplastic materials the ability to become superplastic. Joining sheets prior to SPF is impossible via standard fusion welding practices due to the complete destruction of the fine structure needed for superplasticity. The low heat input and intense deformation which occurs during FSW creates a far superior post weld microstructure allowing sheets to be joined in butt weld and lap weld configurations as well as multisheet structures for internally supported structures. FSW has been shown to be effective for joining 2XXX, 5XXX and 7XXX series aluminium for subsequent high temperature deformation [30].

9.2 Friction Stir Welding of Superplastic Aluminium Alloys

Superplasticity is a phenomenon which is very sensitive to the microstructure of the material which is being deformed. It relies on a set of well defined prerequisite characteristics; however, fulfilling all of the characteristics still does not guarantee that the material will be able to become superplastic. There are many characteristics which are believed to be required for superplastic deformation to occur in aluminium [3, 86, 99]. Of these characteristics the main points are clear; the material must have a fine equiaxed structure typically <10μm with a distribution of hard, second phase particles. The second phase particles are very important to the stability of the materials at high temperatures. Metals experience cycles of recovery,

recrystallization and grain growth in order to reach the preferred state which will be close to equilibrium provided there is enough stored energy within the structure to enable the transformation. The transformation occurs via the three mechanisms mentioned above; which can overlap and compete for the energy within the structure. The most beneficial of these mechanisms, to post weld SPF, is that of recrystallization; the nucleation and growth of deformation-free grains as this provides a fine grain structure. Understanding the state in which the material begins the SPF process is paramount in understanding how the material has evolved into its final structure. There are many excellent works centred on the understanding of all the complex annealing mechanisms which affect the material during heating and deformation process [46, 98, 100, 101]. These theories have been assimilated to provide a clear visualisation of the evolution from a highly strained, banded original structure into the fine equiaxed structure required for SPF and the transformation of the original structure into the equiaxed structure which is characteristic to FSW [27, 49].

9.2.1 AA5083

AA5083 is widely considered to be a non-heat-treatable alloy which gains its strength from solid solution strengthening and strain hardening from extensive cold working. The material starts as a highly deformed, banded structure. The bands are plate shaped grains with large elongations in the rolling direction and moderate elongations in the transverse direction. This structure is full of dislocation tangles which makes the material is extra hard [90]. Upon heating, during the initial preheat stages of SPF, the AA5083 transforms into an equiaxed matrix structure dispersed with fine Al_6Mn particles via static recrystallization [2, 88]. The material is packed full of dislocations and it is these tangled dislocations which provide the energy for structural change when the material is heated. This material is known to begin recrystallizing at temperatures as low as 350°C which is close to the temperatures associated with the friction stir welding process. Dislocations within the structure are assimilated into the subgrain boundaries until the subgrain becomes sufficiently misorientated and becomes a new grain. This structure should now be capable of superplastic deformation due to fulfilling the two main characteristics required for fine-structure superplasticity. The fine SP microstructure will now continue to evolve via dynamic recrystallization and recovery mechanisms until the onset of necking.

Necked regions which exhibit a critical level of strain begin to deform via dynamic recrystallization leading to these areas remaining finer in grain size whilst dynamic recovery and growth occurs outside of the necked area in regions where the strain has not maintained a sufficient, critical level to sustain recrystallization [102]. AA5083 is capable of superplastic elongation but is severely limited to ~500-600% due to its lack of high strength precipitates. Fine Al_6Mn particles are present but these are distributed throughout the entire matrix structure, not preferentially distributed on the grain boundaries and so are not effective at pinning the grains and preventing grain growth [88]. Friction stir welding also causes an evolution of the parent material; the weld region is subjected to localized, intense heat and deformation in the form of material shear [24] and hot extrusion as the tool traverses the material. This involves two competing processes. Firstly the heat and deformation causes the material to become softer by associated annealing and recovery processes, the strain hardening is reduced and the grain size increases. Secondly the deformation provided by the rotating tool adds to the dislocations already present in the material, restoring some of the strength lost through heating, this antagonistic relationship means that the strain hardened parent material does not experience a significant loss of strength in the weld region if a critical level of heat input is not reached. Properties of AA5083 friction stir welds are widely publicised; studies by Svennsson et al [50] and Kristensen et al [64] provide excellent property and microstructural assessments of AA5083-O whilst Peel et al [18] have investigated AA5083-H19 which is the same as the material investigated in this thesis. In the cases for AA5083-O both investigations conclude that the FSW process can have a minor strengthening effect on the material. Since AA5083-O is fully soft, strength cannot be lost due to heating; only flaws in the weld region microstructure can weaken the material. The AA5083-H19 material investigated by Peel et al has undergone significant softening in the weld region leading to an extensive drop in tensile strength and hardness. Without the exact specifications of the tooling and the spindle speeds used it is difficult to make a comparison; however it is surmised that these detrimental effects are caused by significant heat inputs due to the very low welding speeds; low welding speeds lead to increased annealing effects as the tool is traversed. This parallels the hot welding conditions from the work included in this thesis. In this work fast traverse speeds are employed to minimise the annealing phenomena; this accompanied with small diameter tools has enabled high tensile

strengths with joint efficiencies close to 100% and minimal reductions of ≤15% in hardness across the entire weld region. However, the hot welding conditions employed in this investigation have led to the same weakening of the material. In the three examples given above [18, 50, 64] clearly defined weld nuggets are present which also include visible flow patterns. The welds created in this investigation did not exhibit a separate weld nugget, only the TMAZ is present; with the most deformation present in a layer which comprises the top third of the material thickness which is directly influenced by the tool shoulder. During subsequent superplastic forming it is this region which experiences the most grain growth. In the single pass weld created on the ESAB SuperStir the top layer of intensely plasticised material has experienced significant grain growth compared to the material situated further towards the weld root. The grain growth in this sample is confined to the material which has been influenced by the FSW tool providing a stark contrast between the unprocessed and processed material. The difference can now be understood between the unaffected base material and friction stir weld zone in terms of their position within deformation cycle during SPF. The parent material undergoes its transformation into fine equiaxed grains due to recrystallization; subgrain rotation and misorientation leading to new undeformed grains which then begin to coarsen due to recovery during the forming process. In a parallel cycle the weld region contains some fully recrystallized material, with the vast majority comprised of fine grained partially recrystallized material with residual dislocations induced by the forging action of the tool heel. While the parent material is recrystallizing, the weld material is coarsening; large deformation free grains begin to grow and consume the small equiaxed grains. If the parent material was allowed to continue its evolution the recrystallized material would also grow and eventually reach a size where deformation causes failure; however, as the weld material is one stage further into the microstructural evolution this material coarsens and fails well before the parent material. Charit and Mishra [65] have suggested an FSP microstructural evolution which contains recrystallized grains of a larger size than the parent material which have additional deformation induced by the tool heel forging action. It is surmised that the grains which contain the dislocations from the forging action have sufficient energy locked in the structure after cooling to enable recovery to cause grain coarsening during the heating of the material before deformation begins. These grains now have a comparable size advantage over the rest of the weld region and

continue to grow until the stress required for grain boundary separation is reached and the material fails.

The grain growth problem is highlighted further by looking at the triple pass weld in AA5083. The overlapped tool passes make the through-thickness weld region much wider than the single pass weld. However towards the extremities of the weld region only the top third is affected further suggesting that the grain growth is strictly limited to the material which has been dynamically influenced by the tooling. The distinct lack of strengthening precipitates causes the early failure of this material after welding and superplastic forming. The Al_6Mn particles are insufficient to prevent grain growth and maintain the fine structure required for superplastic deformation. Investigations have been carried out on modified Al-Mg alloys with additions of Zr, Mn, Cr and Sc [81, 82, 83]. These strengthening precipitates are used to further refine the grain size and structure of the material as well as maintaining the fine grain size upon heating for superplastic forming. In case of Ma et al [82] and Charit et al [81] the refinement of the grain structure has led to an ultra fine structure which is capable of low temperature SPF; with successful superplastic deformations at temperatures ranging from 175-310°C which equates to superplasticity at 0.48 T_m where T_m is the melting point in K. It is fully accepted that the thermal and deformation cycles experienced by FSW material causes a massive change in the structure of the material and has a huge affect on its stability. Hot welding conditions causes an increase in grain size and leads to grain growth during subsequent SPF. Very cold FSW parameters, coupled with small tools have been found to significantly reduce the grain size and improve the stability of the material. The only major problem with using small tools is the size of the weld region which is produced. The double pass FSW produced using the GSP 5651 tool failed due rupturing of the weld seam. Despite the cold welding conditions, 1.49 mm/rev, and small tool size the weld region remained undeformable and was subsequently pulled apart by deforming parent material. A recent investigation by Charit et al [65] has shown that commercially available AA5083-SPF can exhibit enhanced superplasticity via FSP; this has been shown using micro-tensile test pieces taken from the dynamically recrystallized weld nugget. This does not take into account the rest of the heterogeneous microstructure situated in the TMAZ but does go on to state the sensitive nature of the microstructural stability will mean that FSW/FSP

requires further optimization in order to produce a weld region which is better matched to the parent material and allows superplastic deformation throughout a gage length including parent material, HAZ, TMAZ and nugget regions. Studies on superplastic responses of AA5083 material which have undergone severe plastic deformation exhibit the same deficiencies as the FSW/FSP material discussed above [76, 83], although fine grained structures are possible they lack the stability at superplastic temperatures provided by coherent strengthening precipitates. The AA5083 friction stir welds tested at superplastic temperatures resemble that of fusion welds produced by Davies et al [80]. A relatively small elongation ranging from 40-60% is achievable in the weld region compared to >200% for the parent material; the weld region has a higher flow stress and thus is undeformable at these temperatures.

9.2.2 AA2004

AA2004 is a precipitation strengthened aerospace alloy which has been developed for its superplastic properties. The relatively large addition of zirconium makes this material very stable at high temperatures due to fine, coherent Al_3Zr precipitates preferentially distributed along the grain boundaries. AA2004 has been welded in the as fabricated condition and the structure is similar to the AA5083 in appearance but with the elongation in the rolling direction being significantly larger with flow patterns surrounding the hard second phase particles. This material undergoes a very complex transformation when it is subjected to the heat and deformation of the FSW process. Many authors have made a number of suggestions relating to how the microstructure evolves into the fine equiaxed grains present in the weld nugget and the heterogeneous mixture of fully and partially recrystallized material in the surrounding TMAZ. Some suggest a continuous dynamic recrystallization mechanism [27, 49], whilst other suggest a geometric dynamic recrystallization mechanism [25]. Whether geometric or continuous in nature; dynamic recrystallization is present in the FSW region. This region has been heated and deformed by the tool severely affecting the room temperature properties of the alloy. The FSW process has been shown to degrade the mechanical properties by coarsening of the strengthening precipitates in regions affected by the heat of the tooling but no deformation; making the HAZ the weakest part of the material and resulting in the distinct ‘W’ shaped microhardness plots in most 2XXX series aluminium alloys [7, 12, 30, 43, 103]. The relatively large amounts of Zr in this alloy

have suppressed the recrystallization occurring during FSW; in turn minimising the hardness loss within the weld region and also keeping the grain size small which affects the hardness by the hall-petch relationship. This yields the hardness plots created in this investigation, moderate softening has occurred; yielding a hardness loss of up to 25%, however this is not limited to HAZ but is present across the entire weld region. This small reduction in hardness is mirrored by the tensile strength of the material. Ultimate tensile strength has been reduced as much as 40% for hot welds and large tools and as little as 6% for cold welds created with small tools. The reduction in ultimate tensile strength relates to the break up, distribution and coarsening of strengthening precipitates within the weld region.

A similar transformation occurs during SPF when the parent microstructure evolves into a fine equiaxed structure. An excellent account of this transformation is given by Bate et al [92] the evolution of this material is said to be linked with dynamic grain growth with a reduction in texture intensity. The original banded structure coarsens causing the grain size to increase while they become increasingly misorientated resulting in a weaker more random texture. The true superplastic deformation does not begin until this evolution takes place; once sufficient deformation allows the transformation, from banded structure to equiaxed structure, superplastic deformation occurs via intragranular slip.

During the high temperature deformation of friction stir welds the weld region is in a state where deformation via superplastic creep mechanisms is possible, the parent material is not. The parent material must first transform into a superplastic structure, however, as the weld region is already capable of deformation under the various creep mechanisms associated with SPF this region begins to form first. Dynamic grain growth has led to a reduced flow stress for superplastic deformation; this in turn has restricted most of the deformation to the weld region. Minimal strain occurs in the unaffected sheet with the change in sheet thickness considered to be negligible; looking more closely at the cone tested AA2004 sheets necking is visible on the advancing side weld region where as the retreating side exhibits uniform deformation; it is surmised that this is due to the asymmetric nature of FSW. The particle break up and distribution by the rotating tool coupled with the increased residual stresses on the advancing side of FSW [54] may directly affect the

deformation mechanisms from the retreating side, through the weld nugget and across to the advancing side. The success of this alloy is attributed to the strengthening precipitates. This alloy remains stable at high temperatures; with minimal grain growth and very limited abnormal grain growth. Superplastic strains of greater than 200% have been achieved in SUPRAL 100 sheets after friction stir welding using an MXTriFlute^{TM} tool. Superplastic properties have been retained or induced after friction stir welding/processing in a number of different 2XXX series aluminium alloys including AA2095 [4], Zr modified AA2014 [67] and AA2024 [58]. The dynamic grain refinement which occurs during FSW/FSP is paramount to obtaining superplastic strains at temperatures where microstructures often become unstable. The fine grain sizes and the ability to remain fine during hot deformation allow the first and most vital condition for superplasticity to be achieved. This is further highlighted by the works carried out on 7XXX series alloys: AA7050 [70], AA7075 [68, 69, 71, 72, 73, 74] and AA7475 [70, 75]. These investigations show the enormous potential of FSW for solid state joining of aluminium sheets prior to SPF. A fine equiaxed structure is produced which is capable of superplastic deformation, however all the investigations in 5XXX, 2XXX and 7XXX series aluminium show the same problems in terms of the final friction stir welded/processed microstructures. The FSW structure is heterogeneous in nature, different regions within the weld exhibit slight but significant changes in recrystallization, recovery and grain growth, volume fraction of strengthening precipitates, size of the precipitates, residual stresses and dislocation density. All of these factors affect the final FSW/FSP microstructure's ability to perform well during high temperature deformation. The most significant factors are twofold, firstly the stability is intrinsically linked to the strengthening precipitates included in the parent sheet, additions of Zr, Mn, Sc and Cr are vital in maintaining stability and the fine grain size at high temperature. Secondly the structural evolution of the parent sheet into the superplastic capable structure, the FSW structure is capable of superplastic deformation immediately after welding. The parent sheet has to transform into a superplastic capable structure during the initial stages of SPF, this puts the two structures out of sync. One will deform before the other due to mismatched flow stress, strain rate sensitivity and deformation mechanism.

9.3 Friction Stir Tooling

A number of different tooling variants have been used to create the friction stir welds in this thesis. These range from the highly successful GSP 5651 tool developed by TWI [30] to simple smooth conical probe designs which can be produced very quickly and easily on any mechanical engineering workshop equipment [38]. From the results obtained and presented in this thesis it is clear that the most successful tooling exhibits re-entrant features on the tool probe. These features increase the surface area of the probe whilst simultaneously reducing the static volume. The increased heat input and material flow enhances the friction stir welds made with this tooling type. It increases the field of heat and deformation; allowing excellent weld closure and penetration right to the bottom of the weld root. The simple smooth tooling lacks this penetration and consistently produced a weld defect in the weld root. These root defects run the entire length of the welded section and severely degrade the properties of the weld.

Large diameter tooling has been trialled in order to produce a wide weld seam at high welding rates without the problem of tooling breakages due to under-heated material shearing the probe off of the tool shoulder. The GSP 5651 tool is the smallest tool diameter at 7.5mm. This tool creates welds with excellent room temperature properties, however when tested at elevated temperature the weld seams ruptured due to the weld region becoming undeformable at high temperatures resulting in the deforming parent material pulling the weld apart. The larger tools, 16 and 19mm diameters however create a much larger weld region with intense deformation located towards the centre fading out to a more gentle deformation occurring at the extremities. This weld zone has been able to deform under superplastic conditions before final failure occurs due to grain coarsening. The range and magnitudes of the forces involved in FSW have been shown to be directly linked to the tooling used to create the welds [31, 104, 105] with the diameter of the shoulder being the main factor. Although only standard rotary friction stir welding has been investigated here there are many new and emerging variants of FSW which could possibly improve the ability to join superplastic materials. The asymmetry of FSW creates a big problem in terms of particle break up and distribution within the weld region. Symmetrical FSWs created by experimental FSW variants such as ReStir^{TM} [106] and SkewStir^{TM} [107] could be beneficial in creating FSW/FSP with identical properties on either

side of the joint interface. Another variant of interest is ComStir™ [108]; this uses the combined rotary action of the tooling with an additional orbital movement from the spindle which will create a wider deformation zone meaning more material can be processed for each pass of the tooling. Using the conventional rotary FSW setup advanced tooling such as DualStir™ has been developed to address the problem of the periphery speeds of the rotating probe and tool shoulder. DualStir™ [109] can set the shoulder rotation speed and probe rotation speed independently of each other allowing more finely adjustable welding parameters and more optimised weld region. Removing the shoulder completely has led to the development of shoulderless FSW. The top section of the weld is contained by a skid which is pulled over the top surface of the weld material. The probe is completely immersed in the material via a pilot hole. This creates a very narrow weld region stirred by the rotating tool probe and compressed by the tool skid. This new variant of FSW is of interest due its very low heat input and narrow weld region especially to welding superplastic material where the disruption to the original microstructure is dominated by the tool shoulder deformation [110]. Welding at reduced starting temperatures may also give a substantial advantage to the friction stir welding process for joining superplastic material; a study by Benavides et al [60] has reported a very fine grain structure of 0.8μm when welding is carried out at -30°C. The fine grain size and greatly reduced peak temperature will assist in maintaining a superplastic microstructure after FSW. The peak temperature close to the tool stays below 140°C preventing any relaxing of the structure via annealing processes.

9.4 Friction Stir Welding - Current Research Trends and Opportunities for Future Work

9.4.1 FSP of Aluminium Alloys for Selective Superplastic Properties

Work is currently underway to develop existing superplastic alloys in order to enhance their properties and achieve higher levels of superplastic deformation. The current highest SPF elongation stands at ~8000% [2]. Using FSP to locally adjust the structure of the material further improvements can be made to already successful alloys, allowing for deeper forming and more complex shapes. FSP could also be utilized to remove superplastic properties, this may seem a little strange but the ability to remove the superplastic properties of a material may be of interest in order to develop selective superplasticity. FSP has been shown to be capable of enhancing SPF, being able to manipulate the levels of superplasticity either increasing or decreasing the magnitude of the deformation can enable processed sheets to be created which are tailor made for the SPF process; enhanced areas where deformation is high and removed properties where deformation is minimal and the sheet thickness is important.

9.4.2 Producing Superplasticity in Non-Superplastic Materials

Most of the current works on friction stir technology and superplasticity are centred on obtaining superplastic responses from otherwise non-superplastic materials. The ability for FSW to produce a fine recrystallized structure is important for producing materials which exhibit the prerequisites for fine-structure superplasticity.

9.4.3 FSP to Optimise SPF – Low Temperature SPF and HSRS

Superplastic forming is not currently considered viable for production of mass quantities of parts due to the relatively long forming times associated with the low strain rates required for the process to be successful. High strain rate superplasticity HSRS is a subject area of great interest in order to speed up the production rate. Production of ultra-fine grain structure via FSP has enabled the strain rates used to be increased towards the more favourable strain rates of 10^1 [74]. Another more favourable direction is reduced temperature SPF. Currently the temperature range for superplasticity in aluminium is between 450 and 500°C. Superplastic elongation

have be demonstrated in FSW material at the lower temperature of 430°C, reducing preheat time and therefore reducing energy expenditure [82].

9.4.4 Friction Stir Processing with Deposition of Strengthening Particles

This hypothetical process would utilize the FSW process' ability to plasticise the material and distribute material beneath the tool. If strengthening particles can be deposited on the top surface of the weld material in front of the tooling then the FSW tool can then mix these precipitates into the existing material. This would have the advantage of adding grain refinement elements to the material and increasing the stability at high temperatures. This would allow superplastic welds to be created and have the possibility of creating enhanced superplasticity in the FSW material.

9.5 Summary

Friction stir welding has been carried out on AA5083-H19 and AA2004-F using small (7.5mm) and large (16-19mm) diameter tooling and three machines with varying levels of control and in-process monitoring technology. Excellent room temperature properties are exhibited by both of the alloys covered herein with AA5083 retaining most its strain hardening and successful joining of AA2004 which is deemed difficult to weld using standard fusion welding techniques. High temperature deformation has been shown to be successful in AA2004 due to the inclusion of strengthening precipitates; the AA5083 is not successful in these tests due to coarsening of the structure during heating. Microstructural observations show that both materials coarsen during deformation; however the AA2004 is pinned by the substantial amounts of Al_3Zr keeping the grain size small. Superplastic elongations of >200% are achievable in AA2004 where as non-superplastic elongations of 60-87% are achievable in the AA5083.

10 Conclusions

10.1 Summary

FSW can be successfully carried out on aluminium alloys which are designed to exhibit superplastic deformation. This has been carried out using many different tooling designs. Some of these designs are existing tool designs used for series production and have been thoroughly tested in laboratory experiments by TWI [30], the rest of the tooling designs have been created specifically for this investigation, using design parameters so far unused for this type of material in this thicknesses used in this thesis. Friction stir welds have been created using the different tooling designs and on three very different machines. These range from a very basic milling machine, the kind found in every single university mechanical engineering workshop, to a state of the art dedicated friction stir welding machine, the kind used in industrial FSW. The friction stir welds created have been tested for room temperature mechanical properties and then subsequently tested for microstructural stability and elevated temperature mechanical properties to test for superplastic behaviour. In all cases the welding of the material is possible with FSW microstructures providing good room temperature properties obtained for all tooling sets. The most critical aspect is the consolidation of the weld in the root, failure to provide sufficient deformation to the weld root leads to an inherent flaw which runs the entire length of the weld causing early failure when subjected to tensile stresses; this has been tested using 180° bend tests with the root in tension as a quality control test. The excellent room temperature response is not mimicked for superplastic response as some of the tooling sets produce FSW microstructures which are incapable of superplastic deformation due to disruption to the delicate original structure. Stability of the structure is paramount during elevated temperature deformation, the heterogeneous structure produced by FSW causes the different regions within the structure to firstly evolve into the superplastic microstructure, deform and finally coarsen at different rates. Superplastic deformation has been shown to be possible using specific tools and weld process variables as outlined in the following conclusions.

10.2 Friction Stir Welding of Superplastic Aluminium Alloys

10.2.1 AA5083

- The weld region has undergone varying level of softening due to recovery mechanisms relaxing the strain hardening present in the parent material. Lower heat inputs like those observed form the GSP 5651 tool do not fully soften the material, there is residual strain hardening in the material increasing the joint efficiency.

- The larger tools produce substantially larger heat inputs; meaning the tool has a far greater influence on the material creating material which has been annealed by the tool.

10.2.2 AA2004

- During FSW Al_3Zr precipitates are distributed throughout the weld region via the complex material flow beneath the tooling and subjected to heat and deformation which cause the second phases to coarsen. This has caused the weld region, in all cases, to become extensively softened; with tensile strength and elongations resembling parent material which has been annealed at 350°C.

10.2.3 Hot and Cold Welding Parameters

- The FSW process has shown to be successful using both the hot and cold welding parameters with room temperature responses improving as the weld heat input is reduced.

- The cold welding parameter reduces the amount of heat input to the weld and so reduces the annealing effect of tool as it passes the material.

10.2.4 Tool Performance

- All tooling sets are capable of creating friction stir welds in both of the materials but with varying success. The tooling which include re-entrant feature on the tool probe (TriFlute and TriFlat designs) yield far superior joint efficiencies and

provide sufficient heating and deformation to the weld root to create a sound joint.

- The simple tools (concave and large shoulder designs) lack the ability to stir the material in the weld root which leads to root flaws and ultimately a failed weld.

- Of the re-entrant tooling the most successful are the TriFlute tooling; however these tools are prone to breaking due to the reduction of tool probe material created by the flutes. The most tool failures have been experienced when using the TriFlute tooling designs and cold welding parameters.

10.2.5 FSW Machinery

- The machine used to create the weld has proven to be very influential in the overall quality and success of the welds produced.

- The Parkson milling machine, FW22 and the ESAB SuperStir have all utilized position control; however the ESAB SuperStir is the only machine which uses CNC to position the tooling.

- Both the Parkson mill and FW22 rely on manually setting the plunge depth which will severely affect the accuracy and repeatability of the plunge depth.

- The Parkson milling machine is capable of FSW but is hampered by its limited process variable settings for spindle and traverse speeds and also by the manual plunge depth.

- FW22 is more than capable of FSW but is once again let down by the manual plunge depth setting.

- The ESAB SuperStir machine is a dedicated FSW machine and so is not limited in its ability to perform FSW on the materials and thicknesses used in this thesis. The ESAB SuperStir is the most successful machine used for this investigation, producing single pass welds which can be deformed to superplastic elongations.

10.3 Room Temperature Response

10.3.1 Retention of Strength after Friction Stir Welding

- AA5083 is a strain hardening alloy deriving its strength from dislocation tangles which are relaxed by heating via static recrystallization and recovery mechanisms.

- AA2004 is a precipitation hardening alloy obtaining its strength from a distribution of hard particles within the aluminium matrix. Heat from the FSW process causes these precipitates to coarsen, degrading the strength of the material.

10.3.2 AA5083 – Retention of Strain Hardening

- Once beyond a critical heat input the FSW process fully anneals the AA5083 and produces a softened weld region. All the tools except the GSP 5651 tool produced heat inputs which resulted in annealed weld regions and joint efficiencies ranging from.66-75%. Decreasing the tool size dramatically reduces the heat input and yields an increase in ultimate tensile strength for welds carried out under cold weld conditions.

- For the GSP 5651 tool the joint efficiencies ranged from 67-91%. These over lapping ranges show that the coldest weld parameters; coupled with a 16mm diameter tool produces approximately the same heat input as the hottest weld parameters used in conjunction with the 7.5mm tool. This points to a critical level of heat input, for FSW structures in AA5083, of ~0.1 KJ/mm; above this level all strain hardening is lost.

- Annealing experiments have shown that the AA5083 in the weld region resembles the properties of parent material which has been annealed at 350°C. Annealing of welds at 350°C has led to joint efficiencies ranging from 60-106%.

10.3.3 AA2004 – Disruption and Coarsening of Strengthening Precipitates

- The major risk with precipitation strengthened alloys is the potential for overaging the structure. Overaging causes the second phase particles to coarsen resulting in a drop in strength of the material.

- The FSW process in this case acts as a localised heat and deformation source, disrupting the homogeneous distribution of the precipitates and causing them to coarsen; severely reducing the strength of the weld region.

- AA2004 does not exhibit stain hardening so the deformation and heat both act to soften the material resulting in a tensile strength which ranges from 60-81%, significantly less than the AA5083.

10.4 Superplastic Deformation

10.4.1 AA5083

- The FSW process introduces a region which is partially recrystallized; making this region one stage further into the microstructural evolution which takes place during SPF. As the rest of the parent material is beginning the transformation the weld region which is already recrystallized undergoes static recovery and grain growth.

- As the structure becomes coarser the weld region becomes undeformable much like a typical fusion weld. As the parent material begins to deform the undeformable weld region acts as a block in the middle of the two deforming parent sheets; resisting the deformation until failure of specimen within the weld region.

- For single pass welds it has been shown that each section of the weld region: nugget, TMAZ and HAZ/Parent material coarsens and deforms at different rates, with the most severe coarsening occurring in the centre of the weld and radiating outwards towards the parent material which remains in a relatively fine grained state.

- For triple pass welds the weld has undergone three cycles of heat and deformation and as a result; the structure has coarsened quite considerably. When the structure coarsens it loses its ability to deform; this then leads to the undeformable weld region being pulled apart by the deforming parent material with final failure of the material being situated near the joint interface in the centre of the weld.

- Welds in AA5083 have been formed at high temperature but have only achieved an equivalent SPF strain in the range of 47-79% before failure due to grain coarsening and abnormal grain growth.

10.4.2 AA2004

- The FSW weld region has introduced a band of partially recrystallized material between two regions of unaffected material and so this region will react very differently from the surrounding material. The welded AA2004 material has been partially recrystallized and so while the parent material is transforming, this material begins to deform. This ultimately means that the weld material forms before the parent sheet.

- It has been observed in all the testing of welds in AA2004 that the deformation is not restricted to the weld region but the weld region in all cases has undergone intense deformation whilst the parent material remains relatively unchanged.

- Friction stir welded AA2004 has been shown to be possible of achieving equivalent SPF strains in the range of 70-258% before failure due to grain coarsening.

- The dramatic improvement over the AA5083 results is all due to the strengthening mechanisms employed by the two materials. The relatively large levels of second phase strengthening precipitates present in the AA2004 pins the grain boundaries at SPF temperatures; maintaining a fine equiaxed structure for longer.

10.4.3 Heterogeneous structures

- The FSW process induces a region of heterogeneous structure between the parent sheets. This third body region acts differently for the two alloy systems. In AA5083 the weld region is undeformable due to extreme levels of grain growth and AGG, acting much like a fusion weld; the structure is unstable at high temperatures.

- The AA2004 on the other hand shows accelerated deformation in the weld region. This area has deformed before the parent sheet and as a result has undergone the grain coarsening stage earlier as well.

- For both materials the failure of the cone test has been within the weld region. In most cases it has not been situated on the joint interface; but on the interface between the characteristic FSW microstructure boundary between the weld nugget and TMAZ.

10.5 Strengthening Mechanisms

- AA5083 is a non-heat-treatable alloy which derives its strength from dislocation tangles caused by deformation. During heating these tangles are relaxed and dislocation become free to move resulting in lower strength. A distinct lack of hard second phase particles means that this alloy is unstable high temperatures.

- Material under the FSW tool has been moved and transported throughout the weld region via complex material flows generated by the tooling. This has changed the distribution of Al_6Mn particles which are important for stability of the material. Material in the weld region coarsens at an alarming rate whilst the parent material remains relatively fine grained.

- The AA2004 is a precipitate strengthened alloy and so contains a large amount of hard second phase particles which stabilize the structure under high temperature conditions. The FSW process does affect the distribution of these particles but they are sufficient in number to pin the structure and maintain a fine

grain size throughout the high temperature deformation cycles experienced during SFP.

- Fine precipitates of Al_3Zr have been shown to pin the grains as they appear to be situated mainly on the grain boundaries and there are sufficient numbers to slow grain growth and stop abnormal grain growth.

10.6 Observations Prompting Future work for Greater Optimisation of FSW for Superplastic Response

10.6.1 Matching the Weld Region to the Parent Materials – m values

- The AA5083 has become undeformable in the weld region due to extreme grain coarsening this suggests that the strain rate sensitivity has dropped to less than 0.3; removing the weld region's prerequisite characteristics for superplasticity

- The AA2004 appears to deform at an accelerated rate compared to the base material suggesting that the strain rate sensitivity remains ≥0.3 but with a reduced flow stress for superplastic deformation. The weld region deforms in a superplastic regime with relatively uniform deformation and only minor necking occurring on the advancing side of the weld where the residual stresses are higher.

10.6.2 Minimal Disruption of Original Microstructure

- Creating an FSW microstructure which can undergo the same deformation rates as the parent material can be achieved by cold welding conditions. The cold welding condition causes the least disruption to the parent material.

- This can be improved when the weld region is cooled continuously behind the tooling. Removing heat from the weld region will freeze deformation in the structure. This stored energy can then be utilized during the transformation to fine equiaxed structure during the SPF process.

10.6.3 The use of FSW Variations

- There are several interesting variants of the FSW process which could ultimately improve the performance of deformation of friction stir welded aluminium under superplastic conditions.
- The first variant looked at is a new technology which has been investigated for the FSW of titanium. This involves a rotating probe but no shoulder. In a typical FSW the shoulder provides the most heat, sometimes overheating the top surface of the material, this is removed and replaced by a skid which prevents the weld material from being expelled from the top of the weld and compresses the weld as it passes. This will produce a very narrow weld region which will lack the tapered transverse section characteristics of conventional FSWs.

- The second variant of interest is known as Dual Stir $_{TM}$. This technique employs a shoulder and probe which are independent of each other, this allow the probe and shoulder speeds to set differently to optimise the weld parameters; creating a sound weld without the detrimental property degradation experiences using monolithic tooling.

10.6.4 Designing Welds into the SPF Process

- As it stands the FSW process can produce joins in aluminium which can stand up to the forces experienced during superplastic forming. The weld does not fail at the joint interface and does allow deformation in the surrounding weld region. If the position of the weld is designed into the forming process, i.e. positioned in an area which does not exhibit large biaxial strains, then the weld can experience moderate deformation and still retain its integrity.

References

[1] S. W. Kallee. Friction Stir Welding - How to Weld Aluminium Without Melting it, Innovations for New Rail Business IMechE, London, (2001), http://www.twi.co.uk/j32k/protected/band_8/spswkamy2001.html. (Last Accessed 12/2006).

[2] G. E. Totten, D. S. MacKenzie. Handbook of Aluminum Volume 1 Physical Metallurgy and Processes, (2003), ISBN: 0-8247-0494-0.

[3] T. G. Nieh, J. Lawrence Wadsworth, O. D. Sherby. Superplasticity in Metals and Ceramics, (2005), pp 1-287, ISBN: 0521020344.

[4] H. G. Salem, A.P. Reynolds, J.S. Lyons. Microstructure and retention of superplasticity of friction stir welded superplastic 2095 sheet, Scripta Materialia, (2002), Issue 5, Volume 46, pp 337-342.

[5] W. M. Thomas. Improvements Relating To Friction Welding, PCT/GB92/02203, WO 93/10935, (1993), p 1.

[6] M. A. Sutton, B. Yang, A. P. Reynolds, R. Taylor. Microstructural studies of friction stir welds in 2024-T3 aluminum, Materials Science and Engineering A, (2002), Issue 1-2, Volume 323, pp 160-166.

[7] R. S. Mishra, Z. Y. Ma. Friction stir welding and processing, Materials Science and Engineering: R: Reports, (2005), Issue 1-2, Volume 50, pp 1-78.

[8] T. L. Dickerson, J. Przydatek. Fatigue of friction stir welds in aluminium alloys that contain root flaws, International Journal of Fatigue, (2003), Issue 12, Volume 25, pp 1399-1409.

[9] S. W. Kallee, E. D. Nicholas, W. M. Thomas. Friction Stir Welding: Invention, Innovations and Industrialisation, Berlin, (2002), http://www.twi.co.uk/j32k/protected/band_8/spwkmar2002.html. (Last Accessed 12/2006).

[10] G. J. Grant. Superplastic Forming of Aluminium Multisheet Structures Fabricated Using Friction Stir Welding and Refill Friction Stir Spot Welding, 6th International Symposium on Friction Stir Welding, (2006).

[11] S. W. Kallee. Friction Stir Welding in Series Production, (2005), http://www.twi.co.uk/j32k/protected/band_8/spswkdec2004.html. (Last Accessed 12/2006).

[12] T. Khaled. An Outsider Looks at Friction Stir Welding, Federal Aviation Administration, ANM-112N-05-06, 2005, Pages 1, (2005), http://www.faa.gov/aircraft/air_cert/design_approvals/csta/publications/media/friction_stir_welding.pdf. (Last Accessed 12/2008).

[13] M. Soron, Friction stir welding of high-strength aluminium alloys using an industrial robot system: A feasibility study, 7th International Symposium on Friction Stir Welding, Awaji-Island Japan, (2008).

[14] P. L. Threadgill M. E. Nunn. A review of friction stir welding: Part 1 process overview, TWI, TWI Members Report, 760/2003, February (2003), pp 1-31, http://www.twi.co.uk/j32k/index_mem.xtp.

[15] W. M. Thomas, D. G. Staines, D. E. Nicholas, I. Norris. Skew Stir, TWI Connect Magazine, (2002), Issue 119, pp 1-3, http://www.twi.co.uk/j32k/unprotected/band_1/c1193.html. (Last Accessed 12/2006).

[16] TWI. Friction Stir Welding at Yorkshire, (2005), http:\\www.twi.co.uk/j32k/unprotected/band_1/twi_yorks_fsw.html, (Last Accessed 12/2006).

[17] S. W. Kallee, D. E. Nicholas, W. M. Thomas. Industrialisation of Friction Stir Welding for Aerospace Structures, Structures and Technologies - Challenges for future launchers third European conference, Strasbourg, France, (2001), http://www.twi.co.uk/j32k/protected/band_8/ spswkdec2001.html. (Last Accessed 12/2006).

[18] M. Peel, A. Steuwer, M. Preuss, P. J. Withers. Microstructure, mechanical properties and residual stresses as a function of welding speed in aluminium AA5083 friction stir welds, Acta Materialia, (2003), Issue 16, Volume 51, pp 4791-4801.

[19] P. Threadgill, T. Minton. Minutes from project meeting 29/09/2006.

[20] T. U. Seidel, A. P. Reynolds. Visualization of Material Flow in AA2195 Friction Stir Welds Using a Marker Insert Technique, Metallurgical and Materials Transactions A, (2001), Volume 32A, pp 2879-2884.

[21] M. Guerra, J. C. Schmidt, L. E. McClure, L. E. Murr, A. C. Nunes. Flow Patterns during Friction Stir Welding, Materials Characterization, (2002), Issue 2, Volume 49, pp 95-101.

[22] R. Zettler, S. Lomolino. A study on material flow in FSW of AA 2024-T351 and AA 6056-T4 alloys, Proceedings of 5th International Friction Stir Welding Symposium, Metz, France, (2004), ISBN: 1-903761-04-2.

[23] K. Colligan. Dynamic material deformation during friction stir welding of aluminium, Proceedings of 1st International Friction Stir Welding Symposium, Thousand Oaks, CA, USA, (1999).

[24] Z.W. Chen, T. Pasang, Y. Qi. Shear flow and formation of Nugget zone during friction stir welding of aluminium alloy 5083-O, Materials Science and Engineering: A, (2008), Issue 1-2, Volume 474, pp312-316.

[25] P. B. Prangnell, C. P. Heason. Grain structure formation during friction stir welding observed by the `stop action technique', Acta Materialia, (2005), Issue 11, Volume 53, pp 3179-3192.

[26] G. Buffa, L. Fratini, R. Shivpuri. CDRX Modelling in friction stir welding of AA7075-T6 aluminium alloy: Analytical approaches, Journal of Materials Processing Technology, (2007), Issue 1-3, Volume 191, pp 356-359.

[27] L. Fratini, G. Buffa. CDRX modelling in friction stir welding of aluminium alloys, International Journal of Machine Tools and Manufacture, (2005), Issue 10, Volume 45, pp 1188-1194.

[28] K. N. Krishnan. On the formation of onion rings in friction stir welds, Materials Science and Engineering A, (2002), Issue 2, Volume 327, pp 246-251.

[29] H. K. D. H. Bhadeshia. Friction Stir Welding, http://www.msm.cam.ac.uk/phase-trans/2003/FSW/aaa.html. (Last Accessed 12/2006).

[30] M. J. Russell. Development of improved tool designs and parameters for the friction stir butt welding of 1.2, 6 and 25mm thickness aluminium alloys, TWI, TWI Members Report, 801/2004, May (2004), pp 1-44, http://www.twi.co.uk/j32k/index_mem.xtp.

[31] K. A. Beamish. The effect of the tool shoulder on friction stir welding of 6mm thickness aluminium alloys, TWI, TWI Members Report, 869/2007, April (2007), pp 1-34, http://www.twi.co.uk/j32k/index_mem.xtp.

[32] K. A. Beamish, A. Ezeilo, S. Smith. Development of a low cost friction stir welding monitoring system, 6th International Symposium on Friction Stir Welding, Saint-Sauveur Canada, (2006).

[33] W. M. Thomas, E. D. Nicholas, S. D. Smith. Friction Stir Welding - Tool Developments, Aluminum Joining Symposium, New Orleans USA, (2001), http://www.twi.co.uk/j32k/protected/band_8/spwmtfeb2001.html.

[34] C. J. Dawes, W. M. Thomas, Development of Improved Tool designs for Friction Stir Welding of Aluminium, 1st International Symposium on Friction Stir Welding, Thousand Oaks, CA, USA, (1999).

[35] T. Nagasawa, M. Otsuka. Structure and Mechanical Properties of Friction Stir Weld Joints of Magnesium Alloy AZ31, Magnesium Technology 2000, USA, (2000), pp 383-389, 0-87339-466-6.

[36] M. Boz, A. Kurt. The influence of stirrer geometry on bonding and mechanical properties in friction stir welding process, Mater Des, (2004), Issue 4, Volume 25, pp 343-347.

[37] G. Buffa, L. Fratini. Modelling the Effect of Pin Geometry in Friction Stir Welding of Aluminium Alloys, 8th International conference on Technology of Plasticity, Italy, (2005), 88-87331-74-X.

[38] T. Minton, D. J. Mynors. Utilisation of engineering workshop equipment for friction stir welding, Journal of Materials Processing Technology, (2006), Issue 1-3, Volume 177, pp 336-339.

[39] M. Page. Friction Stir Welding Broadens Applications Base, (2003), http:\\www.manufacturingtalk.com/news/mij/mij107.html. (Last Accessed 12/2006).

[40] TWI. Materials and Thickness, (2005), http:\\www.twi.co.uk/j32k/unprotected/band_1/fswmat.html, (Last Accessed 12/2006).

[41] TWI. Small joints make a big difference, TWI - Connect Magazine, (2006), Issue 143, p 1, http://www.twi.co.uk/j32k/unprotected/band_1/c1431.html.

[42] International Organization for Standardization. http://www.iso.org/iso/home.htm, (Last Accessed 2008).

[43] P. L. Threadgill. Friction stir welding - the state of the art, TWI, TWI Members Report, 678/1999, May (1999), pp 1-50, http://www.twi.co.uk/j32k/index_mem.xtp.

[44] P. L. Threadgill, A. J. Leonard. Macro and microstructural features of friction stir welds in various materials, TWI, TWI Members Report, 693/1999, December (1999), pp 1-19, http://www.twi.co.uk/j32k/index_mem.xtp.

[45] R. A. Prado, L. E. Murr, D. J. Shindo, KF Soto. Tool wear in the friction-stir welding of aluminum alloy 6061+20% Al2O3: a preliminary study, Scripta Materialia, (2001), Issue 1, Volume 45, pp 75-80.

[46] R. D Doherty, D. A. Hughes, F. J. Humphreys, J. J. Jonas, D. J. Jensen, M. E. Kassner. Current issues in recrystallization: a review, Materials Science and Engineering A, (1997), Issue 2, Volume 238, pp 219-274.

[47] H. G. Salem. Friction stir weld evolution of dynamically recrystallized AA 2095 weldments, Scripta Materialia, (2003), Issue 11, Volume 49, pp 1103-1110.

[48] J- Su, T. W. Nelson, R. Mishra, M Mahoney. Microstructural investigation of friction stir welded 7050-T651 aluminium, Acta Materialia, (2003), Issue 3, Volume 51, pp 713-729.

[49] K. V. Jata, S. L. Semiatin. Continuous dynamic recrystallization during friction stir welding of high strength aluminum alloys, Scripta Materialia, (2000), Issue 8, Volume 43, pp 743-749.

[50] L. E. Svensson, L. Karlsson, H. Larsson, B. Karlsson, M. Fazzini, J. Karlsson. Microstructure and mechanical properties of friction stir welded aluminium alloys with special reference to AA 5083 and AA 6082, Science and Technology of Welding and Joining, (2000), Issue 5, Volume 5, pp 285-296.

[51] G. Liu, L. E. Murr, C. Niou, J.C. McClure, F. R. Vega. Microstructural aspects of the friction-stir welding of 6061-T6 aluminum, Scr.Mater, (1997), Issue 3, Volume 37, pp 355-361.

[52] K. Tsuzaki, Huang Xiaoxu, T. Maki. Mechanism of dynamic continuous recrystallization during superplastic deformation in a microduplex stainless steel, Acta Materialia, (1996), Issue 11, Volume 44, pp 4491-4499.

[53] P. Cavaliere, R. Nobile, F. W. Panella, A. Squillace. Mechanical and microstructural behaviour of 2024-7075 aluminium alloy sheets joined by friction stir welding, International Journal of Machine Tools and Manufacture, (2006), Issue 6, Volume 46, pp 588-594.

[54] B. Yang, J. Yan, M. A. Sutton, A. P. Reynolds. Banded microstructure in AA2024-T351 and AA2524-T351 aluminum friction stir welds: Part I. Metallurgical studies, Materials Science and Engineering A, (2004), Issue 1-2, Volume 364, pp 55-65.

[55] R. W. Fonda, J. F. Bingert, K. J. Colligan. Development of grain structure during friction stir welding, Scripta Materialia, (2004), Issue 3, Volume 51, pp 243-248.

[56] J. Yan, M. A. Sutton, A. P. Reynolds. Process-Structure-Property Relationship for Nugget and HAZ Regions of AA2524-T351 FSW Joints, 5th International Symposium on Friction Stir Welding, Metz, France, (2004).

[57] K. A. A. Hassan, A. F. Norman, D. A. Price, P. B. Prangnell. Stability of nugget zone grain structures in high strength Al-alloy friction stir welds during solution treatment, Acta Materialia, (2003), Issue 7, Volume 51, pp 1923-1936.

[58] I. Charit, R. S. Mishra. High strain rate superplasticity in a commercial 2024 Al alloy via friction stir processing, Materials Science and Engineering A, (2003), Issue 1-2, Volume 359, pp 290-296.

[59] T. Hirata, T. Oguri, H. Hagino, T. Tanaka, S. W. Chung, Y. Takigawa. Influence of friction stir welding parameters on grain size and formability in 5083 aluminum alloy, Materials Science and Engineering: A, (2007), Issue 1-2, Volume 456, pp 344-349.

[60] S. Benavides, Y. Li, L. E. Murr, D. Brown, J. C. McClure. Low-temperature friction-stir welding of 2024 aluminum, Scripta Materialia, (1999), Issue 8, Volume 41, pp 809-815.

[61] W. M. Thomas, D. G. Staines, D. E. Nicholas, I. Norris. Novel Developments in Friction Stir Welding - Flared Tools for Lap Welding, TWI - Connect Magazine, 2002, Issue 118, p 3, http://www.twi.co.uk/j32k/unprotected/band_1/c1183.html.

[62] P. L. Threadgill. A review of friction stir welding: Part 2 selection of tool materials, TWI, TWI Members Report, 761/2003, February (2003), pp 1-30, http://www.twi.co.uk/j32k/index_mem.xtp.

[63] H. Fujii, L. Cui, M. Maeda, K. Nogi. Effect of tool shape on mechanical properties and microstructure of friction stir welded aluminum alloys, Materials Science and Engineering: A, (2006), Issue 1-2, Volume 419, pp 25-31.

[64] J. K. Kristensen, C. Dalle-Donne, T. Ghidini. Properties of Friction Stir Welded Joints in the Aluminium Alloys 2024, 5083, 6082/6060 and 7075, 5th International Symposium on Friction Stir Welding, Metz, France, (2004).

[65] I. Charit, R. S. Mishra. Evaluation of microstructure and superplasticity in friction stir processed 5083 Al alloy, J. Mater. Res, (2004), Issue 11, Volume 19, pp 3329-3342.

[66] T. Minton, J. Au. Stability of friction stir welds at superplastic forming temperatures, Key Engineering Materials, (2009), Volume 410-411, pp 117-125.

[67] P. Cavaliere, P. De Marco. Friction stir processing of a Zr-modified 2014 aluminium alloy, Materials Science and Engineering: A, (2007), Issue 1-2, Volume 462, pp 206-210.

[68] M. W. Mahoney, R. Mishra, T. Nelson. High Strain Rate Superplasticity in Thick Section 7050 Aluminium Created by Friction Stir processing, 3rd International Symposium on Friction Stir Welding, Kobe,Japan, (2001).

[69] Z. Y. Ma, R. S. Mishra, M. W. Mahoney. Superplastic deformation behaviour of friction stir processed 7075Al alloy, Acta Materialia, (2002), Issue 17, Volume 50, pp 4419-4430.

[70] M. W. Mahoney. Friction stir welding and processing: A sprinter's start, a marathoner's finish, 7th International Conference on Trends in Welding Research, Georgia USA, (2005).

[71] Z. Y. Ma, R. S. Mishra. Cavitation in superplastic 7075Al alloys prepared via friction stir processing, Acta Materialia, (2003), Issue 12, Volume 51, pp 3551-3569.

[72] P. Cavaliere, A. Squillace. High temperature deformation of friction stir processed 7075 aluminium alloy, Materials Characterization, (2005), Issue 12, Volume 51, pp 136-142.

[73] R. S. Mishra, M. W. Mahoney, S. X. McFadden, N. A. Mara, A. K. Mukherjee. High strain rate superplasticity in a friction stir processed 7075 Al alloy, Scripta Materialia, (1999), Issue 2, Volume 42, pp 163-168.

[74] V. Seetharaman, K. V. Jata, S. L. Semiatin. Plastic flow and Microstructure Development during High Temperature Deformation of a Friction Stir Welded 7050 Aluminium Alloy, 2nd International Symposium on Friction Stir Welding, Gothenburg, Sweden, (2000).

[75] I. Charit, R. S. Mishra, M. W. Mahoney. Multi-sheet structures in 7475 aluminum by friction stir welding in concert with post-weld superplastic forming, Scripta Materialia, (2002), Issue 9, Volume 47, pp 631-636.

[76] M. Furukawa, Z. Horita, M. Nemoto, T. G. Langdon. The use of severe plastic deformation for microstructural control, Materials Science and Engineering A, (2002), Issue 1-2, Volume 324, pp 82-89.

[77] S. Komura, P. B. Berbon, M. Furukawa, Z. Horita, M. Nemoto, T. G. Langdon. High strain rate superplasticity in an Al-Mg alloy containing scandium, Scripta Materialia, (1998), Issue 12, Volume 38, pp 1851-1856.

[78] R. Z. Valiev, D. A. Salimonenko, N.K. Tsenev, P. B. Berbon, T. G. Langdon. Observations of high strain rate superplasticity in commercial aluminium alloys with ultra fine grain sizes, Scripta Materialia, (1997), Volume 37, pp 1945-1950.

[79] M. A. Garcia-Bernal, R. S. Mishra, R. Verma, D. Hernadez-Silva. High strain rate superplasticity in continuous cast Al-Mg alloys prepared via friction stir processing, Scripta Materialia, (2009), Volume 60, pp 850-853.

[80] R. W. Davies, J. S. Vetrano, M. T. Smith, S. G. Pitman. Mechanical properties of aluminum tailor welded blanks at superplastic temperatures, Journal of Materials Processing Technology, (2002), Issue 1-3, Volume 128, pp 38-47.

[81] I. Charit, R. S. Mishra. Low temperature superplasticity in a friction-stir-processed ultrafine grained Al–Zn–Mg–Sc alloy, Acta Materialia, (2005), Issue 15, Volume 53, pp 4211-4223.

[82] Z. Y. Ma, R. S. Mishra. Development of ultrafine-grained microstructure and low temperature (0.48 Tm) superplasticity in friction stir processed Al–Mg–Zr, Scripta Materialia, (2005), Issue 1, Volume 53, pp 75-80.

[83] S. Lee, J. Yeh. Superplasticity of 5083 alloys with Zr and Mn additions produced by reciprocating extrusion, Materials Science and Engineering A, (2007), Volume 460-461, pp 409-419.

[84] Superform-Aluminium, Superform Aluminium homepage, (2006), http://www.superform-aluminium.com/, (Last Accessed 2007).

[85] N. Ridley. Superplastic Forming. In: Handbook of Aluminum Volume 1 Physical Metallurgy and Processes, CRC Press, 2(003). p.1105.

[86] O. D. Sherby. Advances in Superplasticity and in Superplastic Materials, ISIJ International, (1989), Volume 29, pp 698-716.

[87] H. L. Xing, C. W. Wang, K. F. Zhang, Z. R. Wang. Recent development in the mechanics of superplasticity and its applications, Journal of Materials Processing Technology, (2004), Issue 1-3, Volume 151, pp 196-202.

[88] R. Verma, A.K. Ghosh, S. Kim, C. Kim. Grain refinement and superplasticity in 5083 Al, Materials Science and Engineering A, (1995), Issue 1-2, Volume 191, pp 143-150.

[89] A. Smolej, M. Gnamus, E. Slacek. The influence of the thermomechanical processing and forming parameters on superplastic behaviour of the 7475 aluminium alloy, Journal of Materials Processing Technology, (2001), Issue 1-3, Volume 118, pp 397-402.

[90] European Aluminium Association, The University of Liverpool. Alu-Matter, http://aluminium.matter.org.uk, (Last Accessed 2009).

[91] Superform-Aluminium. 5083 Data sheet, (2002).

[92] P.S. Bate, F. J. Humphreys, N. Ridley, B. Zhang. Microstructure and texture evolution in the tension of superplastic Al–6Cu–0.4Zr, Acta Materialia, (2005), Issue 10, Volume 53, pp 3059-3069.

[93] Superform-Aluminium. Material Data sheet 2004 SPF, (1997), Issue 1.

[94] T. Minton, J. Au, R. Bulpett. Friction stir welding of AA5083 and AA2004, commercially available SPF aluminium alloys, for subsequent superplastic forming, 7th International Symposium on Friction Stir Welding, Awaji-Island Japan, (2008).

[95] Buehler Ltd. Buehler SUM-MET^{TM} - The Science Behind Materials Preparation , (2004), pp 1-135.

[96] Oxford Instruments. Electron Backscatter Diffraction, (2005), http://www.ebsd.com/ebsd-explained/, (Last Accessed 2009).

[97] M.F. Ashby, D. R.H. Jones. Engineering Materials 2 An Introduction to Microstructures, Processing and Design, (1986), pp 1-369, ISBN: 0-08-032532-7.

[98] R. D. Doherty. Recrystallization and texture, Progress in Materials Science, (1997), Issue 1-4, Volume 42, pp 39-58.

[99] G. J. Davies, J. W. Edington, C. P. Cutler, K. A. Padmanabhan. Superplasticity: A Review, (1970), pp 1091-1102.

[100] F. J. Humphreys. A unified theory of recovery, recrystallization and grain growth, based on the stability and growth of cellular microstructures—I. The basic model, Acta Materialia, (1997), Issue 10, Volume 45, pp 4231-4240.

[101] F. J. Humphreys. A unified theory of recovery, recrystallization and grain growth, based on the stability and growth of cellular microstructures—II. The effect of second-phase particles, Acta Materialia, (1997), Issue 12, Volume 45, pp 5031-5039.

[102] S. Agarwal, P. E. Krajewski, C. L. Briant. Texture development and dynamic recrystallization in AA5083 during superplastic forming at various strain rates, Advances in Superplasticity and superplastic forming, Charlotte USA, (2004), pp 95-107.

[103] M. G. Dawes, S. A. Karger, J. Przydatek. Fracture toughness of friction stir welds in 2014A, 7075 and 5083 aluminium alloys, TWI, TWI Members Report, 705/2000, April (2000), pp 1-16, http://www.twi.co.uk/j32k/index_mem.xtp.

[104] R. Johnson, N. L. Horrex. Preliminary examination of forces generated during the friction stir welding process, TWI, TWI Members Report, 696/2000, January (2000), pp 1-7, http://www.twi.co.uk/j32k/index_mem.xtp.

[105] R. Johnson. Forces in friction stir welding of aluminium alloys - further studies, TWI, TWI Members Report, 716/2000, December (2000), pp 1-18, http://www.twi.co.uk/j32k/index_mem.xtp.

[106] W. M. Thomas, D. G. Staines, E. R. Watts, Re Stir Reversal Stir Welding, TWI Connect Magazine, (2003), Issue 123, pp 1-3, http://www.twi.co.uk/j32k/unprotected/band_1/c1233.html.

[107] W. M. Thomas, D. G. Staines, D. E. Nicholas, I. Norris. Skew Stir Variation on a Theme, TWI Connect Magazine, (2001), Issue 113, pp 1-3, http://www.twi.co.uk/j32k/unprotected/band_1/c1133.html.

[108] W. M. Thomas. Com Stir Compound Motion for Friction Stir Welding and Machining, (2003), pp 1-6, http://www.twi.co.uk/j32k/unprotected/pdfs/spwmtmar2003.pdf.

[109] E. R. Watts, D. G. Staines, W. M. Thomas, E. D. Nicholas. Dual Rotation Stir Welding Preliminary Trials, (2004), http://www.twi.co.uk/j32k/unprotected/band_1/sperwapr2004a.html, (Last Accessed 2006).

[110] M. J. Russell, P. Threadgill, N. L. Horrex. Recent developments in stationary shoulder FSW of Ti alloys, 7th International Symposium on Friction Stir Welding, Awaji-Island Japan, (2008).

[111] TWI. Friction Stir Welding - Process Advantages, (2005), http://www.twi.co.uk/j32k/unprotected/band_1/fswproc.html, (Last Accessed 2006).

[112] P. Colegrove, P. Threadgill. Trivex Tool for Friction Stir Welding, TWI Connect Magazine, (2003), Issue 124, pp 1, http://www.twi.co.uk/j32k/unprotected/band_1/c1241.html.

[113] H. Ohba, C. Ueda, K. Agatsuma. Hitachi Rail, Innovative vehicle - the "A train", (2001), http://www.hitachi.com/ICSFiles/afieldfile/2004/06/08/r2001_04_102.pdf, (Last Accessed 2009).

[114] R.W. Cahn. A New Theory of Recrystallization Nuclei, Proceedings of the Physical Society. Section A, (1950), Issue 4, Volume 63, pp 323-336.

[115] M. F. Ashby, D. R. H Jones. Engineering Materials 1 An Introduction to their Properties and Applications, Volume34, (1980), pp 1-278, ISBN: 0-08-026138-8.

[116] R. D. Doherty. Primary Recrystallization. In: Encyclopaedia of Materials: Science and Technology, Elsevier Science Ltd, (2005). pp 7847-7850.

[117] A. Ball, M. M. Hutchison. Superplasticity in the aluminum-zinc eutectoid , Metal Sci. J., (1969), Volume 3, pp 1-7.

[118] R.C. Gifkins. Grain-Boundary Sliding and its Accommodation during Creep and Superplasticity. Metal Trans A, (1976), Issue 8, Volume 7 A, pp 1225-1232.

[119] O. D. Sherby, J. Wadsworth. Development and Characterization of Fine-Grain Superplastic Materials., (1984), pp 355-389.

[120] H. Fukuyo, H. C. Tsai, T. Oyama, O. D. Sherby. Superplasticity and Newtonian-viscous flow in fine-grained class I solid solution alloys, ISIJ International, (1991), Issue 1, Volume 31, pp 76-85.

[121] M. F. Ashby, R. A. Verrall. Diffusion-Accommodated Flow and Superplasticity, Acta Metall, (1973), Issue 2, Volume 21, pp 149-163.

[122] W. D. Nix, M. J. Mayo. A model for superplasticity not controlled by grain boundary sliding, pp 1-20, (2004), http://imechanica.org/files/Nabarro.pdf, (Last Accessed 2007).

Appendix A:

Supplementary Information

Appendix A Chapter 1 - Advanced FSW Tooling

A1.1 Advanced FSW Tools and Process Variants.

In rotary FSW the tool simply spins, contacting an area governed by the width of the tool. Other forms or variants of FSW use orbital motion of the tool as well as rotation, others use discontinuous rotation; some possible variants are described below.

A1.2 Com-Stir™

Com-Stir™ is a FSW variant, tested in laboratory conditions by TWI, where the rotation of the tool and an added orbital motion generates friction in the same way as a purely rotary friction stir welding tool does. The added orbiting of the tool creates a wider weld zone and significantly more material flow, see Figure A1.1.a) The relative velocity of a rotational tool varies from its maximum on the circumference of the shoulder to zero at the centre of the probe. Varying the tool rotation and the orbit can create a fully orbital motion or a fully rotational motion; this can be changed before or during welding to suit the condition, further optimising the process.

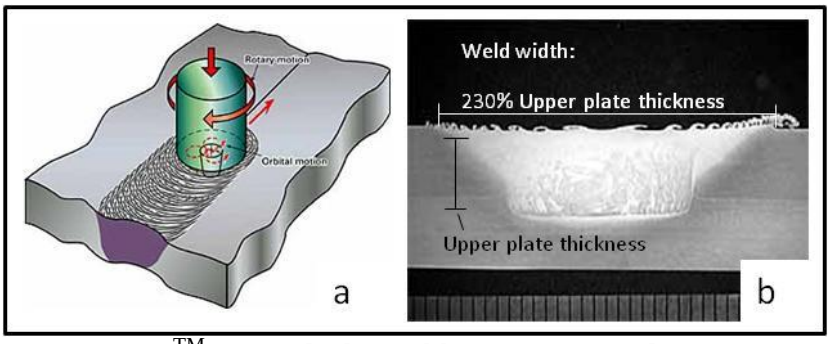

Figure A1.1. a) Com-Stir™ Principle, b) Weld Region Created using Com-Stir™ [108]

The wider weld zone makes this technique well suited for joint configurations such as lap or ‘T’ sections. This wide zone will also benefit friction stir processing. The width of the central weld zone can be as much as 230% of the top plate’s thickness, as shown in Figure A1.1.b) This process variant benefits from a higher heating rate and increased material flow when compared to purely rotary FSW. Further work is being undertaken on this combined motion technique in welding applications and also for milling. The combined motion allows less torque to be applied to the pre-welded

material whilst still obtaining sufficient heating and material flow to create a sound join. This lower torque level also saves on the jigging of the pre-welded material. Less equipment is needed to hold the pieces in place [108].

A1.3 Re Stir™

This technology includes angular reciprocating (rotation reversal after each rotation) and rotary reversal (reversal occurs after a number of rotations). As the name suggest the pre-welded material is stirred in one direction, the tool instantaneously stops and is then rotated in the opposite direction, stirring and then re-stirring the material. Figure A1.2.a) shows the process principle. This variant avoids the problems which arise from an asymmetrical weld produced by a conventional FSW process. The difference between the advancing side and retreating side of the weld in the conventional process may sometimes lead to differing mechanical properties at each side of the weld. The Re Stir™ variant eliminates these problems by producing a symmetrical weld. The rotation reversal effectively balances the work done on each side. Figure A1.2.b) shows a symmetrical lap weld produced using a Re stir™ process.

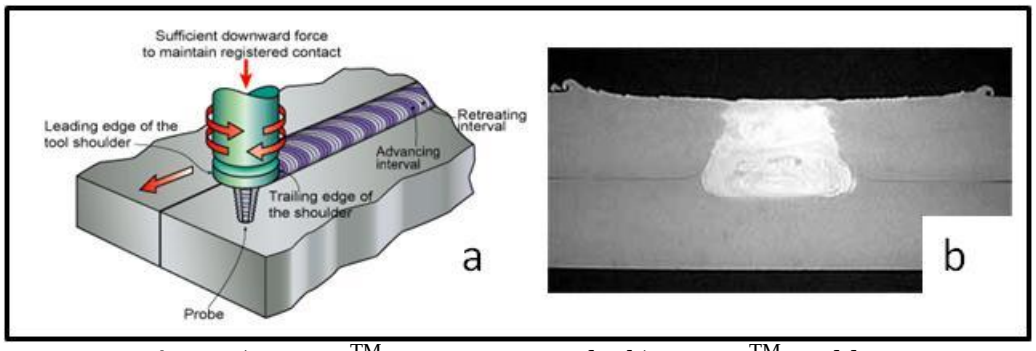

Figure A1.2, a) Re-stir™ Process Principle, b) Re-stir™ Weld Region, [106].

The investigations carried out by TWI indicate that this technology will benefit the production of sound butt and lap joints. The ability to produce symmetrical joint structures reduces the problems associated with conventional FSW and may make Re-Stir™ a favoured process for certain lap, butt, compound lap, spot or processing operation [106].

A1.4 Skew stir

This tool involves a two part design and allows a faster weld speed whilst generating sufficient heat. The shoulder section and probe section of the tool are completely separate components which can be made from materials with similar or different properties, as mentioned previously, a highly durable substance for the probe and a less wear resistant material for the shoulder. The major difference in the construction of this tool from other tools is that the shoulder and probe are not positioned vertically. The tooling orientation has an angle taking it off vertical. The shoulder contact face remains parallel to the pre-welded material top surface as does the probe tip. The skew angle causes a far greater 'dynamic to static probe volume ratio'. I.e. produces a greater flow of plasticised material around the probe. The angle at which the centre line of the shoulder/probe section differs from vertical is known as the skew angle as shown in Figure A1.3 [15]. The point at which the skew axis and vertical axis intersect is known as the focal point. This focal point can be altered to produce different weld parameters. If the focal point lies within close proximity to, or within the thickness of the pre-welded material then the shoulder will produce an orbital motion as well as rotation seen in Figure A1.4. This tool does not rotate on its own axis, and therefore only a specific part of the face of the probe surface is directly in contact with the pre-welded material. This means the inner part of the tool can be removed to improve the flow path of material during welding.

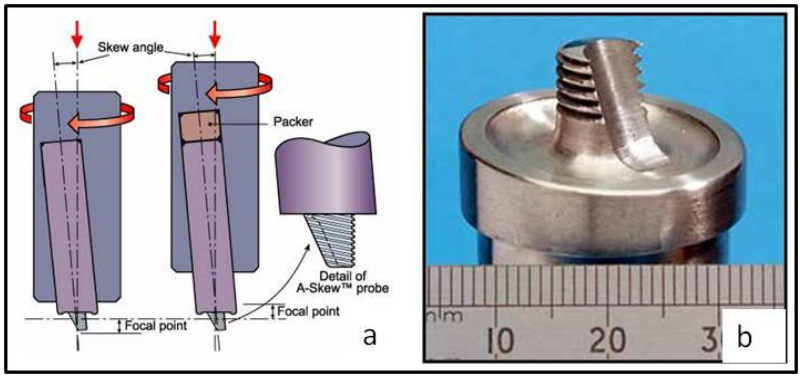

Figure A1.3, a) Skew Stir Tooling Concept. b) Prototype Asymmetric Skew-Stir™ Tool. [15]

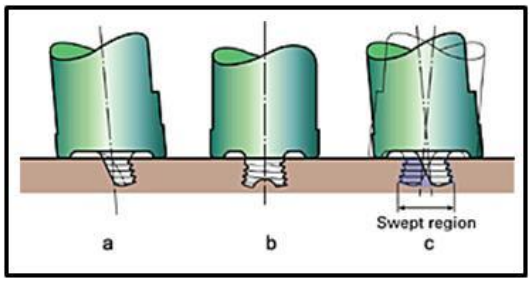

Figure A1.4, Details of Prototype A-Skew™ tool:

a) Side View

b) Front View, Showing Probe Tip Profile

c) Swept Region Encompassed by Skew Action [15].

The increased ratio of the probe's dynamic volume and its static volume means more mixing of the weld material during the process. This ultimately means a better quality of weld. One of the most common causes for failure for a FSW lap joint is insufficient dispersal of the oxide layer between the abutted material sections. This tool disrupts more of the oxide layers due to the increased levels of material flow around the probe. This makes the tool particularly effective for lap and 'T' section joint configurations. This is because the axis of the abutted materials lies perpendicular to the machine axis. The weld region is larger than that produced by a standard conical probed tool. This is also an advantage not only for welding but for FSP too. The wider stir zone gives extra strength to lap and 'T' section joints reducing the effect of the notches on each side of the join. This wider affected zone reduces the number of passes made whilst Friction Stir Processing. Consistent and good results obtained and compared with results from a conventional threaded probe type tool [15].

A1.7 Dual rotation

This is another variant to the FSW process. The basic rotary FSW process is carried out using a special tool which has an independent shoulder and probe. That is they can rotate freely from each other in the same direction or in opposite directions as shown in Figure A1.5. The speed of the effectively separate tool components can be altered before or in process and allows the process to be further optimised. The relative velocity of a rotational tool varies from its maximum on the circumference of the shoulder to zero at the very centre of the probe. Dual Rotation Friction Stir

Welding allows this velocity gradient to be modified to suit the process conditions, for example a high probe rotational speed and slower shoulder rotation. This allows for sufficient heating and material flow around the probe whilst preventing the shoulder from overheating the material beneath it. Over heating of the top surface can lead to cracking of the weld during or after the process has been carried out.

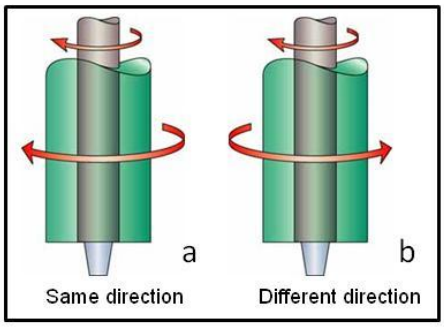

Figure A1.5, Principle of Dual Rotation Friction Stir Welding:
a) Same Direction, b) Opposing Directions, [109].

Further investigation into this technology is done by TWI, the preliminary investigations shows this is a potentially advantageous technique [109].

A1.8 Tool Heel Roller

A simple and now conventional means of tracking the tool's plunge depth is the use of a tool heel roller, see Figure A1.6.

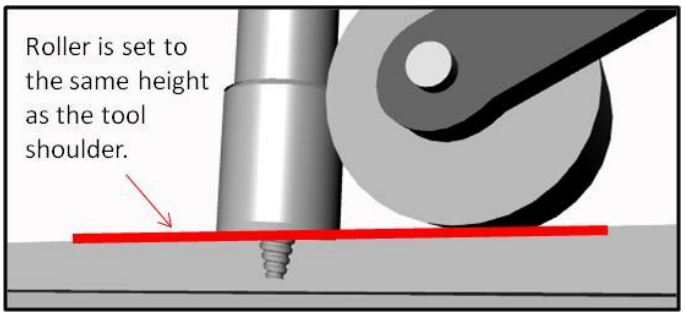

Figure A1.6, Tool Heel Roller.

One or more rollers can be positioned close to the tool to prevent the tool from penetrating too far into the material. On a more advanced machine the use of position or force control is used to control the tool heel plunge depth, and so in this case the use of the roller is different. The roller is used to locally press the material to be joined to the backing plate to prevent deflection of the material being welded [9].

A1.9 TWI Whorl Tool

The distance between the threads can be altered to further tailor the tool to the material and weld specifications. The spacing of these ridges is important to maximise the auger action and thus increase the vertical mixing. TWI's Whorl™ tool, shown in Figure A1.7, is designed so that the spacing between the ridges is different throughout the length of the probe. Larger spaced at the top and smaller towards the tip. The threads also act to break up oxide layers and deform the material as well as mixing and heating the material [1, 111].

Figure A1.7, TWI Designed Whorl™ FSW Tool [1, 111].

A1.10 TWI TriVex Tool

The TriVex tooling as shown in Figure A1.8 has a probe with three flattened sides, each of the three faces themselves are convex. In direct comparison to the above MX Triflute™ tooling, which has the same shoulder and probe dimensions, the TriVex tools allow the force required to traverse the tool through the pre-welded material to be lowered by around 18 – 25% for an unthreaded tool and 12% for a threaded tool. These results have been conducted in laboratory demonstrations by TWI [112]. This suggests that the probe features dictate the force required to traverse the tooling. More prominent features such as threads and flutes trap material within and transport it with the rotation, although beneficial for producing sound welds, the trapping of the material impedes the tool traverse and increases the amount of force required to perform this motion. The external threads are beneficial to the process and the welds

produced, but also act as crack initiation zones reducing the tool life and making the tool considerably harder to produce [112].

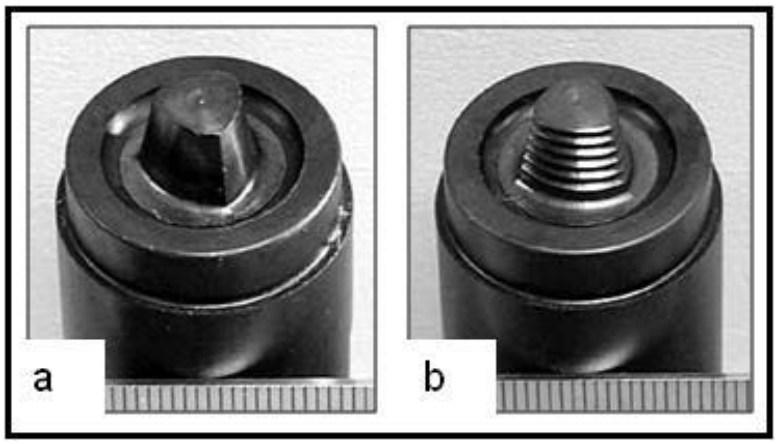

Figure A1.8, TriVex Tooling, a) Unthreaded, b) Threaded [112].

Appendix A Chapter 2 – Advantages of FSW Over Fusion Welding

A2.1 Advantages of the FSW Process

The FSW process has many advantages over conventional welding techniques such as MIG and TIG welding [111].

A2.2 Solid Phase Process

Fusion temperatures are not reached; this reduces any solidification defects and losses of alloying elements in 2xxx and 7xxx series aluminium alloys [14].

A2.3 1-D, 2-D or 3-D

Friction stir welding can be applied to any welding position as gravity plays no part in the welding process allowing it to be carried out in any orientation [14].

A2.4 No environmental hazards

There are no ultra-violet or electromagnetic radiation hazards when carrying out FSW [14].

A2.5 Low Distortion

Friction stir welding provides low distortion welds. The low heat input during the FSW process means that the material will not curl or deflect as much when compared to material welded using conventional fusion welding techniques [111, 113].

A2.6 Minimised Colour Change

The low temperatures experienced during the welding process minimises the amount of colour change. It should be noted that aluminium does not change colour, on heating, due to its tenacious oxide layer so this only applies to materials which change colour when heated, for example steel [111].

A2.7 No Filler Wire

Other welding methods require a filler wire or flux to control the weld properties and allow for variations during fit up (assembly). FSW only requires the tool and the machine to rotate it [14, 111].

A2.8 Reduced Porosity

During fusion welding the weld region is completely melted. A major problem with melted material is that during the cooling of the weld region voids can appear. These tiny spaces in the structure of the weld are known as porosity and cause an area of weakness and a compromised joint, during FSW the weld material is not melted and so the amount of porosity is reduced [111].

A2.9 No Shielding Gas Required

FSW breaks up the oxide coatings on the abutted surfaces therefore minimising the need for a shielding gas, as long as the abutted surfaces of the weld material have been correctly prepared [111].

A2.10 Repeatable, Programmable Process

The process can be fully automated with no manual intervention meaning it is highly repeatable [111].

Appendix A Chapter 3 – Friction Stir Weld Setup

A3.1 Tools designed for specific welding applications

The material thickness is a guide to how long to make the tool probe. The overall probe length required is specific to the application of the weld and equal to the plunge depth or depth of weld required given the circumstances. Thin and thick cross-sections of material can be joined using specially designed tooling as is the general rule for FSW, a different tool for each scenario. The design of the tool will depend on the type of joint to be welded. Different configurations of joints require different probes or shoulder designs. For example circumference welding requires a scroll shoulder and a lap joint requiring a flared probe [33].

A3.2 Weld Configuration, Material Positioning and Clamping

When the tool is plunged into the material the natural reaction for this material is to be forced apart. It is only by constraining this movement that the tool can be plunged and traversed to create the joint. The process can accept a small gap between the material sections to be joined. For a typical butt weld this tolerance is in the order of 10% of the weld depth so for a 5mm thickness the gap tolerance would be 0.5mm [1]. Too large a gap will create flaws such as voids or porosity in the weld. As the tool contacts the material the tool will move the stationary material in the direction of rotation. However, for the process to be a success zero degree of freedom must be maintained. The pre-welded material must resist the motion induced by the tool. The tool produces torque as it contacts and is plunged into the material. The amount of torque is linked with the amount of deformation occurring during the process. A smooth probe will produce less torque than a thread probe due to less deformation. The clamping of the pre-welded materials must be able to handle the torque produced by the tool contact or unsuitable conditions may occur, such as unacceptable gaps between abutted surfaces or movement of the material during process.

A3.3 Tool Fixture and Orientation

The tool is rotated and plunged into the pre-welded material. Then the tool is traversed through the material to be joined. There is rotation, downward and lateral forces acting on the tool as the process is carried out meaning that securing the tool in the spindle is important for a successful weld. The tool is an independent piece from

the machine which is driving it. The tool must be fixed to the spindle of the machine in such a way as to be totally safe. The tool may rotate at speeds reaching or exceeding 2000 rpm and at the same time it is traversed through resistive mediums at speeds exceeding 100 mm/s. For these reasons the tool must be securely fitted to the spindle with no chance of the tool becoming loose. The tool can be tilted as mentioned in Chapter 2. The easiest way for this adjustment, is to tilt the spindle of the machine. A completely vertical spindle can be used if the shoulder has a scroll profile.

Appendix A Chapter 4 – Materials Science Background Information

A4.1 Mechanisms for Microstructural Change

It is important to know the basics of some key microstructural change mechanisms which occur during and after the FSW process has taken place. A brief description of these mechanisms is offered to assist the understanding of the microstructural evolution of a friction stir weld.

A4.1.1 Stored Energy for Microstructural Change

Materials contain energy locked in their structures in the form of internal stress or residual stresses. This energy is part of the driving force for microstructural change. A material will attempt to transform from a high energy state to a low energy state by going through a cycle of recovery, recrystallization and grain growth. A material's stacking fault energy determines the amount of energy required for a dislocation to move through the structure. The higher this value the more energy is required for structural change. Aluminium has a relatively high Stacking Fault Energy (SFE) giving it reluctance to recrystallize [90].

A4.1.2 Recrystallization

Recrystallization in a classical definition is the nucleation and growth of new grains containing fewer dislocations. In solids this is not true nucleation as this would require the grain to grow from something that was not originally there [98]. This process is best described as an evolution of a subgrain into a grain [46,114]. Dislocations within the grains coalesce to form subgrain boundaries, eventually the subgrain will become misorientated in relation to the original grain and can be deemed to be a new grain. The dislocations within the grains give the material strength as these dislocations impede each other's movement [115]. The new recrystallized microstructure contains fewer dislocations and so tends to be accompanied by a reduction in the strength and hardness of the material but also an increase in ductility [46]. The process of recrystallization is strongly related to other processes such as recovery and grain growth. Recrystallization can occur without deformation, ***Static*** recrystallization, or with deformation, ***Dynamic*** recrystallization.

It can also happen heterogeneously, ***Discontinuous*** recrystallization or homogeneously over the entire structure, ***Continuous*** recrystallization.

A4.1.3 Recovery

The mechanism of recovery is similar to that of recrystallization. A classical definition of the mechanism would be all annealing processes occurring within a plastically deformed material which occur without the migration of high angle grain boundaries [97]. Recovery has two stages, first is the annihilation of dislocations with opposite signs. When the temperature of a material is increased dislocations are more mobile and can therefore glide, cross-slip and climb [97], when dislocations of opposite sign interact they cancel each out and their contribution to the stored energy is removed. This leaves only the excess dislocations of a particular sign. The second stage is the rearrangement of the excess dislocations to reduce the stored energy. Dislocations become ordered into arrays which reduced the stored energy by overlapping of their strain fields.

A4.1.4 Grain Growth

Grain growth, also referred to as Abnormal Grain Growth (AGG), secondary recrystallization and grain coarsening, occurs after the mechanisms of recrystallization and recovery have ceased; the only way of further reducing the internal energy of the structure is to decrease the total area of the grain boundaries. This phenomenon can be continuous (normal) or discontinuous (abnormal).

The recovery, recrystallization and grain growth cycle is a subject area of great interest, [27, 46, 49, 100, 101, 116] give thorough explanations and excellent detail on these mechanisms.

Appendix A Chapter 5 – Superplasticity

A5.1 Superplasticity Constituent Equations

By modelling the superplastic deformation process, constituent equations which describe the process have been derived and published. However many of these models do not explain the superplasticity phenomenon in its entirety leading to many different views on how and why materials exhibit these remarkable properties. Some of the more popular views and mechanisms are discussed below.

(A5.1) $\sigma = K \cdot \dot{\varepsilon}^{m}$ [MPa]

Where: σ is the flow stress, *K* is a material constant, ἑ is the strain rate and *m* is the strain rate sensitivity index.

(A5.2) $\sigma = K \cdot \dot{\varepsilon}^{m} \cdot \varepsilon^{n}$ [MPa]

Where: ε is the strain and *n* is the material strain hardening index [87].

If a material is to be considered to be superplastic it must generally have a strain-rate sensitivity index of greater than 0.4. The strain-rate sensitivity is a measure of the relationship between stress and strain-rate and is denoted as "m". This notation is taken from the Backoften equation (A5.1). A material which exhibits ideal Newtonian Viscous behaviour has a strain-rate sensitivity index of m=1 for example hot glass or tar. For most non-superplastic metals, m=0.2, but for superplastic metals this value increases to m>0.33 [3]. This equation however does not take into account any sensitivity to work or strain strengthening/weakening which may be present in the material. Strain hardening is a metal's ability to become strengthened when subjected to plastic deformation. The material's strength is altered by the induction of dislocations into the structure via deformation, these dislocations move through the material when eventually they begin to impede each other's movement, hence improving strength. The strain hardening index is denoted as "n" and is included in the constituent equation by Rossard (A5.2) [87]. Superplasticity can be best described as a special type of creep mechanism. Creep is a permanent, time dependant deformation of material under a constant load or stress. For metals creep is important

when the temperature rises to $0.4T_m$. For a better understanding of superplastic deformation the different creep mechanisms involved are described.

A5.2 Creep Mechanisms

The mechanism by which superplastic deformation occurs is a well known creep mechanism. This deformation initially occurs with little or no cracks or voids forming, over time creep strains build up and cause failure of the material. This means that creep is a time dependent process and is associated with three discrete mechanisms: **1)** Slip by dislocation movement, ***Dislocation creep*** *(n≥3)*. **2)** Directional diffusional flow, ***Diffusional creep*** *(n=1)*. **3)** Sliding of adjacent grains along grain boundaries, ***Grain boundary sliding*** *(n=2)*. The primary mode by which superplastic flow is modelled is Grain Boundary Sliding (GBS) [3]. Dislocation and diffusional creep are explained briefly to aid the understanding of GBS.

Creep can be characterised by a strain versus time curve (creep curve), the creep can be calculated from the gradient of this curve and is shown in Figure A5.1. Figure A5.1.a) represents a metal of relatively high purity and Figure A5.1.b); shows an alloy. The curves depict the balance between two competing mechanisms, these being work hardening and recovery softening. During the steady state region the two mechanisms are in balance and allow for a slow and steady but uniform deformation cycle. Eventually the material will enter the tertiary creep phase and accelerated failure will occur due to formation of cavities and necking. Past studies have used the regions of steady state creep to model and evaluate creep and its mechanisms to derive constituent equations [3].

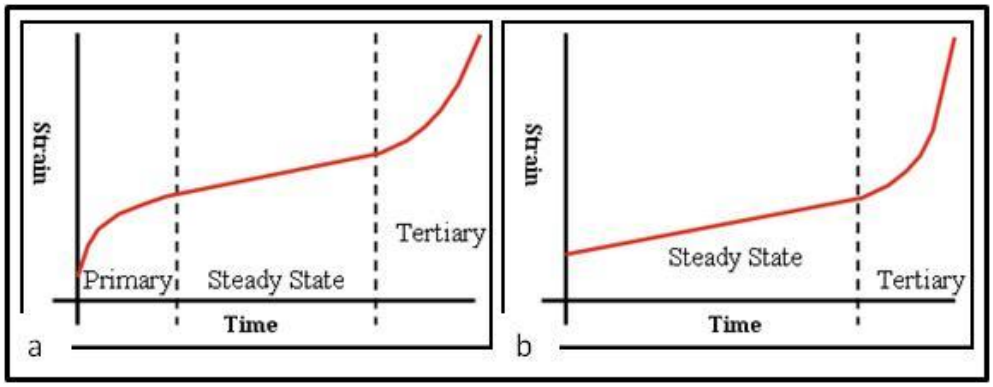

Figure A5.1, Creep Curves: a) Metal Type Creep Curve, b) Alloy Type Creep Curve [3].

A5.2.1 Dislocation Creep

This form of creep is a sequential process involving both slip plane gliding and climb over physical obstacles as shown schematically in Figure A5.2.

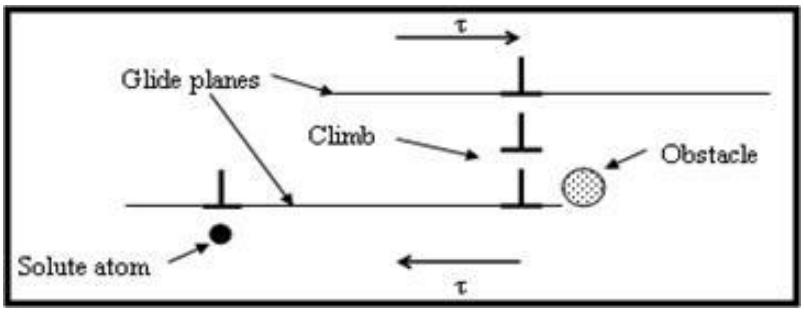

Figure A5.2, Schematic Representation of Dislocation Creep Involving both Glide and Climb [3,115].

This process involves both glide and climb. The slower of the two processes (glide or climb) is the controlling process and determines the creep rate. The creep rate in this form of creep mechanism is independent of grain size.

A5.2.1.1 Glide Controlled Creep

When the gliding process is the rate controlling process solute atoms impede the motion of dislocations through the material. Elongations of typically around 400% are achievable when glide is the controlling process. Materials for which this is the case are usually referred to as Class I solid solutions [3, 115].

A5.2.1.2 Climb Controlled Creep

When the climb process is the rate controlling process, deformation is controlled by dislocations climbing over obstacles. Climb is much more difficult than glide in the majority of metals and alloys [3, 115].

A5.2.2 Diffusional Creep

In this form of creep the transportation of matter is by a process known as diffusion rather than that of dislocation motion. This occurs in fine structure materials, typically at temperatures of around 90% of the absolute melting temperature [3, 115]. Diffusion is caused by non-hydrostatic stress which makes atoms flow from

compression sites towards tension sites. This can be split into two different types of diffusional creep.

A5.2.2.1 Nabarro-Herring Creep

Transportation of atoms occurs through the grain lattice; this is shown in Figure A5.3.a).

A5.2.2.2 Coble Creep

This is a specialized version of the above-mentioned Nabarro-Herring creep. In this case the transportation of atoms occurs due to grain boundary diffusion. This is shown schematically in Figure A5.3.b).

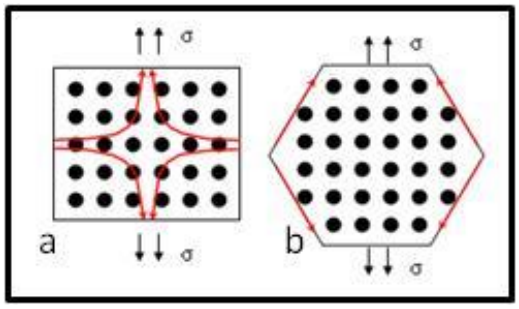

Figure A5.3, Schematic Representation of Diffusional Atom Flow during Creep: a) Nabarro-Herring Creep. b) Coble Creep [3].

A5.2.3 Grain Boundary Sliding

The exact method of superplastic flow in an FSS material is not entirely understood. As a result there have been many studies carried out to investigate this elusive mechanism. There are three modes which many authors believe explain the creep behaviour, these are: **1)** Diffusional flow. **2)** Grain boundary sliding accommodated by diffusional flow. **3)** Grain boundary sliding accommodated by dislocation slip. Of these three modes, GBS accommodated by dislocation slip fits well with many other authors' work [3].

Grain boundary sliding is considered to be the main mechanism behind superplastic flow [2, 3]; however this process requires an accommodation process to accompany it. This accommodation process could be one of the following: Grain boundary migration, recrystallization, diffusional flow or dislocation slip. Without this

accommodation process, premature failures within the specimens will occur due to cavitation. As the grains slide over each other grain boundary separation causes small cavities to appear between the grain boundaries of neighbouring grains. This is an especially common occurrence in the vicinity of hard particles within the matrix structure. The harder particles will impede the movement of grains as they slide over each other. As the particle is harder than the matrix grain, the matrix grains will move around the hard particle rather than through it creating a cavity where the grain boundaries have been separated by the hard particle. Many models for GBS have been proposed for the accommodation of GBS, for slip accommodation these include [117, 118, 119, 120] and for diffusional accommodation [121]. Although these models have aspects which agree with each other, none of them are able to accurately predict the actual creep behaviour in FSS materials. Gifkins' core and mantle model is a popular explanation of the superplastic mechanism. Two processes work independently to cause superplasticity: GBS accommodated by slip in the mantle region (extremities of the grains) and slip in the core of each grain. Only the first scenario will cause superplasticity, with the latter process yielding normal ductility [3].

Figure A5.4 shows a creep curve which represents the general behaviour of high temperature creep; it highlights the two independent but competing processes: GBS with a threshold stress and dislocation controlled slip. Once the threshold stress has been reached the mechanism switches from slip to GBS and results in a superior elongation to failure. The solid red line depicts the creep rate when dislocation creep is rate controlling, the dashed black line represents the creep rate when GBS with a threshold stress (black line) is rate controlling with the fastest one of the two being the rate controlling process. The blue curve is the predicted behaviour. The curve is split into 4 regions: Region 0 - Deformation controlled by slip; Region I - Threshold stress is observed with low ductility; Region II - GBS and superplastic behaviour; and Region III - Deformation controlled by slip. It is the steady state region II which is of most benefit providing large elongations.

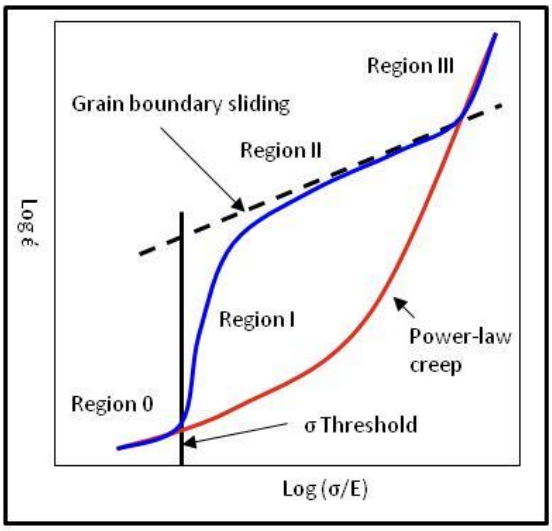

Figure A5.4, Creep Behaviour of FSS Materials [3].

Another, more controversial, view comes in the form of a model for superplasticity which is not controlled by GBS [122]. Although these authors do admit that GBS takes place they believe that it is the accommodation processes which control the process not the GBS itself.

A5.3 Applications for the Superplastic Forming Process

Superplastic forming is currently used for the production of products in the automotive, aeronautic, marine, rail and construction sectors [84]. Currently these are produced in relatively small batches compared to other manufacturing techniques due to the long times required to for each part in some cases parts many require forming times of in excess of 4 hours [85].

A5.3.1 Examples of Products Formed in AA5083

Figure A5.5.a-e shows some examples of superplastically formed products which utilise this alloy, formed by Superform Aluminium (UK).

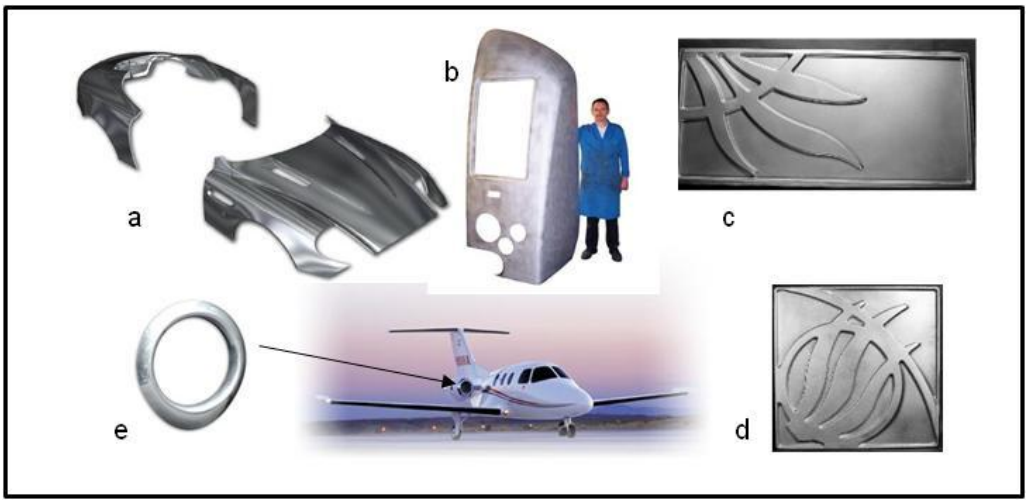

Figure A5.5, a) Aston Martin Vanquish Body Panels. b) Desiro Train Front. c) and d) Decorative Panels from Grady Hospital in Atlanta, Georgia. e) Eclipse 500 Engine Intake Lip Skin [84].

A5.3.2 Examples of Products Formed in AA2004

Figure A5.6 shows some components superplastically formed by Superform Aluminium (UK) in AA2004.

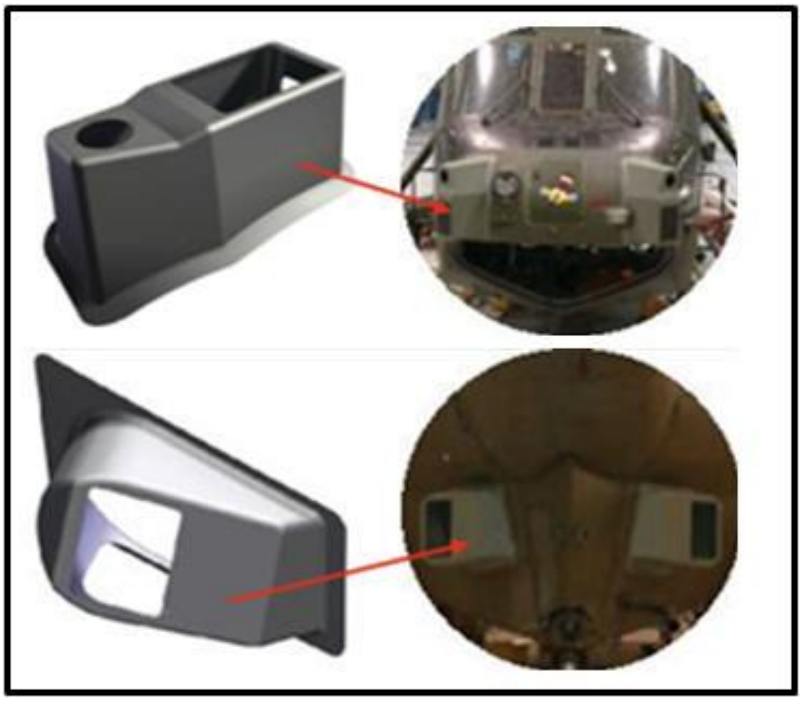

Figure A5.6, Components from a Westland Sea King MK4, Superplastically Formed in AA2004 [84].

A5.4 Superplastic Forming Methods

There are multiple methods of superplastic forming, these include: Bulge forming, Female forming (Cavity forming), Drape forming, Back-Pressure forming, male forming (Bubble forming) and Diaphragm forming [2]. The most commonly used for production, by Superform Aluminium UK, are Cavity and Drape forming and so are described in more detail below.

A5.4.1 Cavity and Drape Forming

This forming operation involves pushing the superplastic sheet into a female die using gas pressure. The die(s) and sheet are heated and maintained at SP temperatures. The pressure forces the sheet into the die cavity as shown schematically in Figure A5.7. The last parts of the sheet to make contact with the die are those contacting the very corners so it is in these areas that the largest strains occur. Drape forming uses the same process only there is a male tool placed in the cavity. As the sheet bulges into the cavity it contacts the male tool and is ‘draped’ over it to produce the required shape.

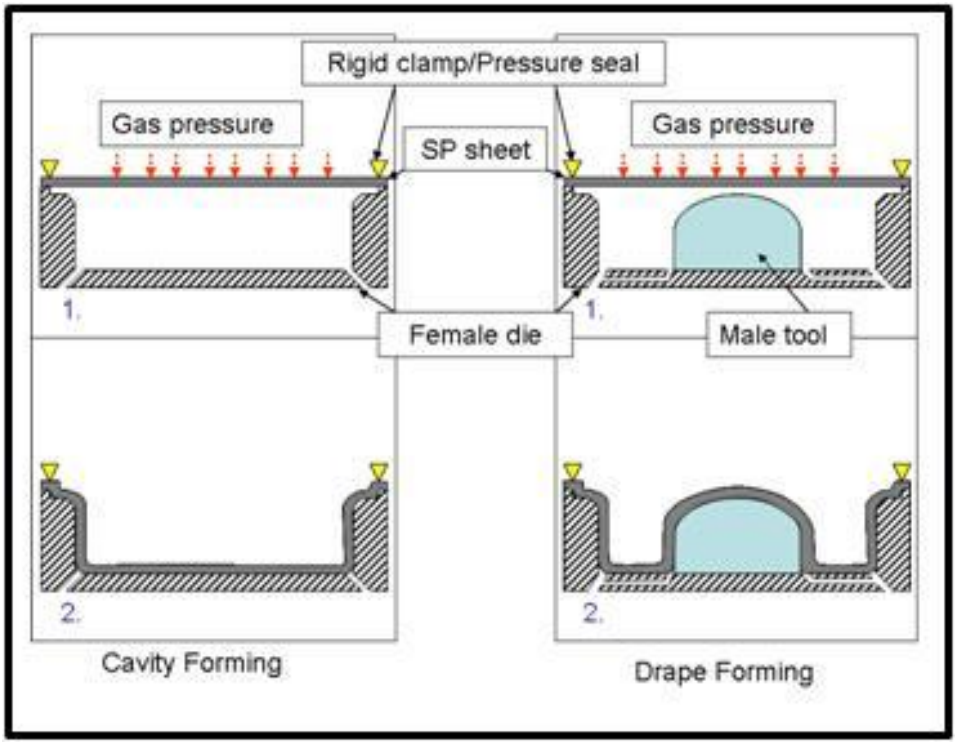

Figure A5.7, Schematic Diagram of a Cavity and Drape Forming Operation, Recreated from [85].

Both of these processes produce parts in a very similar manner and the choice between which of these processes to use is based on the required accuracy for the inner/outer dimension of the part. Female forming produces parts with very accurate outer dimensions. However, if it is the inner dimensions that are more important, a drape forming operation will be used. Parts produced by female forming are thinnest at the pole and corners of the bulged sheet where as drape formed parts are thickest at the pole as shown in Figure A5.8.

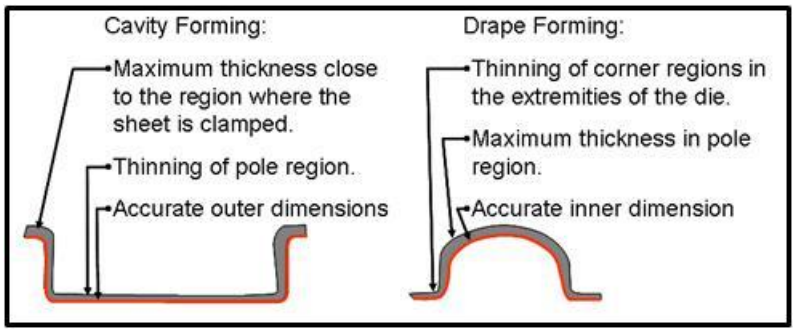

Figure A5.8, Thickness Variations of Parts Produced by Cavity and Drape Forming [85].

Appendix B:

Tooling Designs

Appendix B - FSW tool design specifications

B1.1 Concave Tools

The concave tooling is the simplest tooling set and is comprised of six tools with smooth conical probes with varying probe root diameters. These tools are simple enough to be machined in any university mechanical engineering workshop. Specifications are given in Figure B1.1.

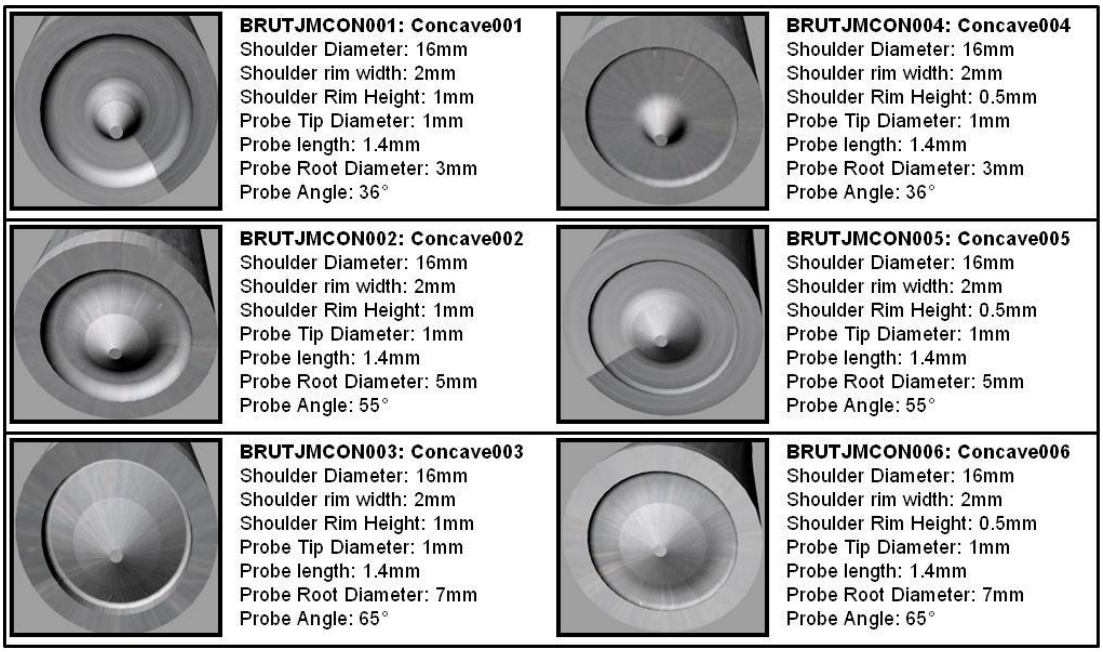

Figure B1.1m Simple Concave Tool Specifications.

B1.2 Triflat Tools

The Triflat tooling is more complex than the concave tooling and so were machined by an external company specialising in precision machining. All of the tools in this set share the same probe design with varying shoulder profiles. The tool probe is cylindrical with left hand threads and three equally spaced flats. Specifications are given in Figure B1.2.

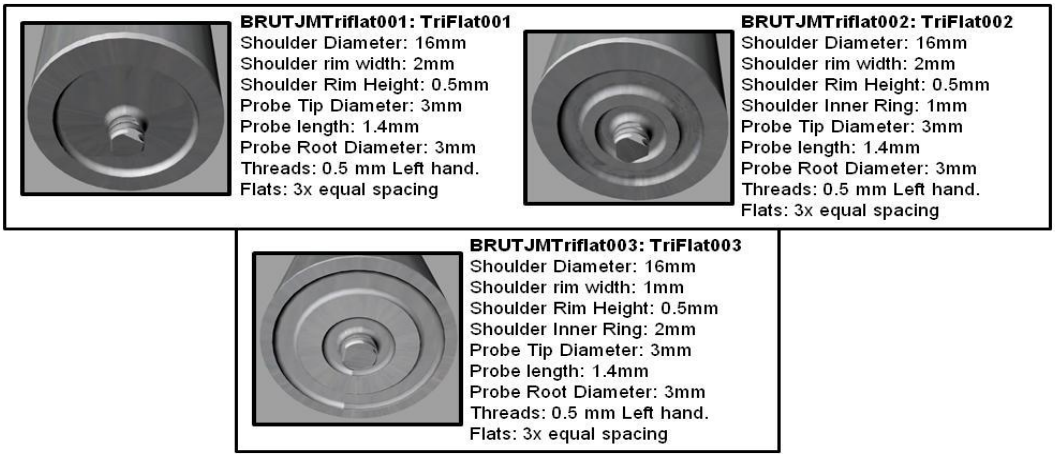

Figure B1.2, Triflat Tool Specifications.

B1.3 Triflute Tools

The Triflute tooling is more complex still. Three small flutes must be machined into the tool probe so these were also machined by an external company specialising in precision machining. All of the tools in this set share the same probe design with varying shoulder profiles. The tool probe is cylindrical with left hand threads and three equally spaced left hand flutes. Specifications are given in Figure B1.3.

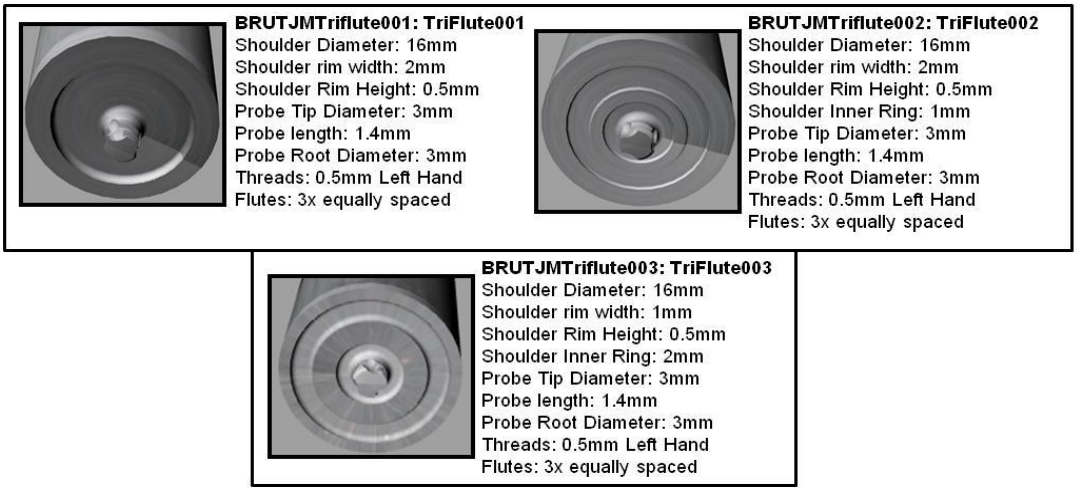

Figure B1.3, Triflute Tool Specifications.

B1.4 GSP 5651 Tool and MX-TriFlute Tools

The GSP 5651 tool and the MXTriflute™ used for welds created on the ESAB machine are both designed by TWI so the specifications are limited.

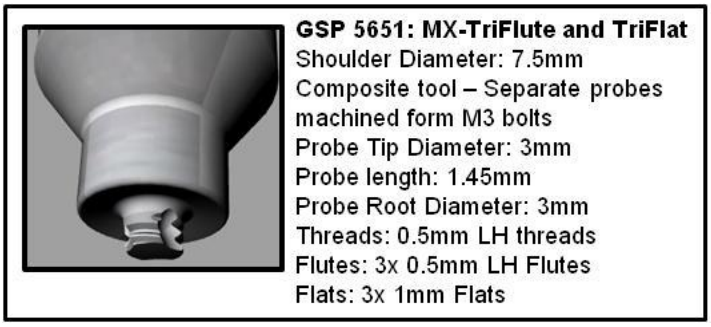

Figure B1.4, GSP 5651 tool specifications.

Figure B1.4 shows the specifications for the 7.5mm GSP5651 tool. The MXTriflute™ tool for the ESAB machine is of similar design but with a much larger shoulder diameter of 15mm and probe diameter of 5mm.

B1.5 Large Shoulder Tools

A set larger shoulder tools were created in order to investigate very wide weld regions created in a single pass. The larger two of the three tools were ineffective and removed from the welding schedule. The smaller of the tools with a diameter of 19mm was used and created the weld which obtained the largest superplastic elongation this is shown in Figure B1.5.

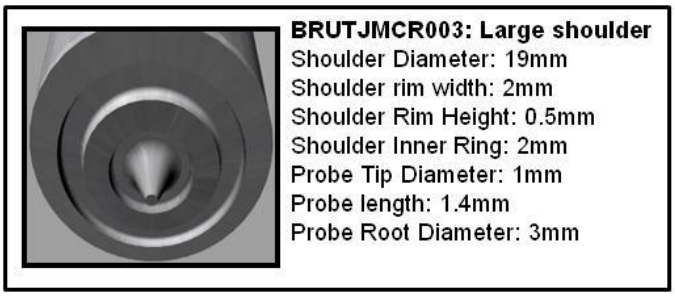

Figure B1.5, Large Shoulder Tool Specification.

Appendix C:

Publications

Appendix C - Publications

C1.1 11th International Conference on Metal Forming 2006

ELSEVIER

Journal of Materials Processing Technology 177 (2006) 336–339

Journal of Materials Processing Technology

www.elsevier.com/locate/jmatprotec

Utilisation of engineering workshop equipment for friction stir welding

T. Minton *, D.J. Mynors

Forming and Manufacturing Group, School of Engineering and Design, Brunel University, Uxbridge, Middlesex UB8 3PH, UK

Abstract

Presented is a description of a methodology for determining if a conventional milling machine is capable of being used to undertake friction stir welding. The methodology is tested by producing same thickness welds of 6.3 mm and 4.6 mm 6082-T6 aluminium sheets. The results from micro-hardness profiles across the tool shoulder diameter are presented in conjunction with tensile test results.

Keywords: Friction stir welding; Milling machine; Aluminium

1. Introduction

This paper describes procedures undertaken to assess whether a conventional manual milling machine could be used to Friction Stir Weld (FSW) butt joints. Trials were undertaken on 6.3 mm and 4.6 mm thick aluminium 6082-T6 sheets using a Parkson Vertical Mill Type A [1]. At the start of the project it was unknown if the milling machine was capable of FSW; hence, a single generic tool was designed for the 6.3 mm sheet (Fig. 1) and truncated for the 4.6 mm sheet. The tools were manufactured from 19 mm diameter silver steel [2]. The pieces to be welded were abutted, bolted to a steel backing plate which was bolted directly to the machine's feed table.

2. Methodology

The determination of the FSW capability window was based on assessing the functional values of the spindle speed, V_s, and feed speed, V_f, for constant probe design, probe positioning and tool tilt angle (1°). Table 1 contains the operating ranges of the Parkson mill. The capability window was assumed to have the same profile as a simple representation of the traditional operating limits (Fig. 2). Hence, the FSW window will fall within A, B, D and E; values for points 1, 2, 4 and 5 need to be determined.

To determine the FSW capability windows for the two thicknesses, trials were undertaken. The first set of trials started with the machine's maximum speed as indicated by point 'A' in Fig. 2. The feed speed was reduced in steps (Table 1), working towards point 'B', until further reductions, based on auditory and visual inspection of the machine and the weld, were inappropriate. This feed speed was then deemed the minimum feed speed, $V_{f_{MIN}}$. Keeping the feed speed constant at $V_{f_{MIN}}$, the spindle speed was set at its maximum and reduced until it was inappropriate to reduce it further, $V_{s_{MIN}}$. The path travelled was parallel to the line 'BD' starting on line 'AB'.

With the coordinates of points 1, 2 and 4 determined, 5 was assumed from symmetry. A statistically valid number of welds were produced (and tested: tensile and hardness) using the values at the corners and centre of the capability window.

3. Results and discussion

3.1. Process window determination

The minimum feed speed was determined for the 6.3 mm and 4.6 mm sheets by setting the spindle speed to the maximum, 1550 rpm, and reducing the feed speed in steps from the maximum of 3.175 mm/s (Table 1). At 0.1 mm/s FSW was possible but resulted in excessive time being required per weld. Hence, $V_{f_{MIN}}$ was defined at the next speed, 0.2646 mm/s.

The minimum spindle speed, $V_{s_{MIN}}$, for both thicknesses was determined by setting the feed speed to $V_{f_{MIN}} = 0.2646$ mm/s and reducing the spindle speed from the maximum. $V_{s_{MIN}}$ was determined to be 620 rpm as below this the manual tool plunge became too physically demanding for the operator and during the welding the acoustic emission from the milling machine indicated that the motor was being too heavily loaded.

Table 2 contains a summary of the determined minimum and maximum speeds, and the closest allowable speeds to the mid-values between the minimum and maximum.

3.2. Weld testing

For the two thicknesses three welds were completed for each of the five test conditions, 1, 2, 3, 4 and 5 (Table 3). Each weld from the centre of tool insertion to the centre of removal was 86 mm in length. Tensile tests were undertaken on each sample using an Instron tensile test machine [3]. Specimens were cut

* Corresponding author. Tel.: +44 1895 265 789; fax: +44 1895 269 763.
E-mail address: Timothy.Minton@brunel.ac.uk (T. Minton).

0924-0136/$ – see front matter © 2006 Elsevier B.V. All rights reserved.
doi:10.1016/j.jmatprotec.2006.03.227

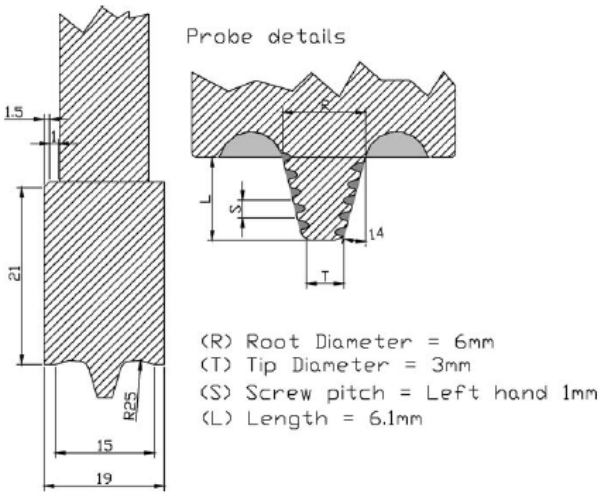

Fig. 1. Tool used for 6.3 mm sheet.

Table 1
Parkson milling machine operating ranges

Spindle speed (rpm)	Feed speed (mm/s)
1550 (maximum)	3.175 (maximum)
1160	2.12
930	1.49
620	0.95
464	0.50
372	0.42
125	0.26
93	0.1 (minimum)
74	
50	Spindle pitch (tool tilt angle) (°)
38	
29 (minimum)	−90° to +90°

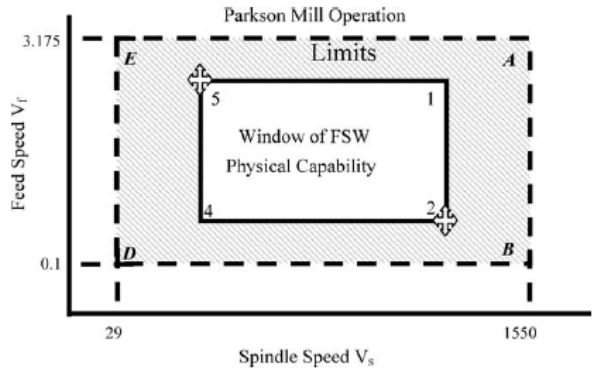

Fig. 2. Parkson mill operational ranges.

Table 2
Speed values

	V_s (rpm)	V_f (mm/s)
Maximum (1)	1550	3.175
Mid-point (3)	1160	1.49
Minimum (4)	620	0.26

Table 3
Weld trial conditions

Condition	V_s (rpm)	V_f (mm/s)
1	1550	3.175
2	1550	0.26
3	1160	1.49
4	620	0.26
5	620	3.175

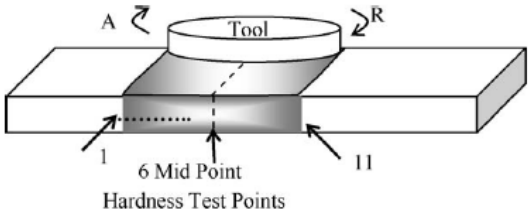

Fig. 3. Hardness profile measurement positions.

from the welds and ground to a suitable surface finish and a micro-hardness profile generated across the weld (Fig. 3), using a Future Tech micro-hardness tester with a 1 kg load [4].

3.2.1. 6.3 mm aluminium

Fig. 4 shows the failure position for each tensile test. Welds produced under condition 5 failed along the weld line. The other 12 welds failed, either within the tool footprint or beyond in the Thermo-Mechanically Affected Zone (TMAZ), C, or Heat Affected Zone (HAZ), B; see reference [5].

Numerous researchers [6–9] have reported failure within the HAZ, the weakest part of the weld, and attribute this to the thermal softening of the material and the lack of compensating deformation. Within the TMAZ the sweeping action of the

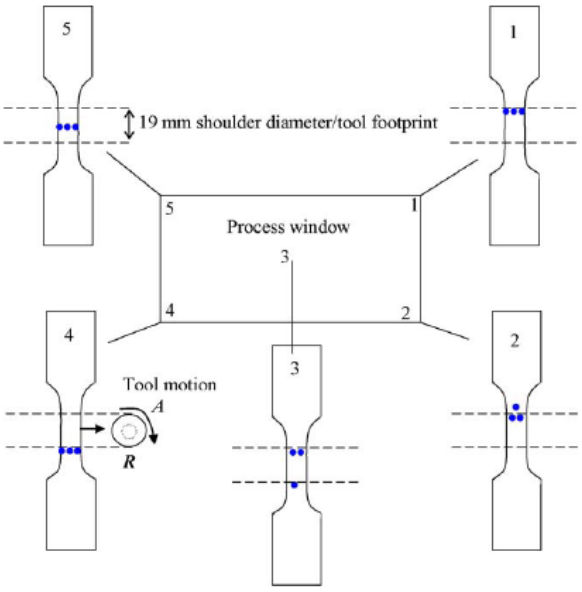

Fig. 4. Tensile test results for 6.3 mm aluminium.

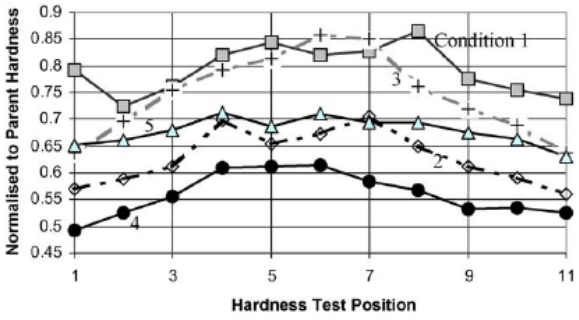

Fig. 5. Hardness profiles for 6.3 mm welds.

probe produces identifiable bands along the join; these affect the material structure and weld properties [9–11]. Their spacing is directly related to the feed speed.

Eight of the 12 welds failed on the advancing side of the tool while the remaining 4 failed on the retreating side. The dominance of 'advancing tool side failure' matches the observations of others [10] and is attributed to the sweeping of the material from the advancing to the retreating side of the tool as it rotates and traverses.

The results indicate that even with a less than an optimal tool the milling machine is capable of producing welds. Fig. 5 demonstrates the relationship between the hardness at 11 positions (Fig. 3) for the 5 conditions. The trends are distinct for each condition, with variations between 50% and 80% of the parent material's hardness.

Hardness plots for points 1, 11 and the mid-point (6) are superimposed on to the normalised spindle and feed speed window (Fig. 6). Inset is a schematic of the hardness trends; the numbers represent the welding conditions. In each case as the feed speed increases for a constant spindle speed the hardness increases. There is little difference in hardness at the extremes of the shoulder footprint; however, there is a considerable difference at the centre, especially under welding condition 3. The tendency for a harder centre region is in line with the heat and deformation seen.

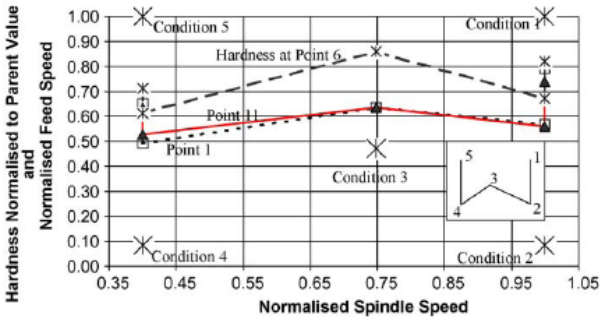

Fig. 6. Hardness trends as a function of speeds for 6.3 mm welds.

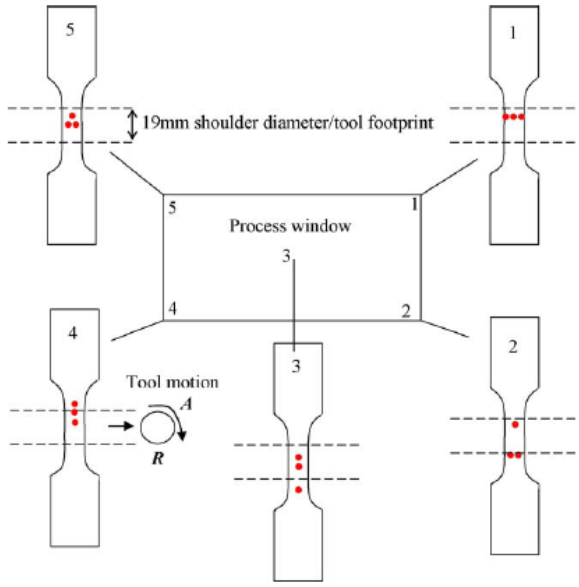

Fig. 7. Tensile test results for 4.6 mm aluminium.

3.2.2. 4.6 mm aluminium

A FSW tool designed for the 6.3 mm aluminium was truncated by 1.7 mm and used to weld the 4.6 mm aluminium. The tool was not specifically designed for 4.6 mm sheet.

Fig. 7 shows the point of the failure for each tensile test. Five of the six welds produced under conditions 3 and 5 failed at the centre. With a few exceptions the welds under conditions 1, 2 and 4 failed within the tool footprint, some at the weld root.

During the welding it was observed that the temperature of the materials being welded and the backing plate were much greater than during the 6.3 mm trials. Fig. 8 shows a very different set of profiles to those in Fig. 5, although the general trends shown in Fig. 9 indicate a similar behaviour to that in Fig. 6.

The less than optimal tool design, the greater amount of heat generated and the large number and type of tensile tests failures are related. For conditions 2 and 4 the excess heat generated appears to have softened excessively the material at the centre (Fig. 8). The relatively large extension seen at the maximum load during the tensile test (Fig. 10) provides additional evidence

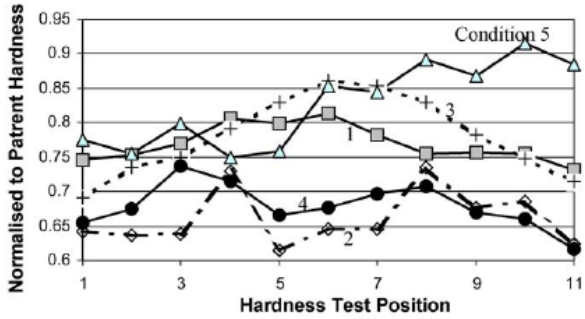

Fig. 8. Hardness profiles for 4.6 mm welds.

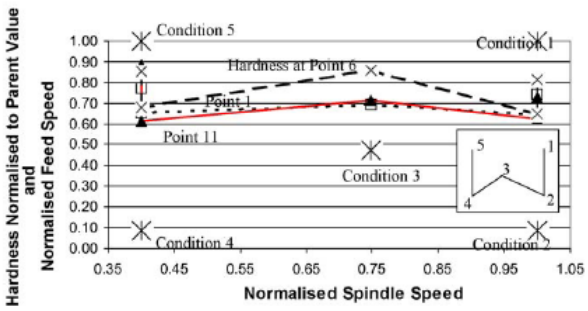

Fig. 9. Hardness trends as a function of speeds for 4.6 mm welds.

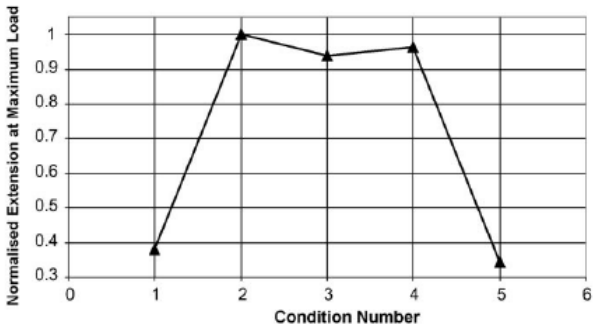

Fig. 10. Extension at maximum load during tensile tests of 4.6 mm welds.

for this. In addition, it is believed that the level of impurities included within the weld was increased because of the raised temperatures, especially at the contact point with the backing plate [8,12] and hence enhanced failures.

The radial bulky tool has demonstrated that large amounts of heat can be generated. However, refining the tool design to improve the welds will require a reduction in the radial dimensions. A question then arises is: at the relatively low achievable speeds, when compared to process specific machines, will a narrower probe be able to withstand the applied loads?

4. Conclusions

A conventional milling machine has been demonstrated capable of performing FSW and producing reasonable welds using a relatively stout tool to join 6.3 mm thick 6082-T6 aluminium. Lesser quality welds were produced when joining 4.6 mm thick 6082-T6 aluminium. Further work is required to establish if the welds in the 4.6 mm can be improved, by enhancing the tool design, while ensuring the tool is sufficiently robust to survive the process.

Acknowledgements

The authors would like to thank the staff at TWI Ltd., Granta Park, Great Abington, Cambridge CB1 6AL, UK, and the EPSRC for their support.

References

[1] J. Parkinson and Son, Parkson 1NA Universal Miller Instruction Manual, Catalogue M23, Second Reprint, J. Parkinson and Son (Shipley) Ltd./Selling Organisation Associated British Machine Tool Makers Ltd., Shipley, Yorkshire, England/London, England, c1950.
[2] RS Components Catalogue, Silver Steel Rod Stock, 1 meter length, 5/8 inch diameter, Part No. QPSZP4377095, RS Stock No. 437-7095, http://rswww.com, last accessed 20/12/2005.
[3] INSTRON, Hydraulic Tensile/Compression Testing Machine, Instron 8501, www.instron.ltd.uk, last accessed 20/12/2005.
[4] Future-Tech Corp., Microhardness Tester, FM-1e, Future Tech, Tokyo, Japan.
[5] G.R. Bradley, M.N. James, Geometry and Microstructure of Metal Inert Gas and Friction Stir Welded Aluminium Alloy 5383-H321, http://www.tech.plymouth.ac.uk/sme/UoA30/Weld_Microstructure.PDF, last accessed 20/12/2005.
[6] TWI Ltd., Granta Park, Great Abington, Cambridge, CB1 6AL, UK, Friction Stir Welding—Intellectual Property Rights, http://www.twi.co.uk/j32k/unprotected/band_1/fswipr.html, 2005.
[7] Y.J. Chao, X. Qi, W. Tang, Heat transfer in friction stir welding—experimental and numerical studies, J. Manuf. Sci. Eng. 125 (2003) 138–140.
[8] T.L. Dickerson, Fatigue of friction stir welds in aluminium alloys that contain root flaws, Int. J. Fatigue 25 (2002) 1399–1409.
[9] H.J. Liu, Tensile properties and fracture location of friction-stir-welded joints of 2017-T351 aluminium alloy, J. Mater. Process. Technol. 142 (2003) 692–696.
[10] M.A. Sutton, Microstructural studies of friction stir welds in 2024-T3 aluminium, Mater. Sci. Eng. A 323 (2002) 160–166.
[11] K.N. Krishnan, On the formation of onion rings in friction stir welds, Mater. Sci. Eng. A 327 (2) (2002) 246–251.
[12] M. Peel, Microstructure, mechanical properties and residual stresses as a function of welding speed in aluminium AA5083 friction stir welds, Acta Mater. 51 (2003) 4791–4801.

Friction Stir Welding of AA5083 and AA2004, commercially available SFP aluminium alloys, for subsequent superplastic forming.

Timothy Minton [1,*], Joe Au [1], Robert Bulpett[2]

1 School of Engineering and Design, Brunel University, Middlesex, UB8 3PH.
2 Experimental Techniques Centre Brunel University, Uxbridge, Middlesex, UB8 3PH.

Corresponding author contact details Email: Timothy.Minton@Brunel.ac.uk.
Phone: 01895267591.

Keywords: Friction Stir Welding, Superplastic forming, Aluminium, AA5083, AA2004.

Abstract:

The effect of tool size, geometry and primary process variables on the existing superplastic (SP) microstructure and properties of two commercially available aluminium alloys are examined. A number of different industrial sectors are now investing in the numerous benefits of friction stir welding (FSW) and friction stir processing (FSP). One of these benefits is the comparatively low heat input compared to fusion welding. Another influential process to gain world wide interest is Superplastic Forming, (SPF). Numerous recent studies have investigated the potential benefits of friction processes to superplasticity. In metals, notably aluminium, superplasticity is usually related to a few prerequisite material characteristics. The most significant is a fine grained structure of <10μm and a fine uniform distribution of strengthening particles. This microstructure is sensitive to heat and deformation and is usually destroyed by fusion welding techniques. The FSW/FSP process can apply a controllable amount of deformation and heat to a specific part of the material creating a fine recrystallized structure which is perfect for superplasticity. The ability to turn a non-SP material into a SP material using FSP has been investigated by many authors, producing micron and nano sized structures capable of the minimum, 200%, elongation required to be deemed superplastic. The retention or improvement of existing superplastic characteristics after FSW/FSP has only been touched on by a few authors but is an area of significant interest, allowing SPF to be carried out on welded sheets. Adapting friction stir processes to SPF will allow for increased flexibility of the SPF process, including, internally stiffened panels, tailor welded blanks and localised modification of properties such as the flow stress or optimum forming temperature. Friction stir welds have been made in 1.6mm thick AA5083 and AA2004 aluminium alloys, in the H19 and F temper conditions respectively, using a multitude of differing tool designs and process variables. Tensile and micro-hardness tests, along with optical light microscopy, have been carried out on samples in an as-welded and annealed condition. Some welds were then reproduced on larger sheets, for cone testing, to assess the SPF qualities of the welds. The results indicate a good acceptance of FSW for the AA5083 producing welds approaching 100% efficiency in the H19 state and consistently ~100% efficiency for the annealed welds. The AA5083 welds decreased in strength as the heat input increased until the material exhibited 'O' temper properties where no further loss of strength is possible. The 2XXX series alloys are a more complex system and are far less tolerant to the FSW trials carried out in this investigation achieving joint efficiencies ranging from 36-85%. It is surmised that above a critical heat input the material is annealed by the FSW/FSP tool as it passes by. The material is softened, losing its strength and possibly its ability to be superplastic.

The amount of disruption to the original microstructure directly affects the superplastic performance. This disruption depends on the tooling used and the FSW

parameters used for the welding process. Small tools, providing a low level of heat input can create an excellent weld that yields efficient room temperature properties. These welds however are highly strained due to the fast welding speeds used. The highly strained weld material does not accommodate superplastic flow, creates a mismatch with the parent material and so is unable to deform in the same manner. When tested at superplastic temperatures the welds which performed the best at room temperature failed quickly in the weld material. Welds which were made using the larger tools and under hot conditions provided room temperature properties which were similar to those of an annealed, fully softened material, but fared better at elevated temperatures. When these welds were cone tested they performed much better than their low temperature counterparts.

The two alloys behave differently under superplastic conditions. The AA5083 welds failed in the weld material at the joint interface. This is due to the mismatch in their structures, the weld material is highly strained from the FSW process and so requires a higher stress to be deformed. The parent material starts to form but the weld material remains undeformed causing a rupture in the weakest part of the specimen. The AA2004 weld managed to withstand the forming gas pressure and continued to ~250% strain. The weld eventually failed due to grain coarsening rather than rupturing of the joint.

Introduction:

It is the challenge of this investigation to create friction stir welds in commercially available superplastic aluminium alloys, AA5083-H19 and AA2004 (SUPRAL100), which can tolerate subsequent SPF conditions to achieve superplastic elongations.

The benefits of friction stir welding (FSW), especially for aluminium and its alloys, have been investigated ever since it was first unleashed into the scientific community and many key industries are now enjoying some of these benefits. One of these benefits is the creation of a modified structure after the weld has been completed. FSW has the ability to change a completely random, heterogeneous structure, for example a casting, into a more homogenous, equiaxed grain structure, which enhances desirable properties such as strength. The realisation of this has opened the door to FSW being used for material processing instead of welding, by carrying out the process on a monolithic sheet. Many authors have, and continue to explore how a relatively simple, mechanical process can completely change the micro and, more recently, nano structures of various metals [1,2]. This ability was immediately recognised as a potential benefit to fine structure superplasticity (FSS). To be considered superplastic a material must be able to deform uniformly to an elongation of 200% or more. For this to be possible the material must be very specifically tailored to exhibit certain characteristics including, an equiaxed matrix grain size <10μm and a fine, uniform distribution of hard second phase particles. These two characteristics are very important, the material's ability to deform to such high elongations relies so heavily on them that if one is removed, the material may loose this ability. This is a major problem when designing using superplastic materials. The material is sensitive to any changes to its structure limiting its manufacturing flexibility.

A typical welding operation is a very traumatic experience for a superplastic material because it will remove the before mentioned characteristics vital for superplasticity. The presence of a very high heat, causing melting of the matrix material, completely disrupts the delicate balance within the structure. Heating the material to the temperatures required for fusion welding causes the structure to become coarse due to the absence of a fine distribution of second phase particles which would stabilise the structure at these temperatures. Recovery occurs more readily than

recrystallization in the aluminium, completely destroying the superplastic properties of the material as the grain size is too large to allow creep mechanisms, such as grain boundary sliding (GBS), to occur. An area, within a superplastic sheet, which does not conform to the perquisites of superplastic behaviour creates a heterogeneous structure and will therefore not deform uniformly and will ultimately fail in or around this area due to a concentration of strain. This area has the potential to become un-deformable under SPF conditions due to a complete mismatch in flow stress in the material.

In stark contrast to this, FSW process produces a fine, equiaxed structure not dissimilar to that of a superplastic material. The presence of deformation and heat allows the material to be dominated by recrystallization instead of recovery. The dramatically lower heat levels produced during FSW also benefits the structure by not destroying the fine distribution of second phase particles. Using the FSW process it should be possible to create a weld that is structurally similar to the parent sheet, minimising any mismatch between them. The retention of superplastic properties after welding has the potential to expand the current capabilities of superplastic forming operations. Successful forming of welds in commercial superplastic aluminium alloys presents a multitude of applications previously difficult or impossible to undertake. Diffusion bonding (DB) is a useful tool in creating superplastically formed internally stiffened panels in titanium, however this process is not readily applicable to aluminium. FSW has been keenly investigated as a replacement for DB to create internally stiffened structures in aluminium. Other applications may include the addition of patches, to increase the material thickness and reinforce key points of the sheet, or using the welding process to intentionally change the properties of the material; creating specifically designed sheets resembling a contour map of varying degrees of superplasticity.

Salem et al [3] and Grant et al [4] have investigated the retention of superplastic properties in superplastic aluminium alloys 2095 and 5083 respectively. Their findings support the use of FSW as an appropriate method of joining superplastic materials. The microstructures produced do exhibit the required characteristics for SPF but do differ from the parent sheet. This difference, no matter how small, will affect the mismatch between the weld material and the parent sheet, causing one to deform before the other. Superplasticity relies on the structure deforming uniformly; when the structure cannot deform uniformly strain concentrates in certain areas and uncontrollable necking will begin, resulting in early failure.

Charit et al [5] have shown that by changing the FSW process variables key aspects of the weld material, such as flow stress, can be tuned to better suit the SPF process and will enable the mismatch of parent and weld flow stresses to be reduced.

Methodology:

The materials chosen for this investigation were considered to be the most commonly used aluminium alloys for SPF, namely AA5083 and AA2004 otherwise known as SUPRAL100; typical compositions can be found in table 1. The two alloys are produced via different thermo-mechanical processing and cold rolling sequences to give very fine grain sizes of <10µm. The material was received as 1.6mm thick 100mmx1000mm strips these were then cut into ~333mm long sections to be secured to the anvil of the machine using finger clamps. The machine is screw driven, the maximum spindle velocity is set to ~1000 rpm and the maximum traverse speed is ~750 mm/minute. The plunge depth on this machine was varied by changing the depth of two bolts which support the mill head when it is lowered. Previously the spindle head was supported by a tool heel roller; however this was

removed to make space for the LoStir device, a real time force monitoring head capable of measuring the welding force, downward force and spindle torque. All the measurements form the Lostir head were taken at 10ms intervals over the entire welding time [6].

A total of 12 tools were used to create the welds. These were separated into 5 groups, Concave, Triflute, Triflat, Large shoulder and GSP 5651. The 5651 tool is a TWI designed tool which has proved successfully in joining aluminium ranging from 1.2-25mm thick [7]. Details of the tools can be found in a summary in figure 1. Each of the 12 tools was used in 10 welding operations, 5 on each alloy. The settings for spindle speed and traverse speed were varied between 500-700rpm and 175-746mm/min respectively This gave 5 different values for the weld pitch (mm/rev) ranging from 0.25, considered to be hot welds to 1.49, considered to be cold welds.

The FSWs were first carried out on monolithic sheets, known as a bead on plate weld, this simulates a perfectly made weld, eliminating defects associated with the set up of the materials, such as plunge depth, starting gap and in process plate separation. Evaluation of the microstructures and properties was carried out to establish the best tools and settings to use for subsequent welding trials. Microscopy samples were taken along with tensile and microhardness specimens. These specimens included welds in the as-welded state and those which had been subsequently annealed at 350°C to give a partially softened material.
Welds which were deemed to be successful in the bead on plate trials were then reproduced using a conventional butt weld configuration. This set up provided many more problems due to setup related defects. The LoStir head was removed and replaced with the tool heel roller to aid the positional accuracy of the tool plunge. Several welds were made in both single and multiple pass operations. These welds were then tested at superplastic temperatures using a cone testing facility, courtesy of Superform-Aluminium UK.

Analysis of the microstructures was carried out using conventional microscopy techniques and an optical light microscope. A five stage preparation procedure was used to prepare both the AA2004 and AA5083. To reveal the microstructure of the different alloys two different methods of etching were used. The AA5083 structure was revealed by electrochemical etching in a 1.8% Barkers reagent (HBF_4) at 10V for 2 minutes. The AA2004 structure was revealed using a two stage chemical etching process. Samples were first immersed in Graff & Sargent's etchant for 2 minutes followed by a dip in Keller's reagent.

Results and discussion:
Many of the first welds were unsuitable for testing and were created to setup the machine and fine tune any variables that resulted in failure of the welding operation. The most difficult and problematic setting was the plunge depth because it has a small tolerance. Due to the thin gauge of the material, the plunge depth of the tool probe has to be perilously close the anvil. Too shallow and the tool shoulder does not make full contact with the top surface of the material and so would not generate sufficient heat to fully plasticise the weld material causing a failure of the tool probe and an inherent flaw in the weld root throughout the length of the weld. Too deep and the tool will impact on the anvil and cause damage to the tool and a failed weld. During the welding operation the tool is forced in to the material to be joined, this force down through the tool is resisted by the material. Once the material is plasticized the resistance is less and the tool can sink into the material causing tool damage, extreme plate thinning accompanied with excessive flash generation and

ultimately a failed weld. This was overcome using a dwell time before the traverse was started and a ramp up of the traverse speed. This allowed the tool to be fully plunged and at a stable depth before any force was applied in the weld direction.

Real-time measurements of welding forces and spindle torque using the LoStir device

Three measurements were taken in real time during the welding experiments. These were weld force (Fx), down force (Fz) and spindle torque. Figure 2 shows an example of the measurements recorded for a hot and cold weld in AA5083, using the same tool. The welds created using the hot conditions have sufficient time to fall into a steady state regime and do so relatively quickly. The cold welds however take longer to establish this regime and sometimes fail to do so before the end of the weld.

It was expected that the magnitude of these measurements would change depending on the FSW process variables as this has been shown in previous works [8,9]. In these investigations and the present study the values of weld force is directly affected by the spindle speed and the traverse rate and so is proportional in some respects to the welding pitch and therefore the weld heat input. A low welding pitch implies a hot welding condition is used and so a drop in weld force is expected when compared to a high weld pitch. It has been shown that there is a maximum welding speed for a given spindle rotation speed that enables the weld material to be ideally softened just before it comes into contact with the tool's probe [10]. In a cold weld the welding force is higher due to insufficient softening of the weld material in front of the tool this is shown in Figure 3 a), thus the weld force increases with increasing weld pitch.

The welding force varies with the amount of softening experienced by the material, in these experiments the weld force increased significantly, ~50-232% higher for a cold weld compared to a hot weld. The softening is mainly due to the processing variables spindle speed and traverse speed but is also related to the tool design and weld material. In all cases the welding force is higher for the AA5083 than for the AA2004, this suggests that the AA5083 requires more energy to sufficiently soften the material beneath the tool [8]. As the frictional heat strives to soften the material the induced strain works antagonistically for the AA5083, strengthening the plasticized material. This results in significantly higher welding forces when compared to the AA2004. At a low welding pitch, hot welding conditions, the difference can be as much as 60% higher. For the high welding pitch, cold welding conditions, the difference can be even higher, as much as 80% higher. This difference can be put down to the critical softening isotherm disused by Russell [7,10], the cold welding conditions mean that the weld experiences less heat for a shorter duration and so there is less time at welding temperature for the material to relax the strain induced by the welding process.

The two alloy systems behave very differently, this is due to their different strengthening mechanisms. AA5083 is a strain hardening material. When welding strain hardening alloys the FSW process combines moderate heat with intense plastic deformation, this produces a weld region which is highly strained. When welding a fully soft, annealed material the weld region can be stronger than the HAZ region and unaffected parent material. The AA2004 relies on precipitation of hard second phases for its strength rather than dislocations so there is no hardening opposing the plasticization of the weld material.

The downwards force is the force acting through the tool, required to maintain a constant contact between the weld material and tool. Figure 3 b) shows the down force versus the weld pitch; it would be expected that as the weld pitch was

increased, from hot to cold welding conditions, the down force would increase due to a greater force being required to plunge the tool into a harder less plasticized material. However during these trials the down force was lower for the cold weld conditions with the exception of the 5651 tool welding the AA2004, in this case the down force did increase. The variation between the hot and cold conditions was quite small ~10-20%. The difference between the two alloy systems is once again highlighted with a higher value for down force for the AA5083 compared to the AA2004, ~5-50% higher, this again suggests that it is harder to plasticise strain hardening alloys, requiring more energy to fully soften the material beneath the tooling.

The torque produced during the process gives a good initial estimate of the amount of heat generated. A high torque value yields a low heat input. Spindle torque can be described as the amount of power required to rotate the tool whilst it is in contact with the resistive weld material. As the weld pitch falls, moving from cold to hot welding conditions, the material is more plasticized resulting in a reduction in the spindle torque. This torque/heat input relationship behaves in the same way as in conventional rotational friction welding. As the heat input rises, the torque decreases, up until a critical point. After this point no further increase in heat input is possible due to extreme softening and localised melting of the material directly beneath the shoulder, resulting in a loss of traction between the tool and the weld material. Figure 3 c) shows the torque versus increasing weld pitch. As the welding pitch is increased the torque rises, the tool is harder to rotate when in contact with a harder material. When the material becomes too soft it can act as a lubricant and so decreases the amount of torque.

The heat input for a friction stir weld is best estimated using the spindle torque. It has been suggested that the rotation of the tool in contact with the weld material accounts for as much as 99% of the total heat generated, with the remaining heat derived from the traverse of the tool. The efficiency factor represents the amount of heat which remains in the work piece and has been estimated to be ~0.85 [10].

(1) $$Q = \varepsilon \frac{2\pi r T}{1000 v}$$ [11]

Q = Heat Input.
ε = Efficiency factor (0.85).
r = Spindle rotation speed (rpm)
T = Spindle torque (Nm).
V = Traverse speed (mm/min)

Figure 3 d) shows the calculated heat input (1) versus the welding pitch. It is clearly visible that as the welding pitch increases the amount of heat supplied falls. This is expected as the higher the welding pitch, the more material is processed for each rotation of the tooling. This supports the notion of using the welding pitch as a preliminary estimate for the heat supplied to the weld.

Room temperature tensile testing:
Of the five tooling types only the GSP 5651 tool showed significant variation of strength over the entire range of process variables. The other four sets had similar sized diameters and produced welds of similar strength regardless of the spindle speed, traverse speed or shoulder and probe profiles used. This due to the heat input of welds being significantly high enough to cause static annealing of the material in the wake of the tooling. Figure 4 shows the results of room temperature

tensile tests and calculations based on an equation for heat input (1) generated during the FSW [12]. The lowest heat input generated for the larger diameter tools corresponded to the highest heat input generated for the much smaller 5651 tool, explaining the overlap of the weld strengths.

AA5083:
The ultimate tensile strength of the parent sheet is ~416 MPa in the H19 form and ~290 MPa for a partially annealed material. For FSWs made in this material the UTs varies from 270-390 MPa. These results correlate with other studies [13,14] which show the strength of 5083 FSWs are similar to those of 5083 material in the 'O' condition; given certain levels of heat input. It can be seen from figure 4 a) that for AA5083 some retention of the H19 strain hardening is possible when using a small tool and a low heat input. Once the heat input reaches a critical level, regardless of tool size, the material becomes soft and strength is lost. For all the larger diameter tools the heat input is similar and this is reflected by the tensile results. All the larger tools created welds which conformed to strength of an annealed material suggesting that the heat input generated by these tools is sufficient to statically anneal the material as the tool passes over it. It should be noted that as the tensile tests are carried out on cross sections of completed welds the UTs results are representative of the weakest part of the weld. AA5083 is a strain-hardening material, therefore when deformation is induced into the material at low temperatures the material shows enhanced strength. This strength is lost when the material is heated above a certain point where annealing takes place. The lowest heat input weld uses the fastest travel speed and so will experience the least annealing in the tool's wake; there is less relaxation of the induced strain so more strain hardening is retained by the weld material. The only variation in tensile strength comes from the lower end of the heat input scale.

AA2004:
The UTs of the parent sheet was tested at ~368 MPa for material in the F condition (As fabricated) and ~250 MPa for annealed material. For AA2004 the results show a range of 245-280 MPa and softening of the material throughout the full range of tooling types and process variables giving an excellent correlation with the annealed parent sheet results, this is shown in figure 4 b). The reason for this is due to the strengthening mechanisms of this material. AA2004 is a precipitation hardening material which gains its strength from the formation of second phase strengthening particles throughout the material. FSW can cause the precipitate distribution to be disrupted, resulting in regions within the weld to be heterogeneous in terms of size and distribution of the second phase causing weakness in some areas. A previous study by Yang et al has demonstrated that the distribution of precipitates changes from one side of the weld to the other as well as longitudinally possibly due to asymmetry of the welding process [15]. The advancing side of the weld combines the angular velocity of the tool with the linear movement of the tooling. For the retreating side the rotation of the tool opposes the linear tool movement. It has been shown that the FSW process creates the weld zone by continuous shearing of small bands of material around the tool probe [16]. Material on the advancing side is moved around the front of the tool and deposited on the retreating side. Material from the retreating side moves the shorter distance around the rear of the tool filling the space behind the tool. This asymmetric material flow causes the precipitates to become distributed throughout the weld zone in a non-uniform manner. This alloy does not gain any strength from the severe plastic deformation occurring in the weld zone to counteract the reduction of strength caused by the annealing of the material and so the effect of the welding process is to lower the strength of the weld material.

Fracture locations:
When tested, the welds predominantly failed in the weld nugget region and on the retreating side of the weld in the TMAZ or HAZ. The only exceptions to this were two welds made in AA5083 using the small 5651 tool; these welds failed on the advancing side. The AA5083 welds showed a stable trend, 89% of the welds fractured in the nugget region of the weld with the remaining 11% split between the TMAZ on the retreating side (8%) and the TMAZ on the advancing side (3%). This trend shows this alloy's susceptibility to strength reductions due to the heat from the process. The general theory, for a strain hardened 5083 alloy, shows that the weld zone will experience a small drop in strength and hardness when compared to the parent material. This area becomes the weakest point in the cross section and so the specimen will predominantly fail here. This trend is not emulated by the AA2004. This alloy showed a greater spread of fracture locations. Predominantly the AA2004 failed in the TMAZ on the retreating side of the weld this accounts for ~56% of the welds. The next highest value was for the weld nugget which accounted for ~31% followed by the HAZ on the retreating side with ~13%. Notice that none of the welds produced in the AA2004 failed on the advancing side. This is possibly due to the asymmetry of the weld, reducing the effectiveness of the precipitation strengthening mechanism on one side more than the other. A typical hardness plot would show a small reduction of strength and hardness in the weld nugget and a far greater reduction in the HAZ regions. The predominance of failure outside the weld nugget coincides with weakest part of the cross section being outside the weld nugget.

Microhardness:
The hardness variations across a transverse section of the welds were measured using a Vickers microhardness tester with a 1kg load. As the hardness of a material is directly related to its strength, it was expected that the hardness of the material in the weld zone would fall, mimicking the fall in tensile strength. A typical hardness profile for a strain hardened 5XXX series weld shows a reduction in hardness in the very centre of the weld, the amount by which the hardness falls is associated with the amount of annealing experienced as the tool passes over the material, this characteristic profile is shown in figure 5 - inset [17]. The profiles for the welds in AA5083 in figure 5 a) show a reduction in hardness, however the reduction is much less than what was expected. It is known that the hardness of a material is also related to the grain size of the material. The smaller the grain size the higher the hardness value. The materials used in this study are used for superplastic forming and so have a very fine grain size possibly explaining the rather small drop in hardness across the weld zone. This may also be deemed to be a result of the strain hardening experienced by the material in the weld zone.

The AA2004 has also produced a hardness plot that does not conform to what is conventionally shown from previous experiments undertaking the friction stir welding of aluminium alloys [17]; this profile is shown in figure 5 b) and has a characteristic profile inset for reference purposes. Usually for a 2XXX series alloy the hardness profile shows a distinct 'W' shape. The minima in this characteristic profile would correspond to the HAZ region where heat, in absence of deformation, causes the strengthening precipitates to coarsen resulting in a drop in hardness in this region. The minima are absent in results shown in figure 5 b); this could possibly be attributed to the composition of the alloy in particular the high Zr content and the low spindle rotation speeds which were used. The microhardness profiles were taken more than a month after the welding operation and so some natural aging would have occurred. The centre of the weld does show a region of reduced hardness with similarities to the inset image, this could be caused by the presence of heat and deformation and the dynamic recrystallization which is associated with the weld nugget of FSW processes carried out on aluminium alloys.

Microstructure:
The AA5083 has a rolling direction which is parallel to the welding direction. The starting microstructure of this material takes the form of fine grains massively elongated in the rolling/welding direction and flattened in the transverse direction. This differs from the AA2004 in this study as the rolling direction for this alloy is perpendicular to the welding direction. The AA2004's grains are highly elongated in the transverse direction; figure 6 shows the microstructures of the two parent materials. The microstructures of the parent materials are stable at superplastic temperatures allowing them to be deformed to strains of 500% and 1000% for the AA5083 and AA2004 respectively [18]. Their microstructures do not resemble that of a characteristic SP microstructure, the fine equiaxed grains <10μm, this is because this structure is obtained by static recrystallization before the SP operation for the AA5083 and dynamic recrystallization during the early parts of the forming operation for the AA2004 [19]. There is a delicate balance between the fine matrix grain and the introduction of a harder second phase to pin the grains during elevated temperatures. The friction stir welding process introduces both heat and plastic deformation to create a solid state bond. This can have the effect of causing changes to the microstructure of the material through many overlapping and competing structural change mechanisms such as dynamic continuous recrystallization, geometric recrystallization, dynamic recovery and abnormal grain growth. Friction stir welding of aluminium usually results a recrystallized, fine equiaxed weld nugget surrounded by a thermo mechanically affected zone which contains regions of differing levels of recrystallization. The difference between the unaffected material and the weld zone can be clearly seen in figure 7, photos a) and c) show the boundary between the undeformed material and the heavily plasticized material beneath the tool. The elongated structure of the parent material is transformed into a more equiaxed structure which is much finer and is shown in figure 7, photos b) and d). This clearly presents a problem when it comes to any subsequent SPF operations carried out on a welded specimen. Although the FSW process creates a solid state join which can exhibit ideal superplastic qualities like a fine grain structure, ultimately the difference in the structures will cause the two areas to deform at different rates. This mismatch in properties will cause the early failure in any superplastic test. A weld zone which requires a lower flow stress to induce a superplastic regime than the parent material will deform first and could form to failure before the parent material. If the weld zone requires a higher flow stress then the weld will act as an undeformable block in the middle of the parent material. The deforming parent material will stretch the undeformable weld zone and cause it to rupture.

Cone testing:
Cone testing is simple repeatable test to determine the superplastic properties of the material. Material is heated to forming temperature and gas pressure is then used to force the material into a conical die. All the tests were carried out at 460°C and with varying gas pressures ranging from 30 to 80 psi. Cone tests were carried out on both single pass and double pass welds to ensure testing could occur with no failure due to any root related defects. The single pass welds did not fare well during the cone tests. Inadequate mixing and therefore bonding of the joint interface in the root of the weld meant a small; approximately 0.1mm section of the joint was not fully bonded. The gas pressure is applied from the weld root side of the test piece, the unbonded section acts as a failure initiation site causing a rupture of the weld seam at the joint interface. To ensure adequate bonding occurs in the root section of the weld re-entrant features on the tool probe such as threads, flutes and flats are utilised. The larger tools do not have such features so root closure is difficult. The 5651 tool uses such features but did not solve the problem as the margin for error with the plunge depth is so small. Double pass welds, which involve welding in a conventional butt

weld configuration, flipping the weld over and repeating the weld on the root side of the plate, were conducted to ensure testing could continue without weld root related failures. The double pass welds were able to maintain gas pressure. The AA2004 weld formed to a strain of ~250%. The cause of failure for this test was coarsening of the grains in the weld region. The weld deformed before the parent material implying that the weld region required a lower flow stress for forming. The AA5083 weld maintained gas pressure but still failed due to rupturing of the weld interface. The strain hardened weld zone did not deform. As the parent material starts to deform the weld material resists the deformation and is pulled apart at the joint interface. This is a similar situation to SPF of tailor welded blanks using conventional fusion welding techniques, the weld material requires a higher flow stress for deformation causing it to resist and remain undeformed [20]. Photos of the cone tested specimens are shown in figure 8 with results shown in table 2.

Conclusions:

- Friction stir welds have been made in commercially available superplastic aluminium alloys which exhibit excellent room temperature properties. Joint efficiencies of ~96% and ~85% for the AA5083 and AA2004 respectively.
- Improved tooling designs and greater control of the positional accuracy of the tool can improve the friction stir welds, removing root defects and increasing joint strength.
- The two alloy systems perform very differently in terms of both room and elevated temperature properties. Excellent room temperature properties do not imply good superplastic properties.
- The microstructure of the weld material differs from the parent sheet causing mismatches of properties. This mismatch causes the weld and parent material to deform at different rates.
- The weld material for the AA2004 deforms before the parent material and fails due to grain coarsening at SPF temperatures. The parent material for AA5083 deforms before the weld material, the undeformable weld material is stretched and ruptures along the joint interface.
- Performance can be improved by removing material from the crown and root of the weld. The scalloping makes left by the FSW process can act as failure initiation sites. The use of tooling which have re-entrant feature on the probe such as flutes, flat and threads can improve the bonding in the root of the weld.

References

[1] ZY Ma, RS Mishra. Development of ultrafine-grained microstructure and low temperature (0.48 Tm) superplasticity in friction stir processed Al–Mg–Zr, Scripta Materialia, 2005, Issue 1, Volume 53, Pages 75-80

[2] S Benavides, Y Li, LE Murr, D Brown, JC McClure. Low-temperature friction-stir welding of 2024 aluminum, Scripta Materialia, 1999/9/10, Issue 8, Volume 41, Pages 809-815

[3] HG Salem, AP Reynolds, JS Lyons. Microstructure and retention of superplasticity of friction stir welded superplastic 2095 sheet, Scripta Materialia, 2002/3/11, Issue 5, Volume 46, Pages 337-342

[4] GJ Grant. Superplastic Forming of Aluminium Multisheet Structures Fabricated Using Friction Stir Welding and Refill Friction Stir Spot Welding, 6th International Symposium on Friction Stir Welding, 2006,

[5] I Charit, RS Mishra. Evaluation of microstructure and superplasticity in friction stir processed 5083 Al alloy, J. Mater. Res., 2004, Issue 11, Volume 19, Pages 3329-3342

[6] K. A. Bemish, A. Ezeilo and S. Smith. Development of a low cost friction stir welding monitoring system, 6th International Symposium on Friction Stir Welding, Saint-Sauveur Canada, 2006,

[7] M. J. Russell. Development of improved tool designs and parameters for the friction stir butt welding of 1.2, 6 and 25mm thickness aluminium alloys, TWI, TWI Members Report, 801/2004, May 2004, Pages 1-44, http://www.twi.co.uk/j32k/index_mem.xtp.

[8] R. Johnson and N. L. Horrex. Preliminary examination of forces generated during the friction stir welding process, TWI, TWI Members Report, 696/2000, January 2000, Pages 1-7, http://www.twi.co.uk/j32k/index_mem.xtp.

[9] R. Johnson. Forces in friction stir welding of aluminium alloys - further studies, TWI, TWI Members Report, 716/2000, December 2000, Pages 1-18, http://www.twi.co.uk/j32k/index_mem.xtp.

[10] M. J. Russell. Development and Modelling of Friction Stir Welding , 2000, Pages 1-154.

[11] P. L. Threadgill and M. E. Nunn. A review of friction stir welding: Part 1 process overview, TWI, TWI Members Report, 760/2003, February 2003, Pages 1-31, http://www.twi.co.uk/j32k/index_mem.xtp.

[12] K. A. Bemish. The effect of the tool shoulder on friction stir welding of 6mm thickness aluminium alloys, TWI, TWI Members Report, 869/2007, April 2007, Pages 1-34, http://www.twi.co.uk/j32k/index_mem.xtp.

[13] LE Svensson, L Karlsson, H Larsson, B Karlsson, M Fazzini, J Karlsson. Microstructure and mechanical properties of friction stir welded aluminium alloys with special reference to AA 5083 and AA 6082, Science and Technology of Welding and Joining, 2000, Issue 5, Volume 5, Pages 285-296

[14] M Peel, A Steuwer, M Preuss, PJ Withers. Microstructure, mechanical properties and residual stresses as a function of welding speed in aluminium AA5083 friction stir welds, Acta Materialia, 2003, Issue 16, Volume 51, Pages 4791-4801

[15] B Yang, J Yan, MA Sutton, AP Reynolds. Banded microstructure in AA2024-T351 and AA2524-T351 aluminum friction stir welds: Part I. Metallurgical studies, Materials Science and Engineering A, 2004, Issue 1-2, Volume 364, Pages 55-65

[16] ZW Chen, T Pasang, Y Qi. Shear flow and formation of Nugget zone during friction stir welding of aluminium alloy 5083-O, Materials Science and Engineering: A, Volume In Press, Corrected Proof,

[17] T. Khaled. An Outsider Looks at Friction Stir Welding, Federal Aviation Adminisration, ANM-112N-05-06, 2005, Pages 1, http://faa.gov/aircraft/air_cert/design_approvals/csta/publications/media/friction_stir_welding.pdf.

[18] GE Totten, DS MacKenzie. Handbook of Aluminum Volume 1 Physiscal Metallurgy and Processes, 2003, 0-8247-0494-0.

[19] PS Bate, FJ Humphreys, N Ridley, B Zhang. Microstructure and texture evolution in the tension of superplastic Al–6Cu–0.4Zr, Acta Materialia, 2005, Issue 10, Volume 53, Pages 3059-3069

[20]RW Davies, JS Vetrano, MT Smith, SG Pitman. Mechanical properties of aluminum tailor welded blanks at superplastic temperatures, Journal of Materials Processing Technology, 2002/10/6, Issue 1-3, Volume 128, Pages 38-47

AA5083							
Si	Fe	Cu	Mn	Mg	Cr	Zn	Ti
0.1245	0.3072	0.0293	0.4791	4.4336	0.0889	0.0109	0.0196
AA2004							
Si	Fe	Cu	Mn	Mg	Zn	Ti	Zr
0.07	0.16	6.05	0.015	0.029	0.084	0.006	0.4

Table 1. Typical composition of superplastic aluminium alloys in weight percentage.

Corresponding photo in figure 8.	Tool (Configuration)	Pitch (mm/rev)	Gas pressure (psi)	Time to failure (Sec)	Failure description
a)	BRUTJMCR003 (DP)	1.49	40	137.92	Grain coarsening
b)	BRUTJMCR003 (DP)	1.49	30	59.27	Weld rupture
c)	GSP 5651 (DP)	1.49	80	2.0	Weld rupture
d)	GSP 5651 (S)	1.49	80	2.0	Weld rupture
e)	Concave005 (S)	1.49	80	1.0	Weld rupture

(S) – Single pas weld (DP) – Double pass weld
Table 2. Results of the cone tests carried out on friction stir welded butt welds.

Group	Shoulder Diameter (mm)	Shoulder Profile	probe Diameter(s) (mm)	probe Profile	004	005	006
Concave	16	Concave	Root: 5,2 & 9 Tip: 2	Smooth Conical			
Triflute	16	Concave/ Concentric rings	Root/Tip: 3	3 x Flutes			
Triflat	16	Concave/ Concentric rings	Root/Tip: 3	3 x Flats			
Large Shoulder	19	Concentric rings	Root: 5 Tip: 2	Smooth Conical			
GSP 5651	7.5	Concave	Root/Tip: 3	3 x Flutes + Threads 3 x Flats + Threads			

Figure 1. Summary of tooling designs

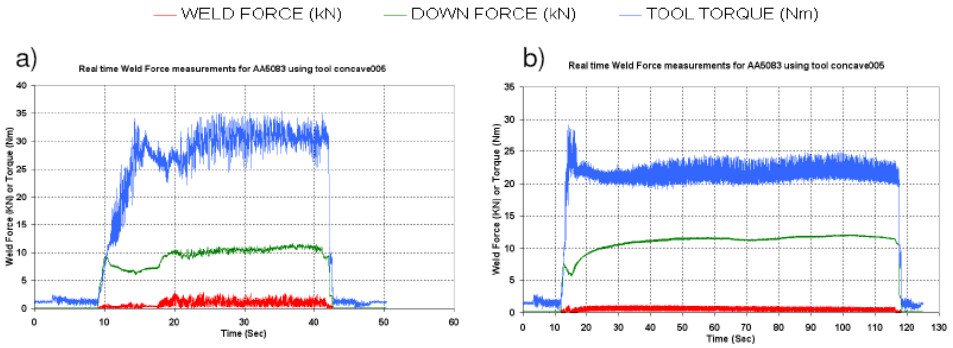

Figure 2. LoStir measurements for Hot and Cold weld conditions

a) Hot welding conditions: weld pitch = 0.25 mm/rev
b) Cold welding conditions: weld pitch = 1.49 mm/rev

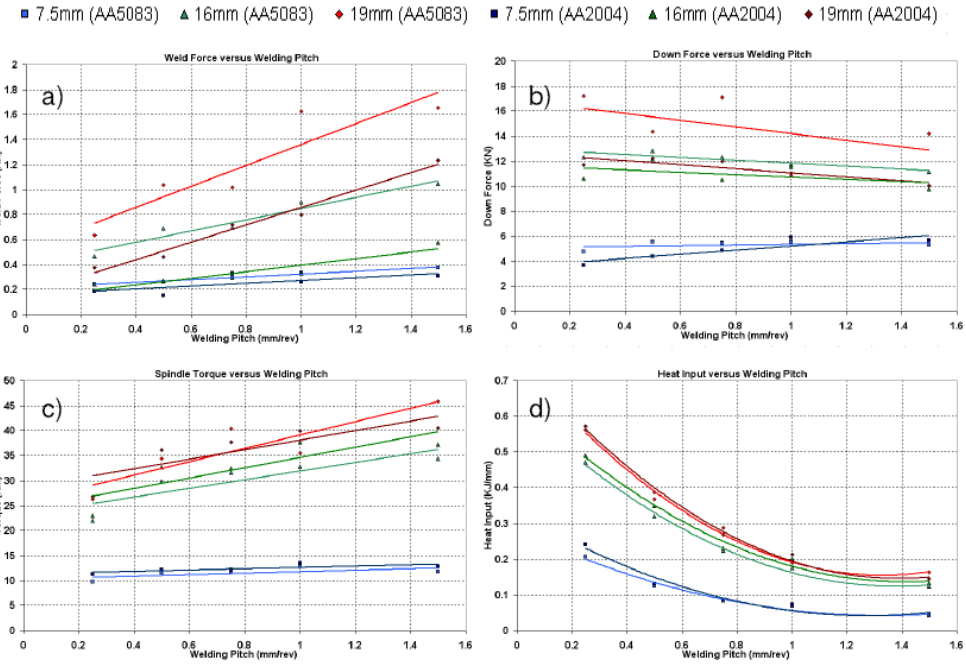

Figure 3. LoStir measurements and calculated heat input values versus Welding pitch.

a) Weld force (Fx)
b) Down force (Fz)
c) Spindle torque
d) Heat input

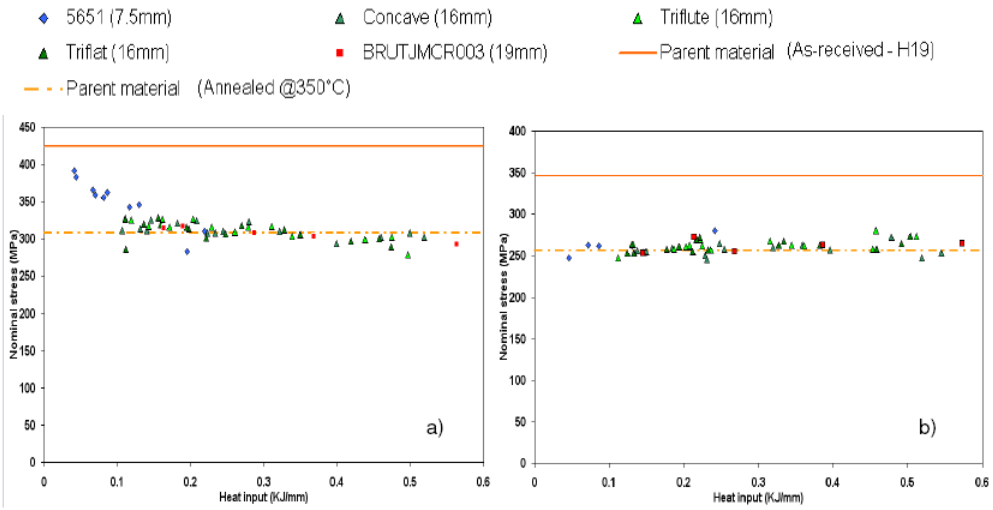

Figure 4. Ultimate tensile strength versus Heat input

a) AA5083
b) AA2004

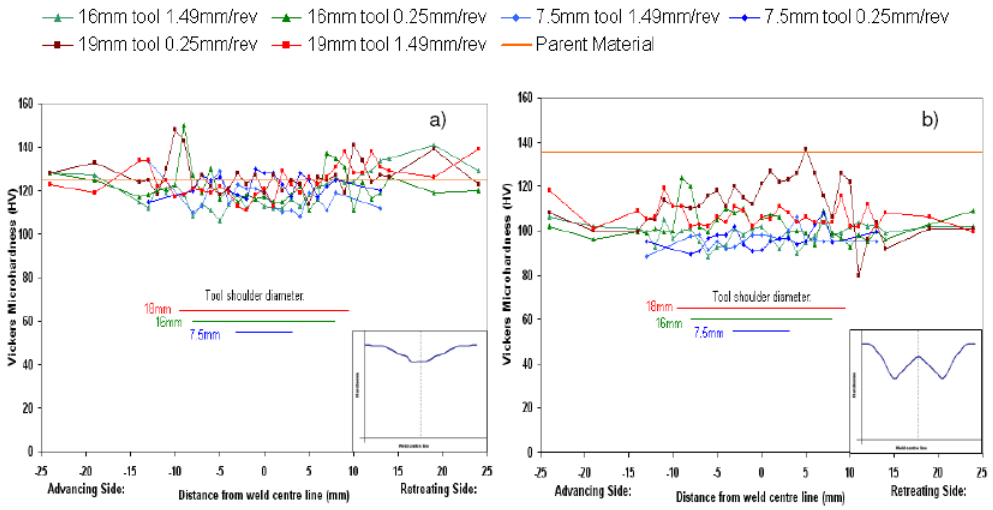

Figure 5. Vickers Hardness versus distance from weld centre

a) AA5083
b) AA2004
Inset: Typical hardness profile from literature [17]

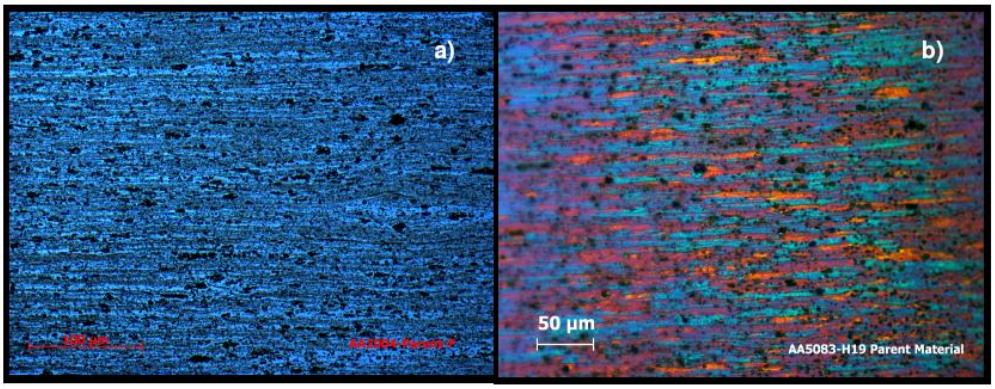

Figure 6. Microstructures of the parent material

a) AA2004-F
b) AA5083-H19

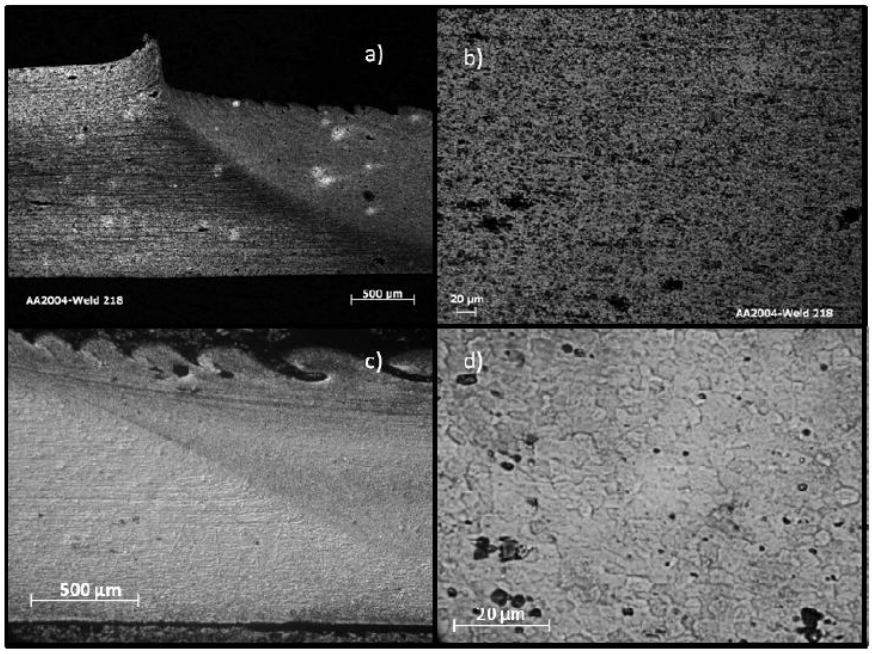

Figure 7. Microstructures of the Weld/Parent material interface with enlarged views of the of the weld material. Weld conditions: 700rpm, 175mm/min, 1.49 mm/rev.

a) AA2004 weld boundary.
b) AA2004 weld material.
c) AA5083 weld boundary.
d) AA5083 weld material.

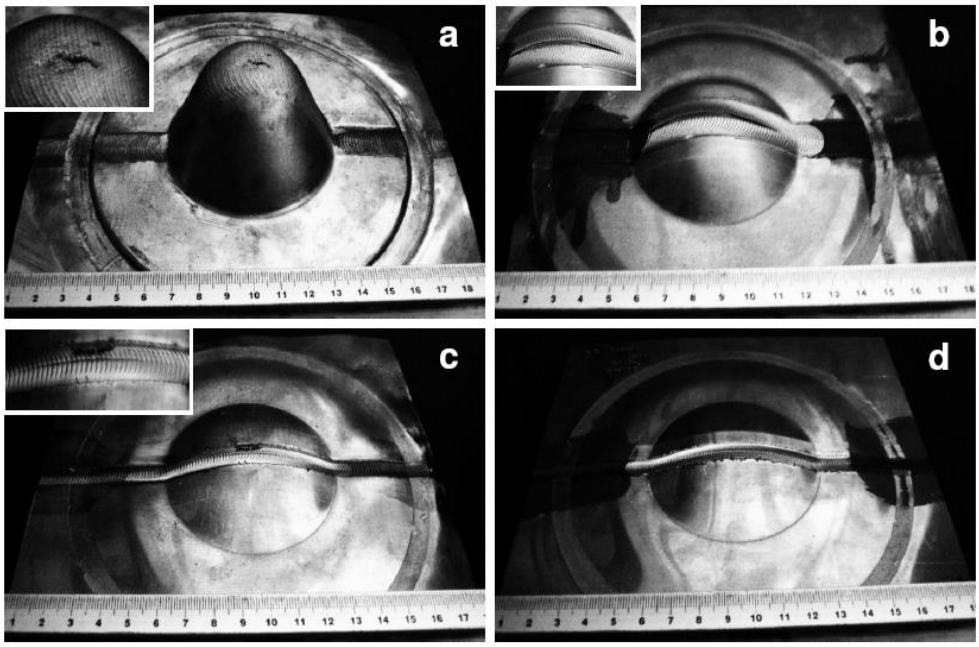

Figure 8. Cone test specimens

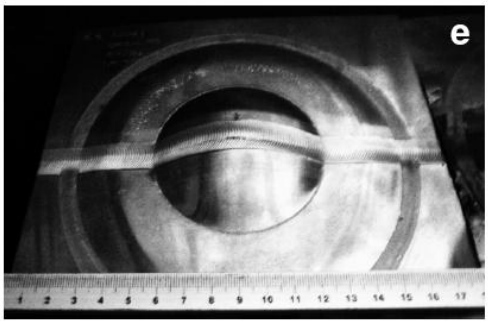

a) Two pass FSW using Large Shoulder tool (AA2004)
b) Two pass FSW using Large Shoulder tool (AA5083)
c) Two pass FSW using GSP5651 tool (AA5083)
d) Single pass FSW using GSP5651 tool (AA5083)
e) Single pass FSW using Concave005 tool (AA5083)

Key Engineering Materials Vols. 410-411 (2009) pp 117-125
online at http://www.scientific.net

Online available since 2009/Mar/02

Stability of Friction Stir Welds at Superplastic Forming Temperatures

T. Minton[1, a] and J. Au[1, b]

[1] School of Engineering and Design, Tower A, Brunel University, Uxbridge, UB8 3PH, UK

[a] Timothy.Minton@Brunel.ac.uk, [b] Joe.Au@Brunel.ac.uk

Keywords: Friction stir welding, Superplasticity, Aluminium, Recrystallization, Grain growth

Abstract. Friction stir welding is a solid state joining process which enables most metals and alloys to be welded without fusion temperatures occurring. The centre of the weld is comprised of dynamically recrystallized material which is beneficial for superplastic deformation. The high temperatures involved with conventional fusion welding techniques disrupt the delicate microstructure of superplastic materials. Superplasticity is heavily reliant on a small grained equiaxed matrix structure pinned by a fine distribution of hard second phase particles to inhibit grain growth during forming of the material. During the superplastic forming operation, the heavily strained structure present in the parent material undergoes a transformation from a banded structure comprising of very long, thin grains to fine equiaxed grains through various static and dynamic recrystallization mechanisms. During forming of friction stir welded materials the stability of the weld region has been investigated. Grain growth is more apparent in the strain hardening of AA5083 due to the relatively small amounts of strengthening precipitates. This material statically recrystallizes during the preheat stage of the superplastic forming process, the grains then begin to grow during a dynamic recovery process becoming far too large to allow superplastic deformation. AA2004 is specially designed superplastic forming (SPF) alloy which contains a large amount of Zr for grain stability. This alloying element is preferentially distributed along the grain boundaries which prevents grain growth during SPF. During the forming process the AA2004 dynamically recrystallizes; disruption to the parent material structure causes discontinuous dynamic recrystallization that results in a heterogeneous structure and makes the material prone to abnormal grain growth. The weld regions of FSWs in AA5083 and AA4004 have been shown to exhibit AGG in weld nugget and shoulder influenced regions. The stability of the superplastic material is reliant on their strengthening precipitates. The Zr in the AA2004 is a much more effective precipitate for maintaining stability.

Introduction

Friction stir welding (FSW) has been in development since its invention by The Welding Institute TWI in 1991 [1]. This joining technique combines frictional heat, generated by a rotating tool in contact with the stationary work piece, and deformation in the form of material flow around the contours of the tooling as it is rotated and traversed through the work piece. A schematic of the friction stir welding process can be seen in Fig. 1. This welding process can be likened to an extrusion process, material is heated and deformed by the tooling and is constrained by the backing plate and the cold unaffected material surrounding the weld region. The intense plastic deformation which occurs within the weld region leads to the creation of a favourable microstructure for subsequent forming operations. The combined heat and deformation allows dynamic recrystallization to occur in the weld nugget and creates a fine equiaxed grain structure. This favourable microstructure has lead to the development of the FSW operation into a processing

operation known as friction stir processing (FSP) which is carried out on monolithic work pieces in order to enhance their material properties.

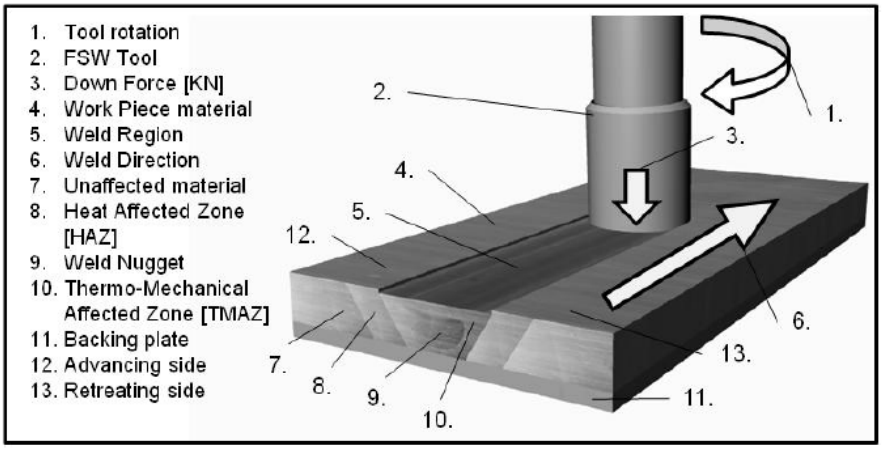

Figure 1. Diagram of the friction stir welding process.

Superplasticity is a phenomenon that allows a material to deform uniformly to extremely large elongations [2-4]. There are prerequisite characteristics which are vital for fine structure superplasticity to be possible these include: an equiaxed matrix grain structure with grains typically <10μm and a fine distribution of hard second phase particles. This second characteristic is critical in maintaining the material's ability to deform in a superplastic mechanism. Superplasticity utilises several creep mechanisms in order for the material to strain uniformly, these include: diffusional creep, grain boundary sliding and dislocation creep [5]. The most common mechanism used to describe superplasticity is grain boundary sliding accommodated by slip [4, 6], this relies on a fine matrix structure and microstructural stability at high temperatures; usually $>0.5T_m$, where T_m is the material melting point. The stability of the matrix structure is vital for allowing the matrix grain to slide over one another without grain boundary separation. Smaller grains slide more easily and larger grains separate more easily.

Aluminium has high stacking fault energy; this gives it a reluctance to recrystallize. During high temperature deformation process the stored energy within the structure drives the structural change mechanisms of recovery, recrystallization and grain growth in order to reduce the stored energy. When the energy available for structural change is low aluminium will recover; internal stresses are relaxed and dislocations find it easier to move within the structure. This preference for recovery over recrystallization then causes grain growth which is detrimental to superplastic deformation. This is where the differences between the two superplastic materials investigated in this study become clear. AA5083 is a strain hardening alloy; the superplastic variant of this alloy, designated H19, has undergone intense warm and cold rolling in order to produce a structure which is suitable for subsequent SPF processes. The internal stresses within this material allow it to statically recrystallize during the initial preheat stage of the superplastic forming process, transforming the highly strained, banded parent structure to a fine equiaxed structure suitable for SPF. The AA2004 is a precipitation hardening alloy, which relies on a fine distribution of hard second phase particles for its strength. During the initial low level straining at the start of the forming operation this material dynamically recrystallizes to transform into the equiaxed structure suitable for SPF.

Welding is usually a very disruptive process for a delicate superplastic material. The ability to weld superplastic materials and subsequently form them is important for increasing the flexibility of the SPF process. The success of the weld region during forming is heavily reliant on the weld region being stable at the temperatures involved during SPF.

Methodology

Two commercially available superplastic alloys have been selected for this investigation, these are AA5083 and AA2004. The typical compositions of these alloys are given in Table 1. Friction stir welds have been created in both bead on plate and butt weld configurations using a converted milling machine and a state of the art dedicated friction stir welding machine. Two sets of tools comprising of 7.5 and 16mm diameter TriFlute and TriFlat tools have been used in conjunction with the bead on plate trials on the converted milling machine. The spindle speed was varied between 500 and 700rpm and the spindle speed varied between 175 and 746mm/min in order to obtain a set of welds with increasing weld pitch from 0.25, deemed to be a hot weld, and 1.49mm/rev deemed to be a cold weld. Real time spindle torque measurements have been recorded, using a low cost FSW data acquisition device developed by TWI [7], and steady state values obtained for use in calculating the FSW heat input. Bead on plate welds have been tested for tensile strength in the as-welded and annealed states. Annealing was carried out in an air furnace at 350°C; the temperature at which AA5083 begins to recrystallize.

Composition of superplastic aluminium alloys.										
AA5083	Mg	Mn	Cr	Fe	Si	Zn	Ti	Cu	Other/Total	Al
	4.0-4.9	0.4-1.0	0.05-0.25	0.4	0.4	0.25	0.15	0.1	0.05/0.15	BAL
AA2004	Cu	Zr	Mg	Si	Fe	Mn	Zn	Ti	Other/Total	Al
	5.5-6.5	0.3-0.5	0.5	0.2	0.2	0.1	0.1	0.05	0.05/0.15	BAL

Table 1. Typical composition of AA5083 and AA2004; superplastic aluminium alloys [wt%].

Microstructural observations of the AA5083 and AA2004 welds have been carried out using standard metallography and light microscopy techniques. Both alloys are prepared and finely polished using colloidal silica before etching in 1% HF for the AA5083 and Keller's reagent for the AA2004. Potentially successful friction stir processed microstructures have then been re-created in butt weld configuration, using an MXTriflute tool and an ESAB SuperStir friction stir welding machine, in order to carry out superplastic cone testing.

Results and discussion

The welding pitch is the ratio of the spindle speed and the welding speed. This value gives the first indication of the heat within the friction stir weld. A high weld pitch indicates a cold welding condition due to more material being welded or processed for every rotation of the FSW tooling. Investigations in to the modelling of FSW have lead to the implementation of FSW heat input equations. The heat input for friction stir welds can be calculated using Eq. 1, taken from Russell et al [8] and Threadgill et al [9]. In this model the vast majority of the FSW heat input is generated

from the tool rotation; with a much smaller fraction, believed to be ~5%, resulting from the tool's movement in the welding direction.

$$Q=E\frac{2\pi rT}{1000v}. \quad (1)$$

Where Q is the FSW heat input (KJ/mm), E is a dimensionless efficiency factor, r is the spindle rotation speed (rpm), T is the steady state spindle torque (Nm) and v is the welding speed (mm/min). This calculated heat input increases as the weld pitch is decreased and is constant for tools with same shoulder diameters. The smallest heat inputs are therefore generated by the 7.5mm tool using the cold welding parameters. From Fig. 2 it can be seen that the two alloy systems respond very differently to the tensile test in the as-welded and annealed [A] conditions. In Fig. 2 a, the AA5083 as-welded samples retain some strain hardening when welded with the small 7.5mm diameter tools and the cold welding condition, producing joint efficiencies of ~85-95%. Above ~0.1KJ/mm the as-welded samples have received enough heat from the FSW tool to completely relax the strain hardening of the H19 material and so causing them resemble a fully annealed material. After annealing the AA5083 samples at 350°C the tensile strength of the welds now resemble that of a fully annealed AA5083-O, producing joint efficiencies of ~73%. The annealing changes the position of the predominant fracture location during tensile testing. For the as-welded samples the fracture location is typically within the weld region, once annealing has been carried out the fracture location switches to outside of the weld region.

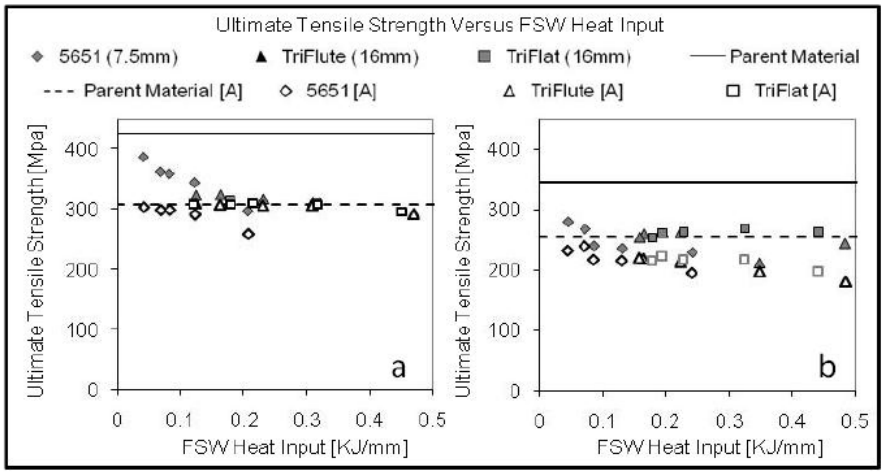

Figure 2. Ultimate tensile strength versus FSW heat input. a) AA5083, b) AA2004.

The AA2004 does not rely on any strain hardening, so there is no retention of strength under any of the conditions used for welding; the material becomes relaxed and the strength from second phase precipitates is disrupted by the deformation and heat from the FSW process causing aging and coarsening. For all the tools and the full range of heat inputs, the strength of the AA2004 is reduced; producing joint efficiencies of ~85%. After the annealing of the AA2004 FSW samples the strength is reduced further to well below that of AA2004-O, this indicates that there is microstructural instability within the FSW weld region during static annealing. Fig. 2 b shows the tensile strength of AA2004 as-welded and annealed FSW samples. In the as-welded condition all the welds

resemble AA2004-O, in the annealed condition the tensile strength of the weld region decreases as the heat input increases.

In the as-welded condition friction stir welds produce refined, recrystallized material within the weld region. The weld regions of the two alloy systems react differently to annealing. The static heat applied to the AA5083 welds allows static recrystallization to occur in both the parent material and the weld region due to the strain hardening of the material providing enough of a driving force for recrystallization. This is shown in Fig. 3, where the material outside of the weld region and the material within the weld region have produced a fine equiaxed structure which appears to be suitable for subsequent superplastic forming operations.

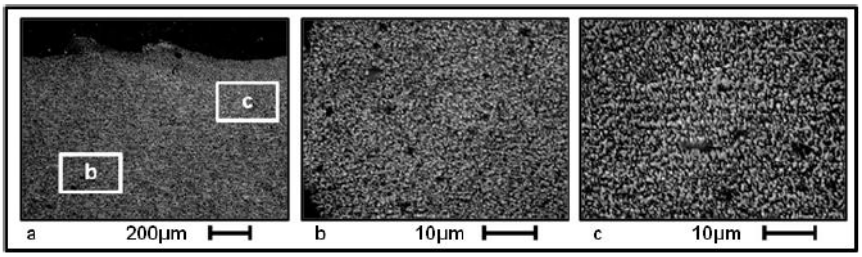

Figure 3. Microstructure of an annealed AA5083 friction stir weld. a) Weld region extremity, b) detail: material outside the weld region, c) detail: material within the weld region.

The friction stir welds in AA2004 react very differently. In the AA5083 welds the residual strain hardening allows static recrystallization. This is not possible for the AA2004 as there is not enough energy within the structure to allow static recrystallization. During static annealing the unaffected material which hasn't been relaxed by the heat field of the FSW tool is able to begin its transformation from banded structure into an equiaxed, recrystallized structure. However the material within the weld region has already been relaxed and recrystallized so the application of heat to this structure does not provide enough energy to drive further recrystallization. In this case the static annealing material causes recovery and leads to abnormal grain growth within the weld region. This is shown in Fig. 4, the most intensely deformed regions of the weld, the weld nugget and the advancing side of the weld have coarsened producing a heterogeneous structure which is unsuitable for SPF.

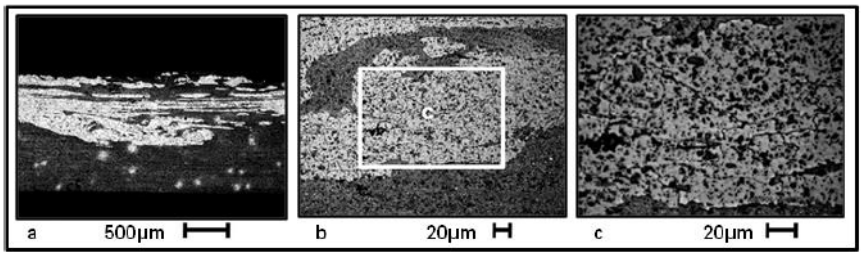

Figure 4. Microstructure of an annealed AA2004 friction stir weld. a) Weld region, b) and c) detail of weld nugget grain growth.

During the superplastic forming process the AA5083 material is heated to 460°C during the preheat phase of the process. During this stage the highly strained parent material transforms from a banded structure to an equiaxed structure via static recrystallization [10]. The friction stir welds in AA5083 have already experienced recrystallization and the strain within the weld region and heat affected zones have been relaxed. When the friction stir welds are subsequently subjected to the SPF preheat the weld region undergoes a cycle of secondary recrystallization and the grain structure rapidly coarsens, as shown in Fig. 5. The coarse structure prevents grain boundary sliding and increases the threshold stress for superplastic deformation. In this case the weld region does not deform. The material outside of the weld regions deforms and pulls the weld seam apart due to grain boundary separation. In the centre of the weld the tool influences material from the weld crown all the way down to the weld root causing grain coarsening through the entire thickness of the weld, this is shown in Fig. 5 b. Fig. 5 a and c, show the extremities of the weld region where the tool shoulder is the only influence on the material. Only the material which has been directly affected by the tool experiences grain coarsening. The material outside of the tool footprint and towards the root of the weld, where the tool lacks influence remains fine. The region where the unaffected fine grained material meets the coarse grains shows evidence of necking, further supporting the notion of an undeformable weld region.

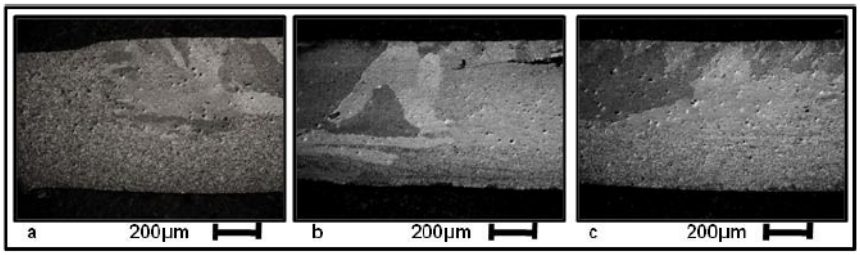

Figure 5. Microstructure of an AA5083 FSW, after SPF, a) Advancing side, b) Weld nugget, c) Retreating side.

The precipitation strengthened AA2004 material undergoes a similar transformation from banded structure to equiaxed structure during the initial low level straining experienced at the start of the SPF process. This transformation occurs via dynamic recrystallization [10, 11]. The fine precipitates distributed throughout the structure act as nucleation sites for recrystallization. Constant misorientation of subgrains leads to these subgrains becoming new deformation free grains with high angle boundaries which are then capable of deformation via grain boundary sliding. As shown in Fig. 6, the grain structure has remained small throughout the entire SPF process; allowing the material to form to strains ≥200%. The high levels of Zr are preferentially distributed along the grain boundaries which pins the grains and prevents grain growth and maintains the necessary fine grain size and high angle boundaries required for GBS. The forming material is still susceptible to coarsening during SPF; however the rate of coarsening is reduced by the pinning of the grain boundaries. Fig 6 a-c show the advancing side, weld nugget and retreating side regions of a formed friction stir weld in AA2004. The grain sizes of the material are similar on the advancing and retreating sides of the weld region; however the weld centre grains are larger. The very centre of the weld, where the tool probe passes through the material, experiences the most heat and deformation. This region therefore experiences the most disruption to the distribution of the second phase pinning precipitates and may become more susceptible to grain coarsening than the weld extremities.

During superplastic forming of friction stir welds in AA2004 all of the welds failed due to grain coarsening in the centre of the weld region. Friction stir welds created under cold welding conditions fared better, obtaining equivalent SPF strains of >200% before failure, with hotter welds achieving strains between 70% and 190% before failure.

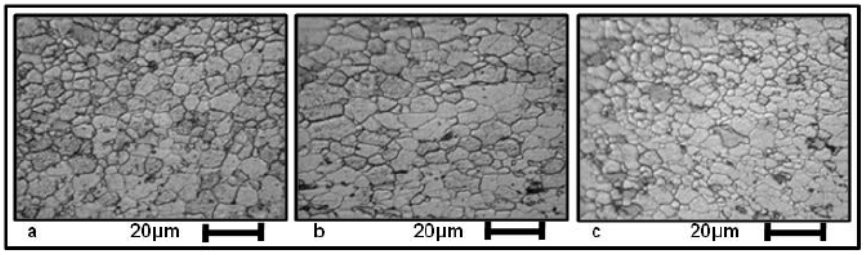

Figure 6. Microstructure of an AA2004 FSW, created using cold welding conditions, after SPF, a) Advancing side, b) Weld nugget, c) Retreating side.

Friction stir welds have been created in two very different alloy systems; these welds have then been subjected to annealing and superplastic forming conditions in order to establish the stability of the welded microstructures. The parent materials start as highly strained, banded structures which transform into an equiaxed grain structure during the SPF process. For the AA5083 this occurs during the preheat stage via static recrystallization and for the AA2004 this occurs via dynamic recrystallization during the initial low level straining at the beginning of the forming operation. A friction stir weld in a superplastic material creates heterogeneity within the structure. The weld region has already undergone intense heat and deformation causing dynamic recrystallization and producing a fine equiaxed grain structure [12], this region therefore skips the transformation stage which is experienced by the unaffected material.

During the preheat stage of SPF the AA5083 recrystallized weld region begins a stage of recovery whilst the parent material is recrystallizing. When the gas pressure is applied dynamic recovery causes grain growth and an increase in the threshold stress for deformation. This makes the weld region undeformable, resembling a fusion weld and creating a block of undeformed material between the deforming parent material sections [13]. To create superplastic AA5083 the material is heavily cold rolled to induce large amounts of strain. This strain is utilised by allowing the material to have stored energy for microstructural change. When heated the strain acts to induce recrystallization, however the FSW weld region is already recrystallized and so there is little stored energy within this region. With low levels of energy, coupled with aluminium's high stacking fault energy, there is insufficient energy for recrystallization so recovery mechanisms take over. The recovery is strictly limited to the region; material which has not been directly affected by the tool remains fine in grain size and begins to deform during SPF. The deforming material then pulls the FSW region apart and causes a weld seam rupture. The weld seam remains the same thickness and width as before the SPF operation further supporting the creation of an undeformable weld region.

The AA2004 FSW region behaves very differently. The large amounts of strain in the AA5083 make it stable under static conditions. The precipitation strengthened AA2004 is not strain hardening and so is more unstable under static conditions. Friction stir welding has recrystallized the weld region and disrupted the fine distribution of second phase Al_3Zr precipitates which pin the structure and prevent grain growth. Under static conditions some grains are not pinned and begin to grow in an abnormal grain growth regime. Over time these grains grow and consume the material

within the weld region. The preheat stage of the SPF process is quite short; approximately 5 minutes. The material is quickly heated to the forming temperature and straining begins as soon as the material has reached the correct temperature. Once the straining begins the material dynamically recrystallizes, the second phase particles act as recrystallization nucleation points and the fine grain size is maintained by the constant misorientation of subgrains which go on to become new grains [2]. Whilst the fine grain size is maintained the material can continue to deform uniformly via grain boundary sliding and allowing this material to be deemed superplastic by achieving strains of > 200%.

Friction stir welding has been shown to be a viable method of joining superplastic materials by enabling the retention of existing superplastic properties within the weld region. Further studies are required in order to improve the obtainable SPF strains by optimising the FSW process to create the best possible microstructure for subsequent forming operations.

Conclusions

- Friction stir welds in AA5083 are intrinsically stable under static annealing conditions due to the high levels of strain within the structure allowing it to statically recrystallize at temperatures of ≥350°C. Under dynamic conditions the material is more unstable due to the lack of pinning forces. Dynamic recovery causes abnormal grain growth which cannot be arrested by the Al_6Mn precipitates which are distributed throughout the structure.
- Friction stir welds in AA2004 are less stable under static conditions due to the dynamically recrystallized weld region lacking the stored energy to allow static recrystallization. The annealing of these samples yields abnormal grain growth. Under superplastic forming conditions the material is given enough energy; dynamic recrystallization occurs, which maintains the fine structure with help from Al_3Zr precipitates which are preferentially distributed along the grain boundaries. Welds in AA2004 are able to retain superplastic properties allowing uniform deformations of >200%.

References

[1] W. M. Thomas. Improvements Relating To Friction Welding, PCT/GB92/02203, WO 93/10935, (1993), p. 1.

[2] G. J. Davies, J. W. Edington, C. P. Cutler, K. A. Padmanabhan. Superplasticity: A Review, (1970), pp. 1091-1102

[3] O. D. Sherby, J. L. Wadsworth. Development and Characterization of Fine-Grain Superplastic Materials, (1984), pp. 355-389.

[4] T. G. Nieh, J. L. Wadsworth, O. D. Sherby. Superplasticity in Metals and Ceramics, (2005), pp. 287, ISBN 0-521-02034-4.

[5] M. F. Ashby, D. R. H. Jones. Engineering Materials 1: An Introduction to Properties, Applications and Design, Third edition, (2005), p. 271, ISBN 0-7506-6380-4.

[6] R. C. Gifkins. Grain-Boundary Sliding and its Accommodation during Creep and Superplasticity. Metal Trans A, Issue 8, Volume 7 A, (1976), pp. 1225-1232.

[7] K. A. Beamish, A. Ezeilo, S. Smith. Development of a low cost friction stir welding monitoring system, 6th International Symposium on Friction Stir Welding, Saint-Sauveur Canada, (2006).

[8] M. J. Russell. Development and Modelling of Friction Stir Welding, Ph.D thesis, Cambridge University UK (2000), pp 1-154.

[9] P. L. Threadgill, M. E. Nunn. A review of friction stir welding: Part 1 process overview, TWI Great Abington Granta Park Cambridge UK, TWI Members Report, 760/2003, (2003), pp 1-31, Information on: http://www.twi.co.uk/j32k/index_mem.xtp.

[10] G. E. Totten, D. S. MacKenzie. Handbook of Aluminum Volume 1 Physiscal Metallurgy and Processes, (2003), ISBN 0-8247-0494-0.

[11] P. S. Bate, F. J. Humphreys, N. Ridley, B. Zhang. Microstructure and texture evolution in the tension of superplastic Al–6Cu–0.4Zr, Acta Materialia, , Issue 10, Volume 53, (2005), pp 3059-3069

[12] K. V. Jata, S. L. Semiatin. Continuous dynamic recrystallization during friction stir welding of high strength aluminum alloys, Scripta Materialia, Issue 8, Volume 43, (2000), pp 743-749

[13] R. W. Davies, J. S. Vetrano, M. T. Smith, S. G. Pitman. Mechanical properties of aluminum tailor welded blanks at superplastic temperatures, Journal of Materials Processing Technology, Issue 1-3, Volume 128, (2002) pp 38-47